DISTRIBUTED CONTROL OF UNDERACTUATED AND HETEROGENEOUS MECHANICAL SYSTEMS

Using Passivity-Based Control by Interconnection and Damping Assignment as a Tool for Distributed Control Design and Human-Machine Interaction

LAURENS VALK

2017–2018

Distributed Control of Underactuated and Heterogeneous Mechanical Systems, Using Passivity-Based Control by Interconnection and Damping Assignment as a Tool for Distributed Control Design and Human-Machine Interaction

SUPERVISORS:
dr.ir. T. Keviczky
prof. dr.ir. H. Vallery

LOCATION:
Delft University Of Technology, Delft Center for Systems and Control
Delft University Of Technology, Department of BioMechanical Engineering

COLOPHON:
Online version typeset with LaTeX *classicthesis* template on June 26, 2018 at 22:04

DISTRIBUTED CONTROL OF UNDERACTUATED AND HETEROGENEOUS MECHANICAL SYSTEMS

Using Passivity-Based Control by Interconnection and Damping Assignment as a Tool for Distributed Control Design and Human-Machine Interaction

MASTER OF SCIENCE THESIS

For the degree of Master of Science in

Systems and Control

at Delft University of Technology

Delft Center for Systems and Control

For the degree of Master of Science in

Mechanical Engineering

at Delft University of Technology

Department of BioMechanical Engineering

LAURENS VALK

July 11, 2018

ABSTRACT

Passivity-based control is a well-established technique for coordinating groups of fully-actuated systems, but existing methods for underactuated systems are limited to groups of homogeneous systems, coordinate synchronization tasks, and to specific applications. We propose a generic distributed control method that enables heterogeneous groups of underactuated and fully-actuated mechanical systems to cooperatively assume desired task-space formations, with or without leaders with constant task-space references.

Extending the method of passivity-based control by interconnection and damping assignment (IDA-PBC) to distributed networks of mechanical systems, we derive matching conditions and control laws to achieve the desired stable group behavior. For a suitable choice of virtual coupling forces between the systems in the task space, we can decouple the matching conditions into three conditions local to each agent, independent of the topology of the undirected and connected network. If these local conditions are satisfied, we show how existing single-system IDA-PBC solutions can be used to construct distributed control laws, thereby enabling distributed control design for a large class of applications.

By shaping the input-output behavior of a system in addition to shaping its total energy, we also show how human operators can interact with groups of underactuated mechanical systems using the proposed distributed control scheme. The procedure is illustrated using simulation studies of networks of unmanned aerial vehicles that can assume formations and dock with underactuated flexible-joint manipulators.

PUBLICATIONS

PUBLICATIONS BASED ON THIS THESIS

[1] L. Valk and T. Keviczky, "Distributed control of heterogeneous underactuated mechanical systems," in *Proceedings of the Conference on Distributed Estimation and Control in Networked Systems*, IFAC, 2018 (Submitted).

[2] L. Valk and T. Keviczky, "Unified passivity-based distributed control of mechanical systems," in *37th Benelux Meeting on Systems and Control*, 2018.

PREVIOUS SCIENTIFIC PUBLICATIONS

[1] L. Valk, A. Berry, and H. Vallery, "Directional singularity escape and avoidance for single-gimbal control moment gyroscopes," *Journal of Guidance, Control, and Dynamics*, vol. 41, no. 5, pp. 1095–1107, 2018.

PREVIOUS EDUCATIONAL PUBLICATIONS

[1] L. Valk, *The LEGO MINDSTORMS EV3 Discovery Book: A Beginner's Guide to Building and Programming Robots*. San Francisco, CA, USA: No Starch Press, 2014.

[2] L. Valk, *LEGO Roboter II: Neue Modelle Bauen mit LEGO MINDSTORMS NXT 2.0*. Heidelberg, DE: Dpunkt Verlag, 2012.

[3] D. J. Perdue and L. Valk, *The Unofficial LEGO MINDSTORMS NXT 2.0 Inventor's Guide*. San Francisco, CA, USA: No Starch Press, 2010.

[4] L. Valk, *The LEGO MINDSTORMS NXT 2.0 Discovery Book: A Beginner's Guide to Building and Programming Robots*. San Francisco, CA, USA: No Starch Press, 2010.

CONTENTS

Symbol	Meaning	Single agent	Multi agent
t	Time	2.1	
$\boldsymbol{0}$	Zero vector	1.4	
$\mathbf{0}$	Zero matrix	1.4	6.1
$\mathbf{I}$	Identity matrix	1.4	6.1
n	Number of states	2.1	6.1
m	Number of control inputs	2.1	6.1
ℓ	Dimension of task-space/communicated variable	3.5	8.2
i or j	Agent index		1.4
N	Number of agents in a network		1.4, 6.1
s	Supply rate	2.4	
S	Storage function	2.4	
$\boldsymbol{q}, \boldsymbol{q}^*$	Generalized coordinates and target	2.1, 3.1	6.1, 6.4
$\boldsymbol{\theta}, \boldsymbol{\theta}^*$	Stabilizable coordinates and target	3.3	
$\boldsymbol{x}, \boldsymbol{x}^*$	Controllable coordinates and target	3.3	
$\boldsymbol{z}, \boldsymbol{z}^*$	Task-space coordinates and target	3.5	8.3
$\boldsymbol{r}^*_{ij}$	Desired difference between $\boldsymbol{z}_j$ and $\boldsymbol{z}_i$		4.2
$\mathcal{Q}^*$	Set of equally desired reference coordinates	3.1	
$\boldsymbol{p}$	Generalized momenta	2.1	6.1
$\boldsymbol{\tau}$	Control input to uncontrolled system	2.1	6.1
$\boldsymbol{\tau}_\mathrm{d}$	Control input to desired closed-loop system	3.1	6.2
$\boldsymbol{\tau}_\mathrm{e}$	Control input through shaped input matrix	9.1	
$\boldsymbol{\tau}_\mathrm{h}$	Human force input	9.1	
$\boldsymbol{\beta}$	State feedback law	3.1	
$\boldsymbol{y}$	Output of uncontrolled system	2.3	6.1
$\boldsymbol{y}_\mathrm{d}$	Output of desired closed-loop system	3.1	6.2, 8.4
$\boldsymbol{y}_\mathrm{e}$	Output with shaped input matrix	9.1	
$\mathbf{R}$	Intrinsic dissipation matrix	2.3	
$\mathbf{C}$	Lagrangian Coriolis force matrix	2.2	

Symbol	Meaning	Single agent	Multi agent
$\mathbf{K}_v$	Desired dissipation matrix	3.1	6.4
$\mathbf{K}_\mathrm{d}$	Desired task dissipation matrix	9.1	10.2
$\mathbf{J}$	Desired gyroscopic force assignment matrix	3.1	6.4
$\mathbf{F}^\perp$	Input matrix annihilator	3.1	8.1
$\mathbf{F}, \mathbf{F}_\mathrm{d}$	Input matrix and desired expression	2.3, 9.3	6.1
$\mathbf{M}, \mathbf{M}_\mathrm{d}$	Generalized mass matrix and desired expression	2.1, 3.1	6.1, 6.2
H, H_d	Hamiltonian and desired expression	2.3, 3.1	6.1, 6.2
V, V_d	Potential energy and desired expression	2.1, 3.1	6.1, 6.2
V_s	Desired stabilization potential energy	3.5	8.2
V_c	Desired (cooperative) tracking potential energy	3.5	8.2
$\mathbf{A}$	Task Jacobian	3.5	7.3
$\boldsymbol{\Psi}$	Input matching matrix	3.5	8.2
$\boldsymbol{\Phi}$	Input matrix for free interaction forces	3.5	8.5
$\boldsymbol{\sigma}$	Internal control except tracking or cooperation	3.5	8.5
$\mathbf{D}_i, \bar{\mathbf{D}}$	Input distribution matrix		10.2
$\boldsymbol{\mathcal{C}}_i$	Task scaling matrix		10.5
$\hat{\boldsymbol{z}}_i, \hat{\boldsymbol{\Psi}}_i$	Unscaled counterparts of $\boldsymbol{z}_i$ and $\boldsymbol{\Psi}_i$		10.5
$\boldsymbol{\alpha}, \boldsymbol{\delta}, \boldsymbol{\zeta}$	Flexible-joint angles and motor angles	3.5	12.1
$\mathcal{V}, \mathcal{T}, \mathcal{E}$	Sets of vertices, leaders, and edges in a network		4.1, 4.2
$\boldsymbol{\mathcal{B}}_i, \boldsymbol{\mathcal{B}}$	Leader matrix and network leader matrix	4.3	4.3
$\boldsymbol{\mathcal{A}}_{ij}, \boldsymbol{\mathcal{L}}$	Adjacency matrix and Laplacian matrix		4.3
$\epsilon, g, M, I, L,$	Constant model parameters	11.1, 11.4	
k, c, a^*	Constant control parameters	11.1, 11.4	
$\boldsymbol{\Upsilon}$	Constant joint stiffness matrix	12.1	

1 INTRODUCTION

1.1 MOTIVATION

The transition from linear control to nonlinear control methods and the rapid increase in computational power has led to robust and adaptive control methods that are now being implemented successfully, even for complex nonlinear plants [1]. More recently, accelerated by the miniaturization and ever decreasing cost of electromechanical systems, there has been an increasing demand for distributed systems, where a complex plant is replaced by a set of simpler plants that cooperatively achieve a similar or superior goal compared to the original plant, by communicating process information or objectives between the subsystems [2]. A distributed approach can reduce operational cost, ease system requirements and increase robustness to failure. The decomposition into small units also allows systems to be scaled up or down, possibly beyond the capabilities of a single complex plant, or to be adapted to changing task requirements [2].

1.1.1 *Applications and objectives of distributed control*

These advantages of a distributed approach are promising for applications such as autonomously operating vehicle platoons [3] or spacecraft constellations [4, 5], collaborative transportation [6], exploration of unknown or dangerous terrains [7], large scale sensing and quality inspection [8, 9], and collaborative construction [10, 11]. Such high level tasks can be decomposed into different, simpler objectives executed sequentially or in parallel [2]. For example, a group of autonomous vehicles may first drive towards a commonly agreed location and then maintain a desired vehicle formation while traversing a stretch of road, to optimize overall fuel efficiency.

This thesis focuses on such low-level cooperative group objectives, known as consensus, agreement, synchronization, or formation problems [2]. These problems are mathematically similar across the wide spectrum of previously mentioned applications, where the cooperative objective is expressed in relevant quantities of the systems under consideration. For example, a group of robotic arms can synchronize (agree on; reach consensus on) their end-effector locations to collaboratively grasp an object, by communicating this position information with one other.

The synchronization and formation control problems are extensively studied in literature, and can be further specialized into studies that address numerous complications that can arise in their practical implementation [12]. One broad class of studies is devoted to communication constraints between the components of a distributed system, where communication delays or connectivity problems can drastically reduce performance or even incur instability of the group.

A second class of distributed control studies addresses the challenges of complex system dynamics, such as nonlinearities or limited actuation capabilities, often while simplifying any adverse affects of communication constraints. This thesis can be placed in this category. In particular, we address the challenges of the distributed control of underactuated mechanical systems, where one or more subsystems have fewer independent actuators than kinematic degrees of freedom.

1.1.2 *Passivity-based distributed control of underactuated mechanical systems*

The solution to the distributed control problem of mechanical systems is well-established for fully-actuated systems, where one typically relies on energy-based analysis techniques such as passivity [13–17]. Although there exist other distributed control techniques including backstepping and optimization-based strategies, we focus on passivity-based techniques due to its potential for proving stability results.

In the context of mechanical systems, passivity implies that the rate at which a system stores energy must be equal to or less than the energy supplied to the system through its input-output pair [1, 18]. This property has been used successfully for individual nonlinear systems such as robotic manipulators [19, 20], resulting in wide range of methods ultimately named passivity-based control (PBC) [21, 22].

While passivity-based control techniques provide simple and effective control solutions for fully-actuated agents or groups thereof, many practical systems are underactuated, such as many ground, aerial [23], water, and space vehicles, as well as some compliant or flexible robotic manipulators [24, 25]. Passivity-based schemes usually do not rule out underactuated applications, but often do not give a constructive solution for such systems.

The single-agent control problem of underactuated mechanical systems is historically a popular research topic both due to its practical applications and challenging nonlinear nature, which has spurred numerous variants of passivity-based control for specific classes of underactuated systems [26]. A successful method for controlling underactuated mechanical systems is passivity-based control by interconnection and damping assignment (IDA-PBC) introduced in [27]. This passivity-based control method uses a static state feedback law to change the open-loop dynamics to match a desired class of stable dynamics, with an asymptotically stable equilibrium at a desired setpoint, corresponding to the minimum of prescribed kinetic and potential energy functions. Constructive single-agent solutions exist for classes of underactuated systems, such as those with only one unactuated coordinate [28].

The distributed control problem of fully-actuated mechanical systems has well-established solutions for various applications, from fully-actuated point masses to systems with Lagrangian and Hamiltonian dynamics [13–17, 29–31], while capturing aspects such as synchronization, formation tasks, obstacle avoidance, and group reference tracking. In some of these methods, solutions are provided to achieve synchronization or formations with or without leaders in a group. Without leaders, a group attains a desired formation, but the final location of the group is arbitrary. When there are one or more leaders in a group, they can guide the followers in the formation to a desired location. Unfortunately, methods such as [13–17] do not extend trivially to networks with one or more underactuated agents.

1.1.3 *Relation to existing work*

An early result for the synchronization of underactuated mechanical systems was given by [32], based on the method of controlled Lagrangians [33, 34], of which the single-agent solution is a special case of IDA-PBC [35]. The method [32] provides control laws for leaderless coordinate synchronization of homogeneous systems which satisfy the so-called simplified matching conditions [33, 34].

An IDA-PBC approach was used to stabilize coordinate synchronization error dynamics in [36]. While this method reduces the synchronization recovery time after a disturbance on a subsystem, all agents require knowledge of the absolute reference, making it technically no longer a distributed control method. Additionally, the communication topology is restricted to a directed ring graph, where each agent communicates state information to one adjacent agent. The solution hinges on the

solvability of a large partial differential equation regarding the error dynamics, for which no systematic solution is provided beyond two examples.

Other passivity-based approaches for controlling networks of underactuated systems provide control laws for specific applications. For example, a coordinate synchronization result for networks of flexible-joint robots was presented in [37]. There, the result amounts to showing that control laws taken from fully-actuated methods can be proven to work for a limited class of underactuated applications as well.

The previously mentioned passivity-based distributed control approaches for underactuated systems share several properties that limit their theoretical and practical applicability, summarized as follows.

- Coordinate and task-space coordination: The methods [32, 36, 37] cooperatively control the generalized coordinates of each underactuated system in the network. In practice, it is more useful to cooperatively control a task-space coordinate, which is generally a nonlinear function of the coordinates. For example, robotic manipulators may control their end-effectors to cooperatively grasp an object, independently from where their base is located. As a special case, coordination of the coordinates remains possible if desired. Task-space coordination is already well-established for the fully-actuated case [38].

- Formations and synchronization: The methods [32, 36, 37] provide control laws for synchronization, whereas formations are more useful in practice. Robotic end-effectors can assume a formation with a desired inter-agent spacing equal to the dimension of the objected to be grasped. On the contrary, synchronization implies zero inter-agent distance, leading to collisions by definition unless they operate, somewhat artificially, in a parallel workspace. Synchronization can still be obtained as special case of a formation. Formations are already possible with methods for fully-actuated agents such as [14].

- Heterogeneity and generality: The method [32] requires that all agents have an identical configuration space, while [37] requires all agents to be of the same system class. In practice, it would be useful if systems can cooperate whether they are underactuated or fully-actuated, regardless of their parameter values or number of coordinates. This is especially useful when combined with the previously mentioned generalizations to task-space formations.

- Methodology and constructiveness: To make a distributed control method useful in practice, it is helpful if it is modular. This means that the ability of an agent to participate in a particular group task can be determined using properties of that agent alone, while the interaction between agents can be constructively obtained based on this capability of each agent. This decoupling of necessary conditions can be found in [32], but not in [36], where a single condition must in general be evaluated for the whole network. Applicability is further enhanced if existing single-agent solutions can be constructively reused and coupled to devise the distributed control laws.

We aim to address each of these generalizations in a constructive distributed control method for achieving stationary heterogeneous formations in the task-space.

1.2 PROBLEM STATEMENT

Our aim is to develop a constructive distributed control method that enables heterogeneous groups of underactuated and fully-actuated mechanical systems to cooperatively assume a desired formation in one or more task coordinates, with or without leaders that steer the formation to a desired location.

Inspired by the generality of the single-agent IDA-PBC problem and solutions [26, 27], and based on the existing synchronization result of homogeneous underactuated agents using the controlled Lagrangians approach [32], our hypothesis is that the single-agent IDA-PBC method can be extended to achieve the desired distributed control objectives. We wish to investigate this hypothesis using the following research question:

How can passivity-based control by interconnection and damping assignment (PBC-IDA) be used as a constructive design tool for distributed control of heterogeneous task-space formations of underactuated and fully-actuated mechanical systems?

The desired outcomes are control laws, one for each agent, that make the group achieve the desired task-space formation in a demonstratively stable fashion. To help find these control laws, we pose the following questions with a more limited scope.

1.2.1 *What conditions must an agent with a local controller satisfy to allow cooperative control in a distributed network?*

Inspired by results for fully-actuated systems [13–17], it is anticipated that the total control law for each agent is the sum of two control signals. One signal pertains to a local objective, such as canceling gravity, inserting damping, or stabilizing a coordinate that is not collaboratively controlled. The other signal could account for helping achieve the group objective.

1.2.2 *How must the coordinates and the equilibrium of each agent be chosen?*

Because underactuated agents have fewer independent actuators than degrees of freedom, not all coordinates can be independently controlled. Single-agent IDA-PBC solutions typically stabilize some coordinates to a fixed setpoint while the setpoints of other coordinates can be chosen freely. When considering a network of distributed systems, the equilibrium or setpoint of all agents may not be known in advance. Does this place constraints on how existing single-agent solutions can be re-used in the distributed control scenario?

1.2.3 *Which information must be communicated with other agents for task-space coordination?*

It is expected that agents must communicate partial state information to one another in order to achieve the group objective. Is it sufficient to communicate only generalized coordinates, or must velocity information also be shared?

Moreover, because task-space objectives are generally of lower dimension than the whole configuration space, it is expected that only part of the configuration space must be coordinated across the network. But which part should that be exactly?

1.2.4 *What degrees of freedom and constraints are there in the distributed control law, and what group objectives can be achieved?*

For underactuated systems, the signals for internal stabilization and for contributing to the group objective are possibly not so easily separated, putting constraints on control signals that make the agents contribute to the group objective. It is therefore

necessary to determine precisely what these conditions are, and whether they pose limitations to the achievable group objectives.

The single-agent PBC-IDA method is especially suited for point tracking, but is less suited for trajectory tracking. This suggests that leaders in a group can track fixed references. However, leaders and followers also move toward one another in synchronization and formation tasks, which implies a moving target. The question then becomes whether existing single-agent solutions can be adapted for this control objective.

1.2.5 *How can human operators interact with underactuated and distributed systems in a stable way?*

In addition to operating autonomously, groups of robots or vehicles can also operate in environments shared with humans, leading to human-machine interaction. This may allow a human operator to steer one or more robots in a supervisory manner while they stabilize themselves or maintain a previously assumed formation. Because the human interaction force cannot be modeled or predicted accurately, it is of interest to investigate how control laws and interaction mechanisms can be designed to maintain stability and the group objective when subjected to an arbitrary human input force. This is especially the case for underactuated systems, which cannot arbitrarily offset all human input force.

1.3 REPORT OVERVIEW

This thesis is split into six parts. Part I introduces passivity-based modeling and control concepts for single agents. The IDA-PBC control problem and solutions are given for several generic classes of systems, along with a coordinate partitioning to prepare for the distributed control approach. Part II gives network modeling concepts from graph theory and gives control objectives that can be pursued by distributed systems. It also presents several existing passivity-based distributed control procedures for fully-actuated mechanical systems in a unified way.

Part III presents the main result of this thesis, by deriving a distributed control law and so-called matching conditions for stable cooperation of underactuated mechanical systems in a distributed system. Part IV extends the proposed method of energy shaping to shaping of the input and output of each system in a network, providing a different interpretation of cooperation between systems, while also allowing a human operator to interact with a group of mechanical systems.

Part V provides two sets of simulation case studies that demonstrate the applicability of the proposed method. This includes a simulation of a group of underactuated unmanned aerial vehicles as well as a simulation of a docking procedure of such a vehicle with two underactuated robotic arms. Part VI summarizes the results and reflects on the achieved results and the research questions.

1.4 TERMINOLOGY AND NOTATION

This section gives a brief overview of the notation used throughout this thesis, including the notation for vectors, matrices and partial derivatives.

1.4.1 *Scalars, vectors, matrices, zeros, and identities*

A scalar symbol c is non-bold and italicized, a vector $\boldsymbol{z}$ is bold and italicized, and a matrix $\mathbf{A}$ is bold and non-italicized. The $n \times n$ identity and zero matrices are

denoted $\mathbf{I}_n$ and $\mathbf{0}_n$. Non-square zero matrices are indexed by the number of rows and columns, respectively (e.g. $\mathbf{0}_{n\times m}$). The vectors $\boldsymbol{0} = [0 \cdots 0]^\top$ and $\boldsymbol{1} = [1 \cdots 1]^\top$ are assumed to have a compatible dimension depending on context.

1.4.2 *Vector, matrix and agent indexing*

Vectors $\boldsymbol{z} \in \mathbb{R}^\ell$ and matrices $\mathbf{A} \in \mathbb{R}^{m\times n}$ have the following elements

$$\boldsymbol{z} = \begin{bmatrix} z_1 \\ \vdots \\ z_\ell \end{bmatrix}, \quad \mathbf{A} = \begin{bmatrix} A_{11} & \cdots & A_{1n} \\ \vdots & & \vdots \\ A_{m1} & \cdots & A_{mn} \end{bmatrix}. \tag{1}$$

In a multi-agent context, agents are usually indexed as $i = 1, \ldots, N$. When multiple subscripts are necessary, the last subscript denotes the agent index:

$$\boldsymbol{z}_i = \begin{bmatrix} z_{1,i} \\ \vdots \\ z_{\ell,i} \end{bmatrix}, \quad \mathbf{A}_i = \begin{bmatrix} A_{11,i} & \cdots & A_{1n,i} \\ \vdots & & \vdots \\ A_{m1,i} & \cdots & A_{mn,i} \end{bmatrix}. \tag{2}$$

A bar is used to designate a property of a network of systems, which is often a collection of the corresponding variables of each agent:

$$\bar{\boldsymbol{z}} = \begin{bmatrix} \boldsymbol{z}_1 \\ \vdots \\ \boldsymbol{z}_N \end{bmatrix}. \tag{3}$$

1.4.3 *Gradients and Jacobian matrices*

A partial derivative of a scalar $c(\boldsymbol{q}) \in \mathbb{R}$, where $\boldsymbol{q} \in \mathbb{R}^n$, is denoted as a column vector, while a Jacobian matrix of a vector function $\boldsymbol{z}(\boldsymbol{q}) \in \mathbb{R}^\ell$ is an $\ell \times n$ matrix:

$$\frac{\partial c}{\partial \boldsymbol{q}} = \begin{bmatrix} \dfrac{\partial c}{\partial q_1} \\ \vdots \\ \dfrac{\partial c}{\partial q_n} \end{bmatrix}, \quad \frac{\partial \boldsymbol{z}}{\partial \boldsymbol{q}} = \begin{bmatrix} \dfrac{\partial z_1}{\partial q_1} & \cdots & \dfrac{\partial z_1}{\partial q_n} \\ \vdots & & \vdots \\ \dfrac{\partial z_\ell}{\partial q_1} & \cdots & \dfrac{\partial z_\ell}{\partial q_n} \end{bmatrix}. \tag{4}$$

For brevity, we introduce the following notation for transposes of these derivatives:

$$\frac{\partial^\top c}{\partial \boldsymbol{q}} = \left(\frac{\partial c}{\partial \boldsymbol{q}}\right)^\top, \quad \frac{\partial^\top \boldsymbol{z}}{\partial \boldsymbol{q}} = \left(\frac{\partial \boldsymbol{z}}{\partial \boldsymbol{q}}\right)^\top. \tag{5}$$

See also Appendix a.3.1 for a definition of the partial derivative $\dfrac{\partial c(\boldsymbol{z}(\boldsymbol{q}))}{\partial \boldsymbol{q}}$.

1.4.4 *Lagrangian versus Hamiltonian notation*

A tilde notation is used to indicate a Lagrangian context, when a function depends on the generalized velocities $\dot{\boldsymbol{q}}$. For example, the total energy of a Lagrangian mechanical system is $\widetilde{H} = \widetilde{H}(\boldsymbol{q}, \dot{\boldsymbol{q}})$. Without the tilde notation, the Hamiltonian context is assumed by default: $H = H(\boldsymbol{q}, \boldsymbol{p})$. No tilde notation is used when a term depends only on the generalized coordinate $\boldsymbol{q}$, such as $\mathbf{M}(\boldsymbol{q})$, in which case the Lagrangian and Hamiltonian interpretation is identical. In most cases, the arguments are dropped after a symbol is first introduced.

Part I

MODELING AND CONTROL OF A SINGLE UNDERACTUATED MECHANICAL SYSTEM

Before considering control methods for distributed systems, this part reviews modeling and passivity-based control techniques for single simple mechanical systems. Chapter 2 gives the Lagrangian and Hamiltonian equations of motion of an uncontrolled system, and reviews relevant passivity and stability properties. Chapter 3 reviews the method of passivity-based control by interconnection and damping assignment, in order to achieve setpoint control for a single mechanical system.

2 MODELING SIMPLE MECHANICAL SYSTEMS

This chapter provides the equations of motion of so-called simple mechanical systems in Sections 2.1–2.3, based on [22, 25]. This class includes ground, water, aerial, and space vehicles, and machines such as robotic manipulators. Passivity and stability of the uncontrolled systems are discussed in Section 2.4, while Section 2.5 provides several modeling assumptions used throughout the thesis.

2.1 ENERGY AND INPUT FORCES

At some time instant t, a simple mechanical system can be uniquely described by a set of generalized coordinates $\boldsymbol{q}(t) \in \mathbb{R}^n$ and their time derivatives $\dot{\boldsymbol{q}}(t) \in \mathbb{R}^n$.

The rate of change of the generalized coordinates is closely related to the energy stored in the system. The total stored energy, denoted $\widetilde{H}(\boldsymbol{q}, \dot{\boldsymbol{q}}) \in \mathbb{R}$, is the sum of the kinetic energy $\widetilde{T}(\boldsymbol{q}, \dot{\boldsymbol{q}}) \in \mathbb{R}$ and the potential energy $V(\boldsymbol{q}) \in \mathbb{R}$, giving

$$\widetilde{H}(\boldsymbol{q}, \dot{\boldsymbol{q}}) = \widetilde{T}(\boldsymbol{q}, \dot{\boldsymbol{q}}) + V(\boldsymbol{q}). \tag{6}$$

The kinetic energy of a simple mechanical system can be described in terms of its generalized mass matrix $\mathbf{M}(\boldsymbol{q}) = \mathbf{M}^\top(\boldsymbol{q}) > \mathbf{0}_n$ as

$$\widetilde{T}(\boldsymbol{q}, \dot{\boldsymbol{q}}) = \frac{1}{2} \dot{\boldsymbol{q}}^\top \mathbf{M}(\boldsymbol{q}) \dot{\boldsymbol{q}}. \tag{7}$$

The system is subject to generalized input forces $\mathbf{F}(\boldsymbol{q})\boldsymbol{\tau} \in \mathbb{R}^n$, where $\boldsymbol{\tau} \in \mathbb{R}^m$ is the control input, $\mathbf{F}(\boldsymbol{q}) \in \mathbb{R}^{n \times m}$ is the input matrix, and m is the number of independent actuators. The system is fully actuated if $m = n$ and rank $\mathbf{F}(\boldsymbol{q}) = n$ for all $\boldsymbol{q}$. Otherwise, if $m < n$, it is underactuated.

Internal dissipative (friction) forces are of the form $-\widetilde{\mathbf{R}}(\boldsymbol{q}, \dot{\boldsymbol{q}})\dot{\boldsymbol{q}}$ with a dissipation matrix $\widetilde{\mathbf{R}}(\boldsymbol{q}, \dot{\boldsymbol{q}}) \geq \mathbf{0}_n$ [22].

2.2 LAGRANGIAN EQUATIONS OF MOTION

The Lagrangian equations for systems with the preceding properties are [25]

$$\mathbf{M}(\boldsymbol{q})\ddot{\boldsymbol{q}} + \widetilde{\mathbf{C}}(\boldsymbol{q}, \dot{\boldsymbol{q}})\dot{\boldsymbol{q}} + \frac{\partial V}{\partial \boldsymbol{q}}(\boldsymbol{q}) + \widetilde{\mathbf{R}}(\boldsymbol{q}, \dot{\boldsymbol{q}})\dot{\boldsymbol{q}} = \mathbf{F}(\boldsymbol{q})\boldsymbol{\tau}. \tag{8}$$

Denoting the k-th row and j-th column of $\mathbf{M}(\boldsymbol{q})$ and $\widetilde{\mathbf{C}}(\boldsymbol{q}, \dot{\boldsymbol{q}})$ as $m_{kj}(\boldsymbol{q})$ and $\widetilde{c}_{kj}(\boldsymbol{q}, \dot{\boldsymbol{q}})$ respectively, the matrix $\widetilde{\mathbf{C}}(\boldsymbol{q}, \dot{\boldsymbol{q}})$ is derived from the mass matrix as [39]

$$\widetilde{c}_{kj}(\boldsymbol{q}, \dot{\boldsymbol{q}}) = \sum_{\ell=1}^{n} c_{\ell jk}(\boldsymbol{q}) \dot{q}_\ell, \tag{9}$$

where

$$c_{\ell jk}(\boldsymbol{q}) = \frac{1}{2} \left(\frac{\partial m_{kj}}{\partial q_\ell}(\boldsymbol{q}) + \frac{\partial m_{k\ell}}{\partial q_j}(\boldsymbol{q}) - \frac{\partial m_{\ell j}}{\partial q_k}(\boldsymbol{q}) \right). \tag{10}$$

As a consequence of (9), (10), the matrix $\widetilde{\dot{\mathbf{M}}}(\boldsymbol{q}, \dot{\boldsymbol{q}}) = \frac{\mathrm{d}}{\mathrm{d}t}\mathbf{M}(\boldsymbol{q})$ satisfies [25]

$$\widetilde{\dot{\mathbf{M}}}(\boldsymbol{q}, \dot{\boldsymbol{q}}) = \widetilde{\mathbf{C}}(\boldsymbol{q}, \dot{\boldsymbol{q}}) + \widetilde{\mathbf{C}}^\top(\boldsymbol{q}, \dot{\boldsymbol{q}}). \tag{11}$$

The state vector of the Lagrangian model is $\widetilde{\boldsymbol{\xi}} = [\boldsymbol{q}^\top \ \dot{\boldsymbol{q}}^\top]^\top \in \mathbb{R}^{2n}$. The state change is $\frac{\mathrm{d}}{\mathrm{d}t}\widetilde{\boldsymbol{\xi}} = [\dot{\boldsymbol{q}}^\top \ \ddot{\boldsymbol{q}}^\top]^\top$, where $\ddot{\boldsymbol{q}}$ is obtained from (8), given the current state. The system output $\widetilde{\boldsymbol{y}} \in \mathbb{R}^m$ is commonly chosen as:

$$\widetilde{\boldsymbol{y}} = \mathbf{F}^\top(\boldsymbol{q})\dot{\boldsymbol{q}}. \tag{12}$$

2.3 HAMILTONIAN EQUATIONS OF MOTION

The Lagrangian equations of motion can be equivalently expressed using generalized momenta $\boldsymbol{p}(t) \in \mathbb{R}^n$ instead of using generalized velocities. The invertible transformation between momenta and velocities is given by

$$\boldsymbol{p} = \mathbf{M}(\boldsymbol{q})\dot{\boldsymbol{q}}. \tag{13}$$

Expressed in the new coordinates, the total energy (6), (7) is the Hamiltonian:

$$H(\boldsymbol{q}, \boldsymbol{p}) = \frac{1}{2}\boldsymbol{p}^\top \mathbf{M}^{-1}(\boldsymbol{q})\boldsymbol{p} + V(\boldsymbol{q}). \tag{14}$$

Likewise, the equations of motion (8) and the conjugate output (12) become [25]

$$\begin{bmatrix} \dot{\boldsymbol{q}} \\ \dot{\boldsymbol{p}} \end{bmatrix} = \begin{bmatrix} \mathbf{0}_n & \mathbf{I}_n \\ -\mathbf{I}_n & -\mathbf{R}(\boldsymbol{q}, \boldsymbol{p}) \end{bmatrix} \begin{bmatrix} \dfrac{\partial H}{\partial \boldsymbol{q}}(\boldsymbol{q}, \boldsymbol{p}) \\ \dfrac{\partial H}{\partial \boldsymbol{p}}(\boldsymbol{q}, \boldsymbol{p}) \end{bmatrix} + \begin{bmatrix} \mathbf{0}_{n\times m} \\ \mathbf{F}(\boldsymbol{q}) \end{bmatrix} \boldsymbol{\tau}, \tag{15}$$

$$\boldsymbol{y} = \mathbf{F}^\top(\boldsymbol{q}) \frac{\partial H}{\partial \boldsymbol{p}}(\boldsymbol{q}, \boldsymbol{p}). \tag{16}$$

The state vector of the Hamiltonian model is $\boldsymbol{\xi} = [\boldsymbol{q}^\top \ \boldsymbol{p}^\top]^\top \in \mathbb{R}^{2n}$.

2.4 PASSIVITY AND STABILITY

A conjugate pair of inputs $\boldsymbol{\tau}(t) \in \mathbb{R}^m$ and outputs $\boldsymbol{y}(t) \in \mathbb{R}^m$ allows a system to exchange energy with other systems or its environment. The rate at which energy flows into the system is called the supply rate, denoted $s(\boldsymbol{\tau}(t), \boldsymbol{y}(t)) \in \mathbb{R}$. During a time interval $[0, t]$, the input $\boldsymbol{\tau}(t)$ steers the state from $\boldsymbol{\xi}(0)$ to $\boldsymbol{\xi}(t)$, while changing the stored energy from $H(\boldsymbol{\xi}(0))$ to $H(\boldsymbol{\xi}(t))$. The change in the stored energy due to the supply during this time interval can be described using dissipativity.

2.4.1 *Dissipativity*

A system with a state $\boldsymbol{\xi}$, an input $\boldsymbol{\tau}$ and an output $\boldsymbol{y}$ is dissipative if there exists a storage function $S(\boldsymbol{\xi}(t)) \geq 0$ such that the dissipation inequality

$$S(\boldsymbol{\xi}(t)) - S(\boldsymbol{\xi}(0)) \leq \int_0^t s(\boldsymbol{\tau}(\sigma), \boldsymbol{y}(\sigma))\mathrm{d}\sigma \tag{17}$$

holds for all admissible controllers $\boldsymbol{\tau}(\cdot)$ that drive the state from $\boldsymbol{\xi}(0)$ to $\boldsymbol{\xi}(t)$ on the interval $[0, t]$ [18, 25]. For continuously differentiable storage functions, the dissipation inequality can be equivalently written as

$$\dot{S} \leq s(\boldsymbol{\tau}, \boldsymbol{y}). \tag{18}$$

Furthermore, if the system satisfies the dissipation inequality

$$\dot{S} \leq \boldsymbol{\tau}^\top \boldsymbol{y} - \varepsilon_{\text{in}} \boldsymbol{\tau}^\top \boldsymbol{\tau} - \varepsilon_{\text{out}} \boldsymbol{y}^\top \boldsymbol{y} \tag{19}$$

for some $\varepsilon_{\text{in}} \geq 0$ and $\varepsilon_{\text{out}} \geq 0$ then it is passive. It is input strictly passive if the condition holds for some $\varepsilon_{\text{in}} > 0$, and output strictly passive if it holds for some $\varepsilon_{\text{out}} > 0$ [40]. The system is lossless if $\dot{S} = \boldsymbol{\tau}^\top \boldsymbol{y}$.

2.4.2 *Passivity of the Lagrangian model*

The Lagrangian system (8), (12) with the storage function (6) is passive. This can be shown by evaluating (19) as

$$\begin{aligned}\frac{\mathrm{d}}{\mathrm{d}t}\widetilde{H}(\boldsymbol{q},\dot{\boldsymbol{q}}) &= \frac{1}{2}\dot{\boldsymbol{q}}^\top\widetilde{\dot{\mathbf{M}}}(\boldsymbol{q},\dot{\boldsymbol{q}})\dot{\boldsymbol{q}} + \dot{\boldsymbol{q}}^\top\mathbf{M}(\boldsymbol{q})\ddot{\boldsymbol{q}} + \dot{\boldsymbol{q}}^\top\boldsymbol{G}(\boldsymbol{q}) \\ &= \dot{\boldsymbol{q}}^\top\left(\frac{1}{2}\left(\widetilde{\mathbf{C}}(\boldsymbol{q},\dot{\boldsymbol{q}}) + \widetilde{\mathbf{C}}^\top(\boldsymbol{q},\dot{\boldsymbol{q}})\right)\dot{\boldsymbol{q}} + \mathbf{F}(\boldsymbol{q})\boldsymbol{\tau} - \widetilde{\mathbf{C}}(\boldsymbol{q},\dot{\boldsymbol{q}})\dot{\boldsymbol{q}} - \widetilde{\mathbf{R}}(\boldsymbol{q},\dot{\boldsymbol{q}})\dot{\boldsymbol{q}}\right) \\ &= \dot{\boldsymbol{q}}^\top\mathbf{F}(\boldsymbol{q})\boldsymbol{\tau} - \dot{\boldsymbol{q}}^\top\widetilde{\mathbf{R}}(\boldsymbol{q},\dot{\boldsymbol{q}})\dot{\boldsymbol{q}} \\ &\leq \boldsymbol{\tau}^\top\widetilde{\boldsymbol{y}}. \end{aligned} \tag{20}$$

The terms containing $\widetilde{\mathbf{C}}(\boldsymbol{q},\dot{\boldsymbol{q}})$ drop because $\widetilde{\mathbf{C}}(\boldsymbol{q},\dot{\boldsymbol{q}}) - \widetilde{\mathbf{C}}^\top(\boldsymbol{q},\dot{\boldsymbol{q}})$ is skew symmetric. The system is output strictly passive if $\widetilde{\mathbf{R}}(\boldsymbol{q},\dot{\boldsymbol{q}}) > 0$.

2.4.3 *Passivity of the Hamiltonian model*

The equivalent Hamiltonian system (15), (16) is naturally also passive, which can be shown similarly by evaluating (19) as:

$$\begin{aligned}\frac{\mathrm{d}}{\mathrm{d}t}H(\boldsymbol{q},\boldsymbol{p}) &= \frac{\partial^\top H}{\partial\boldsymbol{q}}(\boldsymbol{q},\boldsymbol{p})\dot{\boldsymbol{q}} + \frac{\partial^\top H}{\partial\boldsymbol{p}}(\boldsymbol{q},\boldsymbol{p})\dot{\boldsymbol{p}} \\ &= \frac{\partial^\top H}{\partial\boldsymbol{q}}(\boldsymbol{q},\boldsymbol{p})\frac{\partial^\top H}{\partial\boldsymbol{p}}(\boldsymbol{q},\boldsymbol{p}) \\ &\quad + \frac{\partial^\top H}{\partial\boldsymbol{p}}(\boldsymbol{q},\boldsymbol{p})\left(-\frac{\partial H}{\partial\boldsymbol{q}}(\boldsymbol{q},\boldsymbol{p}) - \mathbf{R}(\boldsymbol{q},\boldsymbol{p})\frac{\partial H}{\partial\boldsymbol{p}}(\boldsymbol{q},\boldsymbol{p}) + \mathbf{F}(\boldsymbol{q})\boldsymbol{\tau}\right) \\ &= -\frac{\partial^\top H}{\partial\boldsymbol{p}}(\boldsymbol{q},\boldsymbol{p})\mathbf{R}(\boldsymbol{q},\boldsymbol{p})\frac{\partial H}{\partial\boldsymbol{p}}(\boldsymbol{q},\boldsymbol{p}) + \frac{\partial^\top H}{\partial\boldsymbol{p}}(\boldsymbol{q},\boldsymbol{p})\mathbf{F}(\boldsymbol{q})\boldsymbol{\tau} \\ &\leq \boldsymbol{\tau}^\top\boldsymbol{y}. \end{aligned} \tag{21}$$

The system is output strictly passive if $\mathbf{R}(\boldsymbol{q},\boldsymbol{p}) > \mathbf{0}_n$.

2.4.4 *Stability*

This section gives a Lyapunov stability result for uncontrolled simple mechanical systems due to Lagrange and Dirichlet [25], summarized here for the Hamiltonian model for the case that the potential energy $V(\boldsymbol{q})$ is locally convex around its minimum $V(\boldsymbol{q}^\#) = \boldsymbol{0}$ for a unique $\boldsymbol{q}^\# \in \mathbb{R}^n$. This requires that

$$\frac{\partial V}{\partial\boldsymbol{q}}(\boldsymbol{q}) = \boldsymbol{0} \Leftrightarrow \boldsymbol{q} = \boldsymbol{q}^\#, \tag{22}$$

$$\frac{\partial^2 V}{\partial\boldsymbol{q}^2}(\boldsymbol{q}^\#) > \mathbf{0}_n. \tag{23}$$

Given (22), the state $(\boldsymbol{q},\boldsymbol{p}) = (\boldsymbol{q}^\#,\boldsymbol{0})$ is an equilibrium of the unforced ($\boldsymbol{\tau} = \boldsymbol{0}$) dynamics (15). It is detectable because if $\boldsymbol{\tau} \equiv \boldsymbol{0}$ and $\boldsymbol{p} \equiv \boldsymbol{0}$, then $\frac{\partial V}{\partial\boldsymbol{q}}(\boldsymbol{q}) = \boldsymbol{0}$, implying $\boldsymbol{q} = \boldsymbol{q}^\#$. Then the fixed point $(\boldsymbol{q}^\#,\boldsymbol{0})$ is Lyapunov stable [25]. To prove this, note that the point $(\boldsymbol{q}^\#,\boldsymbol{0})$ is a locally strict minimum of the storage function (14), and because the system is passive, the unforced system satisfies (17) with

$$H(\boldsymbol{q}(t),\boldsymbol{p}(t)) \leq H(\boldsymbol{q}(0),\boldsymbol{p}(0)) \quad \forall\, t \geq 0, \tag{24}$$

implying stability. If the potential energy is globally convex, the equilibrium is globally stable. If additionally $\mathbf{R}(\boldsymbol{q},\boldsymbol{p}) > \mathbf{0}_n$, the equilibrium is asymptotically

stable. This follows from (21) and the observation that only invariant set inside the set $\{(\boldsymbol{q}, \boldsymbol{p}) : \boldsymbol{p} \equiv \boldsymbol{0}\}$ is the equilibrium $(\boldsymbol{q}^{\#}, \boldsymbol{0})$ [25]. Stability of controlled systems and systems with more than one equilibrium are discussed in the next chapter.

2.5 PRACTICAL ASPECTS OF SELECTED SYSTEM MODEL

Although the presented mechanical Lagrangian model (8) and the equivalent mechanical Hamiltonian model (15) can be extended with more realistic friction models, electromechanical actuator dynamics, or phenomena such as motor backlash, we will restrict our analysis to the idealistic case of frictionless systems ($\mathbf{R}(\boldsymbol{q}, \boldsymbol{p}) = \mathbf{0}_n$), and where the control forces $\boldsymbol{\tau} \in \mathbb{R}^m$ can be chosen as desired.

It is assumed that the whole state can be used to define the feedback control law, implying that both generalized positions and velocities can be measured without noise or other measurement errors. Likewise, it is assumed that the state and control signal are measured and implemented in continuous time, without delay or discretization errors. We will briefly reconsider these simplifications and their implications for control in Section 3.7, as well as throughout this thesis by giving references to solutions that address some of these phenomena.

3

PASSIVITY-BASED CONTROL BY INTERCONNECTION AND DAMPING ASSIGNMENT (IDA-PBC)

Passivity-based control (PBC) is a form of nonlinear control that relies on passivity properties to systematically derive asymptotically stabilizing control laws for systems with a known model or model structure. The control goal is achieved by energy shaping instead of assigning a fully-prescribed set of dynamics, in order to exploit rather than destroy the internal dynamics of the original system, thereby reducing the need for high-gain feedback while increasing robustness [1].

Various types of PBC control strategies exist, where the main classification pertains to whether the control signal is determined by a static feedback law or generated by a dynamical system [41]. Among the different state feedback variants, the most general form is known as passivity-based control by interconnection and damping assignment (IDA-PBC) as introduced in [27], which has been successfully used to control various underactuated mechanical systems [42].

Sections 3.1–3.5 review IDA-PBC in the context of simple mechanical systems, when the control objective is tracking of a known, constant setpoint $\boldsymbol{q}^* \in \mathbb{R}^n$. Anticipating the application to networks of mechanical systems, we propose a partitioning of the generalized coordinates of a single agent into coordinates that must be stabilized internally and coordinates that must be cooperatively controlled with other systems. A generic class of IDA-PBC solutions is identified that stabilizes such systems at fixed setpoints, and several classes of systems that have a solution of this form are described in Section 3.6. Finally, Section 3.7 considers the practical applicability of the IDA-PBC method along with several shortcomings.

Related nonlinear control techniques beyond the scope of this thesis are control by interconnection [41], immersion and invariance [43, 44], partial contraction [45, 46], and backstepping [47]. The relation between PBC and the method of controlled Lagrangians is briefly discussed in Section 3.8.

3.1 ENERGY SHAPING FOR SETPOINT TRACKING

Because the open-loop equilibrium $\boldsymbol{q}^\#$ generally differs from the desired setpoint $\boldsymbol{q}^*$, the IDA-PBC method uses state feedback to shape the dynamics and the energy function of the system such that the energy attains a minimum at the desired setpoint, while inserting damping to settle at this setpoint asymptotically.

It is assumed that the open-loop system is frictionless, such that its dynamics are described by

$$\begin{bmatrix} \dot{\boldsymbol{q}} \\ \dot{\boldsymbol{p}} \end{bmatrix} = \begin{bmatrix} \mathbf{0}_n & \mathbf{I}_n \\ -\mathbf{I}_n & \mathbf{0}_n \end{bmatrix} \begin{bmatrix} \dfrac{\partial H}{\partial \boldsymbol{q}} \\ \dfrac{\partial H}{\partial \boldsymbol{p}} \end{bmatrix} + \begin{bmatrix} \mathbf{0}_{n\times m} \\ \mathbf{F} \end{bmatrix} \boldsymbol{\tau}, \tag{25}$$

$$\boldsymbol{y} = \mathbf{F}^\top \frac{\partial H}{\partial \boldsymbol{p}} = \mathbf{F}^\top \mathbf{M}^{-1} \boldsymbol{p}, \tag{26}$$

$$H = \frac{1}{2} \boldsymbol{p}^\top \mathbf{M}^{-1} \boldsymbol{p} + V. \tag{27}$$

This model is equivalent to (15) with the dissipation matrix selected as $\mathbf{R} = \mathbf{0}_n$.

3.1.1 *Desired closed-loop dynamics*

The state feedback law has the form [41]

$$\boldsymbol{\tau} = \boldsymbol{\beta} + \boldsymbol{\tau}_{\mathrm{d}}, \tag{28}$$

where $\boldsymbol{\beta}(\boldsymbol{q}, \boldsymbol{p})$ is the state feedback to be designed and $\boldsymbol{\tau}_{\mathrm{d}}$ is a new input to the resulting closed-loop system.

The control objective is to design $\boldsymbol{\beta}(\boldsymbol{q}, \boldsymbol{p})$ such that the dynamics (25)–(27) attain the desired ("d") closed-loop dynamics given by [28, 41]

$$\begin{bmatrix} \dot{\boldsymbol{q}} \\ \dot{\boldsymbol{p}} \end{bmatrix} = \begin{bmatrix} \mathbf{0}_n & \mathbf{M}^{-1}\mathbf{M}_{\mathrm{d}} \\ -\mathbf{M}_{\mathrm{d}}\mathbf{M}^{-1} & \mathbf{J} - \mathbf{F}\mathbf{K}_v\mathbf{F}^\top \end{bmatrix} \begin{bmatrix} \dfrac{\partial H_{\mathrm{d}}}{\partial \boldsymbol{q}} \\ \dfrac{\partial H_{\mathrm{d}}}{\partial \boldsymbol{p}} \end{bmatrix} + \begin{bmatrix} \mathbf{0}_{n\times m} \\ \mathbf{F} \end{bmatrix} \boldsymbol{\tau}_{\mathrm{d}}, \tag{29}$$

$$\boldsymbol{y}_{\mathrm{d}} = \mathbf{F}^\top \frac{\partial H_{\mathrm{d}}}{\partial \boldsymbol{p}} = \mathbf{F}^\top \mathbf{M}_{\mathrm{d}}^{-1} \boldsymbol{p}, \tag{30}$$

$$H_{\mathrm{d}} = \frac{1}{2} \boldsymbol{p}^\top \mathbf{M}_{\mathrm{d}}^{-1} \boldsymbol{p} + V_{\mathrm{d}}, \tag{31}$$

where $\mathbf{K}_v = \mathbf{K}_v^\top > \mathbf{0}_m$ is the desired dissipation matrix and $\mathbf{J} = -\mathbf{J}^\top \in \mathbb{R}^{n\times n}$ is a free skew-symmetric matrix. The matrix $\mathbf{J}$ does not instantaneously affect stability but it can be chosen freely both to help solve the IDA-PBC problem in the underactuated case and to shape the transient response [28][1].

The desired dynamics and its energy function $H_{\mathrm{d}}(\boldsymbol{q}, \boldsymbol{p})$ are defined in the original coordinates $(\boldsymbol{q}, \boldsymbol{p})$ but with a desired mass matrix $\mathbf{0}_n < \mathbf{M}_{\mathrm{d}}(\boldsymbol{q}) < \alpha \mathbf{I}_n$, $\alpha > 0$ and a desired potential energy function $V_{\mathrm{d}}(\boldsymbol{q})$ which is selected to be minimal at the setpoint $\boldsymbol{q}^*$:

$$\boldsymbol{q}^* = \arg\min_{\boldsymbol{q}} V_{\mathrm{d}}(\boldsymbol{q}). \tag{32}$$

By choosing $V_{\mathrm{d}}(\boldsymbol{q}) \geq 0$ without loss of generality, we may equivalently write

$$V_{\mathrm{d}}(\boldsymbol{q}^*) = 0. \tag{33}$$

Because V_{d} is minimal at $\boldsymbol{q}^*$ we also have

$$\left. \frac{\partial V_{\mathrm{d}}}{\partial \boldsymbol{q}} \right|_{\boldsymbol{q}=\boldsymbol{q}^*} = \boldsymbol{0}. \tag{34}$$

More generally, there may be a continuum of equally desired equilibria rather than a distinct one. The equilibrium set is defined as

$$\boldsymbol{q}^* \in \mathcal{Q}^* \quad \text{with} \quad \mathcal{Q}^* = \{\boldsymbol{q} \mid V_{\mathrm{d}}(\boldsymbol{q}) = 0\}, \tag{35}$$

where each equilibrium point $\boldsymbol{q}^* \in \mathcal{Q}^*$ satisfies the minimality conditions (32), (33). The control objective is then to reach any equilibrium in this set.

If it is possible to obtain the desired closed-loop dynamics (29)–(31), with the previously mentioned minimality properties of the desired potential energy, the asymptotic stability analysis of the desired setpoint $(\boldsymbol{q}, \boldsymbol{p}) = (\boldsymbol{q}^*, \boldsymbol{0})$ can be carried out as in [28].

We review this stability analysis for the cases where V_{d} has a minimum for a unique configuration $\boldsymbol{q}^*$ in Section 3.1.3, and for a range of configurations $\boldsymbol{q}^* \in \mathcal{Q}^*$ in Section 3.1.4. In both cases, the equilibrium and passivity properties of the following subsection apply.

1 The matrix $\mathbf{J}$ is historically referred to as $\mathbf{J}_2$, to distinguish it from another matrix with a similar role not used in this thesis. We omit the subscript "2" to avoid confusion with other subscripts in subsequent chapters.

3.1.2 *Equilibria and passivity properties*

The point $(\boldsymbol{q}^*, \boldsymbol{0})$ is an equilibrium of (29), because $\boldsymbol{p} \equiv \boldsymbol{0}$ and $\boldsymbol{\tau}_\mathrm{d} \equiv \boldsymbol{0}$ implies that $\dot{\boldsymbol{q}} = \boldsymbol{0}$ and likewise

$$\begin{aligned}\dot{\boldsymbol{p}} &= -\mathbf{M}_\mathrm{d}\mathbf{M}^{-1}\left.\frac{\partial H_\mathrm{d}}{\partial \boldsymbol{q}}\right|_{(\boldsymbol{q}^*,\boldsymbol{0})} + \mathbf{J}\frac{\partial H_\mathrm{d}}{\partial \boldsymbol{p}} - \mathbf{F}\mathbf{K}_v\mathbf{F}^\top\frac{\partial H_\mathrm{d}}{\partial \boldsymbol{p}} \\ &= -\mathbf{M}_\mathrm{d}\mathbf{M}^{-1}\left.\frac{\partial V_\mathrm{d}}{\partial \boldsymbol{q}}\right|_{\boldsymbol{q}^*} + \mathbf{J}\mathbf{M}_\mathrm{d}^{-1}\boldsymbol{p} - \mathbf{F}\mathbf{K}_v\mathbf{F}^\top\mathbf{M}_\mathrm{d}^{-1}\boldsymbol{p} = \boldsymbol{0}. \end{aligned} \tag{36}$$

Passivity of the desired closed-loop system is demonstrated using the shaped energy (31) as a storage function and computing its time derivative as

$$\begin{aligned}\dot{H}_\mathrm{d} &= \begin{bmatrix}\frac{\partial^\top H_\mathrm{d}}{\partial \boldsymbol{q}} & \frac{\partial^\top H_\mathrm{d}}{\partial \boldsymbol{p}}\end{bmatrix}\begin{bmatrix}\mathbf{0}_n & \mathbf{M}^{-1}\mathbf{M}_\mathrm{d} \\ -\mathbf{M}_\mathrm{d}\mathbf{M}^{-1} & \mathbf{J} - \mathbf{F}\mathbf{K}_v\mathbf{F}^\top\end{bmatrix}\begin{bmatrix}\frac{\partial H_\mathrm{d}}{\partial \boldsymbol{q}} \\ \frac{\partial H_\mathrm{d}}{\partial \boldsymbol{p}}\end{bmatrix} + \frac{\partial^\top H_\mathrm{d}}{\partial \boldsymbol{p}}\mathbf{F}\boldsymbol{\tau}_\mathrm{d} \\ &= -\frac{\partial^\top H_\mathrm{d}}{\partial \boldsymbol{p}}\mathbf{F}\mathbf{K}_v\mathbf{F}^\top\frac{\partial H_\mathrm{d}}{\partial \boldsymbol{p}} + \frac{\partial^\top H_\mathrm{d}}{\partial \boldsymbol{p}}\mathbf{F}\boldsymbol{\tau}_\mathrm{d} \\ &= -\boldsymbol{y}_\mathrm{d}^\top\mathbf{K}_v\boldsymbol{y}_\mathrm{d} + \boldsymbol{y}_\mathrm{d}^\top\boldsymbol{\tau}_\mathrm{d}. \end{aligned} \tag{37}$$

Because $\mathbf{K}_v > 0$, the system is output strictly passive. For the externally unforced closed loop, where $\boldsymbol{\tau}_\mathrm{d} = \boldsymbol{0}$, we further have

$$\begin{aligned}\dot{H}_\mathrm{d} &= -\boldsymbol{y}_\mathrm{d}^\top\mathbf{K}_v\boldsymbol{y}_\mathrm{d} \\ &= -\boldsymbol{p}^\top\mathbf{M}_\mathrm{d}^{-1}\mathbf{F}\mathbf{K}_v\mathbf{F}^\top\mathbf{M}_\mathrm{d}^{-1}\boldsymbol{p} \leq 0 \\ &= -\lambda_{\min}(\mathbf{K}_v)||\mathbf{F}^\top\mathbf{M}_\mathrm{d}^{-1}\boldsymbol{p}||^2 \leq 0, \end{aligned} \tag{38}$$

where $\lambda_{\min}(\mathbf{K}_v)$ is the minimum eigenvalue of $\mathbf{K}_v$ [28].

3.1.3 *Stability of a unique equilibrium*

If an equilibrium $\boldsymbol{q}^*$ is (locally) a strict minimum of $V_\mathrm{d}(\cdot)$, that is if (locally)

$$V_\mathrm{d}(\boldsymbol{q}) > V_\mathrm{d}(\boldsymbol{q}^*) = 0 \quad \forall \quad \boldsymbol{q} \neq \boldsymbol{q}^*, \tag{39}$$

then the problem is equivalent to [28], in which it is proven that the setpoint $(\boldsymbol{q}^*, \boldsymbol{0})$ is asymptotically stable if it is (locally) detectable from the output $\boldsymbol{y}_\mathrm{d}$.

A summary of the argument is as follows. The continuously differentiable storage function H_d (31) is a positive definite function in a neighborhood of $(\boldsymbol{q}^*, \boldsymbol{0})$. Hence there exists a bounded level set $\Omega_c = \{(\boldsymbol{q}, \boldsymbol{p}) \in \mathbb{R}^{2n} \mid H_\mathrm{d} \leq c\}$ for sufficiently small $c > 0$ [48]. From (38), $\dot{H}_\mathrm{d} \leq 0$ everywhere including in Ω_c. Defining the set $\mathcal{S}$ at which the storage function is stationary as

$$\begin{aligned}\mathcal{S} &= \{(\boldsymbol{q}, \boldsymbol{p}) \in \mathbb{R}^{2n} \mid \dot{H}_\mathrm{d} = 0\} \\ &= \{(\boldsymbol{q}, \boldsymbol{p}) \in \mathbb{R}^{2n} \mid \mathbf{F}^\top\mathbf{M}_\mathrm{d}^{-1}\boldsymbol{p} = \boldsymbol{0}\}, \end{aligned} \tag{40}$$

then under the detectability assumption, no solution can stay in $\mathcal{S}$ other than $\mathcal{M} = \{(\boldsymbol{q}, \boldsymbol{p}) \in \mathbb{R}^{2n} \mid \boldsymbol{p} = \boldsymbol{0},\ \boldsymbol{q} = \boldsymbol{q}^*\}$, because for $\boldsymbol{p} = \boldsymbol{0}$ we have from (29) that

$$\dot{\boldsymbol{p}} = -\mathbf{M}_\mathrm{d}\mathbf{M}^{-1}\frac{\partial V_\mathrm{d}}{\partial \boldsymbol{q}} \neq \boldsymbol{0} \tag{41}$$

if there are no local minima or saddle points for which $\frac{\partial V_\mathrm{d}}{\partial \boldsymbol{q}} = \boldsymbol{0}$ outside $\mathcal{M}$. With $\mathcal{M} \subset \mathcal{S} \subset \Omega_c$, asymptotic stability of the equilibrium $(\boldsymbol{q}^*, \boldsymbol{0})$ then follows from Barbashin's theorem as a corollary of LaSalle's theorem [28, 39, 48].

3.1.4 *Stability of a continuum of desired equilibria*

If there is a continuum of configurations $\boldsymbol{q}^* \in \mathcal{Q}^*$ for which $V_\mathrm{d}(\boldsymbol{q}^*) = 0$, the function V_d is not positive definite and Barbashin's theorem ceases to apply [48]. The energy function H_d in (31) and its time derivative (37) are unchanged, but the set $\boldsymbol{\Omega}_c$ is not bounded in general, which means that the conditions for applying LaSalle's theorem also no longer hold.

For the controlled mechanical systems under consideration, this implies that for those coordinates within $\boldsymbol{q}$ that are free within $\mathcal{Q}^*$ (in which they have equally desired values), we do not prove that they become stationary. For example, for an inverted pendulum-cart system one may choose a V_d that equals zero if the pendulum is upright regardless of the cart position, if the cart position is not of interest in the application. Then the level set $\boldsymbol{\Omega}_c$ is unbounded due to the free cart translation. However, because $\mathbf{K}_v > \mathbf{0}_m$, the system does come to standstill due to the enforced dissipation (38); that is, the trajectories may be bounded due to dissipation. This conjecture is supported by several simulations in Part V.

Another approach to such a problem is to reduce the configuration space by eliminating the coordinate that is not of interest (the cart position in this example), such that the objective for the remaining coordinates is again to attain a unique equilibrium. However, it is often not trivial to obtain such coordinate transformation, and the dynamics may lose the simple structure (29), complicating the stability analysis further. Likewise, in light of the subsequent analysis of networks of mechanical systems, we wish to maintain the structure of the coordinates and the dynamics.

3.1.5 *Semistability*

It may also be possible to analyze this problem in the original coordinates using semistability [49]. An equilibrium is semistable if it is Lyapunov stable and trajectories starting near it converge to a Lyapunov stable point, not necessarily the same one (see Section 4.7 in [49] for a mathematically precise definition). A system is semistable if every equilibrium point is semistable.

The hypothesized application of semistability to this problem is as follows. Define the set $\mathcal{S}$ identically as in (40). For the continuum of equilibria (35), no solution can stay in $\mathcal{S}$ other than $\mathcal{M}_\mathcal{Q} = \{(\boldsymbol{q}, \boldsymbol{p}) \in \mathbb{R}^{2n} \mid \boldsymbol{p} = \boldsymbol{0},\ \boldsymbol{q} = \boldsymbol{q}^* \in \mathcal{Q}^*\}$, under the detectability assumption. Because (38) holds, it may be possible to show that the system (29) is semistable [49] so that we have $\lim_{t\to\infty}(\boldsymbol{q}, \boldsymbol{p}) \in \mathcal{M}_\mathcal{Q}$, achieving the control objective.

3.2 DERIVATION OF THE CONTROL LAW AND MATCHING CONDITIONS

The problem of obtaining the desired stable closed-loop dynamics from the open-loop system amounts to finding the state feedback $\boldsymbol{\beta}(\boldsymbol{q}, \boldsymbol{p})$ that makes (29) and (25) equal. This sections develops the necessary conditions that make this possible, along with an explicit expression for $\boldsymbol{\beta}(\boldsymbol{q}, \boldsymbol{p})$, following the summary given in [28].

Setting the right hand sides of (25) and (29) equal and inserting (28) gives

$$\frac{\partial H}{\partial \boldsymbol{p}} = \mathbf{M}^{-1}\mathbf{M}_\mathrm{d}\frac{\partial H_\mathrm{d}}{\partial \boldsymbol{p}}, \tag{42}$$

and

$$-\frac{\partial H}{\partial \boldsymbol{q}} + \mathbf{F}\boldsymbol{\beta} = -\mathbf{M}_\mathrm{d}\mathbf{M}^{-1}\frac{\partial H_\mathrm{d}}{\partial \boldsymbol{q}} + \mathbf{J}\frac{\partial H_\mathrm{d}}{\partial \boldsymbol{p}} - \mathbf{F}\mathbf{K}_v\mathbf{F}^\top\frac{\partial H_\mathrm{d}}{\partial \boldsymbol{p}}. \tag{43}$$

Equation (42) is automatically satisfied since $\frac{\partial H}{\partial \boldsymbol{p}} = \mathbf{M}^{-1}\boldsymbol{p}$ and likewise

$$\mathbf{M}^{-1}\mathbf{M}_\mathrm{d}\frac{\partial H_\mathrm{d}}{\partial \boldsymbol{p}} = \mathbf{M}^{-1}\mathbf{M}_\mathrm{d}\mathbf{M}_\mathrm{d}^{-1}\boldsymbol{p} = \mathbf{M}^{-1}\boldsymbol{p}. \tag{44}$$

Equation (43) must be satisfied by a suitable choice for the static feedback expression $\boldsymbol{\beta}$, if it exists.

Define a full rank left annihilator of $\mathbf{F}$, denoted $\mathbf{F}^\perp = \mathbf{F}^\perp(\boldsymbol{q}) \in \mathbb{R}^{(n-m)\times n}$ such that $\mathbf{F}^\perp\mathbf{F} = \mathbf{0}_{(n-m)\times m}$ and the matrix $[(\mathbf{F}^\perp)^\top\ \mathbf{F}]^\top \in \mathbb{R}^{n\times n}$ is full rank [28]. Multiplying both sides of (43) with this matrix gives

$$\begin{bmatrix}\mathbf{F}^\perp\\ \mathbf{F}^\top\end{bmatrix}\mathbf{F}\boldsymbol{\beta} = \begin{bmatrix}\mathbf{F}^\perp\\ \mathbf{F}^\top\end{bmatrix}\left(\frac{\partial H}{\partial \boldsymbol{q}} - \mathbf{M}_\mathrm{d}\mathbf{M}^{-1}\frac{\partial H_\mathrm{d}}{\partial \boldsymbol{q}} + \mathbf{J}\frac{\partial H_\mathrm{d}}{\partial \boldsymbol{p}} - \mathbf{F}\mathbf{K}_v\mathbf{F}^\top\frac{\partial H_\mathrm{d}}{\partial \boldsymbol{p}}\right). \tag{45}$$

Since $\mathbf{F}^\perp\mathbf{F}\boldsymbol{\beta} = \boldsymbol{0}$, the first $n-m$ rows of (45) must satisfy

$$\mathbf{F}^\perp\left(\frac{\partial H}{\partial \boldsymbol{q}} - \mathbf{M}_\mathrm{d}\mathbf{M}^{-1}\frac{\partial H_\mathrm{d}}{\partial \boldsymbol{q}} + \mathbf{J}\frac{\partial H_\mathrm{d}}{\partial \boldsymbol{p}} - \mathbf{F}\mathbf{K}_v\mathbf{F}^\top\frac{\partial H_\mathrm{d}}{\partial \boldsymbol{p}}\right) = \boldsymbol{0}. \tag{46}$$

This so-called matching condition can be written more explicitly by expanding the energy functions H and H_d into their kinetic and potential energies, giving

$$\begin{aligned}\mathbf{F}^\perp\left(\frac{1}{2}\frac{\partial\left(\boldsymbol{p}^\top\mathbf{M}^{-1}\boldsymbol{p}\right)}{\partial \boldsymbol{q}} - \frac{1}{2}\mathbf{M}_\mathrm{d}\mathbf{M}^{-1}\frac{\partial\left(\boldsymbol{p}^\top\mathbf{M}_\mathrm{d}^{-1}\boldsymbol{p}\right)}{\partial \boldsymbol{q}} + \mathbf{J}\mathbf{M}_\mathrm{d}^{-1}\boldsymbol{p}\right)\\ + \mathbf{F}^\perp\left(\frac{\partial V}{\partial \boldsymbol{q}} - \mathbf{M}_\mathrm{d}\mathbf{M}^{-1}\frac{\partial V_\mathrm{d}}{\partial \boldsymbol{q}}\right) = \boldsymbol{0}.\end{aligned} \tag{47}$$

The last m rows of (45) yield the expression for $\boldsymbol{\beta}$ because $\mathbf{F}^\top\mathbf{F}$ is full rank:

$$\boldsymbol{\beta} = \left(\mathbf{F}^\top\mathbf{F}\right)^{-1}\mathbf{F}^\top\left(\frac{\partial H}{\partial \boldsymbol{q}} - \mathbf{M}_\mathrm{d}\mathbf{M}^{-1}\frac{\partial H_\mathrm{d}}{\partial \boldsymbol{q}} + \mathbf{J}\frac{\partial H_\mathrm{d}}{\partial \boldsymbol{p}} - \mathbf{F}\mathbf{K}_v\mathbf{F}^\top\frac{\partial H_\mathrm{d}}{\partial \boldsymbol{p}}\right). \tag{48}$$

3.2.1 *The control law*

Substituting (48) and (30) in (28) gives the IDA-PBC control law:

$$\boldsymbol{\tau} = \left(\mathbf{F}^\top\mathbf{F}\right)^{-1}\mathbf{F}^\top\left(\frac{\partial H}{\partial \boldsymbol{q}} - \mathbf{M}_\mathrm{d}\mathbf{M}^{-1}\frac{\partial H_\mathrm{d}}{\partial \boldsymbol{q}} + \mathbf{J}\mathbf{M}_\mathrm{d}^{-1}\boldsymbol{p}\right) - \mathbf{K}_v\boldsymbol{y}_\mathrm{d} + \boldsymbol{\tau}_\mathrm{d}. \tag{49}$$

3.2.2 *The matching equations*

The control law (49) yields the desired closed-loop dynamics (29) if and only if condition (46) is satisfied. This condition is satisfied if the kinetic energy matching equation

$$\mathbf{F}^\perp\left(\frac{\partial\left(\boldsymbol{p}^\top\mathbf{M}^{-1}\boldsymbol{p}\right)}{\partial \boldsymbol{q}} - \mathbf{M}_\mathrm{d}\mathbf{M}^{-1}\frac{\partial\left(\boldsymbol{p}^\top\mathbf{M}_\mathrm{d}^{-1}\boldsymbol{p}\right)}{\partial \boldsymbol{q}} + 2\mathbf{J}\mathbf{M}_\mathrm{d}^{-1}\boldsymbol{p}\right) = \boldsymbol{0}. \tag{50}$$

and the potential energy matching equation

$$\mathbf{F}^\perp\left(\frac{\partial V}{\partial \boldsymbol{q}} - \mathbf{M}_\mathrm{d}\mathbf{M}^{-1}\frac{\partial V_\mathrm{d}}{\partial \boldsymbol{q}}\right) = \boldsymbol{0}. \tag{51}$$

both hold. Solving (50), (51) by choosing appropriate $\mathbf{M}_\mathrm{d}$, V_d, and $\mathbf{J}$ is known as the matching problem. The next sections discuss how this problem can be addressed in the fully-actuated and underactuated case.

3.3 COOPERATIVE AND LOCAL GOALS

When a system works cooperatively in a network, it has two non-conflicting control objectives, each pertaining to a subset of its generalized coordinates, partitioned as $\boldsymbol{q} = (\boldsymbol{x}, \boldsymbol{\theta}) \in \mathbb{R}^n$. The coordinates $\boldsymbol{x} \in \mathbb{R}^\ell$ are to be controlled in cooperation with other agents in the network, while $\boldsymbol{\theta} \in \mathbb{R}^{n-\ell}$ are controlled by each agent individually. Before considering a network of systems, this chapter shows how these separate control goals appear in the single-agent IDA-PBC problem, in which the goal is to reach the setpoint $\boldsymbol{q}^* = (\boldsymbol{x}^*, \boldsymbol{\theta}^*)$, for prescribed values $\boldsymbol{x}^*$ and $\boldsymbol{\theta}^*$

For example, consider the systems in Figure 1 consisting of two point masses m_1 and m_2 located at $q_1 \in \mathbb{R}$ and $q_2 \in \mathbb{R}$, respectively, interconnected by a linear spring with stiffness k. The system in Figure 1a is fully-actuated using the control forces τ_1 and τ_2. The system in Figure 1b is underactuated because only τ_2 is available, resembling a single-link flexible-joint robot without gravity.

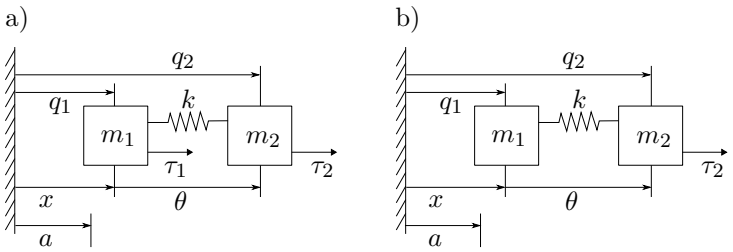

Figure 1: A fully-actuated system (a) and an underactuated system (b).

Suppose that in both cases the control goal is to stabilize both q_1 and q_2 at a prescribed setpoint $a \in \mathbb{R}$. This goal can be equivalently expressed in the coordinates $x = q_1$ and $\theta = q_2 - q_1$, in which case the goal is to reach the setpoints $x^* = a$ and $\theta^* = 0$. A candidate desired potential V_d is

$$V_\mathrm{d}(\boldsymbol{q}) = \frac{1}{2}P_1(x-a)^2 + \frac{1}{2}P_2 k\theta^2 = \frac{1}{2}P_1(q_1-a)^2 + \frac{1}{2}P_2 k(q_2-q_1)^2, \tag{52}$$

where P_1 and P_2 are positive constants. This potential is positive definite and minimal at $x = a$ and $\theta = 0$. Further details for this example will be given in Chapter 12, which considers the case for a multi-link flexible-joint robot.

Whereas in this example it is easy to express the whole equations of motion directly in new coordinates $\tilde{\boldsymbol{q}} = [x \;\; \theta]^\top$, doing so is not necessary. Avoiding the change of coordinates, except for expressing the potential energy V_d, considerably simplifies (or even enables) the analysis of more complicated systems.

3.4 SOLUTIONS FOR THE FULLY-ACTUATED CASE

For the fully actuated case, $\mathbf{F}$ is square and full rank, and the condition (43) immediately yields the control law (49) without having to satisfy any matching condition. In fact, one may assume $\mathbf{F} = \mathbf{I}_n$ without loss of generality. (Otherwise, one could take the system (25)–(27) and use the new signals $\boldsymbol{\tau}_\mathrm{new}$ and $\boldsymbol{y}_\mathrm{new}$ with the transformations $\boldsymbol{\tau} = \mathbf{F}^{-1}\boldsymbol{\tau}_\mathrm{new}$ and $\boldsymbol{y} = \mathbf{F}^\top \boldsymbol{y}_\mathrm{new}$.) With $\mathbf{F} = \mathbf{I}_n$ the control law becomes

$$\boldsymbol{\tau} = \frac{\partial H}{\partial \boldsymbol{q}} - \mathbf{M}_\mathrm{d}\mathbf{M}^{-1}\frac{\partial H_\mathrm{d}}{\partial \boldsymbol{q}} + (\mathbf{J} - \mathbf{K}_v)\,\boldsymbol{y}_\mathrm{d} + \boldsymbol{\tau}_\mathrm{d}. \tag{53}$$

Because the problem is not constrained by matching conditions, the matrices $\mathbf{M}_\mathrm{d}$ and $\mathbf{J}$ only play a role in shaping the transient response, but they can be chosen as $\mathbf{M}_\mathrm{d} = \mathbf{M}$ and $\mathbf{J} = \mathbf{0}_n$ in principle. Doing so leaves the kinetic energy and the

output unchanged ($\boldsymbol{y}_\mathrm{d} = \boldsymbol{y}$), resulting in only potential energy shaping, using the control law

$$\boldsymbol{\tau} = \frac{\partial V}{\partial \boldsymbol{q}} - \frac{\partial V_\mathrm{d}}{\partial \boldsymbol{q}} - \mathbf{K}_v \boldsymbol{y} + \boldsymbol{\tau}_\mathrm{d}. \tag{54}$$

In the example of robotic manipulators, this is equivalent to gravity compensation ($\frac{\partial V}{\partial \boldsymbol{q}}$), proportional control ($-\frac{\partial V_\mathrm{d}}{\partial \boldsymbol{q}}$ with V_d quadratic in $\boldsymbol{q} - \boldsymbol{q}^*$) and damping insertion (using $-\mathbf{K}_v \boldsymbol{y} = -\mathbf{K}_v \dot{\boldsymbol{q}}$) [21].

3.5 SOLUTIONS FOR SELECTED UNDERACTUATED SYSTEMS

Whereas stabilization of the setpoint $\boldsymbol{q}^*$ of an underactuated system primarily requires a suitable choice of V_d to satisfy the minimality condition (32), it is usually also necessary to shape the kinetic energy through $\mathbf{M}_\mathrm{d}$ in order to ensure that the potential energy matching condition (51) has a solution. In turn, kinetic energy shaping may require the assignment of gyroscopic forces through $\mathbf{J}$ to satisfy the kinetic energy matching condition (50). The entangled process of choosing $\mathbf{M}_\mathrm{d}$, V_d, and $\mathbf{J}$ is a nontrivial task, which has spurred numerous research endeavors aiming to find constructive solutions for special types of simple mechanical systems.

3.5.1 *Solution strategies*

The survey [42] states the IDA-PBC problem for systems more general than mechanical systems, and proposes several strategies to simplify the IDA-PBC problem by fixing some degrees of freedom and solving for the remaining terms, if possible.

The results [28, 50] give constructive solutions for systems where only one degree of freedom is unactuated, also known as underactuation-degree one systems. The method in [51] simplifies the matching problem through a change of coordinates and the method in [52] allows the matching conditions to be shaped by the control action to make them solvable. The paper [53] proposes a method to circumvent the problem of solving the partial differential equations for mechanical systems by not requiring that the closed-loop energy function is of the form (29) while [54] avoids solving them by using a dynamic rather than a static controller. The reader is referred to the recent survey [26] for a historic overview of IDA-PBC along with a summary of developments as of 2017.

3.5.2 *Structure of the desired potential energy*

Among the (classes of) systems that can be controlled by IDA-PBC, we are interested in identifying those solutions and system properties that we can exploit to make systems cooperatively control the variable $\boldsymbol{x}$ with other agents in a network while locally stabilizing the coordinates $\boldsymbol{\theta}$.

In some existing IDA-PBC solutions, the objectives to reach $\boldsymbol{x}^*$ and $\boldsymbol{\theta}^*$ can be alternatively represented using a new coordinate $\boldsymbol{z}(\boldsymbol{q}) = \boldsymbol{z}(\boldsymbol{x}, \boldsymbol{\theta}) \in \mathbb{R}^\ell$, chosen such that achieving $\boldsymbol{\theta} = \boldsymbol{\theta}^*$ and $\boldsymbol{z} = \boldsymbol{z}^*$ also implies that $\boldsymbol{x} = \boldsymbol{x}^*$. An appropriate choice of $\boldsymbol{z}$ ensures that the control signal to stabilize $\boldsymbol{z}$ does not violate the matching conditions, which is useful for expressing interaction forces between agents in the network later on. More precisely, we are interested in existing IDA-PBC solutions in which the desired potential energy can be written as

$$V_\mathrm{d}(\boldsymbol{q}) = V_\mathrm{s}(\boldsymbol{q}) + V_\mathrm{c}(\boldsymbol{z}(\boldsymbol{q})), \tag{55}$$

where $\boldsymbol{z}(\boldsymbol{q}) \in \mathbb{R}^\ell$, $\ell \leq m$, and V_c is free in $\boldsymbol{z}$ as long as V_d remains positive definite around the setpoint $\boldsymbol{q}^*$. The term V_s stabilizes the coordinates $\boldsymbol{\theta}$ to their fixed

setpoint $\boldsymbol{\theta}^*$, while V_c stabilizes the cooperative coordinates at the setpoint $\boldsymbol{x}^*$ by steering $\boldsymbol{z}$ to $\boldsymbol{z}^*$, provided V_s and V_c satisfy the matching conditions derived below.

The gradient of $V_\mathrm{d}(\boldsymbol{q})$, which appears in both the control law and the matching conditions, is given by

$$\frac{\partial V_\mathrm{d}}{\partial \boldsymbol{q}} = \frac{\partial V_\mathrm{s}}{\partial \boldsymbol{q}} + \boldsymbol{\Psi}\frac{\partial V_\mathrm{c}}{\partial \boldsymbol{z}}, \tag{56}$$

where $\frac{\partial V_\mathrm{c}}{\partial \boldsymbol{z}}$ depends only on $\boldsymbol{z}$ and $\boldsymbol{\Psi}$ depends only on $\boldsymbol{q}$ (see Appendix a.3.1):

$$\boldsymbol{\Psi}(\boldsymbol{q}) = \begin{bmatrix} \frac{\partial z_1}{\partial \boldsymbol{q}} & \cdots & \frac{\partial z_\ell}{\partial \boldsymbol{q}} \end{bmatrix} = \begin{bmatrix} \frac{\partial z_1}{\partial q_1} & \cdots & \frac{\partial z_\ell}{\partial q_1} \\ \vdots & & \vdots \\ \frac{\partial z_1}{\partial q_n} & \cdots & \frac{\partial z_\ell}{\partial q_n} \end{bmatrix} \in \mathbb{R}^{n\times\ell}. \tag{57}$$

Suppose now that $V_\mathrm{s}(\boldsymbol{q})$ in (55) satisfies

$$\mathbf{F}^\perp\left(\frac{\partial V}{\partial \boldsymbol{q}} - \mathbf{M}_\mathrm{d}\mathbf{M}^{-1}\frac{\partial V_\mathrm{s}}{\partial \boldsymbol{q}}\right) = \boldsymbol{0}, \tag{58}$$

for a given desired mass matrix $\mathbf{M}_\mathrm{d}$ compatible with the kinetic energy matching condition (50). In order to satisfy the potential energy matching condition (51) when $V_\mathrm{c}(\cdot)$ in (55) is free, we must additionally require that

$$\mathbf{F}^\perp\mathbf{M}_\mathrm{d}\mathbf{M}^{-1}\boldsymbol{\Psi} = \mathbf{0}_{(n-m)\times\ell}. \tag{59}$$

Although requiring (58), (59) to hold is more conservative than requiring (51) to hold, it ensures that $V_\mathrm{c}(\cdot)$ is free in $\boldsymbol{z}$, crucial in our solution of the distributed IDA-PBC problem. Classes of IDA-PBC solutions with the partitioning (55)–(59) that satisfy the conditions (58), (59) are given in Section 3.6.

In summary, for the proposed class of systems with the parametrized potential energy (55), the matching problem (50), (51) is solved if (50) is solved by a suitable $\mathbf{M}_\mathrm{d}$ and $\mathbf{J}$, and the parametrized potential energy matching equations (58), (59) are solved by suitable V_s and $\boldsymbol{\Psi}$. Furthermore, if the total desired potential energy (55) is positive definite and minimal at the setpoint, then the single-agent IDA-PBC problem is solved. Furthermore, this system class satisfies the conditions for stable cooperation in a network, as will be derived in subsequent chapters.

3.5.3 *Splitting the control law*

By substituting the proposed parametrization of the desired potential energy (55) into the control law (49), we obtain

$$\begin{aligned}\boldsymbol{\tau} &= \left(\mathbf{F}^\top\mathbf{F}\right)^{-1}\mathbf{F}^\top\left(\frac{\partial H}{\partial \boldsymbol{q}} + \mathbf{J}\mathbf{M}_\mathrm{d}^{-1}\boldsymbol{p} - \frac{1}{2}\mathbf{M}_\mathrm{d}\mathbf{M}^{-1}\frac{\partial \boldsymbol{p}^\top\mathbf{M}_\mathrm{d}^{-1}\boldsymbol{p}}{\partial \boldsymbol{q}} - \mathbf{M}_\mathrm{d}\mathbf{M}^{-1}\frac{\partial V_\mathrm{s}}{\partial \boldsymbol{q}}\right) \\ &\quad - \left(\mathbf{F}^\top\mathbf{F}\right)^{-1}\mathbf{F}^\top\mathbf{M}_\mathrm{d}\mathbf{M}^{-1}\boldsymbol{\Psi}\frac{\partial V_\mathrm{c}}{\partial \boldsymbol{z}} - \mathbf{K}_v\boldsymbol{y}_\mathrm{d} + \boldsymbol{\tau}_\mathrm{d} \\ &= \boldsymbol{\sigma} - \boldsymbol{\Phi}\frac{\partial V_\mathrm{c}}{\partial \boldsymbol{z}} - \mathbf{K}_v\boldsymbol{y}_\mathrm{d} + \boldsymbol{\tau}_\mathrm{d},\end{aligned} \tag{60}$$

where

$$\boldsymbol{\sigma}(\boldsymbol{q},\boldsymbol{p}) = \left(\mathbf{F}^\top\mathbf{F}\right)^{-1}\mathbf{F}^\top\left(\frac{\partial H}{\partial \boldsymbol{q}} + \mathbf{J}\mathbf{M}_\mathrm{d}^{-1}\boldsymbol{p} - \mathbf{M}_\mathrm{d}\mathbf{M}^{-1}\frac{\partial(\frac{1}{2}\boldsymbol{p}^\top\mathbf{M}_\mathrm{d}^{-1}\boldsymbol{p} + V_\mathrm{s})}{\partial \boldsymbol{q}}\right) \tag{61}$$

shapes the kinetic energy and the potential energy component for internal stabilization, equivalent to single-agent IDA-PBC control except for the control force to track $\boldsymbol{x}^*$, and

$$\boldsymbol{\Phi}(\boldsymbol{q}) = \left(\mathbf{F}^\top \mathbf{F}\right)^{-1} \mathbf{F}^\top \mathbf{M}_\mathrm{d} \mathbf{M}^{-1} \boldsymbol{\Psi} \in \mathbb{R}^{m \times \ell} \tag{62}$$

is an input matrix that ensures that the control force $\frac{\partial V_\mathrm{c}}{\partial \boldsymbol{z}}$ that steers $\boldsymbol{z}$ to $\boldsymbol{z}^*$ (and $\boldsymbol{x}$ to $\boldsymbol{x}^*$) does not violate the matching conditions.

3.5.4 *Generality of the desired potential energy structure*

Although beyond the scope of this thesis, it would be useful to investigate the generality and limitations of the proposed structure (55) and the separation of the potential energy matching condition (51) into the internal stabilization condition (58) and the tracking condition (59). A counterexample indicating conservativeness of this approach would be an IDA-PBC solution that allows internal stabilization at a fixed $\boldsymbol{\theta}^*$ and tracking of a free target $\boldsymbol{x}^*$ without the explicit separation of the potential energy and matching conditions. A control by interconnection interpretation of the proposed coordinate partitioning is given in Section 9.3, which supports the generality of the approach based on the properties of $\boldsymbol{z}$ and its time derivative.

As in [55], it is possible to use one combined matching condition instead of separate kinetic and potential energy matching conditions (50), (51). Such an approach can be followed here as well, where one could leave (50) and (58) combined, keeping only the cooperation condition (59) separate. This amounts to combining the goals to reach $\boldsymbol{\theta}^*$ and to stabilize $\boldsymbol{p}$ at zero into a single objective, while tracking $\boldsymbol{x}^*$ is the second objective. In this work we maintain the three separate conditions (50), (58), (59) to emphasize how previously derived single-agent IDA-PBC solutions can be used in our distributed control framework.

3.6 IDA-PBC SOLUTIONS SATISFYING CONDITIONS FOR COOPERATION

In this section we discuss three generic classes of systems with the potential energy (55) that satisfy the previously given conditions (50), (58), (59) to solve the single-agent IDA-PBC problem and allow systems to cooperate in a network.

3.6.1 *Solutions for fully-actuated systems*

Although Section 3.4 provides a straight-forward solution to the IDA-PBC problem for fully-actuated systems, it is useful to consider how the partitioning of the setpoint $\boldsymbol{q}^* = (\boldsymbol{x}^*, \boldsymbol{\theta}^*)$ and the variable $\boldsymbol{z}(\boldsymbol{q})$ appears in the control law (60)–(62) in order to let a fully-actuated system control part or all of its coordinates cooperatively with other agents, which may be underactuated.

Choosing the desired potential energy V_d as in (55), and recalling that for fully-actuated systems we can use $\mathbf{F} = \mathbf{I}_n$, $\mathbf{M}_\mathrm{d} = \mathbf{M}$, $\mathbf{J} = \mathbf{0}_n$, the internal control signal (61) becomes

$$\boldsymbol{\sigma}(\boldsymbol{q}, \boldsymbol{p}) = \frac{\partial V}{\partial \boldsymbol{q}} - \frac{\partial V_\mathrm{s}}{\partial \boldsymbol{q}}, \tag{63}$$

such that the total control law (60) becomes

$$\boldsymbol{\tau} = \frac{\partial V}{\partial \boldsymbol{q}} - \frac{\partial V_\mathrm{s}}{\partial \boldsymbol{q}} - \boldsymbol{\Phi} \frac{\partial V_\mathrm{c}}{\partial \boldsymbol{z}} - \mathbf{K}_v \boldsymbol{y}_\mathrm{d} + \boldsymbol{\tau}_\mathrm{d}. \tag{64}$$

This is a sum of forces, respectively representing: gravity compensation, stabilization of the internal coordinate $\boldsymbol{\theta}$, stabilization of the cooperative coordinates $\boldsymbol{x}$, damping, and a new external control input $\boldsymbol{\tau}_{\mathrm{d}}$. Notice that we could have obtained the same result directly from (54) by substituting V_{d} as in (55).

In some applications, it is sufficient to steer $\boldsymbol{z}$ to $\boldsymbol{z}^*$, without imposing specific requirements on $\boldsymbol{\theta}$ and $\boldsymbol{x}$ other than that they are stationary. Consider the problem of controlling the end-effector of a fully-actuated robotic manipulator. In this example $\boldsymbol{q} \in \mathbb{R}^n$ are the joint angles while $\boldsymbol{z}(\boldsymbol{q}) \in \mathbb{R}^\ell$, is the end-effector position and orientation. For example, $\ell = 3$ for position control in euclidean space. From the definitions (57), (62) we obtain for the fully-actuated system

$$\boldsymbol{\Phi} = \boldsymbol{\Psi} = \begin{bmatrix} \dfrac{\partial z_1}{\partial \boldsymbol{q}} & \cdots & \dfrac{\partial z_\ell}{\partial \boldsymbol{q}} \end{bmatrix} = \mathbf{A}^\top, \tag{65}$$

where $\mathbf{A}(\boldsymbol{q})$ is the Jacobian of the forward kinematics. When choosing a quadratic potential $V_{\mathrm{c}} = \frac{1}{2}(\boldsymbol{z} - \boldsymbol{z}^*)^\top \mathbf{K}_p (\boldsymbol{z} - \boldsymbol{z}^*)$ for a gain $\mathbf{K}_p > \mathbf{0}_\ell$, the single-agent control law (64) becomes

$$\boldsymbol{\tau} = \frac{\partial V}{\partial \boldsymbol{q}} + \mathbf{A}^\top \mathbf{K}_p (\boldsymbol{z}^* - \boldsymbol{z}) - \mathbf{K}_v \boldsymbol{y}_{\mathrm{d}}, \tag{66}$$

which is known as Jacobian-transpose control [56] with gravity compensation and damping insertion. In a redundant robotic arm ($n = m > \ell$), there is a multitude of equilibria for which the end-effector is at the desired location, such that the stability problem can be carried out as in Section 3.1.4, where we require a full rank assumption of $\mathbf{A}(\boldsymbol{q})$ to ensure that there are no undesired equilibria away from the goal in the invariant set.

3.6.2 *Solutions for a class of underactuation degree one*

This section summarizes the IDA-PBC solution provided in [28] for a class of mechanical systems (25)–(27) with underactuation degree one: $m = n - 1$. The input matrix $\mathbf{F}(q_n)$ is assumed to be a function of at most one coordinate, which we take to be q_n for notational convenience. Additionally, the mass matrix $\mathbf{M}$ must not depend on the unactuated coordinate. If the original system does not satisfy this property, a partial feedback linearization can sometimes transform the dynamics into the desired form. We refer the reader to [28] for several other technical assumptions.

In [28], the control goal is to stabilize q_n at a fixed setpoint determined by the system dynamics, while stabilizing $q_1, \ldots, q_m$ at a setpoint that can be freely chosen. In our work, we let the first $\ell \leq m$ coordinates be cooperatively controlled in the network, while stabilizing $q_{\ell+1}, \ldots, q_m$ at an arbitrary desired setpoint, and stabilizing q_n at the fixed setpoint imposed by the system. In the notation of this chapter we have

$$\boldsymbol{q} = \begin{bmatrix} \boldsymbol{x} \\ \boldsymbol{\theta} \end{bmatrix} \quad \text{with} \quad \boldsymbol{x} = \begin{bmatrix} q_1 \\ \vdots \\ q_\ell \end{bmatrix}, \quad \boldsymbol{\theta} = \begin{bmatrix} q_{\ell+1} \\ \vdots \\ q_m \\ \vdots \\ q_n \end{bmatrix}. \tag{67}$$

The ordering of the coordinates is chosen for notational convenience and can be obtained by reordering the coordinates of the original system is necessary.

For systems that satisfy the necessary technical assumptions, [28] derives a constructive procedure to find a desired mass matrix $\mathbf{M}_{\mathrm{d}}(q_n)$ which guarantees the

existence of a $\mathbf{J}(\boldsymbol{q},\boldsymbol{p})$ that solves the kinetic energy matching condition. The desired mass is defined by

$$\mathbf{M}_{\mathrm{d}}(q_n) = \int_{q_n^*}^{q_n} \mathbf{F}(q_n)\boldsymbol{\Xi}(q_n)\mathbf{F}^\top(q_n) + \mathbf{M}_{\mathrm{d}}^0, \tag{68}$$

where $q_n^* = \theta^* \in \mathbb{R}$ is the fixed setpoint of q_n determined by the system equilibrium. The matrices $\mathbf{M}_{\mathrm{d}}^0 > \mathbf{0}_n$ and $\boldsymbol{\Xi}(q_n) = \boldsymbol{\Xi}^\top(q_n) \in \mathbb{R}^{m\times m}$ are free. Once $\mathbf{M}_{\mathrm{d}}$ is obtained, the matrix $\mathbf{J}$ that solves the kinetic energy matching condition (50) can be obtained algebraically as detailed in [28].

The desired mass matrix (68) ensures the existence of a V_{d} of the form (55):

$$V_{\mathrm{d}}(\boldsymbol{q}) = V_{\mathrm{s}}(\boldsymbol{q}) + V_{\mathrm{c}}(z(\boldsymbol{q})), \tag{69}$$

$$\boldsymbol{z}(\boldsymbol{q}) = \begin{bmatrix} a_1(\boldsymbol{q}) \\ \vdots \\ a_\ell(\boldsymbol{q}) \end{bmatrix}. \tag{70}$$

The coordinate transformations $a_j(\boldsymbol{q})$, $j = 1,\dots,m$ are adopted from [28] as

$$a_j = q_j - \int_0^{q_n} \frac{\gamma_j(\mu)}{\gamma_n(\mu)}\mathrm{d}\mu, \tag{71}$$

$$\boldsymbol{\gamma}(q_n) = \begin{bmatrix} \gamma_1 \\ \vdots \\ \gamma_n \end{bmatrix} = \mathbf{M}^{-1}\mathbf{M}_{\mathrm{d}} \left(\mathbf{F}^\perp\right)^\top. \tag{72}$$

and the internal stabilization potential V_{s} is adapted from [28] as

$$V_{\mathrm{s}}(\boldsymbol{q}) = \int_0^{q_n} \frac{b(\mu)}{\gamma_n(\mu)}\mathrm{d}\mu + \phi(a_{\ell+1}(\boldsymbol{q}),\dots,a_m(\boldsymbol{q})), \tag{73}$$

in which ϕ is a free function and

$$b(q_n) = \mathbf{F}^\perp \frac{\partial V}{\partial \boldsymbol{q}}. \tag{74}$$

We now show that the internal stabilization potential satisfies the condition (58). First, the partial derivatives of the coordinate transformations a_j are given by

$$\frac{\partial a_j}{\partial q_i} = \frac{\partial q_j}{\partial q_i} - \frac{\partial}{\partial q_i}\int_0^{q_n} \frac{\gamma_j(\mu)}{\gamma_n(\mu)}\mathrm{d}\mu. \tag{75}$$

Next, noting that the integral in (73) depends only on q_n, the derivative of V_{s} is

$$\begin{aligned} \frac{\partial V_{\mathrm{s}}}{\partial \boldsymbol{q}} &= \begin{bmatrix} 0 \\ \vdots \\ 0 \\ \dfrac{b}{\gamma_n} \end{bmatrix} + \begin{bmatrix} \dfrac{\partial a_{\ell+1}}{\partial q_1} & \cdots & \dfrac{\partial a_m}{\partial q_1} \\ \vdots & & \vdots \\ \dfrac{\partial a_{\ell+1}}{\partial q_n} & \cdots & \dfrac{\partial a_m}{\partial q_n} \end{bmatrix} \begin{bmatrix} \dfrac{\partial \phi}{\partial a_{\ell+1}} \\ \dfrac{\partial \phi}{\partial a_m} \end{bmatrix} \\ &= \begin{bmatrix} 0 \\ \vdots \\ 0 \\ \dfrac{b}{\gamma_n} \end{bmatrix} + \begin{bmatrix} \boldsymbol{e}_{\ell+1} - \dfrac{\gamma_{\ell+1}}{\gamma_n}\boldsymbol{e}_n & \cdots & \boldsymbol{e}_m - \dfrac{\gamma_m}{\gamma_n}\boldsymbol{e}_n \end{bmatrix} \begin{bmatrix} \dfrac{\partial \phi}{\partial a_{\ell+1}} \\ \dfrac{\partial \phi}{\partial a_m} \end{bmatrix}, \end{aligned} \tag{76}$$

where $\boldsymbol{e}_k$ are n-dimensional vectors with zeros except their k-th entry equals 1. Finally, left-multiplication with $\boldsymbol{\gamma}$ gives

$$\boldsymbol{\gamma}^\top \frac{\partial V_\mathrm{s}}{\partial \boldsymbol{q}} = b + \begin{bmatrix} \gamma_{\ell+1} - \frac{\gamma_{\ell+1}}{\gamma_n}\gamma_n & \cdots & \gamma_m - \frac{\gamma_m}{\gamma_n}\gamma_n \end{bmatrix} \begin{bmatrix} \frac{\partial \phi}{\partial a_{\ell+1}} \\ \\ \frac{\partial \phi}{\partial a_m} \end{bmatrix} = b.$$

An assumption $\gamma_n(q_n^*) \neq 0$ is imposed to ensure that the above step is well-defined in a neighborhood of the setpoint q_n^*. Another assumption $\gamma_n(q_n^*)\frac{\mathrm{d}b}{\mathrm{d}q_n}(q_n^*) > 0$ is imposed to ensure positive definiteness of the integral in (73). Substituting the result into (58) provides matching, since:

$$\mathbf{F}^\perp \left(\frac{\partial V}{\partial \boldsymbol{q}} - \mathbf{M}_\mathrm{d}\mathbf{M}^{-1} \frac{\partial V_\mathrm{s}}{\partial \boldsymbol{q}} \right) = b - \boldsymbol{\gamma}^\top \frac{\partial V_\mathrm{s}}{\partial \boldsymbol{q}} = b - b = 0. \tag{77}$$

The process to show that the matching condition (59) is similar. First, we compute the matrix $\boldsymbol{\Psi} \in \mathbb{R}^{n \times \ell}$ (57) where $z_j = a_j$ for $j = 1, \ldots, \ell$:

$$\boldsymbol{\Psi}(\boldsymbol{q}) = \begin{bmatrix} \frac{\partial a_1}{\partial q_1} & \cdots & \frac{\partial a_\ell}{\partial q_1} \\ \vdots & & \vdots \\ \frac{\partial a_1}{\partial q_n} & \cdots & \frac{\partial a_\ell}{\partial q_n} \end{bmatrix} = \begin{bmatrix} \boldsymbol{e}_1 - \frac{\gamma_1}{\gamma_n}\boldsymbol{e}_n & \cdots & \boldsymbol{e}_\ell - \frac{\gamma_\ell}{\gamma_n}\boldsymbol{e}_n \end{bmatrix}. \tag{78}$$

The result can be substituted into (59) to obtain

$$\begin{aligned} \mathbf{F}^\perp \mathbf{M}_\mathrm{d}\mathbf{M}^{-1}\boldsymbol{\Psi} &= \boldsymbol{\gamma}^\top \boldsymbol{\Psi} \\ &= \begin{bmatrix} \gamma_1 - \frac{\gamma_1}{\gamma_n}\gamma_n & \cdots & \gamma_\ell - \frac{\gamma_\ell}{\gamma_n}\gamma_n \end{bmatrix} \\ &= \mathbf{0}_{(n-m)\times \ell}. \end{aligned} \tag{79}$$

Hence, the matching conditions and the condition for cooperation (50), (58), (59) are satisfied for the discussed class of systems.

For the single-agent problem, the free function $V_\mathrm{c}(\boldsymbol{z}(\boldsymbol{q})) = V_\mathrm{c}(a_1(\boldsymbol{q}), \ldots, a_\ell(\boldsymbol{q}))$ in (69) and the free function $\phi(a_{\ell+1}(\boldsymbol{q}), \ldots, a_m(\boldsymbol{q}))$ in (73) play a similar role, both in terms of shaping the total energy V_d and in the matching problem; they are one and the same free function in [28]. In our case, the distinction between stabilizing the internal coordinates and the cooperative coordinates is needed for cooperation between underactuated systems which may have the same ℓ but different m or n.

In the special case that $\ell = m$, when all controllable coordinates are designated as cooperative coordinates, the preceding results become more similar to [28]: there is only one free function V_c, and V_s reduces to only the integral term in (73).

3.6.3 *Solutions for systems with flexible couplings*

We now consider a class of mechanical systems with $n = 2m$ coordinates, partitioned as $\boldsymbol{q} = [\boldsymbol{\alpha}^\top \ \boldsymbol{\delta}^\top]^\top$, where the coordinates of interest $\boldsymbol{\alpha} \in \mathbb{R}^m$ are unactuated while the coordinates $\boldsymbol{\delta} \in \mathbb{R}^m$ are actuated. The coordinates $\boldsymbol{\alpha}$ are indirectly driven by potential forces as a function of the differences $\boldsymbol{\delta} - \boldsymbol{\alpha}$. This class includes compliant mechanisms such as flexible-joint robots.

Here we consider systems with the Hamiltonian equations of motion (25) where

$$\boldsymbol{q} = \begin{bmatrix} \boldsymbol{\alpha} \\ \boldsymbol{\delta} \end{bmatrix}, \quad \mathbf{M} = \begin{bmatrix} \mathbf{M}_\alpha & \mathbf{0}_m \\ \mathbf{0}_m & \mathbf{M}_\delta \end{bmatrix}, \quad \mathbf{F} = \begin{bmatrix} \mathbf{0}_m \\ \mathbf{I}_m \end{bmatrix}, \quad V(\boldsymbol{\delta} - \boldsymbol{\alpha}), \tag{80}$$

where the matrices $\mathbf{M}_\alpha(\boldsymbol{\alpha})$ and $\mathbf{M}_\delta(\boldsymbol{\delta})$ are functions of $\boldsymbol{\alpha}$ and $\boldsymbol{\delta}$, respectively, and potential energy function satisfies $V(\boldsymbol{\delta}-\boldsymbol{\alpha}) \geq 0$, $V(\boldsymbol{0}) = 0$.

We propose a generic single-agent IDA-PBC solution of the form

$$\mathbf{M}_\mathrm{d} = \begin{bmatrix} c\mathbf{M}_\alpha & \mathbf{0}_m \\ \mathbf{0}_m & \mathbf{M}_{\delta,\mathrm{d}} \end{bmatrix}, \quad V_\mathrm{s} = \frac{1}{c}V,$$
$$\mathbf{J} = \mathbf{0}_n, \quad \mathbf{K}_v > \mathbf{0}_m, \quad \mathbf{F}^\perp = \begin{bmatrix} \mathbf{I}_m & \mathbf{0}_m \end{bmatrix}, \tag{81}$$

with the constant $c > 0$, and a desired mass matrix $\mathbf{M}_{\delta,d}$. The variable to be internally stabilized is $\boldsymbol{\theta} = \boldsymbol{\delta} - \boldsymbol{\alpha}$ with $\boldsymbol{\theta}^* = \boldsymbol{0}$. The cooperative variable is chosen as a function of $\boldsymbol{\delta}$ only, which gives

$$\boldsymbol{z}(\boldsymbol{q}) = \boldsymbol{z}(\boldsymbol{\delta}) \in \mathbb{R}^\ell, \quad \boldsymbol{\Psi} = \begin{bmatrix} \frac{\partial z_1}{\partial \boldsymbol{\alpha}} \cdots \frac{\partial z_\ell}{\partial \boldsymbol{\alpha}} \\ \frac{\partial z_1}{\partial \boldsymbol{\delta}} \cdots \frac{\partial z_\ell}{\partial \boldsymbol{\delta}} \end{bmatrix} = \begin{bmatrix} \mathbf{0}_{m\times\ell} \\ \boldsymbol{\Psi}_\delta \end{bmatrix}. \tag{82}$$

Although expressing this variable in terms of $\boldsymbol{\delta}$ can seem restrictive, note that $\boldsymbol{\delta}$ and $\boldsymbol{\alpha}$ converge to each other as $\boldsymbol{\theta}$ converges to $\boldsymbol{0}$. Consequently, $\boldsymbol{z}(\boldsymbol{\alpha})$ asymptotically approaches $\boldsymbol{z}(\boldsymbol{\delta})$, and a control goal $\boldsymbol{z}^*$ can hence be specified as $\boldsymbol{z}^*(\boldsymbol{\alpha}^*)$.

To see that the proposed solution satisfies the matching conditions for cooperation, we write the kinetic energy condition (50) as

$$\begin{bmatrix} \mathbf{I}_m & \mathbf{0}_m \end{bmatrix} \left(\begin{bmatrix} \frac{\partial\left(\boldsymbol{p}^\top \mathbf{M}_\alpha^{-1}\boldsymbol{p}\right)}{\partial \boldsymbol{\alpha}} \\ \frac{\partial\left(\boldsymbol{p}^\top \mathbf{M}_\delta^{-1}\boldsymbol{p}\right)}{\partial \boldsymbol{\delta}} \end{bmatrix} - \begin{bmatrix} c\mathbf{M}_\alpha\mathbf{M}_\alpha^{-1} & \mathbf{0}_m \\ \mathbf{0}_m & \mathbf{M}_{\delta,\mathrm{d}}\mathbf{M}_\delta^{-1} \end{bmatrix} \begin{bmatrix} \frac{1}{c}\frac{\partial\left(\boldsymbol{p}^\top \mathbf{M}_\alpha^{-1}\boldsymbol{p}\right)}{\partial \boldsymbol{\alpha}} \\ \frac{\partial\left(\boldsymbol{p}^\top \mathbf{M}_{\delta,d}^{-1}\boldsymbol{p}\right)}{\partial \boldsymbol{\delta}} \end{bmatrix} \right) = \boldsymbol{0}. \tag{83}$$

Likewise, the stabilization potential energy matching condition (58) gives

$$\begin{aligned} \mathbf{F}^\perp &\left(\frac{\partial V}{\partial \boldsymbol{q}} - \mathbf{M}_\mathrm{d}\mathbf{M}^{-1}\frac{\partial V_\mathrm{s}}{\partial \boldsymbol{q}} \right) \\ &= \begin{bmatrix} \mathbf{I}_m & \mathbf{0}_m \end{bmatrix} \left(\begin{bmatrix} \frac{\partial V}{\partial \boldsymbol{\alpha}} \\ \frac{\partial V}{\partial \boldsymbol{\delta}} \end{bmatrix} - \begin{bmatrix} c\mathbf{M}_\alpha\mathbf{M}_\alpha^{-1} & \mathbf{0}_m \\ \mathbf{0}_m & \mathbf{M}_{\delta,\mathrm{d}}\mathbf{M}_\delta^{-1} \end{bmatrix} \begin{bmatrix} \frac{1}{c}\frac{\partial V}{\partial \boldsymbol{\alpha}} \\ \frac{1}{c}\frac{\partial V}{\partial \boldsymbol{\delta}} \end{bmatrix} \right) \\ &= \frac{\partial V}{\partial \boldsymbol{\alpha}} - \begin{bmatrix} \mathbf{I}_m & \mathbf{0}_m \end{bmatrix} \begin{bmatrix} \frac{\partial V}{\partial \boldsymbol{\alpha}} \\ \frac{1}{c}\mathbf{M}_{\delta,\mathrm{d}}\mathbf{M}_\delta^{-1}\frac{\partial V}{\partial \boldsymbol{\delta}} \end{bmatrix} = \boldsymbol{0}. \end{aligned} \tag{84}$$

Finally, the condition for cooperation (59) is

$$\mathbf{F}^\perp\mathbf{M}_\mathrm{d}\mathbf{M}^{-1}\boldsymbol{\Psi} = \begin{bmatrix} \mathbf{I}_m & \mathbf{0}_m \end{bmatrix} \begin{bmatrix} c\mathbf{M}_\alpha\mathbf{M}_\alpha^{-1} & \mathbf{0}_m \\ \mathbf{0}_m & \mathbf{M}_{\delta,\mathrm{d}}\mathbf{M}_\delta^{-1} \end{bmatrix} \begin{bmatrix} \mathbf{0}_{m\times\ell} \\ \boldsymbol{\Psi}_\delta \end{bmatrix} = \mathbf{0}_{m\times\ell}, \tag{85}$$

which holds independently of $\boldsymbol{\Psi}_\delta$ and hence independently of the structure of $\boldsymbol{z}(\boldsymbol{\delta})$.

An example application for a flexible-joint robot will be given in Chapter 12.

3.7 PRACTICAL ASPECTS OF IDA-PBC

Throughout this thesis and in many IDA-PBC results, friction is assumed to be negligible. Several starting points for including friction models, along with a successful experimental demonstration of IDA-PBC, are given in [57] for an inverted

pendulum-cart model. It is shown that unknown linear friction in the actuated coordinates can be embedded in the desired dynamics in a similar fashion as the damping matrix $\mathbf{K}_v$, leading to additional damping which only strengthens the stability result. Friction compensation techniques can be used to offset some of the effects of coulomb friction in these coordinates. For friction in the unactuated coordinates however, it leads to an additional dissipation matching condition that must hold in order to obtain the desired dynamics. This is not always restrictive, because friction in the unactuated coordinate is sometimes very small precisely because there are no actuators, as is the case in the pendulum-cart example or the UAV example discussed later in this thesis.

Furthermore, our focus is on single-agent IDA-PBC solutions that provide tracking of a fixed setpoint. It will be shown that these solutions are sufficient for our intended cooperative control procedure, but a more generic application could also consider tracking time-varying references. This is addressed for classes of Hamiltonian systems in [58]. Another practical extension is to apply IDA-PBC without the availability of velocity measurements, as addressed in [28]. See also the recent survey [26] for recent developments on robustness and observers for perturbed systems.

3.8 RELATION TO CONTROLLED LAGRANGIANS

An alternative approach for designing controllers for underactuated mechanical systems is the method of controlled Lagrangians, introduced in [33, 34]. Although derived from different geometric principles, the method of controlled Lagrangians can be seen as a special case of IDA-PBC. A treatment and comparison of both methods in a consistent formulation is given in [35]. Similarly, although the geometric methods can offer mathematical and physical insight when solving the design problem, the controlled Lagrangians method suffers from the same difficulties in solving the partial differential equations of the matching conditions (50), (51).

The method of controlled Lagrangians and IDA-PBC have been almost simultaneously developed around the year 2000, which has led to some novelty disputes between the associated research groups. Some comments from the point of view of the IDA-PBC research groups can be found in [26, 28]. We will readdress the relation with this method for networks of underactuated systems in Chapter 8.

Part II

MODELING AND CONTROL OF DISTRIBUTED SYSTEMS

This part presents modeling and control techniques for networks of the simple mechanical systems studied in the previous part. Chapter 4 begins by introducing energy-based network modeling concepts along with standard tools such as graph theory, and defines control objectives that can be pursued by a group of agents. Chapter 5 shows how these techniques have been used in literature to devise distributed control strategies for groups of fully-actuated mechanical systems.

4 MODELING NETWORKS OF MECHANICAL SYSTEMS

High-level, application-specific control objectives of distributed systems can be decomposed into generic types of group behaviors such as synchronization or assuming formations [2, 12]. This chapter describes modeling techniques and mathematical tools to analyze distributed systems that pursue such group behaviors.

Section 4.1 begins by introducing concepts from graph theory to mathematically specify the role of each agent in the network and the information exchange between them. Group control objectives are defined in Section 4.2. Section 4.3 describes how the deviation from the group objectives can be compactly described by a quadratic error function, which will be used several times throughout this thesis.

4.1 INFORMATION EXCHANGE ON GRAPHS

Distributed systems (also called networks) consisting of information-exchanging agents (also called systems) can be described using graphs. This section reviews the concepts of graph theory needed to describe several existing and new energy-based distributed control strategies.

Each agent i has the dynamics (25), with the generalized coordinates $\boldsymbol{q}_i \in \mathbb{R}^{n_i}$, the generalized momenta $\boldsymbol{p}_i \in \mathbb{R}^{n_i}$, the input $\boldsymbol{\tau}_i \in \mathbb{R}^{m_i}$, and the output $\boldsymbol{y}_i \in \mathbb{R}^{m_i}$. The dimensions n_i and $m_i \leq n_i$ may be different for each agent.

4.1.1 *Modeling communication on graphs*

This subsection is based on [12]. A graph represents a group of N systems as a set of vertices $\mathcal{V} = \{i, \ldots, N\}$, and it represents their interconnections by a set of edges $\mathcal{E} \subset \mathcal{V} \times \mathcal{V}$. An edge is an ordered pair of distinct vertices. The edge (i, j) is outgoing from vertex i and incoming on vertex j, as represented by an arrow pointing from i to j. The existence of an edge implies communication from one agent to another; the arrow designates the direction of information flow.

If the edges (i, j) and (j, i) both exist, the information exchange between agents i and j is bidirectional and the edge is undirected (as opposed to directed). Bidirectional information flows are designated using an arrow with two heads, as shown in Figure 2. All edges in this thesis are undirected unless specified otherwise.

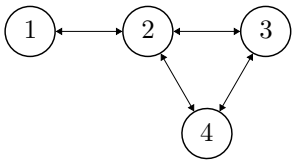

Figure 2: A connected undirected graph of four agents

The existence of an undirected edge between agent i and j implies that i is a neighbor of j and that j is a neighbor of i. A path is a sequence of edges of the form (i, k), (k, j), $\ldots$, (z, y), (y, a). A graph is connected if there is a path between every distinct pair of vertices. It is fully connected if there is an edge between every distinct pair of vertices.

4.1.2 *Information exchange*

In order to achieve a group objective collaboratively, agents exchange information with their neighbors in the form of a vector quantity $\boldsymbol{z}_i \in \mathbb{R}^\ell$. The information exchange implies that agent i knows its own $\boldsymbol{z}_i$ as well as the quantities $\boldsymbol{z}_j \in \mathbb{R}^\ell$ from its neighbors j. Agent i may obtain these quantities from explicit wireless messages from the neighbors j, or by sensing the quantities $\boldsymbol{z}_j$ through other equipment. In some of the presented results in this thesis, it is sufficient for agent i to know only the relative quantities $\boldsymbol{z}_j - \boldsymbol{z}_i$ for all neighbors j.

The vector quantity $\boldsymbol{z}_i \in \mathbb{R}^\ell$ is the transformed coordinate $\boldsymbol{z}_i(\boldsymbol{q}_i) \in \mathbb{R}^\ell$ introduced in Chapter 3. This generalizes many solutions from literature where $\boldsymbol{z}_i(\cdot)$ is the identity map ($\boldsymbol{z}_i = \boldsymbol{q}_i$). In some of the presented results, a second objective is to be achieved collaboratively, and agents use a second graph to exchange the vector quantity $\boldsymbol{y}_i \in \mathbb{R}^\ell$. This graph has the same vertices $\mathcal{V}$ but may have different edges $\mathcal{E}$, such that agent i may have different neighbors k on this graph.

In this thesis we assume the quantities $\boldsymbol{z}_j$ and $\boldsymbol{y}_k$ to be available to agent i at all times, without delay, without quantization errors, noise, changes in network topology, or other discrepancies.

4.2 GENERALIZED LOCAL AND GROUP CONTROL OBJECTIVES

Unlike in the previous chapter, where a single agent had to steer $\boldsymbol{z}_i$ towards a known target $\boldsymbol{z}_i^*$, the agents now exchange the information $\boldsymbol{z}_i$ to achieve a common goal. This section formalizes the local group objectives which a distributed system can pursue in this thesis, expressed in terms of the variables $\boldsymbol{q}_i = (\boldsymbol{x}_i, \boldsymbol{\theta}_i) \in \mathbb{R}^{n_i}$ and $\boldsymbol{z}_i \in \mathbb{R}^\ell$,introduced in the previous chapter.

4.2.1 *Stabilization*

As before, we restrict the control objective to stationary solutions, which means that we require $\boldsymbol{p}_i$ to reach zero asymptotically for all agents:

$$\lim_{t\to\infty} ||\boldsymbol{p}_i(t)|| = 0 \quad \forall\, i = 1, \ldots, N. \tag{86}$$

Likewise, each agent must stabilize the coordinates $\boldsymbol{\theta}_i \in \mathbb{R}^{n_i-\ell}$ at a target $\boldsymbol{\theta}_i^*$, independently of any interactions with other agents, which requires that

$$\lim_{t\to\infty} ||\boldsymbol{\theta}_i(t) - \boldsymbol{\theta}_i^*|| = 0 \quad \forall\, i = 1, \ldots, N. \tag{87}$$

4.2.2 *Leaderless formations*

The most general group objective discussed in this thesis is the creation of a formation between all agents, expressed in the variables $\boldsymbol{z}_i \in \mathbb{R}^\ell$, as shown in Figure 3 for the planar case ($\ell = 2$) when the communication graph corresponds to Figure 2.

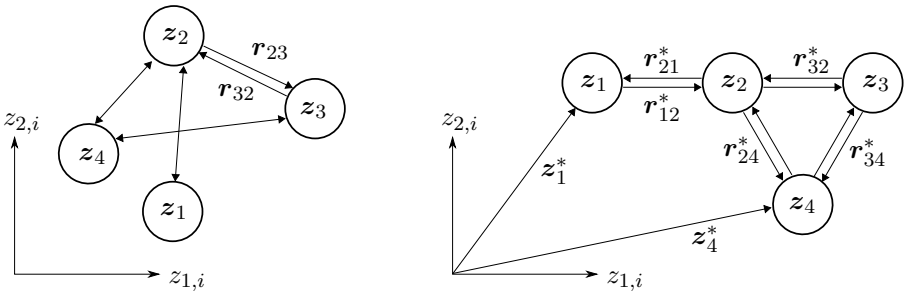

Figure 3: Initial configuration (left) and target formation with two leaders (right).

Initially at an arbitrary state, the communicated variables are at a relative configuration $\boldsymbol{r}_{ij}(t) = \boldsymbol{z}_j(t) - \boldsymbol{z}_i(t)$ that changes in time as a function of the system dynamics. A formation objective specifies the desired inter-agent configurations $\boldsymbol{r}^*_{ij} = -\boldsymbol{r}^*_{ji} \in \mathbb{R}^\ell$ for all neighboring agents. Specifically, the objective is

$$\lim_{t\to\infty} ||\boldsymbol{z}_i(t) - \boldsymbol{z}_j(t) + \boldsymbol{r}^*_{ij}|| = 0 \quad \forall\ (i,j) \in \mathcal{E}. \tag{88}$$

We require the graph to be connected, implying that between every two distinct agents a and e there is a fixed desired configuration $\boldsymbol{r}^*_{ae} = \boldsymbol{r}^*_{ab} + \cdots + \boldsymbol{r}^*_{de}$, even if agents a and e are not connected through a single link (when the edges (a,e) and (e,a) do not exist). This means that if (88) is achieved, we obtain a unique formation, specified by the edges that do exist.

Whereas the formation shape is unique, the location at which the formation comes to standstill (due to the stationarity objective (86)) is not unique, since the objective (88) would still be satisfied when translating all variables $\boldsymbol{z}_i$ and $\boldsymbol{z}_j$ by some constant $\boldsymbol{c} \in \mathbb{R}^\ell$

4.2.3 *Formations with leaders*

One or more agents $i \in \mathcal{T}$ may additionally have a known, fixed target $\boldsymbol{z}^*_i$, similar to the single-agent case, as shown in Figure 3. Agents that know such a target are called leaders. All other agents are followers, and know only inter-agent targets $\boldsymbol{r}^*_{ij}$. The objective of all leaders $i \in \mathcal{T}$ reaching their targets asymptotically becomes

$$\lim_{t\to\infty} ||\boldsymbol{z}_i(t) - \boldsymbol{z}^*_i|| = 0 \quad \forall\ i \in \mathcal{T} \tag{89}$$

The absolute targets $\boldsymbol{z}^*_i$ and relative targets $\boldsymbol{r}^*_{ij}$ must be chosen to be mutually compatible, meaning that the objectives (88), (89) are non-conflicting. For example, in Figure 3 agents 1 and 4 have fixed targets $\boldsymbol{z}^*_1$ and $\boldsymbol{z}^*_4$, and so we require that the sum of the inter-agent targets of all paths between 1 and 4 match the desired difference $\boldsymbol{z}^*_1 - \boldsymbol{z}^*_4$. In example, $\boldsymbol{z}^*_4 - \boldsymbol{z}^*_1 = \boldsymbol{r}^*_{12} + \boldsymbol{r}^*_{24} = \boldsymbol{r}^*_{12} + \boldsymbol{r}^*_{23} + \boldsymbol{r}^*_{34}$.

In this group objective, not only the shape of the formation is uniquely specified, but also the location at which the group comes to standstill.

4.2.4 *Internal objectives and the communicated variable*

Depending on the application, the true group objective may not be to obtain a formation in the variables $\boldsymbol{z}_i(\boldsymbol{x}_i, \boldsymbol{\theta}_i)$ but rather directly in the variables $\boldsymbol{x}_i$. Because the formation goals in either $\boldsymbol{x}_i$ or $\boldsymbol{z}_i$ are both expressed as an asymptotic objective, they are related by the asymptotically stabilized variable $\boldsymbol{\theta}^*_i$. Therefore, a desired formation in the variables $\boldsymbol{x}_i$ can be obtained using the same control objectives (88), (89) by an appropriate choice of $\boldsymbol{r}^*_{ij}$ and $\boldsymbol{z}^*$, if possible.

As an example, we consider the case where $\boldsymbol{z}_i(\boldsymbol{q}_i) = \boldsymbol{x}_i + \boldsymbol{g}_i(\boldsymbol{\theta}_i)$ for some function $\boldsymbol{g}_i(\cdot)$, in which case the objective (88) becomes equivalent to

$$\lim_{t\to\infty} ||\boldsymbol{x}_i(t) - \boldsymbol{x}_j(t) + \boldsymbol{g}_i(\boldsymbol{\theta}_i(t)) - \boldsymbol{g}_j(\boldsymbol{\theta}_j(t)) + \boldsymbol{r}^*_{ij}|| = 0 \quad \forall\ (i,j) \in \mathcal{E}. \tag{90}$$

We already require that all $\boldsymbol{\theta}_i$ converge to $\boldsymbol{\theta}^*_i$ as in (87). Hence, to reach a desired relative configuration $\boldsymbol{r}^{*x}_{ij}$ for the difference $\boldsymbol{x}_j - \boldsymbol{x}_i$, one may aim for a formation in $\boldsymbol{z}_i$ as in (90) and choose $\boldsymbol{r}^*_{ij} = \boldsymbol{r}^{*x}_{ij} - \boldsymbol{g}_i(\boldsymbol{\theta}^*_i) + \boldsymbol{g}_j(\boldsymbol{\theta}^*_j)$. The same extension holds for the case with leaders, where we obtain

$$\lim_{t\to\infty} ||\boldsymbol{x}_i(t) + \boldsymbol{g}_i(\boldsymbol{\theta}_i(t)) - \boldsymbol{z}^*_i|| = 0 \quad \forall\ i \in \mathcal{T}. \tag{91}$$

Hence, to reach a desired target $\boldsymbol{x}^*_i$, this example requires $\boldsymbol{z}^*_i = \boldsymbol{x}^*_i + \boldsymbol{g}_i(\boldsymbol{\theta}^*_i)$ to be chosen as the target for $\boldsymbol{z}_i$.

4.2.5 *Distance-based formations*

The objective (88) imposes a rigid configuration and orientation of the formation in which each agent has a fixed location [59]. This is beneficial in terms of demonstrating mathematically that the goal can be reached asymptotically, but it may be restrictive in some applications. The objective (88) can be relaxed in several ways, such as by imposing the configuration shape but allowing free rotations in addition to free translations.

Alternatively, the relative configurations may be specified as relative scalar distances d_{ij} [59], resulting in a distance-based formation of the form

$$\lim_{t\to\infty} ||\boldsymbol{z}_i(t) - \boldsymbol{z}_j(t)|| - d_{ij} = 0 \quad \forall\ (i,j) \in \mathcal{E}. \tag{92}$$

Depending on the selected graph, the final configuration may not be unique, which may or may not be desirable depending on the application. If we additionally allow changes in the network topology, applications may be realized where agents communicate only with their nearest neighbors, which can be advantageous in very large networks. We refer the reader to [59] for further details on distance-based formations and non-rigid graphs.

In this thesis we restrict the applications to the configuration-based formation objective (88) with or without leaders (89) in order to demonstrate mathematically the feasibility of our proposed methods, and to derive new insights in distributed control of mechanical systems. Further research can extend these insights to applications with other formation objectives and network properties, in which case their validity can be obtained through simulations or more advanced analysis methods.

4.2.6 *Synchronization, agreement, rendezvous, consensus*

A special case of the formation objective (88) arises when all inter-agent configurations or distances are zero ($\boldsymbol{r}^*_{ij} = \boldsymbol{0}\ \ \forall\ (i,j) \in \mathcal{E}$). The resulting objective is

$$\lim_{t\to\infty} ||\boldsymbol{z}_i(t) - \boldsymbol{z}_j(t)|| = 0 \quad \forall\ (i,j) \in \mathcal{E}, \tag{93}$$

which is commonly called synchronization, agreement, rendezvous, or consensus, depending on the application and research area [2]. For a connected graph, this implies that all $\boldsymbol{z}_i$ converge to the same constant value asymptotically, following the same reasoning as for the formation objective in Section 4.2.2.

This goals may be achieved with or without leaders. When there are leaders as in (89), we require $\boldsymbol{z}^*_i = \boldsymbol{c}$ for all $i \in \mathcal{T}$ and some constant $\boldsymbol{c} \in \mathbb{R}^\ell$. In this problem, one typically considers the case where $\boldsymbol{c} = \boldsymbol{0}$. The special case where all agents know their target is sometimes called controlled synchronization [15].

4.3 SELECTED PROPERTIES OF UNDIRECTED GRAPHS

This section discusses several mathematical properties of graph theory which will be useful for designing distributed control laws in the remaining chapters, and re-derives several known properties for the purposes of exchanging vector information.

4.3.1 *Adjacency and Laplacian matrices*

If agent i is a leader, it has an associated leader weight $\boldsymbol{\mathcal{B}}_i = \boldsymbol{\mathcal{B}}_i^\top > \mathbf{0}_\ell$. If agent j is a follower, its leader weight satisfies $\boldsymbol{\mathcal{B}}_j = \mathbf{0}_\ell$. The leader matrix is defined as

$$\boldsymbol{\mathcal{B}} = \begin{bmatrix} \mathcal{B}_1 & & \\ & \ddots & \\ & & \mathcal{B}_N \end{bmatrix} \geq \mathbf{0}_{N\ell}, \quad \boldsymbol{\mathcal{B}}_i = \begin{bmatrix} \boldsymbol{\mathcal{B}}_{i,11} & \cdots & \boldsymbol{\mathcal{B}}_{i,1\ell} \\ \vdots & & \vdots \\ \boldsymbol{\mathcal{B}}_{i,1\ell} & \cdots & \boldsymbol{\mathcal{B}}_{i,\ell\ell} \end{bmatrix}. \tag{94}$$

For each pair of edges (i,j), (j,i) between agents, there is associated symmetric matrix weight $\boldsymbol{\mathcal{A}}_{ij} = \boldsymbol{\mathcal{A}}_{ji} > \mathbf{0}_\ell$ with $\boldsymbol{\mathcal{A}}_{ij} = \boldsymbol{\mathcal{A}}_{ij}^\top$, defined as

$$\boldsymbol{\mathcal{A}}_{ij} = \begin{bmatrix} \mathcal{A}_{ij,11} & \mathcal{A}_{ij,12} & \cdots & \mathcal{A}_{ij,1\ell} \\ \mathcal{A}_{ij,12} & \mathcal{A}_{ij,22} & & \\ \vdots & & \ddots & \\ \mathcal{A}_{ij,1\ell} & & & \mathcal{A}_{ij,\ell\ell} \end{bmatrix}. \tag{95}$$

If there are no edges between vertex i and j, then $\boldsymbol{\mathcal{A}}_{ij} = \boldsymbol{\mathcal{A}}_{ji} = \mathbf{0}_\ell$. Self-edges are not allowed, such that $\boldsymbol{\mathcal{A}}_{ii} = \mathbf{0}_\ell$.

The adjacency components $\boldsymbol{\mathcal{A}}_{ij}$ can be used to construct a symmetric Laplacian matrix $\boldsymbol{\mathcal{L}} \in \mathbb{R}^{N\ell \times N\ell}$ that encodes the network topology, defined as

$$\boldsymbol{\mathcal{L}} = \begin{bmatrix} \sum_{j=1}^N \boldsymbol{\mathcal{A}}_{1j} & -\boldsymbol{\mathcal{A}}_{12} & \cdots & -\boldsymbol{\mathcal{A}}_{1N} \\ -\boldsymbol{\mathcal{A}}_{12} & \sum_{j=1}^N \boldsymbol{\mathcal{A}}_{2j} & & \\ \vdots & & \ddots & \\ -\boldsymbol{\mathcal{A}}_{1N} & & & \sum_{j=1}^N \boldsymbol{\mathcal{A}}_{Nj} \end{bmatrix}. \tag{96}$$

4.3.2 *Laplacian properties for scalar adjacency elements*

Most literature considers the case where all $\mathcal{A}_{ij}$ and $\mathcal{B}_i$ are scalars, in which case the Laplacian matrix (96) has at least one zero eigenvalue with the corresponding eigenvector $\boldsymbol{1}$ [12]. All its nonzero eigenvalues are positive. If the graph is connected, there is only one zero eigenvalue and the other eigenvalues are positive.

Furthermore, if the graph is connected and there is at least one leader (at least one $\mathcal{B}_i > 0$), the matrix

$$\boldsymbol{\mathcal{L}} + \boldsymbol{\mathcal{B}} > \mathbf{0}_N \tag{97}$$

is symmetric positive definite [12].

4.3.3 *Laplacian properties for matrix adjacency elements*

When the adjacency weights $\boldsymbol{\mathcal{A}}_{ij}$ are matrices, the definition (96) is not a Laplacian matrix in the classical sense. For example, a scalar on the diagonal of (96) is

generally not the sum of the remaining elements on the same row, as is the case when $\mathcal{A}_{ij}$ are scalars.

In this section we re-derive several necessary positivity properties of the provided Laplacian matrix (96) and leader matrix (94) to show that they hold equivalently when the adjacency weights $\boldsymbol{\mathcal{A}}_{ij}$ are matrices, which will prove useful for the exchange of vector quantities $\boldsymbol{z}_i$ on the graph.

All information being exchanged at a given instant is contained in the vector $\bar{\boldsymbol{z}} \in \mathbb{R}^{N\ell}$, given as

$$\bar{\boldsymbol{z}} = \begin{bmatrix} \boldsymbol{z}_1 \\ \vdots \\ \boldsymbol{z}_N \end{bmatrix}. \tag{98}$$

Positivity of the matrices $\boldsymbol{\mathcal{L}}$ and $\boldsymbol{\mathcal{B}}$ can be assessed by expanding a quadratic form into a sum of scalar quadratic terms, giving

$$\bar{\boldsymbol{z}}^\top \boldsymbol{\mathcal{L}} \bar{\boldsymbol{z}} = \frac{1}{2} \sum_{i=1}^{N} \sum_{j=1}^{N} (\boldsymbol{z}_i - \boldsymbol{z}_j)^\top \boldsymbol{\mathcal{A}}_{ij} (\boldsymbol{z}_i - \boldsymbol{z}_j) \geq 0, \tag{99}$$

$$\bar{\boldsymbol{z}}^\top \boldsymbol{\mathcal{B}} \bar{\boldsymbol{z}} = \sum_{i=1}^{N} \boldsymbol{z}_i^\top \boldsymbol{\mathcal{B}}_i \boldsymbol{z}_i \geq 0, \tag{100}$$

where the steps to obtain the summation (99) are given in Appendix a. It follows immediately that $\boldsymbol{\mathcal{L}} \geq \mathbf{0}_{\mathbf{N}\ell}$ and $\boldsymbol{\mathcal{B}} \geq \mathbf{0}_{\mathbf{N}\ell}$ are positive semi-definite. Their sum $\boldsymbol{\mathcal{L}} + \boldsymbol{\mathcal{B}} \geq \mathbf{0}_{\mathbf{N}\ell}$ is also positive semi-definite since

$$\bar{\boldsymbol{z}}^\top (\boldsymbol{\mathcal{L}} + \boldsymbol{\mathcal{B}}) \bar{\boldsymbol{z}} = \bar{\boldsymbol{z}}^\top \boldsymbol{\mathcal{L}} \bar{\boldsymbol{z}} + \bar{\boldsymbol{z}}^\top \boldsymbol{\mathcal{B}} \bar{\boldsymbol{z}} \geq 0 \tag{101}$$

The matrix $\boldsymbol{\mathcal{L}} + \boldsymbol{\mathcal{B}}$ is positive definite if and only if the graph is connected and there is at least one leader. Otherwise, it is positive semi-definite.

Proof: From (101) it follows that $\bar{\boldsymbol{z}}^\top (\boldsymbol{\mathcal{L}} + \boldsymbol{\mathcal{B}}) \bar{\boldsymbol{z}} \geq 0$, such that $\boldsymbol{\mathcal{L}} + \boldsymbol{\mathcal{B}}$ is at least positive semi-definite. To show definiteness, it remains to show that $\bar{\boldsymbol{z}}^\top (\boldsymbol{\mathcal{L}} + \boldsymbol{\mathcal{B}}) \bar{\boldsymbol{z}} = 0$ if and only if $\bar{\boldsymbol{z}} = \boldsymbol{0}$. Clearly $\bar{\boldsymbol{z}}^\top (\boldsymbol{\mathcal{L}} + \boldsymbol{\mathcal{B}}) \bar{\boldsymbol{z}} = 0$ when $\bar{\boldsymbol{z}} = \boldsymbol{0}$. To see that the reverse also holds, first note that the quadratic form (101) equals zero if and only if (99) and (100) equal zero. The term (99) being zero implies that for all neighbors i and j, which satisfy $\boldsymbol{\mathcal{A}}_{ij} > \mathbf{0}_\ell$, there must hold $\boldsymbol{z}_i = \boldsymbol{z}_j$, and hence $\boldsymbol{z}_i = \boldsymbol{z}_j = ... = \boldsymbol{z}_y$ for all agents $i, j, \ldots, y$ on a path. If the graph is connected, there is a path between every pair of distinct agents, and hence the term (99) being zero implies that $\boldsymbol{z}_i = \boldsymbol{z}_j \ \forall \ i, j = 1, \ldots, N$. The term (100) being zero implies that all leaders i, which satisfy $\boldsymbol{\mathcal{B}}_i > \mathbf{0}_\ell$, must have $\boldsymbol{z}_i = \boldsymbol{0}$. Therefore, when there is at least one leader, we have that $\boldsymbol{z}_i = \boldsymbol{z}_j = \boldsymbol{0} \ \forall \ i, j = 1, \ldots, N$ and hence we must have $\bar{\boldsymbol{z}} = \boldsymbol{0}$, completing the proof.

4.3.4 *Quadratic forms*

When pursuing the formation control objectives (88), (89), it is useful to define an error function $\varphi(t)$ that expresses the deviation from the desired formation at any given time. Throughout this thesis we will frequently use a scalar quadratic error function given by

$$\begin{aligned} \varphi = \frac{1}{4} \sum_{i=1}^{N} \sum_{j=1}^{N} \left(\boldsymbol{z}_i - \boldsymbol{z}_j + \boldsymbol{r}_{ij}^* \right)^\top \boldsymbol{\mathcal{A}}_{ij} \left(\boldsymbol{z}_i - \boldsymbol{z}_j + \boldsymbol{r}_{ij}^* \right) \\ + \frac{1}{2} \sum_{i=1}^{N} \left(\boldsymbol{z}_i - \boldsymbol{z}_i^* \right)^\top \boldsymbol{\mathcal{B}}_i \left(\boldsymbol{z}_i - \boldsymbol{z}_i^* \right) \geq 0, \end{aligned} \tag{102}$$

which is a weighted sum of the deviations of the inter-agent configurations $\boldsymbol{z}_j - \boldsymbol{z}_i$ from their desired values $\boldsymbol{r}_{ij}^*$, and the distances of the leaders from their targets $\boldsymbol{z}_i^*$.

The function (102) is nonnegative since $\boldsymbol{\mathcal{A}}_{ij} \geq \boldsymbol{0}_\ell$ and $\boldsymbol{\mathcal{B}}_i \geq \boldsymbol{0}_\ell$, and it equals zero when the desired formation is reached. It is convex in $\bar{\boldsymbol{z}}$, which can be shown by writing it as a single quadratic function of the form

$$\varphi = \frac{1}{2}\bar{\boldsymbol{z}}^\top(\boldsymbol{\mathcal{L}} + \boldsymbol{\mathcal{B}})\bar{\boldsymbol{z}} + \boldsymbol{c}_1^\top \bar{\boldsymbol{z}} + c_0, \tag{103}$$

with a constant vector $\boldsymbol{c}_1 \in \mathbb{R}^{N\ell}$ and a constant $c_0 \in \mathbb{R}$ given by

$$\boldsymbol{c}_1 = \begin{bmatrix} -\boldsymbol{\mathcal{B}}_1 \boldsymbol{z}_1^* + \sum_{j=1}^{N} \boldsymbol{\mathcal{A}}_{1j} \boldsymbol{r}_{1j}^* \\ \vdots \\ -\boldsymbol{\mathcal{B}}_N \boldsymbol{z}_N^* + \sum_{j=1}^{N} \boldsymbol{\mathcal{A}}_{Nj} \boldsymbol{r}_{Nj}^* \end{bmatrix} \tag{104}$$

$$c_0 = \frac{1}{4}\sum_{i=1}^{N}\sum_{j=1}^{N} (\boldsymbol{r}_{ij}^*)^\top \boldsymbol{\mathcal{A}}_{ij} \boldsymbol{r}_{ij}^* + \frac{1}{2}\sum_{i=1}^{N} (\boldsymbol{z}_i^*)^\top \boldsymbol{\mathcal{B}}_i \boldsymbol{z}_i^* \tag{105}$$

A derivation for (103)–(105) is given in Appendix a. Convexity in $\bar{\boldsymbol{z}}$ follows from $\boldsymbol{\mathcal{L}} + \boldsymbol{\mathcal{B}} \geq \boldsymbol{0}_{N\ell}$ as determined previously. The Jacobian of (103) is given by

$$\frac{\partial \varphi}{\partial \bar{\boldsymbol{z}}} = (\boldsymbol{\mathcal{B}} + \boldsymbol{\mathcal{L}})\bar{\boldsymbol{z}} + \boldsymbol{c}_1 \tag{106}$$

$$= \begin{bmatrix} \boldsymbol{\mathcal{B}}_1(\boldsymbol{z}_1 - \boldsymbol{z}_1^*) + \sum_{j=1}^{N} \boldsymbol{\mathcal{A}}_{1j}(\boldsymbol{z}_1 - \boldsymbol{z}_j + \boldsymbol{r}_{1j}^*) \\ \vdots \\ \boldsymbol{\mathcal{B}}_N(\boldsymbol{z}_N - \boldsymbol{z}_N^*) + \sum_{j=1}^{N} \boldsymbol{\mathcal{A}}_{Nj}(\boldsymbol{z}_N - \boldsymbol{z}_j + \boldsymbol{r}_{Nj}^*) \end{bmatrix} \tag{107}$$

The minimum is reached when the Jacobian is zero:

$$\frac{\partial \varphi}{\partial \bar{\boldsymbol{z}}} = \boldsymbol{0} \quad \Leftrightarrow \quad \varphi = 0 \tag{108}$$

At this point, all elements of the Jacobian are zero, which leads to

$$\frac{\partial \varphi}{\partial \bar{\boldsymbol{z}}} = \boldsymbol{0} \;\Leftrightarrow\; \boldsymbol{\mathcal{B}}_i(\boldsymbol{z}_i - \boldsymbol{z}_i^*) + \sum_{j=1}^{N} \boldsymbol{\mathcal{A}}_{ij}(\boldsymbol{z}_i - \boldsymbol{z}_j + \boldsymbol{r}_{ij}^*) = \boldsymbol{0} \quad \forall\, i = 1, \ldots, N \tag{109}$$

4.3.5 *Minimizing the quadratic function with one or more leaders*

If $\boldsymbol{\mathcal{L}} + \boldsymbol{\mathcal{B}} > \boldsymbol{0}_{Nm}$, there is a unique $\bar{\boldsymbol{z}}^*$ for which the minimum of (102)–(103) is reached when (109) holds. This happens when the desired formation (88), (89) is obtained, such that $\boldsymbol{z}_i = \boldsymbol{z}_i^*$ and $\boldsymbol{z}_j - \boldsymbol{z}_i = \boldsymbol{r}_{ij}^*$. Because the minimum is unique, the reverse is also true, implying that the formation is reached when the Jacobian of the error function is zero. Hence, for a connected graph with at least one leader there holds

$$\frac{\partial \varphi}{\partial \bar{\boldsymbol{z}}} = \boldsymbol{0} \quad \Leftrightarrow \quad \varphi = 0 \quad \Leftrightarrow \quad \begin{cases} \boldsymbol{z}_i = \boldsymbol{z}_i^* \\ \\ \boldsymbol{z}_j - \boldsymbol{z}_i = \boldsymbol{r}_{ij}^* \end{cases} \quad \forall\, i, j = 1, \ldots, N. \tag{110}$$

4.3.6 *Minimizing the quadratic function without leaders*

If there are no leaders ($\boldsymbol{\mathcal{B}} = \mathbf{0}_{N\ell}$), then $\boldsymbol{\mathcal{L}} + \boldsymbol{\mathcal{B}} = \boldsymbol{\mathcal{L}} \geq \mathbf{0}_{N\ell}$. Although the vector $\bar{\boldsymbol{z}}$ for which the minimum is reached is then not unique, it satisfies

$$\frac{\partial \varphi}{\partial \bar{\boldsymbol{z}}} = \boldsymbol{\mathcal{L}}\bar{\boldsymbol{z}} + \boldsymbol{c}_1 = \boldsymbol{0} \;\Leftrightarrow\; \sum_{j=1}^{N} \boldsymbol{\mathcal{A}}_{ij}(\boldsymbol{z}_i - \boldsymbol{z}_j + \boldsymbol{r}^*_{ij}) = \boldsymbol{0} \quad \forall\, i = 1, \ldots, N \tag{111}$$

For some free variable $\boldsymbol{z}_f \in \mathbb{R}^\ell$, (111) is satisfied by all solutions of the form

$$\bar{\boldsymbol{z}}^* = \begin{bmatrix} \boldsymbol{z}_f^\top & \boldsymbol{z}_f^\top & \cdots & \boldsymbol{z}_f^\top \end{bmatrix} + \begin{bmatrix} 0^\top & (\boldsymbol{r}^*_{12})^\top & \cdots & (\boldsymbol{r}^*_{1N})^\top \end{bmatrix}^\top \tag{112}$$

since then $\boldsymbol{z}_j - \boldsymbol{z}_i = \boldsymbol{z}_f + \boldsymbol{r}^*_{1j} - \boldsymbol{z}_f - \boldsymbol{r}^*_{1i} = \boldsymbol{r}^*_{ij}$. For the same reason, these solutions satisfy the leaderless formation control objectives (88).

Hence, for a connected graph without leaders ($\boldsymbol{\mathcal{B}}^z = \mathbf{0}_N$, $\boldsymbol{\mathcal{L}}^z \geq \mathbf{0}_N$) there holds

$$\frac{\partial \varphi}{\partial \bar{\boldsymbol{z}}} = \boldsymbol{0} \quad \Leftrightarrow \quad \varphi = 0 \quad \Leftrightarrow \quad \boldsymbol{z}_j - \boldsymbol{z}_i = \boldsymbol{r}^*_{ij} \quad \forall\, i, j = 1, \ldots, N \tag{113}$$

Proof: It is easy to see from (103)–(105) that $\boldsymbol{z}_j - \boldsymbol{z}_i = \boldsymbol{r}^*_{ij}$ implies that $\varphi = 0$. It remains to show that the reverse must also hold. From (103), $\varphi = 0$ if and only if $\boldsymbol{z}_j - \boldsymbol{z}_i = \boldsymbol{r}^*_{ij}$ for all agents connected by an edge (with $\boldsymbol{\mathcal{A}}_{ij} > 0$). Hence, all agents a and b on a path are at a configuration $\boldsymbol{z}_b - \boldsymbol{z}_a = \boldsymbol{r}^*_{a\ldots} + \cdots + \boldsymbol{r}^*_{\ldots b} = \boldsymbol{r}^*_{ab}$. Because the graph is assumed to be connected, every pair of distinct agents is connected by a path. Hence, all agents $\boldsymbol{z}_j - \boldsymbol{z}_i$ are at the desired relative configuration $\boldsymbol{r}^*_{ij}$, which completes the proof.

5

EXISTING PASSIVITY-BASED DISTRIBUTED CONTROL OF FULLY-ACTUATED SYSTEMS: A UNIFIED APPROACH

This chapter reviews and compares five existing passivity-based distributed control methodologies for networks of fully-actuated mechanical systems [13–17]. While these distributed control methods are derived from similar passivity principles, the control laws differ depending on the desired group behaviors, the information exchange (positions, velocities, or both), the method of energy dissipation (by the network, the agents, or both), and the presence of a group reference.

It will be shown that for undirected networks without time delays, each control method can be derived from a unified control scheme (Sections 5.1–Section 5.4). Each specialization to obtain the methods [13–17] has a physical or task-specific interpretation, facilitating a comparison between the control schemes (Section 5.5).

This unified presentation of existing methodologies for fully-actuated systems also provides a benchmark for analyzing the distributed control method for underactuated systems proposed in Part III. Specifically, the unified scheme presented here will later be shown to be a special case of the newly proposed scheme for underactuated systems, in case of constant reference signals or leaderless consensus.

As the subsequent chapters take a different distributed control design approach, this stand-alone chapter may be considered as optional reading. The results of this chapter have been previously presented in [60].

5.1 LOCAL AND DISTRIBUTED CONTROL OBJECTIVES

The overlapping objective between the methods [13–17] is asymptotic synchronization of the generalized coordinates $\boldsymbol{q}_i$:

$$\lim_{t\to\infty} ||\boldsymbol{q}_i(t) - \boldsymbol{q}_j(t)|| = 0 \quad \forall\ (i,j) \in \mathcal{E}. \tag{114}$$

Additionally, the method [14] facilitates tracking of a group velocity reference $\dot{\boldsymbol{q}}_d(t)$ while [15] also specifies an absolute group reference $\boldsymbol{q}_d(t)$. The method [17] specifies a constant group reference $\boldsymbol{q}_d$. These objectives may be summarized as:

$$\lim_{t\to\infty} ||\boldsymbol{q}_i(t) - \boldsymbol{q}_d(t)|| = 0 \quad \forall\ i = 1,\dots,N. \tag{115}$$

For brevity, this literature survey chapter will not elaborate on the case where only a subset of the agents knows the reference $\boldsymbol{q}_d$; this will be discussed for the newly proposed distributed control scheme in Part III.

5.2 EQUIVALENT SINGLE-AGENT BEHAVIOR

The dynamics of fully-actuated ($\mathbf{F} = \mathbf{I}_n$) mechanical systems are commonly represented using the frictionless Lagrangian equations of motion (8), repeated here for agent i as

$$\mathbf{M}_i\ddot{\boldsymbol{q}}_i + \widetilde{\mathbf{C}}_i\dot{\boldsymbol{q}}_i + \frac{\partial V_i}{\partial \boldsymbol{q}_i} = \boldsymbol{\tau}_i, \tag{116}$$

with the generalized coordinates $\boldsymbol{q}_i \in \mathbb{R}^n$ and control signal $\boldsymbol{\tau}_i \in \mathbb{R}^n$, with an equal number of coordinates (n) for all agents. Passivity of input-output pair $(\boldsymbol{\tau}_i, \dot{\boldsymbol{q}}_i)$ with respect to the total energy $\widetilde{H}_i$ is obtained using (20).

5.2.1 *Desired single-agent dynamics*

The key similarity in the methods [13–17] is that each agent uses a control law $\boldsymbol{\tau}_i$ to transform the dynamics (116) into the form

$$\mathbf{M}_i\dot{\boldsymbol{y}}_i + \widetilde{\mathbf{C}}_i\boldsymbol{y}_i + \mathbf{K}_i\boldsymbol{y}_i = \boldsymbol{u}_i, \tag{117}$$

with different choices for a new input $\boldsymbol{u}_i \in \mathbb{R}^n$, a new output $\boldsymbol{y}_i(\boldsymbol{q}_i, \dot{\boldsymbol{q}}_i) \in \mathbb{R}^n$, and a damping matrix $\mathbf{K} \in \mathbb{R}^{n\times n}$. Regardless of the choice of $\boldsymbol{y}_i$, this system is passive with respect to the input $\boldsymbol{u}_i$, output $\boldsymbol{y}_i$ and the storage function S_i given by

$$S_i = \frac{1}{2}\boldsymbol{y}_i^\top \mathbf{M}_i \boldsymbol{y}_i. \tag{118}$$

Passivity is demonstrated by taking the time derivative of S_i and exploiting the mass matrix property (11) to write

$$\begin{aligned}\dot{S}_i &= \boldsymbol{y}_i^\top \mathbf{M}_i\dot{\boldsymbol{y}}_i + \frac{1}{2}\boldsymbol{y}_i^\top\left(\widetilde{\mathbf{C}}_i + \widetilde{\mathbf{C}}_i^\top\right)\boldsymbol{y}_i,\\ &= \boldsymbol{y}_i^\top \boldsymbol{u}_i - \boldsymbol{y}_i^\top\mathbf{K}_i\boldsymbol{y}_i + \frac{1}{2}\boldsymbol{y}_i^\top\left(\widetilde{\mathbf{C}}^\top - \widetilde{\mathbf{C}}_i\right)\boldsymbol{y}_i,\\ &= \boldsymbol{y}_i^\top \boldsymbol{u}_i - \boldsymbol{y}_i^\top\mathbf{K}_i\boldsymbol{y}_i.\end{aligned} \tag{119}$$

The system is passive if $\mathbf{K}_i = \mathbf{0}_n$ and output strictly passive if $\mathbf{K}_i > \mathbf{0}_n$.

5.2.2 *Modified passive output*

The modified output $\boldsymbol{y}_i$ is a linear combination of the generalized velocities and coordinates, and an optional reference signal $\boldsymbol{q}_d(t)$:

$$\boldsymbol{y}_i = (\dot{\boldsymbol{q}}_i - \dot{\boldsymbol{q}}_d) + \boldsymbol{\Lambda}(\boldsymbol{q}_i - \boldsymbol{q}_d) \tag{120}$$

where, depending on the method, $\boldsymbol{\Lambda} = \mathbf{0}_n$ or $\boldsymbol{\Lambda} > \mathbf{0}_n$, and $\boldsymbol{q}_d(t) \in \mathbb{R}^n$ is either a twice differentiable function of time or identically set to zero. For notational convenience, we introduce the modified reference velocity $\boldsymbol{v}(t)$ as

$$\boldsymbol{v} = \dot{\boldsymbol{q}}_d + \boldsymbol{\Lambda}\boldsymbol{q}_d, \tag{121}$$

such that (120) can also be written as $\boldsymbol{y}_i = \dot{\boldsymbol{q}}_i + \boldsymbol{\Lambda}\boldsymbol{q}_i - \boldsymbol{v}$.

5.2.3 *Internal control law*

To obtain the desired agent dynamics (117) from the original dynamics (116), each agent uses the control law

$$\boldsymbol{\tau}_i = \frac{\partial V_i}{\partial \boldsymbol{q}_i} + \mathbf{M}_i(\dot{\boldsymbol{v}} - \boldsymbol{\Lambda}\dot{\boldsymbol{q}}_i) + \widetilde{\mathbf{C}}_i(\boldsymbol{v} - \boldsymbol{\Lambda}\boldsymbol{q}_i) - \mathbf{K}_i\boldsymbol{y}_i + \boldsymbol{u}_i, \tag{122}$$

where the implementation varies depending on the presence of a reference, and whether the matrices $\boldsymbol{\Lambda}$ and $\mathbf{K}_i$ are zero or positive definite. No acceleration measurements are required for any of the resulting variants.

5.3 UNIFIED DISTRIBUTED CONTROL SCHEME

Although the distributed control schemes [13–17] are presented in different ways and for different applications, they can be represented by the unified control scheme shown in Figure 4, consisting of N agents (116) with the internal feedback law (122)

and a distributed feedback block $\mathbf{\Gamma}$, interconnected through negative feedback. This section covers the design and implementation of the distributed control law.

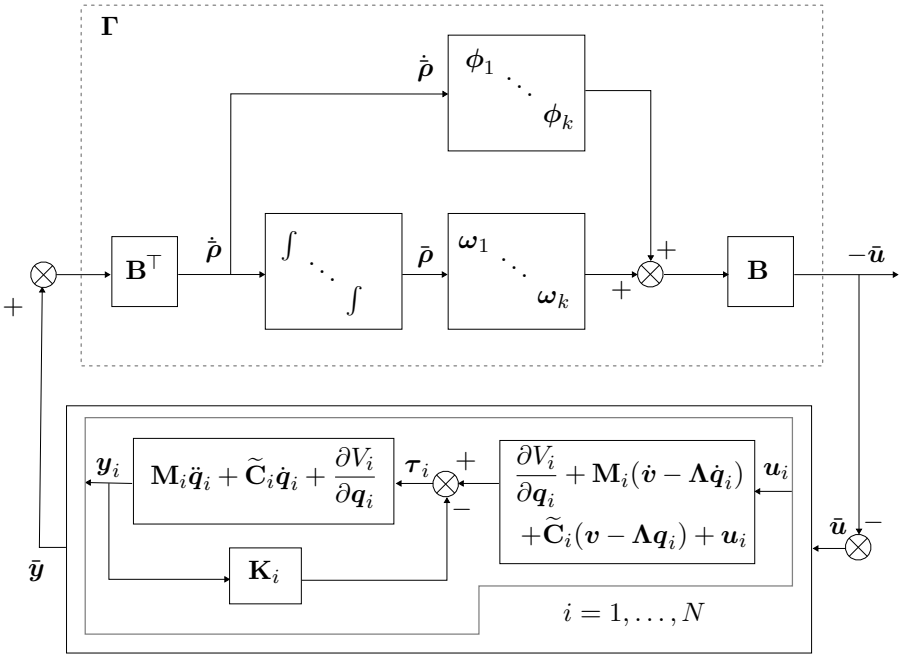

Figure 4: Unified passivity-based distributed control scheme for fully-actuated agents. Adapted from [14].

5.3.1 *Incidence matrix*

The network is modeled using the techniques introduced in Chapter 4. In a network with ν undirected edge pairs, all pairs $(i,j),(j,i)$ are numbered (arbitrarily) from 1 to ν. For each undirected edge with the number k, the agent with the highest index is said to be the positive end of the k-th edge. The other end is its negative end. Then the incidence matrix $\mathbf{B}$ of the network can be defined as [14]

$$\mathbf{B} = \begin{bmatrix} b_{11}\mathbf{I}_n & \cdots & b_{1\nu}\mathbf{I}_n \\ \vdots & & \vdots \\ b_{N1}\mathbf{I}_n & \cdots & b_{N\nu}\mathbf{I}_n \end{bmatrix}, \tag{123}$$

where

$$b_{ik} = \begin{cases} +1 & \text{if the } i\text{-th agent is at the positive end of link } k, \\ -1 & \text{if the } i\text{-th agent is at the negative end of link } k, \\ 0 & \text{otherwise.} \end{cases} \tag{124}$$

The (arbitrary) assignment of a positive end serves only for mathematical convenience; the information flow between two neighboring agents remains bidirectional.

If we now define the vectors

$$\bar{\boldsymbol{y}} = \begin{bmatrix} \boldsymbol{y}_1 \\ \vdots \\ \boldsymbol{y}_N \end{bmatrix}, \quad \bar{\boldsymbol{u}} = \begin{bmatrix} \boldsymbol{u}_1 \\ \vdots \\ \boldsymbol{u}_N \end{bmatrix}, \quad \bar{\boldsymbol{\rho}} = \begin{bmatrix} \boldsymbol{\rho}_1 \\ \vdots \\ \boldsymbol{\rho}_\nu \end{bmatrix}, \tag{125}$$

then an important property is that the product of $\mathbf{B}^\top$ and $\boldsymbol{y}$ gives the differences in the output signals $\boldsymbol{y}_a$ and $\boldsymbol{y}_b$ for each edge (a, b). Specifically,

$$\dot{\boldsymbol{\rho}}_k = \sum_{i=1}^{N} b_{ik}\boldsymbol{y}_i = \begin{cases} \boldsymbol{y}_a - \boldsymbol{y}_b & \text{if the } a\text{-th agent is at the positive end of link } k, \\ \boldsymbol{y}_b - \boldsymbol{y}_a & \text{if the } b\text{-th agent is at the positive end of link } k, \\ \boldsymbol{0} & \text{otherwise.} \end{cases} \tag{126}$$

From the definition of the modified output signals (120), this gives the differences

$$\begin{aligned} \boldsymbol{y}_a - \boldsymbol{y}_b &= (\dot{\boldsymbol{q}}_a - \dot{\boldsymbol{q}}_d) + \boldsymbol{\Lambda}(\boldsymbol{q}_a - \boldsymbol{q}_d) - ((\dot{\boldsymbol{q}}_b - \dot{\boldsymbol{q}}_d) + \boldsymbol{\Lambda}(\boldsymbol{q}_b - \boldsymbol{q}_d)) \\ &= \dot{\boldsymbol{q}}_a - \dot{\boldsymbol{q}}_b + \boldsymbol{\Lambda}(\boldsymbol{q}_a - \boldsymbol{q}_b). \end{aligned} \tag{127}$$

When $\boldsymbol{\Lambda} = \mathbf{0}_n$, the output differences $\dot{\boldsymbol{\rho}}_k$ hence represent relative velocities and their integrals $\boldsymbol{\rho}_k$ represent relative positions $\boldsymbol{q}_a - \boldsymbol{q}_b$. If $\boldsymbol{\Lambda} > \mathbf{0}_n$, then $\boldsymbol{\rho}_k$ also includes an integral of the relative positions.

5.3.2 *Distributed control law*

The relative velocities $\dot{\boldsymbol{\rho}}_k$ and positions $\boldsymbol{\rho}_k$ are then passed through the vector functions $\boldsymbol{\phi}_k(\cdot)$ and $\boldsymbol{\omega}_k(\cdot)$, respectively, as shown in Figure 4. The vector function $\boldsymbol{\phi}_k(\dot{\boldsymbol{\rho}}_k) \in \mathbb{R}^n$ satisfies [13]

$$\begin{aligned} \boldsymbol{\phi}_k(\boldsymbol{0}) &= \boldsymbol{0}, \\ \boldsymbol{\phi}_k(-\dot{\boldsymbol{\rho}}_k) &= -\boldsymbol{\phi}_k(\dot{\boldsymbol{\rho}}_k), \\ \dot{\boldsymbol{\rho}}_k^\top \boldsymbol{\phi}_k(\dot{\boldsymbol{\rho}}_k) &\geq 0, \end{aligned} \tag{128}$$

and the functions $\boldsymbol{\omega}_k(\boldsymbol{\rho}_k) \in \mathbb{R}^N$ are gradients of potential functions $\Omega_k(\boldsymbol{\rho}_k) \geq 0$:

$$\boldsymbol{\omega}_k(\boldsymbol{\rho}_k) = \frac{\partial \Omega_k}{\partial \boldsymbol{\rho}_k}. \tag{129}$$

In the simplest case, both $\boldsymbol{\phi}_k(\cdot)$ and $\boldsymbol{\omega}_k(\cdot)$ are positive linear maps. With $\dot{\boldsymbol{\rho}}_k$ as in (126) the total distributed control law is

$$u = -\mathbf{B}(\bar{\boldsymbol{\phi}} + \bar{\boldsymbol{\omega}}), \quad \bar{\boldsymbol{\phi}} = \begin{bmatrix} \boldsymbol{\phi}_1 \\ \vdots \\ \boldsymbol{\phi}_\nu \end{bmatrix}, \quad \bar{\boldsymbol{\omega}} = \begin{bmatrix} \boldsymbol{\omega}_1 \\ \vdots \\ \boldsymbol{\omega}_\nu \end{bmatrix}. \tag{130}$$

5.3.3 *Passivity of the feedback path and closed loop*

The system highlighted as the dashed block $\boldsymbol{\Gamma}$ in Figure 4 has the input $\boldsymbol{y}$ and output $-\boldsymbol{u}$. It is passive with respect to the storage function

$$\bar{\Omega} = \sum_{k=1}^{\nu} \Omega_k, \tag{131}$$

since its time derivative is

$$\begin{aligned} \dot{\bar{\Omega}} &= \sum_{k=1}^{\nu} \frac{\partial^\top \Omega_k}{\partial \boldsymbol{\rho}_k} \dot{\boldsymbol{\rho}}_k \\ &= \dot{\bar{\boldsymbol{\rho}}}^\top (\bar{\boldsymbol{\omega}} + \bar{\boldsymbol{\phi}}) - \dot{\bar{\boldsymbol{\rho}}}^\top \bar{\boldsymbol{\phi}} \\ &= \bar{\boldsymbol{y}}^\top \mathbf{B}(\bar{\boldsymbol{\omega}} + \bar{\boldsymbol{\phi}}) - \dot{\bar{\boldsymbol{\rho}}}^\top \bar{\boldsymbol{\phi}} \\ &= \bar{\boldsymbol{y}}^\top (-\bar{\boldsymbol{u}}) - \dot{\bar{\boldsymbol{\rho}}}^\top \bar{\boldsymbol{\phi}} \\ &\leq \bar{\boldsymbol{y}}^\top (-\bar{\boldsymbol{u}}), \end{aligned} \tag{132}$$

where the last step follows from (128). Strict passivity is obtained if the inequality in (128) is strict for all $\dot{\boldsymbol{\rho}}_k \neq \boldsymbol{0}$.

The system $\boldsymbol{\Gamma}$ is connected with the internally controlled mechanical agents with the passive dynamics (117) through a negative feedback interconnection, yielding an overall passive system [14] with respect to the total storage function S:

$$\bar{S} = \bar{\Omega} + \sum_{i=1}^{N} S_i = \sum_{k=1}^{\nu} \Omega_k + \sum_{i=1}^{N} S_i. \tag{133}$$

The storage function can be interpreted as the total energy contained in each system and each undirected edge between them. The storage function also serves as a Lyapunov function to assess closed-loop stability.

Combining (119) with (132), the rate of change of this storage function is

$$\dot{\bar{S}} = \dot{\bar{\Omega}} + \sum_{i=1}^{N} \dot{S}_i = -\sum_{k=1}^{\nu} \dot{\boldsymbol{\rho}}_k^{\top} \boldsymbol{\phi}_k - \sum_{i=1}^{N} \boldsymbol{y}_i^{\top} \mathbf{K}_i \boldsymbol{y}_i \leq 0. \tag{134}$$

Energy contained in the closed loop can hence be dissipated by each system i at a rate $\boldsymbol{y}_i^{\top} \mathbf{K}_i \boldsymbol{y}_i$ and by each undirected edge k at a rate $\dot{\boldsymbol{\rho}}_k^{\top} \boldsymbol{\phi}_k$.

5.4 EXISTING RESULTS AS SPECIAL CASES

The generic single-agent control law (122) and the distributed control law (130) can be implemented in several different ways. The possible variations include:

- $\boldsymbol{\Lambda} = \mathbf{0}_n$ or $\boldsymbol{\Lambda} > \mathbf{0}_n$,
- $\mathbf{K}_i = \mathbf{0}_n$ or $\mathbf{K}_i > \mathbf{0}_n$,
- $\boldsymbol{q}_d(t)$ is either undefined or defined as a function of time,
- $\dot{\boldsymbol{q}}_d(t)$ is either zero or equal to $\frac{\mathrm{d}}{\mathrm{d}t}\boldsymbol{q}_d$,
- $\boldsymbol{\phi}_k(\cdot)$ is either the zero map or satisfies (128),
- $\boldsymbol{\omega}_k(\cdot)$ is as in (129), either for $\Omega_k = 0$ or $\Omega_k \geq 0$.

Table 1 summarizes how each of the methods discussed in [13–17] can be obtained from the previously given single-agent and distributed control laws for a specific combination of design choices, for undirected networks without time delays.

	$\mathbf{K}_i$	$\boldsymbol{\Lambda}$	$\boldsymbol{q}_d$	$\dot{\boldsymbol{q}}_d$	$\boldsymbol{\phi}$	$\Omega, \boldsymbol{\omega}$	Storage	Dissipation	Exchange
[13]	$= \mathbf{0}_n$	$> \mathbf{0}_n$	$\boldsymbol{0}$	$\boldsymbol{0}$	(128)	$\boldsymbol{0}$	agents	network	$\boldsymbol{q}_i$, $\dot{\boldsymbol{q}}_i$
[14]	$> \mathbf{0}_n$	$= \mathbf{0}_n$	n/a	$\dot{\boldsymbol{q}}_d$	$\boldsymbol{0}$	(129)	both	agents	$\boldsymbol{q}_i$
[15]	$> \mathbf{0}_n$	$> \mathbf{0}_n$	$\boldsymbol{q}_d$	$\dot{\boldsymbol{q}}_d$	(128)	$\boldsymbol{0}$	agents	both	$\boldsymbol{q}_i$, $\dot{\boldsymbol{q}}_i$
[16]	$> \mathbf{0}_n$	$= \mathbf{0}_n$	$\boldsymbol{0}$	$\boldsymbol{0}$	(128)	(129)	both	both	$\boldsymbol{q}_i$, $\dot{\boldsymbol{q}}_i$
[17]	$> \mathbf{0}_n$	$= \mathbf{0}_n$	$\boldsymbol{0}$	$\boldsymbol{0}$	$\boldsymbol{0}$	(129)	both	agents	$\boldsymbol{q}_i$

Table 1: Specializations to obtain the control laws of [13–17].

Although the necessary notational conversions to each method are quite straightforward to obtain using Table 1, it is worth noting that the modified reference velocity called "$\boldsymbol{q}_{i,r}$" in [15] corresponds to $\boldsymbol{v} - \boldsymbol{\Lambda}\boldsymbol{q}_i = \dot{\boldsymbol{q}}_d + \boldsymbol{\Lambda}(\boldsymbol{q}_d - \boldsymbol{q}_i)$ in the notation of this chapter.

5.5 METHODOLOGICAL DIFFERENCES

Each design choice corresponds to a specific task objective or damping mechanism, and also defines which information agents must exchange over the network. Each choice also effects the transient response and can have consequences for robustness.

5.5.1 *Model-based and model-free distributed control*

Depending on the selected design, the resulting control law requires knowledge of the model matrices $\mathbf{M}_i$ and $\widetilde{\mathbf{C}}_i$. The need for these matrices in the internal control law (122) arises from $\boldsymbol{v} - \boldsymbol{\Lambda}\boldsymbol{q}_i$ being nonzero, which happens for two distinct reasons.

First, a nonzero reference velocity $\boldsymbol{v}$ implies that the model matrices are needed to provide a generalized feed-forward force $\mathbf{M}_i\dot{\boldsymbol{v}} + \widetilde{\mathbf{C}}_i\boldsymbol{v}$ in order to keep tracking the reference. A second model dependency arises from the selection of $\boldsymbol{\Lambda} > 0$, which is done in order to simultaneously control the generalized coordinates $\boldsymbol{q}_i$ and the velocities $\dot{\boldsymbol{q}}_i$ by controlling only $\boldsymbol{y}_i$. By this definition, [16] and [17] (and [14] if $\dot{\boldsymbol{q}}_d = \boldsymbol{0}$) are model-free distributed PD controllers, though knowledge of the gravity compensation term $\frac{\partial V_i}{\partial \boldsymbol{q}_i}$ is still required in all cases.

The need for model matrices can pose robustness constraints and makes implementation comparatively more complex than the distributed PD control methods.

5.5.2 *Storage and dissipation mechanisms, and velocity information exchange*

The total energy (133) contained in the closed-loop system is distributed across the systems and the edges between them. The methods [14, 16, 17] use both storage mechanisms, while [13, 15] store energy only in the agents, as reflected by Ω_k being zero in Table 1.

Independently of where the energy is stored, energy can be dissipated by either the agents or the edges between them, or both, as clarified by (134). Dissipation by the agents is achieved through damping their individual generalized velocities by choosing $\mathbf{K}_i > \mathbf{0}_N$ (in [14–17]). Dissipation in the edges occurs due to damping of relative velocities between the agents using nonzero $\boldsymbol{\phi}_k(\cdot)$ (in [13, 15, 16]).

Although damping relative velocities may lead to faster convergence to the group objective, applying damping internally does not require velocity information to be coordinated over the network, potentially enhancing robustness in the presence of time delays and noise.

5.5.3 *Position coupling mechanisms*

The generalized coordinates $\boldsymbol{q}_i$ and $\boldsymbol{q}_j$ of agents i and j are coupled in two distinct ways. First, when $\Omega_k > 0$, the coupling forces arise as the gradients of potentials between coupled agents, as in (129), (130). Otherwise, if $\boldsymbol{\Lambda} > 0$, the relative positions are coupled because the damping forces $\boldsymbol{\phi}_k(\cdot)$ act on the relative outputs $\boldsymbol{y}_i - \boldsymbol{y}_j = \dot{\boldsymbol{q}}_i - \dot{\boldsymbol{q}}_j + \boldsymbol{\Lambda}(\boldsymbol{q}_i - \boldsymbol{q}_j)$ that relate both the positions and the velocities.

None of the previously discussed control schemes uses both coupling mechanisms simultaneously (no method has both $\Omega_k > 0$ and $\boldsymbol{\Lambda} > 0$). Both couplings being active would imply a form of integral control because the control scheme in Figure 4 integrates the signals $\dot{\boldsymbol{\rho}}_k$ (126), (127), which contains both velocities and positions when $\boldsymbol{\Lambda} > 0$. The resulting distributed PID controller could be further explored to investigate its potentially more robust response to small disturbances.

Part III

DISTRIBUTED CONTROL OF UNDERACTUATED AND HETEROGENEOUS MECHANICAL SYSTEMS

This part presents the main result of this thesis. We present the problem and solution of cooperatively controlling a group of fully-actuated, underactuated, and heterogeneous mechanical systems in a distributed control scheme. Chapter 6 presents the generic distributed IDA-PBC control problem for a network of mechanical systems, and contrasts it to existing distributed control design techniques. Chapter 7 uses the proposed method to derive control laws for networks of fully-actuated agents, while Chapter 8 gives a solution for the case where one or more systems are underactuated.

6 THE DISTRIBUTED IDA-PBC PROBLEM

This chapter shows how the distributed control problem of mechanical systems can be cast as a control problem described in the language of passivity-based control by interconnection and damping assignment. By considering the network of uncontrolled systems as one large mechanical system, we show how IDA-PBC can be used to derive control laws and matching conditions for the whole network.

Section 6.1 gives an explicit description of the uncontrolled dynamics of a network of decoupled mechanical systems. Section 6.2 gives the prescribed desired dynamics, and Section 6.3 provides the control law and matching conditions to obtain these dynamics. Section 6.4 interprets the resulting design problem and its implications for a network of mechanical systems, preparing for the solutions given in the next chapters. Finally, Section 6.5 contrasts this top-down control design procedure to the more commonly used bottom-up procedure of designing internal control laws for each agent and finding stable interconnections.

6.1 A NETWORK OF MECHANICAL SYSTEMS AS ONE SYSTEM

As introduced in Part II, we consider a network of N agents, where each agent has the uncontrolled and frictionless dynamics (25)–(27), given for each agent i as

$$\begin{bmatrix} \dot{\boldsymbol{q}}_i \\ \dot{\boldsymbol{p}}_i \end{bmatrix} = \begin{bmatrix} \mathbf{0}_{n_i} & \mathbf{I}_{n_i} \\ -\mathbf{I}_{n_i} & \mathbf{0}_{n_i} \end{bmatrix} \begin{bmatrix} \dfrac{\partial H_i}{\partial \boldsymbol{q}_i} \\ \dfrac{\partial H_i}{\partial \boldsymbol{p}_i} \end{bmatrix} + \begin{bmatrix} \mathbf{0}_{n_i \times m_i} \\ \mathbf{F}_i \end{bmatrix} \boldsymbol{\tau}_i, \tag{135}$$

$$\boldsymbol{y}_i = \mathbf{F}_i^\top \frac{\partial H_i}{\partial \boldsymbol{p}_i} = \mathbf{F}_i^\top \mathbf{M}_i^{-1} \boldsymbol{p}_i, \tag{136}$$

$$H_i = \frac{1}{2} \boldsymbol{p}_i^\top \mathbf{M}_i^{-1} \boldsymbol{p}_i + V_i, \tag{137}$$

where as before, $\boldsymbol{q}_i \in \mathbb{R}^{n_i}$ are the generalized coordinates of agent i, $\boldsymbol{p}_i \in \mathbb{R}^{n_i}$ are its generalized momenta, $\boldsymbol{\tau}_i \in \mathbb{R}^{m_i}$ and $\boldsymbol{y}_i \in \mathbb{R}^{m_i}$ are its generalized input and output, $\mathbf{F}_i(\boldsymbol{q}_i) \in \mathbb{R}^{n_i \times m_i}$ is its input matrix, $\mathbf{M}_i(\boldsymbol{q}_i) = \mathbf{M}_i^\top(\boldsymbol{q}_i) > \mathbf{0}_{n_i}$ is its mass matrix, and $\mathbf{V}_i \in \mathbb{R}$ is its potential energy. All terms may be different for each agent, including the dimensions n_i and $m_i \leq n_i$.

Then we can write the open-loop dynamics of all agents in the network as a single simple mechanical system of the form

$$\begin{bmatrix} \dot{\bar{\boldsymbol{q}}} \\ \dot{\bar{\boldsymbol{p}}} \end{bmatrix} = \begin{bmatrix} \mathbf{0}_{\bar{n}} & \mathbf{I}_{\bar{n}} \\ -\mathbf{I}_{\bar{n}} & \mathbf{0}_{\bar{n}} \end{bmatrix} \begin{bmatrix} \dfrac{\partial \bar{H}}{\partial \bar{\boldsymbol{q}}} \\ \dfrac{\partial \bar{H}}{\partial \bar{\boldsymbol{p}}} \end{bmatrix} + \begin{bmatrix} \mathbf{0}_{\bar{n} \times \bar{m}} \\ \bar{\mathbf{F}} \end{bmatrix} \bar{\boldsymbol{\tau}}, \tag{138}$$

$$\bar{\boldsymbol{y}} = \bar{\mathbf{F}}^\top \frac{\partial \bar{H}}{\partial \bar{\boldsymbol{p}}} = \bar{\mathbf{F}}^\top \bar{\mathbf{M}}^{-1} \bar{\boldsymbol{p}}, \tag{139}$$

$$\bar{H} = \frac{1}{2} \bar{\boldsymbol{p}}^\top \bar{\mathbf{M}}^{-1} \bar{\boldsymbol{p}} + \bar{V}, \tag{140}$$

where the coordinate and input dimensions are

$$\bar{n} = \sum_{i=1}^{N} n_i, \quad \bar{m} = \sum_{i=1}^{N} m_i, \tag{141}$$

and the corresponding network terms are given by

$$\bar{\boldsymbol{q}} = \begin{bmatrix} \boldsymbol{q}_1 \\ \vdots \\ \boldsymbol{q}_N \end{bmatrix}, \quad \bar{\boldsymbol{p}} = \begin{bmatrix} \boldsymbol{p}_1 \\ \vdots \\ \boldsymbol{p}_N \end{bmatrix}, \quad \bar{\boldsymbol{\tau}} = \begin{bmatrix} \boldsymbol{\tau}_1 \\ \vdots \\ \boldsymbol{\tau}_N \end{bmatrix}, \quad \bar{\boldsymbol{y}} = \begin{bmatrix} \boldsymbol{y}_1 \\ \vdots \\ \boldsymbol{y}_N \end{bmatrix}, \tag{142}$$

$$\bar{\mathbf{M}} = \begin{bmatrix} \mathbf{M}_1 & & \\ & \ddots & \\ & & \mathbf{M}_N \end{bmatrix}, \quad \bar{\mathbf{F}} = \begin{bmatrix} \mathbf{F}_1 & & \\ & \ddots & \\ & & \mathbf{F}_N \end{bmatrix}, \quad \bar{V} = \sum_{i=1}^{N} V_i. \tag{143}$$

A brief derivation is given in Appendix a.

We assume that there is no physical contact between the systems, but interaction arises due to their control signals. Generally, the control law $\boldsymbol{\tau}_i$ of agent i can be a function of its own state and of information it receives from other agents. Because the uncontrolled network is still a simple mechanical system, the previously introduced IDA-PBC control law, matching conditions, and stability analysis still apply. This concept forms the basis of this chapter and the next.

6.2 DESIRED CLOSED LOOP NETWORK DYNAMICS AND INTERACTION

Similar to single system case discussed in Chapter 3, the feedback control law is designed to turn the open-loop network dynamics (138)–(140) into the asymptotically stable or semi-stable closed-loop dynamics given by

$$\begin{bmatrix} \dot{\bar{\boldsymbol{q}}} \\ \dot{\bar{\boldsymbol{p}}} \end{bmatrix} = \begin{bmatrix} \mathbf{0}_{\bar{n}} & \bar{\mathbf{M}}^{-1}\bar{\mathbf{M}}_{\mathrm{d}} \\ -\bar{\mathbf{M}}_{\mathrm{d}}\bar{\mathbf{M}}^{-1} & \bar{\mathbf{J}} - \bar{\mathbf{F}}\bar{\mathbf{K}}_v\bar{\mathbf{F}}^{\top} \end{bmatrix} \begin{bmatrix} \dfrac{\partial \bar{H}_{\mathrm{d}}}{\partial \bar{\boldsymbol{q}}} \\ \dfrac{\partial \bar{H}_{\mathrm{d}}}{\partial \bar{\boldsymbol{p}}} \end{bmatrix} + \begin{bmatrix} \mathbf{0}_{\bar{n}\times\bar{m}} \\ \bar{\mathbf{F}} \end{bmatrix} \bar{\boldsymbol{\tau}}_{\mathrm{d}}, \tag{144}$$

$$\bar{\boldsymbol{y}}_{\mathrm{d}} = \bar{\mathbf{F}}^{\top}\frac{\partial \bar{H}_{\mathrm{d}}}{\partial \bar{\boldsymbol{p}}} = \bar{\mathbf{F}}^{\top}\bar{\mathbf{M}}_{\mathrm{d}}^{-1}\bar{\boldsymbol{p}}, \tag{145}$$

$$\bar{H}_{\mathrm{d}} = \frac{1}{2}\bar{\boldsymbol{p}}^{\top}\bar{\mathbf{M}}_{\mathrm{d}}^{-1}\bar{\boldsymbol{p}} + \bar{V}_{\mathrm{d}}. \tag{146}$$

A control objective is achieved by shaping the closed-loop energy of the network and inserting damping such that the system asymptotically reaches a desired equilibrium $\bar{\boldsymbol{q}}^*$ or a desired set of equilibria $\bar{\mathcal{Q}}^*$, as discussed further in Section 6.4.

In principle, the definitions of the design variables $\bar{\mathbf{J}} = -\bar{\mathbf{J}}_2^{\top} \in \mathbb{R}^{\bar{n}\times\bar{n}}$, $\bar{\mathbf{K}}_v > \mathbf{0}_{\bar{m}}$, $\mathbf{0}_{\bar{n}} < \bar{\mathbf{M}}_{\mathrm{d}} < \alpha\mathbf{I}_{\bar{n}}$, $\alpha > 0$, and $\bar{V}_{\mathrm{d}} \in \mathbb{R}$ extend equivalently to the distributed case, but they now play roles in both the local agent behavior and in the interaction between agents. This will be discussed for each term in the sections and chapters that follow.

6.3 DISTRIBUTED CONTROL LAW AND MATCHING CONDITIONS

Extending (49) to the networked case gives the distributed IDA-PBC control law:

$$\bar{\boldsymbol{\tau}} = \left(\bar{\mathbf{F}}^{\top}\bar{\mathbf{F}}\right)^{-1}\bar{\mathbf{F}}^{\top}\left(\frac{\partial \bar{H}}{\partial \bar{\boldsymbol{q}}} - \bar{\mathbf{M}}_{\mathrm{d}}\bar{\mathbf{M}}^{-1}\frac{\partial \bar{H}_{\mathrm{d}}}{\partial \bar{\boldsymbol{q}}} + \bar{\mathbf{J}}\bar{\mathbf{M}}_{\mathrm{d}}^{-1}\bar{\boldsymbol{p}}\right) - \bar{\mathbf{K}}_v\bar{\boldsymbol{y}}_{\mathrm{d}} + \bar{\boldsymbol{\tau}}_{\mathrm{d}}. \tag{147}$$

Equivalently to the single-agent case, the control law (147) achieves the desired dynamics (144)–(146) only if the matching conditions are satisfied. From (50), the distributed kinetic energy matching condition becomes:

$$\bar{\mathbf{F}}^{\perp}\left(\frac{\partial\left(\bar{\boldsymbol{p}}^{\top}\bar{\mathbf{M}}^{-1}\bar{\boldsymbol{p}}\right)}{\partial \bar{\boldsymbol{q}}} - \bar{\mathbf{M}}_{\mathrm{d}}\bar{\mathbf{M}}^{-1}\frac{\partial\left(\bar{\boldsymbol{p}}^{\top}\bar{\mathbf{M}}_{\mathrm{d}}^{-1}\bar{\boldsymbol{p}}\right)}{\partial \bar{\boldsymbol{q}}} + 2\bar{\mathbf{J}}\bar{\mathbf{M}}_{\mathrm{d}}^{-1}\bar{\boldsymbol{p}}\right) = \boldsymbol{0}. \tag{148}$$

From (51), the distributed potential energy matching equation becomes:

$$\bar{\mathbf{F}}^{\perp}\left(\frac{\partial \bar{V}}{\partial \bar{\boldsymbol{q}}} - \bar{\mathbf{M}}_{\mathrm{d}}\bar{\mathbf{M}}^{-1}\frac{\partial \bar{V}_{\mathrm{d}}}{\partial \bar{\boldsymbol{q}}}\right) = \boldsymbol{0}. \tag{149}$$

6.4 DISTRIBUTED POTENTIAL AND KINETIC ENERGY SHAPING

While the distributed IDA-PBC strategy is mathematically identical to the single-agent case, the uncontrolled system (138)–(140) is not a single physical system but a decoupled set of mechanical systems. This has implications for the implementation of the control law, the conditions for matching, as well as the design problem of potential and kinetic energy shaping. This section briefly elaborates on these topics before addressing them one at a time in subsequent chapters.

6.4.1 *Local and distributed implementation*

The distributed control signal $\bar{\boldsymbol{\tau}} \in \mathbb{R}^{\bar{m}}$ (142), (147) is implemented as N separate control signals $\boldsymbol{\tau}_i \in \mathbb{R}^{m_i}$. Most generally, each control signal $\boldsymbol{\tau}_i(\bar{\boldsymbol{q}}, \bar{\boldsymbol{p}})$ may be a function of its own state and the states of all other agents in the system. Which state information is needed by each agent defines which information must be communicated between the agents. In turn, this depends on the selected design parameters of the desired dynamics (144)–(146). Consequently, if constraints are imposed on the allowed communication, this limits the choices that can be made in energy shaping.

6.4.2 *Local and distributed potential energy shaping*

The desired potential energy $\bar{V}_{\mathrm{d}}(\bar{\boldsymbol{q}})$ of the closed-loop system is generally a function of the generalized coordinates $\boldsymbol{q}_i$ of all agents. This energy must be chosen such that it attains a minimum when the control objectives are achieved:

$$\bar{\boldsymbol{q}}^{*} = \arg\min \bar{V}_{\mathrm{d}}(\bar{\boldsymbol{q}}), \tag{150}$$

where $\bar{\boldsymbol{q}}^{*}$ is either a unique equilibrium or an element of a set of equally desired equilibria. Agents can pursue a group objective such as a formation as well as local objectives like stabilizing one or more internal coordinates, as discussed in Chapter 4. The potential energy $\bar{V}_{\mathrm{d}}(\bar{\boldsymbol{q}})$ must be minimal when both the group objective and the local objectives are achieved. As in the single-agent case, this choice is constrained by the potential energy matching condition (149).

The energy $\bar{V}_{\mathrm{d}}(\bar{\boldsymbol{q}})$ appears in the distributed control law (147) through the gradient of $\bar{H}_{\mathrm{d}}$. Local objectives to agent i are expressed in an energy term that depends only on $\boldsymbol{q}_i$, which through the gradient results in a control force acting only on agent i. A group objective shared by agent j and k appears as an energy function of both $\boldsymbol{q}_j$ and $\boldsymbol{q}_k$, leading to interaction control forces on both agent j and k and the need to exchange information. This is equivalent to the principle of energy storage in the interconnections discussed in Chapter 5. Potential energy shaping is of critical importance for the distributed IDA-PBC solutions presented in Chapter 7 and 8.

6.4.3 *Local and distributed kinetic energy shaping*

The desired kinetic energy is determined by the desired mass matrix $\bar{\mathbf{M}}_\mathrm{d} = \bar{\mathbf{M}}_\mathrm{d}^\top$, which we may partition without loss of generality as

$$\bar{\mathbf{M}}_\mathrm{d} = \begin{bmatrix} \mathbf{M}_{\mathrm{d},1} & \mathbf{M}_{\mathrm{d},12} & \cdots & \mathbf{M}_{\mathrm{d},1N} \\ \mathbf{M}_{\mathrm{d},21} & \mathbf{M}_{\mathrm{d},2} & & \\ \vdots & & \ddots & \\ \mathbf{M}_{\mathrm{d},N1} & & & \mathbf{M}_{\mathrm{d},N} \end{bmatrix}, \tag{151}$$

where symmetry implies $\mathbf{M}_{\mathrm{d},ij} = \mathbf{M}_{\mathrm{d},ji}^\top \in \mathbb{R}^{n_i \times n_j}$ and $\mathbf{M}_{\mathrm{d},i} = \mathbf{M}_{\mathrm{d},i}^\top \in \mathbb{R}^{n_i \times n_i}$. The kinetic energy expression $\frac{1}{2}\bar{\boldsymbol{p}}^\top \bar{\mathbf{M}}_\mathrm{d}^{-1} \bar{\boldsymbol{p}}$ in (146) is generally not simply the sum of the desired kinetic energies for the single systems, unless $\mathbf{M}_{\mathrm{d},ij} = \mathbf{0}_{n_i \times n_j}$. Choosing nonzero $\mathbf{M}_{\mathrm{d},ij}$ creates energy terms expressed simultaneously in $\boldsymbol{q}_i$, $\boldsymbol{p}_i$, $\boldsymbol{q}_j$ and $\boldsymbol{p}_j$.

Even if $\mathbf{M}_{\mathrm{d},ij} = \mathbf{0}_n$, the diagonal blocks $\mathbf{M}_{\mathrm{d},i}$ can be used to change the interaction between agents. Increasing or decreasing the desired mass of one agent compared to another enables cooperation between heterogeneous systems with significantly different masses. For example, pure potential shaping without kinetic energy shaping would set a lightweight system in oscillatory motion while the heavyweight system would hardly move. Kinetic energy shaping can normalize these relative effects to considerably improve the transient response. This is illustrated for an example application in Chapter 11.

6.4.4 *Local and distributed damping*

The damping matrix $\bar{\mathbf{K}}_v = \bar{\mathbf{K}}_v{}^\top > \mathbf{0}_{\bar{m}}$ can be partitioned as

$$\bar{\mathbf{K}}_v = \begin{bmatrix} \mathbf{K}_{v,1} & \mathbf{K}_{v,12} & \cdots & \mathbf{K}_{v,1N} \\ \mathbf{K}_{v,21} & \mathbf{K}_{v,2} & & \\ \vdots & & \ddots & \\ \mathbf{K}_{v,N1} & & & \mathbf{K}_{v,N} \end{bmatrix}, \tag{152}$$

where $\mathbf{K}_{v,i} \in \mathbb{R}^{m_i \times m_i}$ and $\mathbf{K}_{v,ij} = \mathbf{K}_{v,ji}^\top \in \mathbb{R}^{m_i \times m_j}$. Damping forces appear in the control law (147) as the expression

$$-\bar{\mathbf{K}}_v \bar{\boldsymbol{y}}_\mathrm{d} = -\bar{\mathbf{K}}_v \bar{\mathbf{F}}^\top \bar{\mathbf{M}}_\mathrm{d}^{-1} \bar{\boldsymbol{p}}. \tag{153}$$

Depending on the chosen $\bar{\mathbf{M}}_\mathrm{d}^{-1}$ and $\bar{\mathbf{K}}_v$, the damping force for agent i is a function of its own coordinates and momenta as well as those of other agents j. Chapter 7 discusses several special choices of $\bar{\mathbf{K}}_v$ that minimize the need to exchange momenta information between agents.

6.4.5 *Local gyroscopic forces and energy routing*

The skew symmetric matrix $\bar{\mathbf{J}}$ may be partitioned as

$$\bar{\mathbf{J}} = \begin{bmatrix} \mathbf{J}_1 & \mathbf{J}_{12} & \cdots & \mathbf{J}_{1N} \\ \mathbf{J}_{21} & \mathbf{J}_2 & & \\ \vdots & & \ddots & \\ \mathbf{J}_{N1} & & & \mathbf{J}_N \end{bmatrix}, \tag{154}$$

where $\mathbf{J}_i = -\mathbf{J}_i^\top \in \mathbb{R}^{n_i \times n_i}$ and $\mathbf{J}_{ij} = -\mathbf{J}_{ji}^\top \in \mathbb{R}^{n_i \times n_j}$. In principle, all elements of $\bar{\mathbf{J}}$ may be functions of all $\bar{\boldsymbol{q}}$ and $\bar{\boldsymbol{p}}$, so long as the distributed kinetic energy matching condition (148) is satisfied. As in the single-agent case, the matrix $\bar{\mathbf{J}}$ does not change the stability result, but can be used to help solve the matching conditions and alter the transient response.

The corresponding "gyroscopic" control forces appear in the control law (147) as

$$\left(\bar{\mathbf{F}}^\top \bar{\mathbf{F}}\right)^{-1} \bar{\mathbf{F}}^\top \bar{\mathbf{J}} \bar{\mathbf{M}}_{\mathrm{d}}^{-1} \bar{\boldsymbol{p}}, \tag{155}$$

in which the matrices $\mathbf{J}_i$ assign gyroscopic forces as in the single-agent case and the matrices $\mathbf{J}_{ij}$ are responsible for routing energy between systems without changing the overall energy balance, an extension discussed in Section 13.4.

6.5 TOP-DOWN AND BOTTOM-UP DISTRIBUTED CONTROL

This section discusses two generic approaches for designing distributed control laws. In the commonly used bottom-up approach, each agent is given its own controller and interactions are sought to devise a stable network. In the top-down approach, the starting point is a stable class of network dynamics, from which the internal and distributed control laws are derived.

6.5.1 *Bottom-up: from local and distributed control to a stable network*

Typical passivity-based distributed control methods follow bottom-up design approaches, which consider how passive systems can be interconnected to preserve passivity. Weighted sums of the storage functions of each subsystem are used as candidate Lyapunov functions in order to assess closed-loop stability [13–17].

This approach is especially successful for networks of fully-actuated systems like robot manipulators, where internal control laws render each system passive with respect to an output that ensures synchronization of both generalized coordinates and velocities between systems, as discussed in Chapter 5. Unfortunately, this approach does not easily generalize to underactuated systems, complicating the procedure of finding internal control laws and stable interconnections.

6.5.2 *Top down: from a stable network to local and distributed control*

This thesis uses a top-down approach instead, starting from a class of stable desired dynamics (144) for the whole network (138), and deriving the control law (147) and interconnection conditions (148), (149) to preserve the desired dynamics and stability. Any remaining degrees of freedom (151)–(154) can be used to address the transient response of the network and its subsystems, and to find a distributed implementation of the control law.

This approach is well-suited for networks of fully-actuated and underactuated systems, and combinations thereof. Whereas choosing a desired class of dynamics may appear more restrictive than allowing arbitrary dynamics and Lyapunov functions, the structure of the solution reveals both the potential force and damping mechanisms commonly found in a bottom-up approach, but also non-trivial gyroscopic coupling forces (155) while preserving stability.

If the resulting control laws and matching conditions can be sufficiently decoupled, such that all energy terms in the total storage function can be assigned to specific subsystems or interconnections, the top-down result can be equivalently written as a bottom-up design. Then the main difference is the transparent derivation and simplified stability analysis, which is the case for the solutions in the next chapters.

7 SOLUTIONS FOR THE FULLY-ACTUATED CASE

This chapter uses the proposed approach of passivity-based control by damping and interconnection assignment to re-derive several known results in distributed control of fully-actuated mechanical systems, setting the stage for new results for the underactuated case in Chapter 8.

Section 7.1 gives the generic distributed control law, while Sections 7.2 and 7.3 specialize this result to coordinate formations and task-space formations.

7.1 DISTRIBUTED CONTROL LAW

Repeating the steps in Section 3.4 for the fully-actuated network of mechanical systems, there are no matching conditions that have to be satisfied, and we may assume $\bar{\mathbf{F}} = \mathbf{I}_{\bar{n}}$. If there are no further external inputs to the network ($\bar{\boldsymbol{\tau}}_\mathrm{d} = \boldsymbol{0}$) the total control law (147) reduces to

$$\bar{\boldsymbol{\tau}} = \frac{\partial \bar{H}}{\partial \bar{\boldsymbol{q}}} - \bar{\mathbf{M}}_\mathrm{d}\bar{\mathbf{M}}^{-1}\frac{\partial \bar{H}_\mathrm{d}}{\partial \bar{\boldsymbol{q}}} + (\bar{\mathbf{J}} - \bar{\mathbf{K}}_v)\,\bar{\boldsymbol{y}}_\mathrm{d}. \tag{156}$$

Likewise, in the absence of matching conditions, the matrices $\bar{\mathbf{M}}_\mathrm{d}$ and $\bar{\mathbf{J}}$ only play a role in shaping the transient response, and they can be chosen as $\bar{\mathbf{M}}_\mathrm{d} = \bar{\mathbf{M}}$ and $\bar{\mathbf{J}} = \mathbf{0}_{\bar{n}}$. This results in only potential energy shaping, using the control law

$$\bar{\boldsymbol{\tau}} = \frac{\partial \bar{V}}{\partial \bar{\boldsymbol{q}}} - \frac{\partial \bar{V}_\mathrm{d}}{\partial \bar{\boldsymbol{q}}} - \bar{\mathbf{K}}_v\bar{\boldsymbol{y}}. \tag{157}$$

As in the single-agent case, the term $\frac{\partial \bar{V}}{\partial \bar{\boldsymbol{q}}}$ amounts to gravity compensation. Recalling that $\bar{V}(\boldsymbol{q}) = V_i(\boldsymbol{q}_i) + \cdots + V_N(\boldsymbol{q}_N)$, it follows that the associated component in the control signal $\boldsymbol{\tau}_i$ for each agent equals $\frac{\partial V_i}{\partial \boldsymbol{q}_i}(\boldsymbol{q}_i)$, which each agent can implement using only the local information $\boldsymbol{q}_i$.

Following the standard single-agent IDA-PBC design procedure, a control objective can be achieved by shaping the potential energy in such a away that it attains its minimum when the control objectives are satisfied. In the distributed scenario, the total closed-loop potential energy V_d should be minimal when the group formation objective is satisfied, which is when $\bar{\boldsymbol{q}} = \bar{\boldsymbol{q}}^*$ or $\bar{\boldsymbol{q}} \in \bar{\mathcal{Q}}^*$.

7.2 POTENTIAL ENERGY SHAPING FOR COORDINATE FORMATIONS

A common distributed control objective is to cooperatively control all coordinates $\boldsymbol{q}_i \in \mathbb{R}^n$ of a set of N fully-actuated mechanical systems with an equal number of coordinates ($m_i = n_i = m = n = \ell$ for all i). This means that the coordinated variable reduces to $\boldsymbol{z}_j = \boldsymbol{x}_j = \boldsymbol{q}_j$, with no coordinates $\boldsymbol{\theta}_i$ to be stabilized internally.

The group objective can be described as in Section 4.2, such that the objective of a stationary formation with or without leaders becomes

$$\lim_{t\to\infty} ||\boldsymbol{p}_i(t)|| = 0 \quad \forall\, i = 1, \ldots, N, \tag{158}$$

$$\lim_{t\to\infty} ||\boldsymbol{q}_i(t) - \boldsymbol{q}_j(t) + \boldsymbol{r}^*_{ij}|| = 0 \quad \forall\, (i,j) \in \mathcal{E}, \tag{159}$$

$$\lim_{t\to\infty} ||\boldsymbol{q}_i(t) - \boldsymbol{q}^*_i|| = 0 \quad \forall\, i \in \mathcal{T}. \tag{160}$$

When the group objective is coordinate synchronization, $\boldsymbol{r}_{ij}^* = \boldsymbol{0}$. When there are no leaders, the objective (160) vanishes, and the group comes to standstill at one of a range of possible states $\bar{\boldsymbol{q}}^* \in \bar{\mathcal{Q}}^*$, all satisfying the formation objective.

7.2.1 *Quadratic potential energy function*

The simplest coupling potential can be obtained directly as a sum of squares of the deviation from the formation objective. Using the adjacency and leader weights, this sum can be compactly written by summing over the agents and each of their neighbors as detailed in Section 4.3. This gives

$$\begin{aligned}\bar{V}_{\mathrm{d}} = \frac{1}{4}\sum_{i=1}^{N}\sum_{j=1}^{N}\left(\boldsymbol{q}_i - \boldsymbol{q}_j + \boldsymbol{r}_{ij}^*\right)^{\top}\boldsymbol{\mathcal{A}}_{ij}\left(\boldsymbol{q}_i - \boldsymbol{q}_j + \boldsymbol{r}_{ij}^*\right) \\ + \frac{1}{2}\sum_{i=1}^{N}\left(\boldsymbol{q}_i - \boldsymbol{q}_i^*\right)^{\top}\boldsymbol{\mathcal{B}}_i\left(\boldsymbol{q}_i - \boldsymbol{q}_i^*\right) \geq 0.\end{aligned} \tag{161}$$

The choice (161) ensures that $V_{\mathrm{d}} \geq 0$ and $V_{\mathrm{d}} = 0$ if and only if the formation objective is achieved. Likewise, the Jacobian

$$\frac{\partial \bar{V}_{\mathrm{d}}}{\partial \bar{\boldsymbol{q}}} = \begin{bmatrix} \boldsymbol{\mathcal{B}}_1(\boldsymbol{q}_1 - \boldsymbol{q}_1^*) + \sum_{j=1}^{N}\boldsymbol{\mathcal{A}}_{1j}(\boldsymbol{q}_1 - \boldsymbol{q}_j + \boldsymbol{r}_{1j}^*) \\ \vdots \\ \boldsymbol{\mathcal{B}}_N(\boldsymbol{q}_N - \boldsymbol{q}_N^*) + \sum_{j=1}^{N}\boldsymbol{\mathcal{A}}_{Nj}(\boldsymbol{q}_N - \boldsymbol{q}_j + \boldsymbol{r}_{Nj}^*) \end{bmatrix} \tag{162}$$

equals zero if and only if the formation goal is satisfied.

7.2.2 *Absolute and relative damping*

In this section we show how the damping condition $\bar{\mathbf{K}}_v > \mathbf{0}_{\bar{n}}$ can be satisfied either locally or by communicating velocity information across the network. Assume we have a second communication graph for velocity or momenta information exchange, which need not be the same as the graph for position exchange. For this second graph, we denote the Laplacian matrix as $\boldsymbol{\mathcal{L}}^v$ and the leader matrix as $\boldsymbol{\mathcal{B}}^v$. An agent is a leader on the velocity graph if it can measure its own velocities $\dot{\boldsymbol{q}}_i$ or its momenta $\boldsymbol{p}_i = \mathbf{M}_i\dot{\boldsymbol{q}}_i$.

Damping is inserted through the damping force $-\bar{\mathbf{K}}_v\bar{\boldsymbol{y}}$ in (157). A necessary damping condition for asymptotic stability is $\bar{\mathbf{K}}_v > \mathbf{0}_{\bar{n}}$. Following (152), we propose to partition $\bar{\mathbf{K}}_v$ as

$$\bar{\mathbf{K}}_v = \boldsymbol{\mathcal{L}}^v + \boldsymbol{\mathcal{B}}^v > 0. \tag{163}$$

This matrix is positive definite if the graph is connected and there is at least one velocity leader. It is also positive definite if all agents are leaders on the velocity graph (when $\boldsymbol{\mathcal{B}}^v > \mathbf{0}_{\bar{n}}$). An intermediate variant is also possible, were all agents are connected to at least one leader, but this case is not discussed here. Using (107), the damping force expressed in velocities $\dot{\boldsymbol{q}}_i = \mathbf{M}_i^{-1}\boldsymbol{p}_i$ equals

$$-\bar{\mathbf{K}}_v\bar{\boldsymbol{y}} = -\bar{\mathbf{K}}_v\bar{\mathbf{M}}^{-1}\bar{\boldsymbol{p}} = -\bar{\mathbf{K}}_v\dot{\bar{\boldsymbol{q}}} = \begin{bmatrix} -\boldsymbol{\mathcal{B}}_1^v\dot{\boldsymbol{q}}_1 - \sum_{j=1}^{N}\boldsymbol{\mathcal{A}}_{1j}^v(\dot{\boldsymbol{q}}_1 - \dot{\boldsymbol{q}}_j) \\ \vdots \\ -\boldsymbol{\mathcal{B}}_N^v\dot{\boldsymbol{q}}_N - \sum_{j=1}^{N}\boldsymbol{\mathcal{A}}_{Nj}^v(\dot{\boldsymbol{q}}_N - \dot{\boldsymbol{q}}_j) \end{bmatrix}. \tag{164}$$

The first component in each block row damps the absolute velocity $\dot{\boldsymbol{q}}_i$ whereas the second component damps the relative velocities between agent i and its neighbors j.

Several practical results can be obtained from the damping condition (163) and the implementation (164). The first term in (164) can be implemented using only local information, achieving absolute damping. If all $\boldsymbol{\mathcal{B}}_i^v > 0$, then (163) is satisfied without having to communicate velocity information between neighbors ($\boldsymbol{\mathcal{A}}_{ij}^v = 0$), thus reducing the detrimental effects of communication time delays.

The single-agent damping conditions $\boldsymbol{\mathcal{B}}_i^v > \mathbf{0}_n$ can be relaxed to $\boldsymbol{\mathcal{B}}_i^v \geq \mathbf{0}_n$ as long as (163) holds. This is achieved if the velocity communication graph is connected and at least one $\boldsymbol{\mathcal{B}}_j^v > \mathbf{0}_n$. This situation may occur in practice if only leaders in a swarm of UAVs have accurate ground velocity information, while the other agents can only sense velocities relative to their neighbors, to apply relative damping.

7.2.3 *Control law for coordinate formations*

From (157), (162), and (164), the distributed control law to achieve a desired formation in all coordinates becomes, for each agent,

$$\boldsymbol{\tau}_i = \frac{\partial V_i}{\partial \boldsymbol{q}_i} + \boldsymbol{\mathcal{B}}_i(\boldsymbol{q}_i^* - \boldsymbol{q}_i) - \boldsymbol{\mathcal{B}}_i^v \dot{\boldsymbol{q}}_i + \sum_{j=1}^{N} \boldsymbol{\mathcal{A}}_{ij}(\boldsymbol{q}_j - \boldsymbol{q}_i - \boldsymbol{r}_{ij}^*) + \sum_{j=1}^{N} \boldsymbol{\mathcal{A}}_{ij}^v(\dot{\boldsymbol{q}}_j - \dot{\boldsymbol{q}}_i). \quad (165)$$

The control law simplifies depending on the group objective, summarized as:

- Formation with one or more leaders: $\exists\, i \,|\, \boldsymbol{\mathcal{B}}_i > \mathbf{0}_n$, and $\exists\, (i,j) \,|\, \boldsymbol{r}_{ij}^* \neq \boldsymbol{0}$,
- Synchronization with one or more leaders: $\exists\, i \,|\, \boldsymbol{\mathcal{B}}_i > \mathbf{0}_n$, and $\boldsymbol{r}_{ij}^* = \boldsymbol{0}$,
- Leaderless formation: $\boldsymbol{\mathcal{B}} = \mathbf{0}_{N\ell}$, and $\exists\, (i,j) \,|\, \boldsymbol{r}_{ij}^* \neq \boldsymbol{0}$,
- Leaderless synchronization: $\boldsymbol{\mathcal{B}} = \mathbf{0}_{N\ell}$ and $\boldsymbol{r}_{ij}^* = \boldsymbol{0}$.

Each objective may further be specialized to either absolute damping where all agents satisfy $\boldsymbol{\mathcal{B}}_i^v > \mathbf{0}_n$, and all $\boldsymbol{\mathcal{A}}_{ij}^v = \mathbf{0}_n$, or relative damping, where at least one $\boldsymbol{\mathcal{B}}_i^v > \mathbf{0}_n$ and the velocity graph is connected.

The resulting distributed PD control law is equivalent to a special case of the unified control scheme for fully-actuated systems discussed in Chapter 5, when the reference trajectory is constant.

7.3 POTENTIAL ENERGY SHAPING FOR TASK-SPACE FORMATIONS

Another practical distributed control objective of fully-actuated systems is a formation in workspace coordinates rather than in configuration coordinates. For example, a group of fully-actuated robotic manipulators can place their end-effectors in a formation in order to collaboratively grasp an object.

The task-space coordinate of one system is a nonlinear function of its generalized coordinates, denoted as $\boldsymbol{z}_i(\boldsymbol{q}_i) \in \mathbb{R}^\ell$, as shown in Figure 5 for $\ell = 2$. In this section we show that the quantities $\boldsymbol{z}_i$ can be collaboratively controlled using the previously introduced methods and control laws combined with the single-agent result given in Section 3.6.1.

As before, the network is made up of N agents, but they are allowed to have a different number of coordinates as long as each agent satisfies $\ell \leq n_i = m_i$. There is no secondary goal of stabilizing $\boldsymbol{\theta}_i$, other than making all coordinates stationary. The objectives of obtaining a stationary formation in $\boldsymbol{z}_i$ with or without leaders is summarized in (86), (88), (89).

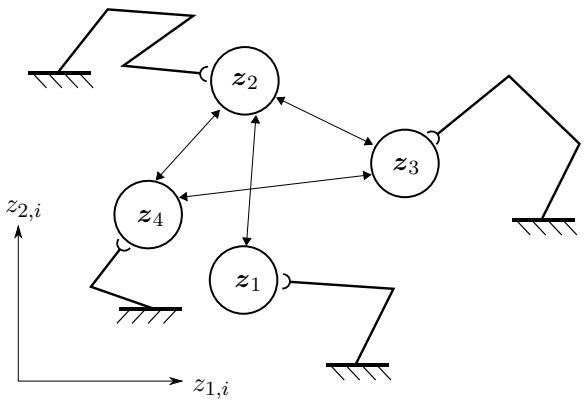

Figure 5: A heterogeneous group of fully-actuated robots collaboratively assume a formation in the task space by aiming to reach desired inter-agent configurations $\boldsymbol{r}_{ij}^*$.

7.3.1 *Control law for task-space formations*

In evaluating the fully-actuated distributed control law (157), a key role is played by the gradient of the desired potential energy, which we write as a function of the $\boldsymbol{z}_i$ variables, as $\bar{V}_\mathrm{d}(\boldsymbol{z}_1(\boldsymbol{q}_1), \dots, \boldsymbol{z}_N(\boldsymbol{q}_N))$. As shown in Appendix a.3.1, the gradient of such a scalar function with respect to the original coordinates $\boldsymbol{q}_i$ becomes:

$$\frac{\partial V_\mathrm{d}}{\partial \boldsymbol{q}_i} = \begin{bmatrix} \dfrac{\partial z_{1,i}}{\partial q_{1,i}} & \cdots & \dfrac{\partial z_{\ell,i}}{\partial q_{1,i}} \\ \vdots & & \vdots \\ \dfrac{\partial z_{1,i}}{\partial q_{n_i,i}} & \cdots & \dfrac{\partial z_{\ell,i}}{\partial q_{n_i,i}} \end{bmatrix} \frac{\partial V_\mathrm{d}}{\partial \boldsymbol{z}_i} = \boldsymbol{\Psi}_i \frac{\partial V_\mathrm{d}}{\partial \boldsymbol{z}_i} = \mathbf{A}_i^\top \frac{\partial V_\mathrm{d}}{\partial \boldsymbol{z}_i},$$

where $\mathbf{A}_i$ is often called the task-space Jacobian [56]. Choosing the absolute damping method of Section 7.2.2 and using the quadratic formation error potential (102), the distributed control law becomes, for each agent,

$$\boldsymbol{\tau}_i = \frac{\partial V_i}{\partial \boldsymbol{q}_i} + \mathbf{A}_i^\top \boldsymbol{\mathcal{B}}_i(\boldsymbol{z}_i^* - \boldsymbol{z}_i) + \mathbf{A}_i^\top \sum_{j=1}^{N} \boldsymbol{\mathcal{A}}_{ij}(\boldsymbol{z}_j - \boldsymbol{z}_i - \boldsymbol{r}_{ij}^*) - \mathbf{K}_{v,i}\boldsymbol{y}_i. \tag{166}$$

This result is similar to [38, 61], but it does not suffer from excessive joint rates near singular configurations, as briefly addressed for a simulation example in Section 12.2.3. A variation where damping is inserted using the absolute or relative end-effector velocities instead of through the joint rates is also possible (see Chapter 9).

8 SOLUTIONS FOR SELECTED UNDERACTUATED SYSTEMS

This chapter presents a solution to the distributed IDA-PBC problem of Chapter 6 for underactuated mechanical systems of the class described in Chapter 3.

Section 8.1 begins by formulating the assumptions for the single-agent solution in the context of the distributed IDA-PBC problem problem and shows how this leads to a solution of the distributed kinetic energy matching condition. Section 8.2 proposes a particular structure for the distributed closed-loop potential energy such that the distributed potential energy matching condition is always satisfied.

Section 8.3 continues by presenting a closed-loop potential energy that not only satisfies the matching condition, but which also satisfies the necessary positivity properties to achieve group objectives such as synchronization or formations. The resulting local and distributed control laws are given in Sections 8.4 and 8.5. Section 8.6 discusses the relation to the previously referenced stability proof, and Section 8.7 relates the result to distributed controlled Lagrangian systems.

8.1 DISTRIBUTED KINETIC ENERGY MATCHING CONDITION

The main assumption in this chapter is that for each system in the network, a single-agent IDA-PBC solution of the form given in Section 3.5.2 is known. This implies that $\mathbf{M}_\mathrm{d}(\boldsymbol{q})$, $\mathbf{J}(\boldsymbol{q},\boldsymbol{p})$, and $V_\mathrm{s}(\boldsymbol{q})$ in (29), (55) are known for each agent i. Using these known terms, we introduce the block diagonal matrices

$$\bar{\mathbf{F}}^\perp = \begin{bmatrix} \mathbf{F}_1^\perp & & \\ & \ddots & \\ & & \mathbf{F}_N^\perp \end{bmatrix} \quad \text{with} \quad \mathbf{F}_i^\perp = \mathbf{F}_i^\perp(\boldsymbol{q}_i), \tag{167}$$

$$\bar{\mathbf{M}}_\mathrm{d} = \begin{bmatrix} \mathbf{M}_{\mathrm{d},1} & & \\ & \ddots & \\ & & \mathbf{M}_{\mathrm{d},N} \end{bmatrix} \quad \text{with} \quad \mathbf{M}_{\mathrm{d},i} = \mathbf{M}_{\mathrm{d},i}(\boldsymbol{q}_i), \tag{168}$$

$$\bar{\mathbf{J}} = \begin{bmatrix} \mathbf{J}_1 & & \\ & \ddots & \\ & & \mathbf{J}_N \end{bmatrix} \quad \text{with} \quad \mathbf{J}_i = \mathbf{J}_i(\boldsymbol{q}_i,\boldsymbol{p}_i), \tag{169}$$

where each block corresponding to the i-th agent depends only on the state of the i-th agent. The inverse $\bar{\mathbf{M}}_\mathrm{d}^{-1}$ is a block diagonal matrix of the inverses $\mathbf{M}_{\mathrm{d},i}^{-1}$.

Substituting these block matrices into the distributed kinetic energy matching condition (148) gives

$$\bar{\mathbf{F}}^\perp \left(\frac{\partial\left(\sum_{i=1}^N \boldsymbol{p}_i^\top \mathbf{M}_i^{-1} \boldsymbol{p}_i\right)}{\partial \bar{\boldsymbol{q}}} - \bar{\mathbf{M}}_\mathrm{d}\bar{\mathbf{M}}^{-1} \frac{\partial\left(\sum_{i=1}^N \boldsymbol{p}_i^\top \mathbf{M}_{\mathrm{d},i}^{-1} \boldsymbol{p}_i\right)}{\partial \bar{\boldsymbol{q}}} + 2\bar{\mathbf{J}}\bar{\mathbf{M}}_\mathrm{d}^{-1}\bar{\boldsymbol{p}} \right) = \boldsymbol{0}. \tag{170}$$

Because each element i in the summed terms above only depends on on the state of agent i and because of the block diagonal structure, this gives N independent kinetic energy matching conditions of the form

$$\mathbf{F}_i^\perp \left(\frac{\partial\left(\boldsymbol{p}_i^\top \mathbf{M}_i^{-1} \boldsymbol{p}_i\right)}{\partial \boldsymbol{q}_i} - \mathbf{M}_{\mathrm{d},i}\mathbf{M}_i^{-1} \frac{\partial\left(\boldsymbol{p}_i^\top \mathbf{M}_{\mathrm{d},i}^{-1} \boldsymbol{p}_i\right)}{\partial \boldsymbol{q}_i} + 2\mathbf{J}_i\mathbf{M}_{\mathrm{d},i}^{-1}\boldsymbol{p}_i \right) = \boldsymbol{0} \quad \forall\, i = 1,\ldots,N. \tag{171}$$

Each matching condition corresponds directly to the single-agent kinetic energy matching condition (50), which is satisfied by the assumption that a single-agent solution is known for each agent.

8.2 DISTRIBUTED POTENTIAL ENERGY MATCHING CONDITION

Using the proposed partitioning of $\bar{\mathbf{M}}_\mathrm{d}$ in (168), the distributed potential energy matching condition (149) becomes

$$\begin{bmatrix} \mathbf{F}_1^\perp & & \\ & \ddots & \\ & & \mathbf{F}_N^\perp \end{bmatrix} \left(\begin{bmatrix} \frac{\partial V_1}{\partial \boldsymbol{q}_1} \\ \vdots \\ \frac{\partial V_N}{\partial \boldsymbol{q}_N} \end{bmatrix} - \begin{bmatrix} \mathbf{M}_{\mathrm{d},1}\mathbf{M}_1^{-1} & & \\ & \ddots & \\ & & \mathbf{M}_{\mathrm{d},N}\mathbf{M}_N^{-1} \end{bmatrix} \begin{bmatrix} \frac{\partial \bar{V}_\mathrm{d}}{\partial \boldsymbol{q}_1} \\ \vdots \\ \frac{\partial \bar{V}_\mathrm{d}}{\partial \boldsymbol{q}_N} \end{bmatrix} \right) = \boldsymbol{0}, \quad (172)$$

which can be separated into N block rows, given by

$$\mathbf{F}_i^\perp \left(\frac{\partial V_i}{\partial \boldsymbol{q}_i} - \mathbf{M}_{\mathrm{d},i}\mathbf{M}_i^{-1} \frac{\partial \bar{V}_\mathrm{d}}{\partial \boldsymbol{q}_i} \right) = \boldsymbol{0} \quad \forall\, i = 1, \ldots, N. \quad (173)$$

Whereas the term $\frac{\partial V_i}{\partial \boldsymbol{q}_i}$ in (173) depends only on $\boldsymbol{q}_i$, the term $\frac{\partial \bar{V}_\mathrm{d}}{\partial \boldsymbol{q}_i}$ generally depends on all coordinates $\bar{\boldsymbol{q}}$. This means that the distributed potential energy matching condition is not trivially satisfied using only the single-agent solution. Rather, we must choose a $\bar{V}_\mathrm{d}$ that satisfies (173) for all agents, while simultaneously ensuring that the desired group objective is achieved when $\bar{V}_\mathrm{d}$ reaches its minimum.

8.2.1 *Splitting the potential energy matching condition*

This section follows the steps in Section 3.5.2 to split the potential energy into components for internal stabilization of each agent and a component for achieving the group objective. To this end, we propose a desired potential energy of the network of the form

$$\bar{V}_\mathrm{d} = \bar{V}_\mathrm{c} + \sum_{i=1}^{N} V_{\mathrm{s},i}, \quad (174)$$

where $V_{\mathrm{s},i}$ are the known potentials V_s for each single-agent solution, and $\bar{V}_\mathrm{c}$ is a potential to be designed for achieving the group objective. Inserting (174) into the matching conditions (173) we obtain

$$\mathbf{F}_i^\perp \left(\frac{\partial V_i}{\partial \boldsymbol{q}_i} - \mathbf{M}_{\mathrm{d},i}\mathbf{M}_i^{-1} \frac{\partial V_{\mathrm{s},i}}{\partial \boldsymbol{q}_i} - \mathbf{M}_{\mathrm{d},i}\mathbf{M}_i^{-1} \frac{\partial \bar{V}_\mathrm{c}}{\partial \boldsymbol{q}_i} \right) = \boldsymbol{0} \quad \forall\, i = 1, \ldots, N. \quad (175)$$

Because the single-agent solution is known, we know a V_s that solves (58) for each agent. Specifically, for each agent we know that there holds:

$$\mathbf{F}_i^\perp \left(\frac{\partial V_i}{\partial \boldsymbol{q}_i} - \mathbf{M}_{\mathrm{d},i}\mathbf{M}_i^{-1} \frac{\partial V_{\mathrm{s},i}}{\partial \boldsymbol{q}_i} \right) = \boldsymbol{0} \quad \forall\, i = 1, \ldots, N \quad (176)$$

This simplifies the distributed potential energy matching condition (175) to

$$\mathbf{F}_i^\perp \mathbf{M}_{\mathrm{d},i}\mathbf{M}_i^{-1} \frac{\partial \bar{V}_\mathrm{c}}{\partial \boldsymbol{q}_i} = \boldsymbol{0} \quad \forall\, i = 1, \ldots, N. \quad (177)$$

8.2.2 *Solving the potential energy matching condition*

The condition (177) does not immediately extend from the single-agent condition (59) because $\bar{V}_\mathrm{c}$ generally depends on the coordinates of all agents. Instead, we propose a structure for $\bar{V}_\mathrm{c}$ of the form

$$\bar{V}_\mathrm{c}(\bar{\boldsymbol{z}}(\bar{\boldsymbol{q}})) = \bar{V}_\mathrm{c}(\boldsymbol{z}_1(\boldsymbol{q}_1), \dots, \boldsymbol{z}_N(\boldsymbol{q}_N)). \tag{178}$$

For this choice, the partial derivative to the coordinates of the i-th agent is

$$\frac{\partial \bar{V}_\mathrm{c}}{\partial \boldsymbol{q}_i} = \boldsymbol{\Psi}_i \frac{\partial \bar{V}_\mathrm{c}}{\partial \boldsymbol{z}_i}, \tag{179}$$

where as derived explicitly in Appendix a.3.2, the matrices $\boldsymbol{\Psi}_i$ are given by

$$\boldsymbol{\Psi}_i(\boldsymbol{q}_i) = \frac{\partial^\top \boldsymbol{z}_i}{\partial \boldsymbol{q}_i} = \begin{bmatrix} \frac{\partial z_{1,i}}{\partial q_{1,i}} & \cdots & \frac{\partial z_{\ell,i}}{\partial q_{1,i}} \\ \vdots & & \vdots \\ \frac{\partial z_{1,i}}{\partial q_{n_i,i}} & \cdots & \frac{\partial z_{\ell,i}}{\partial q_{n_i,i}} \end{bmatrix} \in \mathbb{R}^{n_i \times \ell}. \tag{180}$$

For the single-agent solution (59) holds, meaning that all agents satisfy

$$\mathbf{F}_i^\perp \mathbf{M}_{\mathrm{d},i} \mathbf{M}_i^{-1} \boldsymbol{\Psi}_i = \mathbf{0}_{(n_i - m_i)\times \ell} \quad \forall\, i = 1, \dots, N. \tag{181}$$

Then it follows that (177) holds since

$$\mathbf{F}_i^\perp \mathbf{M}_{\mathrm{d},i} \mathbf{M}_i^{-1} \frac{\partial \bar{V}_\mathrm{c}}{\partial \boldsymbol{q}_i} = \mathbf{F}_i^\perp \mathbf{M}_{\mathrm{d},i} \mathbf{M}_i^{-1} \boldsymbol{\Psi}_i \frac{\partial \bar{V}_\mathrm{c}}{\partial \boldsymbol{z}_i} = \boldsymbol{0} \quad \forall\, i = 1, \dots, N. \tag{182}$$

From the fact that (176), (177) hold, it follows that (175) and in turn (173), (172) hold, and we finally obtain that the distributed potential energy matching condition (149) holds. Because we have previously established that the distributed kinetic energy matching condition holds, the distributed matching problem is solved by choosing (168), (169), (174) if each agent has a single-agent solution of the form (55) and satisfies the conditions (50), (58), (59).

It is important to note that (171), (176), (177) are *local* matching conditions to each agent, depending only on their own coordinates and parameters. Consequently, no communication is required to satisfy the distributed potential energy matching condition or the distributed kinetic energy matching condition, enhancing robustness against communication delays or switching network topologies. Matching still holds if the agents are heterogeneous, whether they have different parameter values, different dynamics, or a different number of coordinates.

8.3 CONTROL OBJECTIVES AND THE CLOSED-LOOP POTENTIAL ENERGY

Although $\bar{V}_\mathrm{c}(\bar{\boldsymbol{z}})$ may be chosen freely as far as the matching problem is concerned, it should be chosen such that the total closed-loop potential energy (174) is positive (semi-)definite, and such that it reaches its minimum when the local and group objectives are met.

The local stabilization objectives are specified by (86)–(87) and the distributed formation objective in the cooperative coordinate $\boldsymbol{z}_i$ is specified by (88). If the

group has leaders that pursue fixed targets $\boldsymbol{z}_i^*$ the objective (89) also applies. These objectives are repeated here for completeness, giving

$$\begin{aligned}
&\lim_{t\to\infty} ||\boldsymbol{p}_i(t)|| = 0 \quad \forall\, i = 1,\dots,N,\\
&\lim_{t\to\infty} ||\boldsymbol{\theta}_i(t) - \boldsymbol{\theta}_i^*|| = 0 \quad \forall\, i = 1,\dots,N,\\
&\lim_{t\to\infty} ||\boldsymbol{z}_i(t) - \boldsymbol{z}_j(t) + \boldsymbol{r}_{ij}^*|| = 0 \quad \forall\, (i,j) \in \mathcal{E},\\
&\lim_{t\to\infty} ||\boldsymbol{z}_i(t) - \boldsymbol{z}_i^*|| = 0 \quad \forall\, i \in \mathcal{T}.
\end{aligned}$$

As before, $\boldsymbol{r}_{ij}^* = \boldsymbol{0}$ simplifies the group objective to (partial) synchronization.

The simplest coupling potential can be obtained directly as a sum of squares of the deviation from the formation objective. Using the adjacency and leader weights, this sum can be compactly written by summing over the agents and each of their neighbors as detailed in Section 4.3, giving

$$\begin{aligned}
\bar{V}_{\mathrm{c}} = \frac{1}{4}\sum_{i=1}^{N}\sum_{j=1}^{N} \left(\boldsymbol{z}_i - \boldsymbol{z}_j + \boldsymbol{r}_{ij}^*\right)^{\top} \boldsymbol{\mathcal{A}}_{ij} \left(\boldsymbol{z}_i - \boldsymbol{z}_j + \boldsymbol{r}_{ij}^*\right)\\
+ \frac{1}{2}\sum_{i=1}^{N} \left(\boldsymbol{z}_i - \boldsymbol{z}_i^*\right)^{\top} \boldsymbol{\mathcal{B}}_i \left(\boldsymbol{z}_i - \boldsymbol{z}_i^*\right) \geq 0,
\end{aligned} \tag{183}$$

The choice (183) ensures that $\bar{V}_{\mathrm{c}} \geq 0$ and $\bar{V}_{\mathrm{c}} = 0$ if and only if the formation objective is achieved. Likewise, the Jacobian

$$\frac{\partial \bar{V}_{\mathrm{c}}}{\partial \tilde{\boldsymbol{z}}} = \begin{bmatrix} \boldsymbol{\mathcal{B}}_1(\boldsymbol{z}_1 - \boldsymbol{z}_1^*) + \sum_{j=1}^{N} \boldsymbol{\mathcal{A}}_{1j}(\boldsymbol{z}_1 - \boldsymbol{z}_j + \boldsymbol{r}_{1j}^*) \\ \vdots \\ \boldsymbol{\mathcal{B}}_N(\boldsymbol{z}_N - \boldsymbol{z}_N^*) + \sum_{j=1}^{N} \boldsymbol{\mathcal{A}}_{Nj}(\boldsymbol{z}_N - \boldsymbol{z}_j + \boldsymbol{r}_{Nj}^*) \end{bmatrix} \tag{184}$$

equals zero if and only if the formation goal is satisfied. The total potential energy $\bar{V}_{\mathrm{d}}$ (174) equals zero when additionally all $V_{\mathrm{s},i}$ are zero, which is when the local control objectives are also achieved.

8.4 DISTRIBUTED DAMPING CONDITION

The damping criterion is similar to the fully-actuated case in Section 7.2.2. We now repeat those steps for the underactuated case. Damping is inserted through the damping force $-\bar{\mathbf{K}}_v \bar{\boldsymbol{y}}_{\mathrm{d}}$ in (147), based on the closed-loop output $\bar{\boldsymbol{y}}_{\mathrm{d}}$ given in (145) In addition to detectability, a damping condition for asymptotic stability is $\bar{\mathbf{K}}_v > \mathbf{0}_{\bar{m}}$. We propose to partition $\bar{\mathbf{K}}_v \in \mathbb{R}^{\bar{m}\times\bar{m}}$ as

$$\bar{\mathbf{K}}_v = \boldsymbol{\mathcal{L}}^v + \boldsymbol{\mathcal{B}}^v > \mathbf{0}_{\bar{m}}, \tag{185}$$

where $\boldsymbol{\mathcal{L}}^v$ and $\boldsymbol{\mathcal{B}}^v$ are the Laplacian and leader matrix corresponding to the closed-loop output information exchange graph. Using (184), the damping force equals

$$-\bar{\mathbf{K}}_v \bar{\boldsymbol{y}}_{\mathrm{d}} = \begin{bmatrix} -\boldsymbol{\mathcal{B}}_1^v \boldsymbol{y}_{\mathrm{d},1} - \sum_{j=1}^{N} \boldsymbol{\mathcal{A}}_{1j}^v (\boldsymbol{y}_{\mathrm{d},1} - \boldsymbol{y}_{\mathrm{d},j}) \\ \vdots \\ -\boldsymbol{\mathcal{B}}_N^v \boldsymbol{y}_{\mathrm{d},N} - \sum_{j=1}^{N} \boldsymbol{\mathcal{A}}_{Nj}^v (\boldsymbol{y}_{\mathrm{d},N} - \boldsymbol{y}_{\mathrm{d},j}) \end{bmatrix}, \tag{186}$$

where

$$\boldsymbol{y}_{\mathrm{d},i} = \mathbf{F}_i^\top \mathbf{M}_{\mathrm{d},i}^{-1} \boldsymbol{p}_i \in \mathbb{R}^{m_i}. \tag{187}$$

The first component in each block row damps the closed-loop output $\boldsymbol{y}_{\mathrm{d},i}$ whereas the second component damps the relative closed-loop output between agent i and its neighbors j.

Note that in this form, relative damping occurs in the configuration space, which is only possible if each system has an equal number of coordinates. A generalization that avoids this restriction is the exchange of task-space velocity information, as discussed in Part IV.

8.5 DISTRIBUTED CONTROL LAWS

Having satisfied the necessary matching conditions and having derived a total closed-loop potential energy function that satisfies the stability requirements, this section provides explicit descriptions of the control laws that must be implemented to achieve the desired closed-loop behavior.

The total control law is equal to (147) with, but we can use the previously made design choices to simplify the control expression and derive an explicit implementation for each agent in the network.

8.5.1 *Gradient of closed-loop energy*

We begin by deriving the expression $\frac{\partial \bar{H}_\mathrm{d}}{\partial \boldsymbol{q}_i}$ for each agent, with $\bar{\mathbf{M}}_\mathrm{d}$ given by (168) and $\bar{V}_\mathrm{d}$ given by (174):

$$\begin{aligned}
\frac{\partial \bar{H}_\mathrm{d}}{\partial \boldsymbol{q}_i} &= \frac{1}{2} \frac{\partial \bar{\boldsymbol{p}}^\top \bar{\mathbf{M}}_\mathrm{d}^{-1} \bar{\boldsymbol{p}}}{\partial \boldsymbol{q}_i} + \frac{\partial \bar{V}_\mathrm{d}}{\partial \boldsymbol{q}_i} \\
&= \frac{1}{2} \frac{\partial \left(\sum_{i=1}^N \boldsymbol{p}_i^\top \mathbf{M}_{\mathrm{d},i}^{-1} \boldsymbol{p}_i \right)}{\partial \boldsymbol{q}_i} + \left(\sum_{i=1}^N \frac{\partial V_{\mathrm{s},i}}{\partial \boldsymbol{q}_i} \right) + \frac{\partial \bar{V}_\mathrm{c}}{\partial \boldsymbol{q}_i} \\
&= \frac{1}{2} \frac{\partial \left(\boldsymbol{p}_i^\top \mathbf{M}_{\mathrm{d},i}^{-1} \boldsymbol{p}_i \right)}{\partial \boldsymbol{q}_i} + \frac{\partial V_{\mathrm{s},i}}{\partial \boldsymbol{q}_i} + \boldsymbol{\Psi}_i \frac{\partial \bar{V}_\mathrm{c}}{\partial \boldsymbol{z}_i}.
\end{aligned} \tag{188}$$

Substituting now the quadratic potential V_c (183) and its Jacobian (184) we obtain

$$\begin{aligned}
\frac{\partial \bar{H}_\mathrm{d}}{\partial \boldsymbol{q}_i} = \frac{1}{2} \frac{\partial \left(\boldsymbol{p}_i^\top \mathbf{M}_{\mathrm{d},i}^{-1} \boldsymbol{p}_i \right)}{\partial \boldsymbol{q}_i} + \frac{\partial V_{\mathrm{s},i}}{\partial \boldsymbol{q}_i} \\
- \boldsymbol{\Psi}_i \left(\boldsymbol{\mathcal{B}}_i (\boldsymbol{z}_i^* - \boldsymbol{z}_i) + \sum_{j=1}^N \boldsymbol{\mathcal{A}}_{ij} (\boldsymbol{z}_j - \boldsymbol{z}_i - \boldsymbol{r}_{ij}^*) \right).
\end{aligned} \tag{189}$$

8.5.2 *Inserting known terms*

The next step is to substitute the damping force (186) into the control law (147). Setting $\bar{\boldsymbol{\tau}}_\mathrm{d} = \boldsymbol{0}$ and restricting the result to absolute damping, we obtain for each agent

$$\boldsymbol{\tau}_i = \left(\mathbf{F}_i^\top \mathbf{F}_i \right)^{-1} \mathbf{F}_i^\top \left(\frac{\partial H_i}{\partial \boldsymbol{q}_i} - \mathbf{M}_{\mathrm{d},i} \mathbf{M}_i^{-1} \frac{\partial \bar{H}_\mathrm{d}}{\partial \boldsymbol{q}_i} + \mathbf{J}_i \mathbf{M}_{\mathrm{d},i}^{-1} \boldsymbol{p}_i \right) - \boldsymbol{\mathcal{B}}_i^v \boldsymbol{y}_{\mathrm{d},i}. \tag{190}$$

Finally, inserting (189) gives

$$\begin{aligned}\boldsymbol{\tau}_i = &\left(\mathbf{F}_i^\top \mathbf{F}_i\right)^{-1} \mathbf{F}_i^\top \left(\frac{\partial H_i}{\partial \boldsymbol{q}_i} + \mathbf{J}_i \mathbf{M}_{\mathrm{d},i}^{-1} \boldsymbol{p}_i - \mathbf{M}_{\mathrm{d},i} \mathbf{M}_i^{-1} \frac{\partial \left(\frac{1}{2} \boldsymbol{p}_i^\top \mathbf{M}_{\mathrm{d},i}^{-1} \boldsymbol{p}_i + V_{\mathrm{s},i} \right)}{\partial \boldsymbol{q}_i} \right) \\ &+ \left(\mathbf{F}_i^\top \mathbf{F}_i\right)^{-1} \mathbf{F}_i^\top \mathbf{M}_{\mathrm{d},i} \mathbf{M}_i^{-1} \boldsymbol{\Psi}_i \left(\boldsymbol{\mathcal{B}}_i (\boldsymbol{z}_i^* - \boldsymbol{z}_i) + \sum_{j=1}^{N} \boldsymbol{\mathcal{A}}_{ij} (\boldsymbol{z}_j - \boldsymbol{z}_i - \boldsymbol{r}_{ij}^*) \right) \\ &- \boldsymbol{\mathcal{B}}_i^v \boldsymbol{y}_{\mathrm{d},i}. \end{aligned} \tag{191}$$

8.5.3 *Control law per agent*

Following Section 3.5.3, the control laws may be abbreviated as

$$\boldsymbol{\tau}_i = \boldsymbol{\sigma}_i + \boldsymbol{\Phi}_i \left(\boldsymbol{\mathcal{B}}_i (\boldsymbol{z}_i^* - \boldsymbol{z}_i) + \sum_{j=1}^{N} \boldsymbol{\mathcal{A}}_{ij} (\boldsymbol{z}_j - \boldsymbol{z}_i - \boldsymbol{r}_{ij}^*) \right) - \boldsymbol{\mathcal{B}}_i^v \boldsymbol{y}_{\mathrm{d},i}, \tag{192}$$

where

$$\boldsymbol{\sigma}_i(\boldsymbol{q}_i, \boldsymbol{p}_i) = \left(\mathbf{F}_i^\top \mathbf{F}_i\right)^{-1} \mathbf{F}_i^\top \left(\frac{\partial H_i}{\partial \boldsymbol{q}_i} + \mathbf{J}_i \mathbf{M}_{\mathrm{d},i}^{-1} \boldsymbol{p}_i - \mathbf{M}_{\mathrm{d},i} \mathbf{M}_i^{-1} \frac{\partial \left(\frac{1}{2} \boldsymbol{p}_i \mathbf{M}_{\mathrm{d},i}^{-1} \boldsymbol{p}_i + V_{\mathrm{s},i} \right)}{\partial \boldsymbol{q}_i} \right) \tag{193}$$

locally shapes the kinetic energy and the potential energy component for internal stabilization, and

$$\boldsymbol{\Phi}_i(\boldsymbol{q}_i) = \left(\mathbf{F}_i^\top \mathbf{F}_i\right)^{-1} \mathbf{F}_i^\top \mathbf{M}_{\mathrm{d},i} \mathbf{M}_i^{-1} \boldsymbol{\Psi}_i \tag{194}$$

is an input matrix that ensures that the tracking control force $\frac{\partial V_{\mathrm{c}}}{\partial \boldsymbol{z}_i}$ does not violate the matching conditions local to each agent i.

The distributed control law (192) has a stabilization term $\boldsymbol{\sigma}_i(\boldsymbol{q}_i, \boldsymbol{p}_i) \in \mathbb{R}^{m_i}$ and a damping term $-\boldsymbol{\mathcal{B}}_i^v \boldsymbol{y}_{\mathrm{d},i}$, each depending only on local information, and a coupling force $-\boldsymbol{\Phi}_i(\boldsymbol{q}_i) \frac{\partial V_{\mathrm{c}}}{\partial \boldsymbol{z}_i}$ that depends on both local information and information $\boldsymbol{z}_j$ received from neighboring agents.

The control law simplifies depending on the group objective, summarized as:

- Formation with one or more leaders: $\exists\, i \,|\, \boldsymbol{\mathcal{B}}_i > \mathbf{0}_\ell$, and $\exists\, (i,j) \,|\, \boldsymbol{r}_{ij}^* \neq \boldsymbol{0}$,
- Synchronization with one or more leaders: $\exists\, i \,|\, \boldsymbol{\mathcal{B}}_i > \mathbf{0}_\ell$, and $\boldsymbol{r}_{ij}^* = \boldsymbol{0}$,
- Leaderless formation: $\boldsymbol{\mathcal{B}} = \mathbf{0}_{N\ell}$, and $\exists\, (i,j) \,|\, \boldsymbol{r}_{ij}^* \neq \boldsymbol{0}$,
- Leaderless synchronization: $\boldsymbol{\mathcal{B}} = \mathbf{0}_{N\ell}$ and $\boldsymbol{r}_{ij}^* = \boldsymbol{0}$.

8.5.4 *Relation to the fully-actuated result*

The control law (192)–(194) is a generalization of the fully-actuated control law (166). Recall that for the fully-actuated case $\mathbf{F}_i = \mathbf{I}_n$ and $\boldsymbol{\Psi}_i = \mathbf{A}_i^\top$. The mass matrix is unchanged ($\mathbf{M}_{\mathrm{d},i} = \mathbf{M}_i$) and accordingly (194) gives $\boldsymbol{\Phi}_i = \boldsymbol{\Psi}_i = \mathbf{A}_i^\top$. Finally, $V_{\mathrm{s},i} = 0$ and $\mathbf{J}_i = \mathbf{0}_{n_i}$ further reduces (193) to $\boldsymbol{\sigma}_i = \frac{\partial V_i}{\partial \boldsymbol{q}_i}$. This amounts to gravity compensation. Substituting these simplification into the distributed IDA-PBC control law (192) gives precisely the distributed Jacobian-transpose controller with gravity compensation given in (166).

8.6 RELATION TO STABILITY RESULT

Although the closed-loop system (144) has arguably more complex dynamics than a single controlled system (29), the structure of the dynamics and the corresponding stability analysis is equivalent. With the proposed solution in this chapter, the closed-loop potential energy $\bar{V}_\mathrm{d}$ has a unique minimum if the control objective is a stationary formation with one or more leaders, following Section 4.3.5 and the fact that all $V_{\mathrm{s},i}$ are minimal at the desired setpoints $\boldsymbol{\theta}_i^*$. The stability analysis then corresponds to the single-agent problem with a fixed target as discussed in Section 3.1.3.

If one or more coordinates $\boldsymbol{\theta}_i$ are free, or if the objective is a stationary formation without leaders, there is a range of equilibria and the analysis of Sections 4.3.6 and 3.1.4 applies. Care must be taken to analyze local extrema of the potential energy, where $\frac{\partial \bar{V}_\mathrm{d}}{\partial \boldsymbol{q}} = \boldsymbol{0}$, which may prevent the group from reaching their objective if simultaneously $\bar{\boldsymbol{p}} = \boldsymbol{0}$. This is discussed for a simulation example in Chapter 12.

8.7 RELATION TO THE METHOD OF CONTROLLED LAGRANGIANS

The method presented in this chapter has parallels to the distributed control method that uses the method of controlled Lagrangians [32], by virtue of the similarities of the single-agent solutions of CL and IDA-PBC [35]. This section treats several methodological and mathematical similarities and differences, and gives an overview of the additions provided by the method of this thesis.

8.7.1 *Distributed control approach*

Although the methods of controlled Lagrangians (CL) and IDA-PBC both suffer from the complexity of solving partial differential equations [35], the so-called simplified matching conditions [33, 34] used in CL reduce their complexity by restricting applications to systems that satisfy certain algebraic conditions on the uncontrolled mass matrix $\mathbf{M}_i$ and potential energy $\mathbf{V}_i$.

The work [32] restricts treatment to networks of mechanical systems that satisfy these simplified matching conditions. Using a similar top-down approach, a single Lagrangian model of the total uncontrolled network dynamics is constructed, and conditions and control laws are derived to obtain a desired controlled Lagrangian model that again satisfies the simplified matching conditions.

Through an appropriate set of coordinate transformations, a potential energy coupling mechanism is derived that can be satisfied by each agent independent of the network topology. This property is similar to (or possibly a special case of) the properties of the potential energy coupling mechanism and the decoupled matching conditions discussed in Section 8.2.2.

8.7.2 *Additions of distributed IDA-PBC*

For the single-agent case, the increased generality of IDA-PBC compared to CL has been a source of debate during the simultaneous development of both methods [26, 35]. Rather than restating the single-agent differences, we focus instead on the practical additions of the proposed distributed IDA-PBC method in terms of network interaction coupling mechanisms and task objectives.

Although some mechanisms exist to include dissipation and gyroscopic forces externally in CL methods [35], the assignable matrices $\bar{\mathbf{J}}$ and $\bar{\mathbf{K}}_v$ are absent in [32],

complicating the application and analysis of damping (Section 8.4), and conservative energy exchange (Section 13.4).

Additionally, the four main practical advantages of the method of this thesis are cooperation in task-space coordinates, cooperation between heterogeneous systems with a different configuration space, and the ability to create formations, with or without leaders. This contrasts to leaderless coordinate synchronization of homogeneous systems in [32].

These additions are made possible in part due to the simplified stability analysis followed in this thesis. By avoiding the explicit coordinate transformations in the desired dynamics (144), the conditions on the task-space variables $\boldsymbol{z}_i$ reduce to minimality conditions of the total desired potential energy. This contrasts to making $\boldsymbol{z}_i$ or $\boldsymbol{z}_i - \boldsymbol{z}_j$ a state variable and deriving its closed-loop dynamics to prove convergence to a (relative) target, which may not be possible if the mapping $\boldsymbol{z}_i(\boldsymbol{q}_i)$ is not invertible, as is typically the case with the end-effector of robotic manipulators. This poses no restrictions in our approach, as highlighted with an example in Chapter 12.

Part IV

INTERACTION WITH UNDERACTUATED AND DISTRIBUTED SYSTEMS

In the previous parts, the agents operated autonomously or cooperatively in a network. This part investigates how the presented single-agent and distributed control solutions can be used to shape not only the agent or network dynamics, but also how the agents or network can interact with external inputs and outputs.

Chapter 9 begins by further analyzing the single-agent IDA-PBC solution for shaping the input matrix of the desired dynamics, while Chapter 10 extends this result to the networked case. In both cases, we study how a human operator can use the altered input-output behavior to control a system or network in a supervisory manner, to alter its trajectory while the systems stabilize themselves internally.

9 INPUT MATRIX SHAPING FOR CONTROL BY INTERCONNECTION AND HUMAN INTERACTION

Typical single-agent IDA-PBC control techniques focus on assigning desired stable closed-loop dynamics, where less attention is given to the response of the closed-loop system to new external inputs, other than satisfying a passivity property. An overview of most standard PBC variants is given in [41], where the control laws are of the form $\boldsymbol{\tau} = \boldsymbol{\beta} + \boldsymbol{\tau}_{\mathrm{d}}$. This is the form (28) we have considered until now.

In this chapter we generalize this approach for the single-agent case, and derive how new control inputs can be designed to benefit from the energy shaping properties already obtained by the state feedback $\boldsymbol{\beta} \in \mathbb{R}^m$. This augments the shaping process to include shaping of the input-output dynamics rather than shaping of only the energy of the internal dynamics.

Section 9.1 and 9.2 generalize standard IDA-PBC to obtain the desired input-output shaping with an extended control law and an extended set of matching conditions. Section 9.3 interprets the result to stabilize systems using dynamical controllers connected to input-output pairs, while Section 9.4 uses the proposed control law to shape the way a human operator interacts with a mechanical system.

9.1 ORIGINAL AND DESIRED DYNAMICS

We now extend the original single-agent dynamics of Chapter 3 with the effect of an external input $\boldsymbol{\tau}_{\mathrm{h}} \in \mathbb{R}^\ell$ acting on the system at the location $\boldsymbol{z}(\boldsymbol{q}) \in \mathbb{R}^\ell$. The variable $\boldsymbol{z}(\boldsymbol{q})$ is defined as before, and may be considered to be a generalized "end-effector" position or task coordinate. The generalized input force $\boldsymbol{\tau}_{\mathrm{h}}$ acts on this point, yielding a generalized force $\boldsymbol{\Psi}\boldsymbol{\tau}_{\mathrm{h}}$, where $\boldsymbol{\Psi}$ is as in (57). This gives

$$\begin{bmatrix} \dot{\boldsymbol{q}} \\ \dot{\boldsymbol{p}} \end{bmatrix} = \begin{bmatrix} \mathbf{0}_n & \mathbf{I}_n \\ -\mathbf{I}_n & \mathbf{0}_n \end{bmatrix} \begin{bmatrix} \dfrac{\partial H}{\partial \boldsymbol{q}} \\ \dfrac{\partial H}{\partial \boldsymbol{p}} \end{bmatrix} + \begin{bmatrix} \mathbf{0}_{n\times m} \\ \mathbf{F} \end{bmatrix} \boldsymbol{\tau} + \begin{bmatrix} \mathbf{0}_{n\times \ell} \\ \boldsymbol{\Psi} \end{bmatrix} \boldsymbol{\tau}_{\mathrm{h}}, \tag{195}$$

$$\boldsymbol{y} = \mathbf{F}^\top \frac{\partial H}{\partial \boldsymbol{p}} = \mathbf{F}^\top \mathbf{M}^{-1} \boldsymbol{p}, \tag{196}$$

$$H = \frac{1}{2} \boldsymbol{p}^\top \mathbf{M}^{-1} \boldsymbol{p} + V. \tag{197}$$

The input force $\boldsymbol{\tau}_{\mathrm{h}}$ can be a disturbance or a human input force, which is assumed to be measurable by a sensor whose deformations are assumed to be negligible.

The desired dynamics are similar to (29), augmented with an additional dissipation term with the matrix $\mathbf{K}_{\mathrm{d}}$, a new external control input $\boldsymbol{\tau}_{\mathrm{e}} \in \mathbb{R}^\ell$ acting through a new input matrix $\mathbf{F}_{\mathrm{d}} \in \mathbb{R}^{n\times \ell}$, and a new output $\boldsymbol{y}_{\mathrm{e}} \in \mathbb{R}^\ell$, given by

$$\begin{bmatrix} \dot{\boldsymbol{q}} \\ \dot{\boldsymbol{p}} \end{bmatrix} = \begin{bmatrix} \mathbf{0}_n & \mathbf{M}^{-1}\mathbf{M}_{\mathrm{d}} \\ -\mathbf{M}_{\mathrm{d}}\mathbf{M}^{-1} & \mathbf{J} - \mathbf{F}\mathbf{K}_v\mathbf{F}^\top - \mathbf{F}_{\mathrm{d}}\mathbf{K}_{\mathrm{d}}\mathbf{F}_{\mathrm{d}}^\top \end{bmatrix} \begin{bmatrix} \dfrac{\partial H_{\mathrm{d}}}{\partial \boldsymbol{q}} \\ \dfrac{\partial H_{\mathrm{d}}}{\partial \boldsymbol{p}} \end{bmatrix} + \begin{bmatrix} \mathbf{0}_{n\times \ell} \\ \mathbf{F}_{\mathrm{d}} \end{bmatrix} \boldsymbol{\tau}_{\mathrm{e}}, \tag{198}$$

$$\boldsymbol{y}_{\mathrm{e}} = \mathbf{F}_{\mathrm{d}}^\top \frac{\partial H_{\mathrm{d}}}{\partial \boldsymbol{p}} = \mathbf{F}_{\mathrm{d}}^\top \mathbf{M}_{\mathrm{d}}^{-1} \boldsymbol{p}, \tag{199}$$

$$H_{\mathrm{d}} = \frac{1}{2} \boldsymbol{p}^\top \mathbf{M}_{\mathrm{d}}^{-1} \boldsymbol{p} + V_{\mathrm{d}}. \tag{200}$$

The desired dynamics are passive with respect to the input $\boldsymbol{\tau}_\mathrm{e}$, output $\boldsymbol{y}_\mathrm{e}$ and the storage function H_d, which can be shown as before, using

$$\begin{aligned}\dot{H}_\mathrm{d} &= \begin{bmatrix}\dfrac{\partial^\top H_\mathrm{d}}{\partial \boldsymbol{q}} & \dfrac{\partial^\top H_\mathrm{d}}{\partial \boldsymbol{p}}\end{bmatrix}\begin{bmatrix}\mathbf{0}_n & \mathbf{M}^{-1}\mathbf{M}_\mathrm{d} \\ -\mathbf{M}_\mathrm{d}\mathbf{M}^{-1} & \mathbf{J}-\mathbf{F}\mathbf{K}_v\mathbf{F}^\top-\mathbf{F}_\mathrm{d}\mathbf{K}_\mathrm{d}\mathbf{F}_\mathrm{d}^\top\end{bmatrix}\begin{bmatrix}\dfrac{\partial H_\mathrm{d}}{\partial \boldsymbol{q}} \\ \dfrac{\partial H_\mathrm{d}}{\partial \boldsymbol{p}}\end{bmatrix} \\ &\quad + \begin{bmatrix}\dfrac{\partial^\top H_\mathrm{d}}{\partial \boldsymbol{q}} & \dfrac{\partial^\top H_\mathrm{d}}{\partial \boldsymbol{p}}\end{bmatrix}\begin{bmatrix}\mathbf{0}_{n\times\ell} \\ \mathbf{F}_\mathrm{d}\end{bmatrix}\boldsymbol{\tau}_\mathrm{e} \\ &= -\frac{\partial^\top H_\mathrm{d}}{\partial \boldsymbol{p}}\left(\mathbf{F}\mathbf{K}_v\mathbf{F}^\top+\mathbf{F}_\mathrm{d}\mathbf{K}_\mathrm{d}\mathbf{F}_\mathrm{d}^\top\right)\frac{\partial H_\mathrm{d}}{\partial \boldsymbol{p}}+\frac{\partial^\top H_\mathrm{d}}{\partial \boldsymbol{p}}\mathbf{F}_\mathrm{d}\boldsymbol{\tau}_\mathrm{e} \\ &\leq \boldsymbol{y}_\mathrm{e}^\top\boldsymbol{\tau}_\mathrm{e}. \end{aligned} \tag{201}$$

9.2 CONTROL LAW AND MATCHING CONDITIONS

This section follows the strategy of Chapter 3 to re-derive the IDA-PBC control law and matching conditions that turn the augmented open-loop dynamics (195) into the augmented desired dynamics (198), by setting them equal and solving for the control signal $\boldsymbol{\tau}$. This yields the equality

$$\begin{aligned}\begin{bmatrix}\mathbf{F}^\perp \\ \mathbf{F}^\top\end{bmatrix}\mathbf{F}\boldsymbol{\tau} &= \begin{bmatrix}\mathbf{F}^\perp \\ \mathbf{F}^\top\end{bmatrix}\left(\frac{\partial H}{\partial \boldsymbol{q}}-\mathbf{M}_\mathrm{d}\mathbf{M}^{-1}\frac{\partial H_\mathrm{d}}{\partial \boldsymbol{q}}+\mathbf{J}\mathbf{M}_\mathrm{d}^{-1}\boldsymbol{p}\right) \\ &\quad+\begin{bmatrix}\mathbf{F}^\perp \\ \mathbf{F}^\top\end{bmatrix}\left(-\mathbf{F}\mathbf{K}_v\mathbf{F}^\top\mathbf{M}_\mathrm{d}^{-1}\boldsymbol{p}-\mathbf{F}_\mathrm{d}\mathbf{K}_\mathrm{d}\mathbf{F}_\mathrm{d}^\top\mathbf{M}_\mathrm{d}^{-1}\boldsymbol{p}+\mathbf{F}_\mathrm{d}\boldsymbol{\tau}_\mathrm{e}-\boldsymbol{\Psi}\boldsymbol{\tau}_\mathrm{h}\right),\end{aligned} \tag{202}$$

where the top block row yields the matching condition and the bottom row yields the control law, given by

$$\begin{aligned}\boldsymbol{\tau} &= \left(\mathbf{F}^\top\mathbf{F}\right)^{-1}\mathbf{F}^\top\left(\frac{\partial H}{\partial \boldsymbol{q}}-\mathbf{M}_\mathrm{d}\mathbf{M}^{-1}\frac{\partial H_\mathrm{d}}{\partial \boldsymbol{q}}+\mathbf{J}\mathbf{M}_\mathrm{d}^{-1}\boldsymbol{p}\right)-\mathbf{K}_v\boldsymbol{y}_\mathrm{d} \\ &\quad-\left(\mathbf{F}^\top\mathbf{F}\right)^{-1}\mathbf{F}^\top\mathbf{F}_\mathrm{d}\mathbf{K}_\mathrm{d}\mathbf{F}_\mathrm{d}^\top\mathbf{M}_\mathrm{d}^{-1}\boldsymbol{p}+\left(\mathbf{F}^\top\mathbf{F}\right)^{-1}\mathbf{F}^\top\left(\mathbf{F}_\mathrm{d}\boldsymbol{\tau}_\mathrm{e}-\boldsymbol{\Psi}\boldsymbol{\tau}_\mathrm{h}\right).\end{aligned} \tag{203}$$

Standard IDA-PBC control (49) is obtained when $\mathbf{K}_\mathrm{d}=\mathbf{0}_\ell$, $\mathbf{F}_\mathrm{d}=\mathbf{F}$, and $\boldsymbol{\tau}_\mathrm{e}=\boldsymbol{\tau}_\mathrm{d}$. The matching condition obtained from (202) is

$$\begin{aligned}\boldsymbol{0} &= \mathbf{F}^\perp\left(\frac{\partial H}{\partial \boldsymbol{q}}-\mathbf{M}_\mathrm{d}\mathbf{M}^{-1}\frac{\partial H_\mathrm{d}}{\partial \boldsymbol{q}}+\mathbf{J}\mathbf{M}_\mathrm{d}^{-1}\boldsymbol{p}\right) \\ &\quad+\mathbf{F}^\perp\left(-\mathbf{F}\mathbf{K}_v\mathbf{F}^\top\mathbf{M}_\mathrm{d}^{-1}\boldsymbol{p}-\mathbf{F}_\mathrm{d}\mathbf{K}_\mathrm{d}\mathbf{F}_\mathrm{d}^\top\mathbf{M}_\mathrm{d}^{-1}\boldsymbol{p}+\mathbf{F}_\mathrm{d}\boldsymbol{\tau}_\mathrm{e}-\boldsymbol{\Psi}\boldsymbol{\tau}_\mathrm{h}\right),\end{aligned} \tag{204}$$

where the first term is equal to the standard IDA-PBC condition (46) that we (conservatively) split to the kinetic and potential energy conditions (50), (58), (59), and the second term simplifies to

$$\mathbf{F}^\perp\left(-\mathbf{F}_\mathrm{d}\mathbf{K}_\mathrm{d}\mathbf{F}_\mathrm{d}^\top\mathbf{M}_\mathrm{d}^{-1}\boldsymbol{p}+\mathbf{F}_\mathrm{d}\boldsymbol{\tau}_\mathrm{e}-\boldsymbol{\Psi}\boldsymbol{\tau}_\mathrm{h}\right)=\boldsymbol{0}. \tag{205}$$

The augmented IDA-PBC problem thus comes with an additional matching condition that imposes limitations on the new external input $\boldsymbol{\tau}_\mathrm{e}$ and the assignable input matrices $\mathbf{F}_\mathrm{d}$, for a given human input or disturbance $\boldsymbol{\tau}_\mathrm{h}$.

Two separate solutions are presented in the next sections, which differ in whether a human input is present ($\boldsymbol{\tau}_\mathrm{h}\neq\boldsymbol{0}$ in Section 9.4) or not ($\boldsymbol{\tau}_\mathrm{h}=\boldsymbol{0}$ in Section 9.3).

9.3 CONTROL BY INTERCONNECTION

This section revisits the single-agent IDA-PBC solution of Chapter 3 (without human input) to obtain identical closed-loop behavior using a control by interconnection approach [41], by splitting the desired closed-loop dynamics into a dynamically shaped system with the input $\boldsymbol{\tau}_\mathrm{e}$ and output $\boldsymbol{y}_\mathrm{e}$, and a dynamical controller.

9.3.1 *Solution to the input matrix matching condition*

Without human input ($\boldsymbol{\tau}_\mathrm{h} = \boldsymbol{0}$), the input matching condition (205) becomes

$$\mathbf{F}^\perp \left(-\mathbf{F}_\mathrm{d} \mathbf{K}_\mathrm{d} \mathbf{F}_\mathrm{d}^\top \mathbf{M}_\mathrm{d}^{-1} \boldsymbol{p} + \mathbf{F}_\mathrm{d} \boldsymbol{\tau}_\mathrm{e} \right) = \boldsymbol{0}. \tag{206}$$

Because we wish the new input $\boldsymbol{\tau}_\mathrm{e} \in \mathbb{R}^\ell$ to be free, we obtain a matching condition for the shaped input matrix $\mathbf{F}_\mathrm{d} \in \mathbb{R}^{n \times \ell}$, given by

$$\mathbf{F}^\perp \mathbf{F}_\mathrm{d} = \mathbf{0}_{(n-m)\times \ell}. \tag{207}$$

This condition can be satisfied by the previously imposed matching condition (59), which implies that we can choose

$$\mathbf{F}_\mathrm{d} = \mathbf{M}_\mathrm{d} \mathbf{M}^{-1} \boldsymbol{\Psi}. \tag{208}$$

9.3.2 *Passive input-output pair*

For the selected input matrix $\mathbf{F}_\mathrm{d}$, we obtain an explicit expression for the output $\boldsymbol{y}_\mathrm{e}$, which shows that the output is the time derivative of the coordinate $\boldsymbol{z}(\boldsymbol{q})$:

$$\boldsymbol{y}_\mathrm{e} = \mathbf{F}_\mathrm{d}^\top \frac{\partial H_\mathrm{d}}{\partial \boldsymbol{p}} = \mathbf{F}_\mathrm{d}^\top \mathbf{M}_\mathrm{d}^{-1} \boldsymbol{p} = \boldsymbol{\Psi}^\top \mathbf{M}^{-1} \boldsymbol{p} = \frac{\partial \boldsymbol{z}}{\partial \boldsymbol{q}} \dot{\boldsymbol{q}} = \frac{\mathrm{d}}{\mathrm{d}t} \boldsymbol{z}. \tag{209}$$

9.3.3 *Externalizing the feedback signal*

Recall from Chapter 3 that the desired Hamiltonian is of the form

$$H_\mathrm{d}(\boldsymbol{q}, \boldsymbol{p}) = \frac{1}{2} \boldsymbol{p}^\top \mathbf{M}_\mathrm{d}^{-1}(\boldsymbol{q}) \boldsymbol{p} + V_\mathrm{s}(\boldsymbol{q}) + V_\mathrm{c}(\boldsymbol{z}(\boldsymbol{q})). \tag{210}$$

If we introduce an energy term $H_{\mathrm{d/c}}(\boldsymbol{q}, \boldsymbol{p}) = H_\mathrm{d}(\boldsymbol{q}, \boldsymbol{p}) - V_\mathrm{c}(\boldsymbol{z}(\boldsymbol{q}))$ we can write the dynamics (198) equivalently as

$$\begin{aligned} \begin{bmatrix} \dot{\boldsymbol{q}} \\ \dot{\boldsymbol{p}} \end{bmatrix} = & \begin{bmatrix} \mathbf{0}_n & \mathbf{M}^{-1}\mathbf{M}_\mathrm{d} \\ -\mathbf{M}_\mathrm{d}\mathbf{M}^{-1} & \mathbf{J} - \mathbf{F}\mathbf{K}_v\mathbf{F}^\top \end{bmatrix} \begin{bmatrix} \dfrac{\partial H_{\mathrm{d/c}}}{\partial \boldsymbol{q}} \\ \dfrac{\partial H_{\mathrm{d/c}}}{\partial \boldsymbol{p}} \end{bmatrix} + \begin{bmatrix} \mathbf{0}_{n\times\ell} \\ \mathbf{F}_\mathrm{d} \end{bmatrix} \boldsymbol{\tau}_\mathrm{e} \\ & + \begin{bmatrix} \mathbf{0}_n \\ -\mathbf{M}_\mathrm{d}\mathbf{M}^{-1} \end{bmatrix} \frac{\partial V_\mathrm{c}}{\partial \boldsymbol{q}} + \begin{bmatrix} \mathbf{0}_n \\ -\mathbf{F}_\mathrm{d}\mathbf{K}_\mathrm{d}\mathbf{F}_\mathrm{d}^\top \end{bmatrix} \frac{\partial H_{\mathrm{d/c}}}{\partial \boldsymbol{p}}. \end{aligned} \tag{211}$$

Using definition (208) for $\mathbf{F}_\mathrm{d}$, this can be compactly written as the dynamical system

$$\begin{bmatrix}\dot{\boldsymbol{q}}\\ \dot{\boldsymbol{p}}\end{bmatrix} = \begin{bmatrix}\mathbf{0}_n & \mathbf{M}^{-1}\mathbf{M}_\mathrm{d}\\ -\mathbf{M}_\mathrm{d}\mathbf{M}^{-1} & \mathbf{J}-\mathbf{F}\mathbf{K}_v\mathbf{F}^\top\end{bmatrix}\begin{bmatrix}\dfrac{\partial H_{\mathrm{d/c}}}{\partial \boldsymbol{q}}\\ \dfrac{\partial H_{\mathrm{d/c}}}{\partial \boldsymbol{p}}\end{bmatrix} + \begin{bmatrix}\mathbf{0}_{n\times\ell}\\ \mathbf{F}_\mathrm{d}\end{bmatrix}\boldsymbol{u}_\mathrm{d}, \tag{212}$$

$$\boldsymbol{y}_\mathrm{e} = \mathbf{F}_\mathrm{d}^\top\mathbf{M}_\mathrm{d}^{-1}\boldsymbol{p} = \frac{\mathrm{d}}{\mathrm{d}t}\boldsymbol{z}, \tag{213}$$

$$H_{\mathrm{d/c}} = \frac{1}{2}\boldsymbol{p}^\top\mathbf{M}_\mathrm{d}^{-1}\boldsymbol{p} + V_\mathrm{s}, \tag{214}$$

$$\boldsymbol{u}_\mathrm{d} = \boldsymbol{\tau}_\mathrm{e} + \boldsymbol{\tau}_\mathrm{z}, \tag{215}$$

where the signal $\boldsymbol{\tau}_\mathrm{z} \in \mathbb{R}^\ell$ must be defined as $\boldsymbol{\tau}_\mathrm{z} = -\frac{\partial V_\mathrm{c}}{\partial \boldsymbol{z}} - \mathbf{K}_\mathrm{d}\boldsymbol{y}_\mathrm{e}$. We have obtained a system equivalent to (198), but part of the stabilization and damping forces are externalized in $\boldsymbol{\tau}_\mathrm{z}$ rather than being embedded in the energy function gradient and dissipation.

9.3.4 *Control signal generation*

The feedback signal $\boldsymbol{\tau}_\mathrm{z}$ can be obtained as the negative of the output of a dynamical controller. Define the controller with input $\boldsymbol{u}_\xi \in \mathbb{R}^\ell$, output $\boldsymbol{y}_\xi \in \mathbb{R}^\ell$, state $\boldsymbol{\xi}_\xi \in \mathbb{R}^\ell$ and storage function $H(\boldsymbol{\xi}_\xi) \in \mathbb{R}$ as

$$\dot{\boldsymbol{\xi}}_\xi = \boldsymbol{u}_\xi, \tag{216}$$

$$\boldsymbol{y}_\xi = \frac{\partial H_\xi(\boldsymbol{\xi}_\xi)}{\partial \boldsymbol{\xi}_\xi} + \mathbf{K}_\mathrm{d}\boldsymbol{u}_\xi. \tag{217}$$

The control signal is obtained as the negative feedback interconnection $\boldsymbol{\tau}_\mathrm{z} = -\boldsymbol{y}_\xi$ and $\boldsymbol{u}_\xi = \boldsymbol{y}_\mathrm{e}$. In this case the state $\boldsymbol{\xi}_\xi$ is the integral of $\boldsymbol{y}_\mathrm{e}$, such that it plays the role of $\boldsymbol{z}$ in the original dynamics, when initialized at time t_0 as $\boldsymbol{\xi}_\xi(t_0) = \boldsymbol{z}(\boldsymbol{q}(t_0))$.

9.3.5 *Port-controlled dynamics*

The dynamical controller and its interconnection with the system can be represented schematically as shown in Figure 6. Because the closed-loop dynamics are equivalent to the stable system (198), this interconnection is also stable.

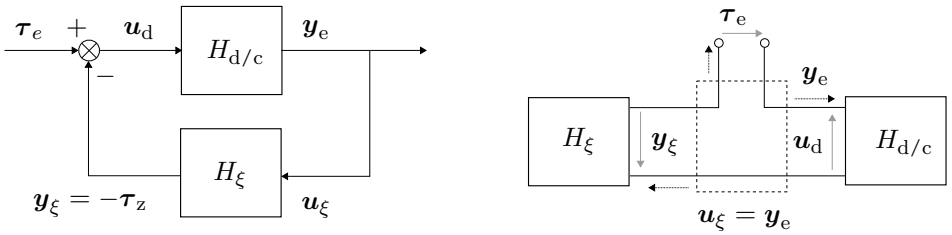

Figure 6: Negative feedback interconnection of the dynamical controller (216), (217) with the shaped IDA-PBC system (212)–(214). The feedback diagram (left) is equivalent to the power-based representation [41] (right).

A different stability analysis can be carried out based on passivity properties, by noting that the two subsystems are passive and that they are connected using a passivity preserving interconnection. Passivity (or strict passivity) of the shaped

IDA-PBC system can be obtained as before. To see that the dynamical controller is passive with respect to its storage function H_ξ we can write

$$\frac{\mathrm{d}}{\mathrm{d}t}H_\xi = \frac{\partial^\top H_\xi}{\partial \boldsymbol{\xi}_\xi}\dot{\boldsymbol{\xi}}_\xi = (\boldsymbol{y}_\xi^\top - \boldsymbol{u}_\xi^\top \mathbf{K}_\mathrm{d})\boldsymbol{u}_\xi = \boldsymbol{y}_\xi^\top \boldsymbol{u}_\xi - \boldsymbol{u}_\xi^\top \mathbf{K}_\mathrm{d}\boldsymbol{u}_\xi, \tag{218}$$

which gives input strict passivity if $\mathbf{K}_\mathrm{d} > \mathbf{0}_\ell$. An in-depth passivity analysis of negative feedback interconnections is given in [25].

The properties of the resulting single-agent input-output behavior are closely related to the requirements for agents in a bottom-up distributed control scheme. Some implications of this are discussed for further exploration in Section 13.2.

9.4 INPUT SHAPING FOR HUMAN-MACHINE INTERACTION

This section considers the control problem of shaping the dynamics of a system along with its input-output behavior, to alter the way a system responds to a human input force, as shown in Figure 7. For example, if the physical system has a high mass, an internal control law can be used to amplify the measured human force to make it easier to manipulate the system. Likewise, it can be used to simplify the end-effector behavior of a nonlinear robotic manipulator. The next chapter describes how this approach can be extended to teleoperation of a remote system.

The internal control objective is to choose the actuator signals $\boldsymbol{\tau}$ such that we obtain a desired system behavior as a function of the human input $\boldsymbol{\tau}_\mathrm{h}$, while simultaneously canceling any effects of the real force $\boldsymbol{\tau}_\mathrm{h}$ acting on the system, as shown in Figure 7. The uncontrolled dynamics subject to the human input are given by (195).

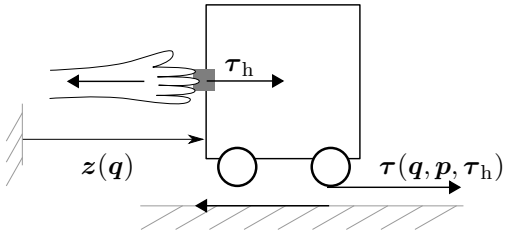

Figure 7: The controlled system exerts a control force $\boldsymbol{\tau}$ as a function of the measured human input $\boldsymbol{\tau}_\mathrm{h}$. This yields a total force $\boldsymbol{\tau}_\mathrm{h} + \boldsymbol{\tau}$ that results in an acceleration as a function of $\boldsymbol{\tau}_\mathrm{h}$ through a desired set of dynamics. This makes it possible to prescribe the perceived mass of the system.

9.4.1 *Desired dynamics*

In order to emulate any desired mechanical system, the desired behavior is described by (198), where we wish the virtual input $\boldsymbol{\tau}_\mathrm{e}$ to be the human input $\boldsymbol{\tau}_\mathrm{h}$, giving

$$\begin{bmatrix}\dot{\boldsymbol{q}}\\ \dot{\boldsymbol{p}}\end{bmatrix} = \begin{bmatrix}\mathbf{0}_n & \mathbf{M}^{-1}\mathbf{M}_\mathrm{d}\\ -\mathbf{M}_\mathrm{d}\mathbf{M}^{-1} & \mathbf{J} - \mathbf{F}\mathbf{K}_v\mathbf{F}^\top - \mathbf{F}_\mathrm{d}\mathbf{K}_\mathrm{d}\mathbf{F}_\mathrm{d}^\top\end{bmatrix}\begin{bmatrix}\dfrac{\partial H_\mathrm{d}}{\partial \boldsymbol{q}}\\ \dfrac{\partial H_\mathrm{d}}{\partial \boldsymbol{p}}\end{bmatrix} + \begin{bmatrix}\mathbf{0}_{n\times\ell}\\ \mathbf{F}_\mathrm{d}\end{bmatrix}\boldsymbol{\tau}_\mathrm{h}, \tag{219}$$

$$\boldsymbol{y}_\mathrm{e} = \mathbf{F}_\mathrm{d}^\top\frac{\partial H_\mathrm{d}}{\partial \boldsymbol{p}} = \mathbf{F}_\mathrm{d}^\top\mathbf{M}_\mathrm{d}^{-1}\boldsymbol{p}, \tag{220}$$

$$H_\mathrm{d} = \frac{1}{2}\boldsymbol{p}^\top\mathbf{M}_\mathrm{d}^{-1}\boldsymbol{p} + V_\mathrm{d}. \tag{221}$$

The control law (203) and and input shaping matching condition (205) are as before, with $\boldsymbol{\tau}_\mathrm{e}$ replaced by $\boldsymbol{\tau}_\mathrm{h}$.

9.4.2 *Human input matching condition*

With $\boldsymbol{\tau}_\mathrm{e} = \boldsymbol{\tau}_\mathrm{h}$ the matching condition (205) becomes

$$\mathbf{F}^\perp \left(-\mathbf{F}_\mathrm{d}\mathbf{K}_\mathrm{d}\mathbf{F}_\mathrm{d}^\top \mathbf{M}_\mathrm{d}^{-1}\boldsymbol{p} + \mathbf{F}_\mathrm{d}\boldsymbol{\tau}_\mathrm{h} - \boldsymbol{\Psi}\boldsymbol{\tau}_\mathrm{h} \right) = \boldsymbol{0}. \tag{222}$$

Like any previously given matching condition, this condition imposes constraints on the forces and desired dynamics that can be produced or assigned, in the case of underactuation.

In this case, the condition imposes limitations on the assignable damping of the output $\boldsymbol{y}_\mathrm{e}$ as well as on the allowed human input forces $\boldsymbol{\tau}_\mathrm{h}$. This arises because the physical effect of the human input force in (195), given by $\boldsymbol{\Psi}\boldsymbol{\tau}_\mathrm{h}$, does not appear in the desired dynamics (198); it is canceled and a new desired force $\mathbf{F}_\mathrm{d}\boldsymbol{\tau}_\mathrm{h}$ is added instead. This is possible only if the matching condition holds, which reflects the presence of the term $\mathbf{F}_\mathrm{d}\boldsymbol{\tau}_\mathrm{h} - \boldsymbol{\Psi}\boldsymbol{\tau}_\mathrm{h}$.

Limitations on the human input and conjugate output are clearly undesirable, as the human operator may produce unknown input forces and ultimately unknown changes in the output. Hence, we are interested in solving the condition for any input $\boldsymbol{\tau}_\mathrm{h}$, at the cost of imposing more constraints on other design parameters. Allowing any $\boldsymbol{\tau}_\mathrm{h}$ and any damping $\mathbf{K}_\mathrm{d}\boldsymbol{y}_\mathrm{e}$ implies that we must require

$$\mathbf{F}^\perp \mathbf{F}_\mathrm{d} = \mathbf{0}_{(n-m)\times \ell}, \tag{223}$$

$$\mathbf{F}^\perp \boldsymbol{\Psi} = \mathbf{0}_{(n-m)\times \ell}. \tag{224}$$

The potential energy condition (59) already imposes that $\mathbf{F}^\perp \mathbf{M}_\mathrm{d}\mathbf{M}^{-1}\boldsymbol{\Psi} = \mathbf{0}_{(n-m)\times \ell}$. This means that a conservative way to satisfy (223), (224) is to choose $\mathbf{F}_\mathrm{d} = \boldsymbol{\Psi}$ and to require that $\mathbf{M}_\mathrm{d} = \mathbf{M}$, implying that we can only shape the input matrix of underactuated systems when there is no kinetic energy shaping.

A less conservative statement is to require that only the kinetic energy of unactuated coordinates cannot be shaped when allowing free human inputs. This will be exploited in Chapter 10, where a human operator can control a group of underactuated robots through a fully-actuated control interface.

9.4.3 *Human input force shaping in the fully-actuated case*

Contrary to the underactuated case, no matching conditions are imposed on fully-actuated systems, implying that $\mathbf{F}_\mathrm{d}$ may be chosen as desired. However, choosing

$$\mathbf{F}_\mathrm{d} = \mathbf{M}_\mathrm{d}\mathbf{M}^{-1}\boldsymbol{\Psi} \tag{225}$$

provides several beneficial effects in terms of amplifying the human input force in a desired way, while still allowing the mass $\mathbf{M}_\mathrm{d}$ to be as desired, as discussed next.

9.4.4 *Passive input-output pair*

In the fully-actuated case, the input matrix $\mathbf{F}_\mathrm{d} = \mathbf{M}_\mathrm{d}\mathbf{M}^{-1}\boldsymbol{\Psi}$ results in an output $\boldsymbol{y}_\mathrm{e}$, which is the time derivative of the coordinate $\boldsymbol{z}(\boldsymbol{q})$:

$$\boldsymbol{y}_\mathrm{e} = \mathbf{F}_\mathrm{d}^\top \frac{\partial H_\mathrm{d}}{\partial \boldsymbol{p}} = \mathbf{F}_\mathrm{d}^\top \mathbf{M}_\mathrm{d}^{-1}\boldsymbol{p} = \boldsymbol{\Psi}^\top \mathbf{M}^{-1}\boldsymbol{p} = \frac{\partial \boldsymbol{z}}{\partial \boldsymbol{q}}\dot{\boldsymbol{q}} = \frac{\mathrm{d}}{\mathrm{d}t}\boldsymbol{z}. \tag{226}$$

In the underactuated case without kinetic energy shaping and $\mathbf{F}_\mathrm{d} = \boldsymbol{\Psi}$ we obtain equivalently,

$$\boldsymbol{y}_\mathrm{e} = \mathbf{F}_\mathrm{d}^\top \frac{\partial H_\mathrm{d}}{\partial \boldsymbol{p}} = \mathbf{F}_\mathrm{d}^\top \mathbf{M}^{-1}\boldsymbol{p} = \frac{\partial \boldsymbol{z}}{\partial \boldsymbol{q}}\dot{\boldsymbol{q}} = \frac{\mathrm{d}}{\mathrm{d}t}\boldsymbol{z}. \tag{227}$$

The power supplied by the human operator to the system is the inner product of the input force $\boldsymbol{\tau}_\mathrm{h}$ and the velocity $\frac{\mathrm{d}}{\mathrm{d}t}\boldsymbol{z} = \boldsymbol{y}_\mathrm{e}$ at the application point of the generalized force, such that the supplied power is $\boldsymbol{\tau}_\mathrm{h}^\top \boldsymbol{y}_\mathrm{e}$, which corresponds to the power balance (201), as expected.

9.4.5 *Passive force and power supply amplification*

Whereas the increase of H_d (201) equals the power supplied by the human operator minus dissipation, the actual energy contained in the system grows at a different rate because the real system also has an input $\boldsymbol{\tau}$. The actuators supply energy at a rate of $\boldsymbol{\tau}^\top \dot{\boldsymbol{q}} = \boldsymbol{\tau}^\top \mathbf{M}^{-1}\boldsymbol{p}$ (see Figure 7). From (195) the real energy rate is

$$\begin{aligned}\dot{H} &= \begin{bmatrix} \dfrac{\partial^\top H}{\partial \boldsymbol{q}} & \dfrac{\partial^\top H}{\partial \boldsymbol{p}} \end{bmatrix} \left(\begin{bmatrix} \mathbf{0}_{n\times m} \\ \mathbf{F} \end{bmatrix} \boldsymbol{\tau} + \begin{bmatrix} \mathbf{0}_{n\times \ell} \\ \boldsymbol{\Psi} \end{bmatrix} \boldsymbol{\tau}_\mathrm{h} \right) \\ &= \boldsymbol{p}^\top \mathbf{M}^{-1}\mathbf{F}\boldsymbol{\tau} + \boldsymbol{p}^\top \mathbf{M}^{-1}\boldsymbol{\Psi}\boldsymbol{\tau}_\mathrm{h}. \end{aligned} \tag{228}$$

If we insert the control law (203) with $\boldsymbol{\tau}_\mathrm{e} = \boldsymbol{\tau}_\mathrm{h}$ and represent all terms that are not a function of $\boldsymbol{\tau}_\mathrm{h}$ by $(\star)$, we have

$$\boldsymbol{\tau} = (\star) + \left(\mathbf{F}^\top \mathbf{F}\right)^{-1} \mathbf{F}^\top \left(\mathbf{F}_\mathrm{d}\boldsymbol{\tau}_\mathrm{h} - \boldsymbol{\Psi}\boldsymbol{\tau}_\mathrm{h}\right), \tag{229}$$

which gives

$$\dot{H} = \boldsymbol{p}^\top \mathbf{M}^{-1}\mathbf{F}\,(\star) + \boldsymbol{p}^\top \mathbf{M}^{-1}\mathbf{F}\left(\mathbf{F}^\top \mathbf{F}\right)^{-1} \mathbf{F}^\top \left(\mathbf{F}_\mathrm{d}\boldsymbol{\tau}_\mathrm{h} - \boldsymbol{\Psi}\boldsymbol{\tau}_\mathrm{h}\right) + \boldsymbol{p}^\top \mathbf{M}^{-1}\boldsymbol{\Psi}\boldsymbol{\tau}_\mathrm{h}.$$

Finally, for the fully-actuated case ($\mathbf{F} = \mathbf{I}_n$) with $\mathbf{F}_\mathrm{d}$ as in (225), we obtain

$$\begin{aligned}\dot{H} &= \boldsymbol{p}^\top \mathbf{M}^{-1}\,(\star) + \boldsymbol{p}^\top \mathbf{M}^{-1}\mathbf{F}_\mathrm{d}\boldsymbol{\tau}_\mathrm{h} \\ &= \boldsymbol{p}^\top \mathbf{M}^{-1}\,(\star) + \boldsymbol{p}^\top \mathbf{M}^{-1}\mathbf{M}_\mathrm{d}\mathbf{M}^{-1}\boldsymbol{\Psi}\boldsymbol{\tau}_\mathrm{h}. \end{aligned} \tag{230}$$

Consequently, the real power supply due to the generalized input forces $\boldsymbol{\Psi}\boldsymbol{\tau}_\mathrm{h}$ and their conjugate velocities $\dot{\boldsymbol{q}} = \mathbf{M}^{-1}\boldsymbol{p}$ is amplified by a factor $\mathbf{M}_\mathrm{d}\mathbf{M}^{-1}$. Likewise, from (229), the total force acting on the system equals the human input amplified by $\mathbf{M}_\mathrm{d}\mathbf{M}^{-1}$:

$$\boldsymbol{\tau} + \boldsymbol{\Psi}\boldsymbol{\tau}_\mathrm{h} = (\star) + \mathbf{F}_\mathrm{d}\boldsymbol{\tau}_\mathrm{h} - \boldsymbol{\Psi}\boldsymbol{\tau}_\mathrm{h} + \boldsymbol{\Psi}\boldsymbol{\tau}_\mathrm{h} = (\star) + \mathbf{M}_\mathrm{d}\mathbf{M}^{-1}\boldsymbol{\Psi}\boldsymbol{\tau}_\mathrm{h}. \tag{231}$$

An important result is that although the real power supply and force can be amplified as desired through a suitable choice of $\mathbf{M}_\mathrm{d}$, passivity is preserved with respect to the metric H_d and the human power supply.

9.4.6 *Perceived mass*

Counter-intuitively, the desired mass matrix $\mathbf{M}_\mathrm{d}$ is not the mass perceived by the human operator. To get a better understanding of the perceived mass, consider again the fully-actuated case and assume $\mathbf{M}(\boldsymbol{q})$ and $\mathbf{V}(\boldsymbol{q})$ are constant. In this case $\dot{\boldsymbol{p}} = \mathbf{M}\ddot{\boldsymbol{q}}$, which yields

$$\dot{\boldsymbol{p}} = \mathbf{M}\ddot{\boldsymbol{q}} = (\star) + \mathbf{M}_\mathrm{d}\mathbf{M}^{-1}\boldsymbol{\Psi}\boldsymbol{\tau}_\mathrm{h}, \tag{232}$$

and hence

$$\mathbf{M}\mathbf{M}_\mathrm{d}^{-1}\mathbf{M}\ddot{\boldsymbol{q}} = \mathbf{M}\mathbf{M}_\mathrm{d}^{-1}(\star) + \boldsymbol{\Psi}\boldsymbol{\tau}_\mathrm{h}. \tag{233}$$

Consequently, the observed acceleration $\ddot{\boldsymbol{q}}$ resulting from a given operator force $\boldsymbol{\tau}_\mathrm{h}$ corresponds to a perceived mass of $\mathbf{M}\mathbf{M}_\mathrm{d}^{-1}\mathbf{M}$. Consequently, choosing a higher $\mathbf{M}_\mathrm{d}$ yields a lower perceived mass, and vice versa.

10 INTERACTING WITH DISTRIBUTED SYSTEMS

The previous chapter presented a method to shape the dynamics of a single mechanical system to obtain a desired input-output behavior, and showed how this enables a form of human-machine interaction. This chapter extends this result to interaction with a distributed system consisting of fully-actuated and underactuated agents. In addition to enabling interaction with groups of systems, this approach can be used to alleviate constraints imposed by the human input matching condition, enabling haptic control of one or more underactuated systems even when direct interaction is not possible.

Although haptic control and teleoperation is a broad research field, this chapter does not aim to provide an in-depth comparison with existing methods. Rather, this chapter illustrates a potential range of additional applications of our main result, which is the distributed IDA-PBC framework.

A thorough introduction to teleoperation is given in [62] and references therein. A detailed study of teleoperation of a group of fully-actuated point-mass robots including force feedback through a haptic manipulator is given in [63]. The recent work [64] considers teleoperation of groups of fully-actuated robots with physical coupling constraints in the Hamiltonian framework. In this chapter, fully-actuated haptic manipulators are used to control fully-actuated and underactuated systems. The opposite problem is considered in [65], where an underactuated haptic manipulator is used to control a manipulator in a virtual environment.

Section 10.1 begins by describing several task objectives when interacting with one or more systems, while Section 10.2 shows how these objectives can be captured by a unified class of desired dynamics. The objective of obtaining these dynamics leads to matching conditions for the human interaction force as well as a set of control laws, as described in Sections 10.3 and 10.4. Extensions to teleoperation at different spatial scales and to remote force sensation are discussed in Sections 10.5 and 10.6.

10.1 CONTROL OBJECTIVES IN THE TASK SPACE

Human interaction can be used to steer a robot towards its goal. The robot stabilizes internally, for example to compensate for gravity, while the human exerts a small force to guide the robot. Depending on the task to be executed, this guidance force may be exerted directly on the system (equivalent to Chapter 9), as shown in Figure 8a, or remotely through a teleoperation control device (Figure 8b).

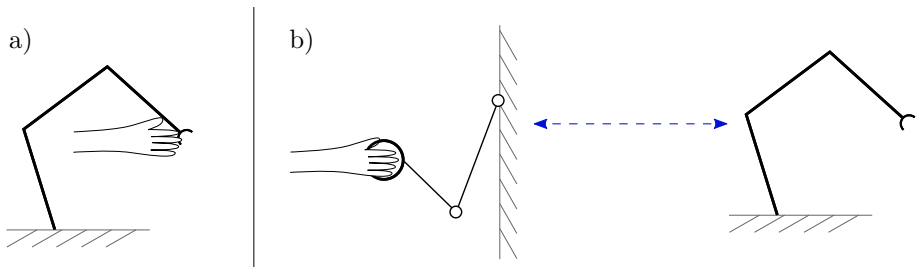

Figure 8: Direct interaction (a) and teleoperation (b) to control the robot end-effector location. A dashed arrow indicates information exchange between systems.

10.1.1 *Teleoperation through synchronization*

The field of teleoperation is broad, with many conceptually different ways to control a robot using a human input from a distance. In this chapter we demonstrate how our previously presented distributed IDA-PBC approach can be used to synchronize the control device and one or more remote machines in the variables $\boldsymbol{z}_i(\boldsymbol{q})$. By exerting forces to manipulate the control device, the remote machine moves along, while the human operator experiences force feedback trough the control device when the systems are not completely synchronized. We also consider the case where the measured force generates an immediate effect on the remote system to improve its response to manipulation of the input device.

10.1.2 *Controlling groups of systems*

A similar direct or remote control procedure can be used to guide a group of robots towards their goal. For example, a leaderless group of robots may attain a prescribed formation while the human leader steers the group towards the desired location, either directly (Figure 9a) or through a teleoperation device (Figure 9b).

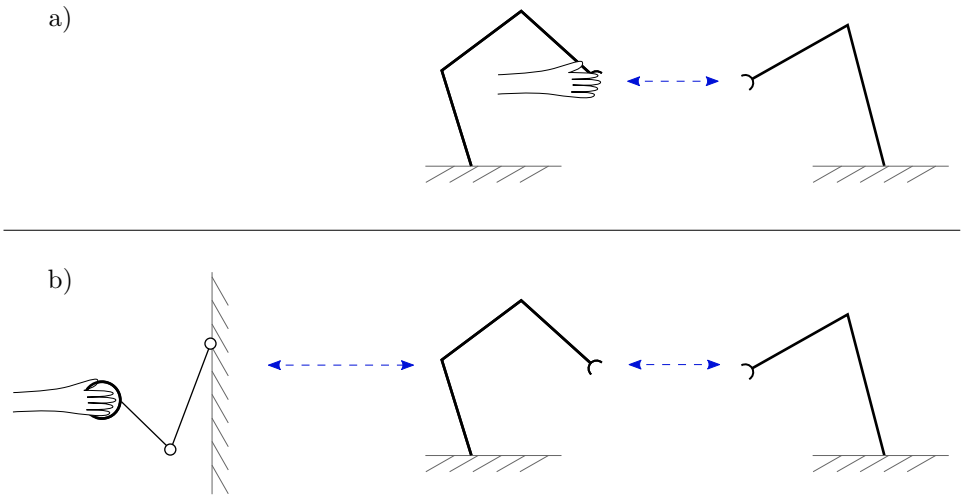

Figure 9: Direct interaction with a group of cooperative robots (a) and interaction through a teleoperation device (b).

10.1.3 *Haptic control of underactuated agents*

A suitable definition of $\boldsymbol{z}_i(\boldsymbol{q})$ variables across heterogeneous systems can be exploited to stably control underactuated agents using fully-actuated input devices that allow arbitrary human input forces, thereby simplifying the process of remotely controlling such systems.

To illustrate this procedure, Figure 10 shows the process of interactively and remotely controlling an unmanned aerial vehicle (UAV) through a two-link input manipulator. The manipulator end-effector in the plane is synchronized with the landing gear location of the UAV, while the UAV autonomously stabilizes its attitude to remain horizontal. The UAV can be steered to a desired vertical and horizontal position by moving the end-effector of the manipulator. Several important considerations such as achieving large translations with comparatively small movement of the input device are discussed in Section 10.5.

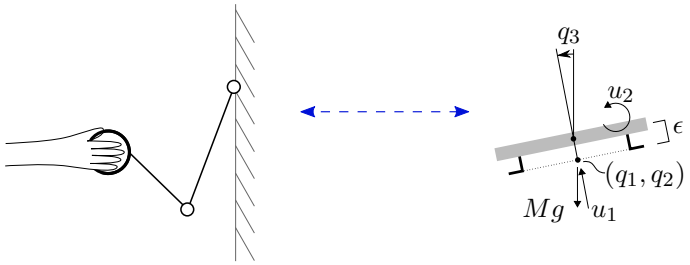

Figure 10: Haptic control of an underactuated UAV through a fully-actuated input device.

10.2 DYNAMICS WITH A HAPTIC CONTROL INTERFACE

In the teleoperation scenarios of Figure 8b and Figure 9b, the haptic control input device is considered to be a simple mechanical system that together with the remote machines forms a distributed mechanical system.When viewing the input device as yet another mechanical system, these schemes are equivalent to the direct interaction scenarios of Figure 8a and Figure 9a. Consequently, we can treat all scenarios mathematically as a distributed system of simple mechanical systems where one system is subject to an additional physical and measured human input force.

10.2.1 *Uncontrolled dynamics*

The physical human input is assumed to act on agent 1, for notational convenience. Agent 1 is assumed to be fully-actuated while the other agents are allowed to be either fully-actuated or underactuated, as long as each one has a known single-agent IDA-PBC solution. Extending the network dynamics (138) with a single human input as in (195), we can write the open-loop dynamics of all agents in the network as a single simple mechanical system of the form

$$\begin{bmatrix} \dot{\bar{\boldsymbol{q}}} \\ \dot{\bar{\boldsymbol{p}}} \end{bmatrix} = \begin{bmatrix} \mathbf{0}_{\bar{n}} & \mathbf{I}_{\bar{n}} \\ -\mathbf{I}_{\bar{n}} & \mathbf{0}_{\bar{n}} \end{bmatrix} \begin{bmatrix} \dfrac{\partial \bar{H}}{\partial \bar{\boldsymbol{q}}} \\ \dfrac{\partial \bar{H}}{\partial \bar{\boldsymbol{p}}} \end{bmatrix} + \begin{bmatrix} \mathbf{0}_{\bar{n}\times\bar{m}} \\ \bar{\mathbf{F}} \end{bmatrix} \bar{\boldsymbol{\tau}} + \begin{bmatrix} \mathbf{0}_{\bar{n}\times\ell} \\ \boldsymbol{\Psi}_1 \\ \mathbf{0}_{(\bar{n}-n_1)\times\ell} \end{bmatrix} \boldsymbol{\tau}_{\mathrm{h}}, \tag{234}$$

$$\bar{\boldsymbol{y}} = \bar{\mathbf{F}}^\top \frac{\partial \bar{H}}{\partial \bar{\boldsymbol{p}}} = \bar{\mathbf{F}}^\top \bar{\mathbf{M}}^{-1} \bar{\boldsymbol{p}}, \tag{235}$$

$$\bar{H} = \frac{1}{2} \bar{\boldsymbol{p}}^\top \bar{\mathbf{M}}^{-1} \bar{\boldsymbol{p}} + \bar{V}, \tag{236}$$

where $\bar{\boldsymbol{\tau}} \in \mathbb{R}^{\bar{m}}$ are the actuator control inputs and $\boldsymbol{\tau}_{\mathrm{h}} \in \mathbb{R}^{\ell}$ is a physical human input force acting on system 1 at its end-effector location $\boldsymbol{z}_1(\boldsymbol{q})$ where it is also measured, and $\boldsymbol{\Psi}_1$ is defined using $\boldsymbol{z}_1(\boldsymbol{q}_1)$ as in (57).

10.2.2 *Desired dynamics with human input*

Similarly, combining the desired network dynamics (237) with the desired dynamics of a single system with human input (219), we propose to write the desired dynamics of the distributed system with human input as

$$\begin{bmatrix} \dot{\bar{\boldsymbol{q}}} \\ \dot{\bar{\boldsymbol{p}}} \end{bmatrix} = \begin{bmatrix} \mathbf{0}_{\bar{n}} & \bar{\mathbf{M}}^{-1}\bar{\mathbf{M}}_{\mathrm{d}} \\ -\bar{\mathbf{M}}_{\mathrm{d}}\bar{\mathbf{M}}^{-1} & \bar{\mathbf{J}} - \bar{\mathbf{F}}\bar{\mathbf{K}}_v\bar{\mathbf{F}}^\top - \bar{\mathbf{F}}_{\mathrm{d}}\bar{\mathbf{K}}_{\mathrm{d}}\bar{\mathbf{F}}_{\mathrm{d}}^\top \end{bmatrix} \begin{bmatrix} \dfrac{\partial \bar{H}_{\mathrm{d}}}{\partial \bar{\boldsymbol{q}}} \\ \dfrac{\partial \bar{H}_{\mathrm{d}}}{\partial \bar{\boldsymbol{p}}} \end{bmatrix} + \begin{bmatrix} \mathbf{0}_{\bar{n}\times\bar{m}} \\ \bar{\mathbf{F}}_{\mathrm{d}} \end{bmatrix} \bar{\mathbf{D}}\boldsymbol{\tau}_{\mathrm{h}}, \tag{237}$$

$$\bar{\boldsymbol{y}}_{\mathrm{d}} = \bar{\mathbf{F}}^{\top}\bar{\mathbf{M}}_{\mathrm{d}}^{-1}\bar{\boldsymbol{p}}, \tag{238}$$

$$\bar{\boldsymbol{y}}_{\mathrm{e}} = \bar{\mathbf{D}}^{\top}\bar{\mathbf{F}}_{\mathrm{d}}^{\top}\bar{\mathbf{M}}_{\mathrm{d}}^{-1}\bar{\boldsymbol{p}}, \tag{239}$$

$$\bar{H}_{\mathrm{d}} = \frac{1}{2}\bar{\boldsymbol{p}}^{\top}\bar{\mathbf{M}}_{\mathrm{d}}^{-1}\bar{\boldsymbol{p}} + \bar{V}_{\mathrm{d}}. \tag{240}$$

where the shaped input matrix $\bar{\mathbf{F}}_{\mathrm{d}}$ and the measured input distribution matrix $\bar{\mathbf{D}}$ are given by

$$\bar{\mathbf{F}}_{\mathrm{d}} = \begin{bmatrix} \mathbf{F}_{\mathrm{d},1} & & \\ & \ddots & \\ & & \mathbf{F}_{\mathrm{d},N} \end{bmatrix}, \quad \bar{\mathbf{D}} = \begin{bmatrix} \mathbf{D}_1 \\ \vdots \\ \mathbf{D}_N \end{bmatrix}. \tag{241}$$

The desired dynamics (237) are similar to the stable distributed system dynamics as discussed in Chapter 6, with an optional additional damping term when $\bar{\mathbf{K}}_{\mathrm{d}} \geq \mathbf{0}_{N\ell}$, and an adjustable input matrix $\bar{\mathbf{F}}_{\mathrm{d}}$ that determines the response to the external input. The input acting on this system is $\bar{\mathbf{D}}\boldsymbol{\tau}_{\mathrm{h}}$, where $\mathbf{D}_i$ is $\mathbf{I}_\ell$ if we wish $\boldsymbol{\tau}_{\mathrm{h}}$ to act on the shaped system i and $\mathbf{D}_i = \mathbf{0}_\ell$ otherwise.

10.2.3 *Deriving the control law and matching conditions*

As before, the control law and matching conditions are obtained by setting the uncontrolled dynamics and desired dynamics equal and solving for $\bar{\boldsymbol{\tau}}$. For the distributed system with human input this yields the necessary equality

$$-\frac{\partial \bar{H}}{\partial \bar{\boldsymbol{q}}} + \bar{\mathbf{F}}\bar{\boldsymbol{\tau}} + \begin{bmatrix} \boldsymbol{\Psi}_1\boldsymbol{\tau}_{\mathrm{h}} \\ \mathbf{0}_{(\bar{n}-n_1)\times 1} \end{bmatrix} =$$

$$-\bar{\mathbf{M}}_{\mathrm{d}}\bar{\mathbf{M}}^{-1}\frac{\partial \bar{H}_{\mathrm{d}}}{\partial \bar{\boldsymbol{q}}} + \left(\bar{\mathbf{J}} - \bar{\mathbf{F}}\bar{\mathbf{K}}_v\bar{\mathbf{F}}^{\top} - \bar{\mathbf{F}}_{\mathrm{d}}\bar{\mathbf{K}}_{\mathrm{d}}\bar{\mathbf{F}}_{\mathrm{d}}^{\top}\right)\frac{\partial \bar{H}_{\mathrm{d}}}{\partial \bar{\boldsymbol{p}}} + \bar{\mathbf{F}}_{\mathrm{d}}\bar{\mathbf{D}}\boldsymbol{\tau}_{\mathrm{h}}. \tag{242}$$

Because agent 1 is fully actuated, its input matrix is $\mathbf{F}_1 = \mathbf{I}_{n_1}$ without loss of generality. This means that the network input matrix $\bar{\mathbf{F}}$ and its annihilator can be written as

$$\bar{\mathbf{F}} = \begin{bmatrix} \mathbf{I}_{n_1} & & & \\ & \mathbf{F}_2 & & \\ & & \ddots & \\ & & & \mathbf{F}_N \end{bmatrix}, \quad \bar{\mathbf{F}}^{\perp} = \begin{bmatrix} \mathbf{0}_{(n_2-m_2)\times n_1} & \mathbf{F}_2^{\perp} & & \\ \vdots & & \ddots & \\ \mathbf{0}_{(n_N-m_N)\times n_1} & & & \mathbf{F}_N^{\perp} \end{bmatrix}. \tag{243}$$

Following the same procedure as in Chapter 3, left-multiplication by the full-rank matrix $[(\bar{\mathbf{F}}^{\perp})^{\top}\ \bar{\mathbf{F}}]^{\top}$ gives

$$-\begin{bmatrix} \bar{\mathbf{F}}^{\perp} \\ \bar{\mathbf{F}}^{\top} \end{bmatrix}\frac{\partial \bar{H}}{\partial \bar{\boldsymbol{q}}} + \begin{bmatrix} \bar{\mathbf{F}}^{\perp} \\ \bar{\mathbf{F}}^{\top} \end{bmatrix}\bar{\mathbf{F}}\bar{\boldsymbol{\tau}} + \begin{bmatrix} \bar{\mathbf{F}}^{\perp} \\ \bar{\mathbf{F}}^{\top} \end{bmatrix}\begin{bmatrix} \boldsymbol{\Psi}_1\boldsymbol{\tau}_{\mathrm{h}} \\ \mathbf{0}_{(\bar{n}-n_1)\times 1} \end{bmatrix} = \begin{bmatrix} \bar{\mathbf{F}}^{\perp} \\ \bar{\mathbf{F}}^{\top} \end{bmatrix}\bar{\mathbf{F}}_{\mathrm{d}}\bar{\mathbf{D}}\boldsymbol{\tau}_{\mathrm{h}}$$

$$-\begin{bmatrix} \bar{\mathbf{F}}^{\perp} \\ \bar{\mathbf{F}}^{\top} \end{bmatrix}\bar{\mathbf{M}}_{\mathrm{d}}\bar{\mathbf{M}}^{-1}\frac{\partial \bar{H}_{\mathrm{d}}}{\partial \bar{\boldsymbol{q}}} + \begin{bmatrix} \bar{\mathbf{F}}^{\perp} \\ \bar{\mathbf{F}}^{\top} \end{bmatrix}\left(\bar{\mathbf{J}} - \bar{\mathbf{F}}\bar{\mathbf{K}}_v\bar{\mathbf{F}}^{\top} - \bar{\mathbf{F}}_{\mathrm{d}}\bar{\mathbf{K}}_{\mathrm{d}}\bar{\mathbf{F}}_{\mathrm{d}}^{\top}\right)\frac{\partial \bar{H}_{\mathrm{d}}}{\partial \bar{\boldsymbol{p}}}.$$

The top and bottom block rows give the matching conditions and control law, respectively. The matching condition becomes

$$\bar{\mathbf{F}}^{\perp}\left(\frac{\partial \bar{H}}{\partial \bar{\boldsymbol{q}}} - \bar{\mathbf{M}}_{\mathrm{d}}\bar{\mathbf{M}}^{-1}\frac{\partial \bar{H}_{\mathrm{d}}}{\partial \bar{\boldsymbol{q}}} + \bar{\mathbf{J}}\frac{\partial \bar{H}_{\mathrm{d}}}{\partial \bar{\boldsymbol{p}}}\right) + \bar{\mathbf{F}}^{\perp}\left(-\bar{\mathbf{F}}_{\mathrm{d}}\bar{\mathbf{K}}_{\mathrm{d}}\bar{\mathbf{F}}_{\mathrm{d}}^{\top}\frac{\partial \bar{H}_{\mathrm{d}}}{\partial \bar{\boldsymbol{p}}} + \bar{\mathbf{F}}_{\mathrm{d}}\bar{\mathbf{D}}\boldsymbol{\tau}_{\mathrm{h}}\right) = \boldsymbol{0}, \tag{244}$$

while the control law becomes, for $\mathbf{F}_1 = \mathbf{I}_{n_1}$,

$$\bar{\boldsymbol{\tau}} = \left(\bar{\mathbf{F}}^\top\bar{\mathbf{F}}\right)^{-1}\bar{\mathbf{F}}^\top\left(\frac{\partial\bar{H}}{\partial\bar{\boldsymbol{q}}} - \bar{\mathbf{M}}_\mathrm{d}\bar{\mathbf{M}}^{-1}\frac{\partial\bar{H}_\mathrm{d}}{\partial\bar{\boldsymbol{q}}} + \bar{\mathbf{J}}\bar{\mathbf{M}}_\mathrm{d}^{-1}\bar{\boldsymbol{p}}\right) - \bar{\mathbf{K}}_v\bar{\boldsymbol{y}}_\mathrm{d} \tag{245}$$

$$- \left(\bar{\mathbf{F}}^\top\bar{\mathbf{F}}\right)^{-1}\bar{\mathbf{F}}^\top\bar{\mathbf{F}}_\mathrm{d}\bar{\mathbf{K}}_\mathrm{d}\bar{\mathbf{F}}_\mathrm{d}^\top\bar{\mathbf{M}}_\mathrm{d}^{-1}\bar{\boldsymbol{p}} + \left(\bar{\mathbf{F}}^\top\bar{\mathbf{F}}\right)^{-1}\bar{\mathbf{F}}^\top\bar{\mathbf{F}}_\mathrm{d}\bar{\mathbf{D}}\boldsymbol{\tau}_\mathrm{h} - \begin{bmatrix}\boldsymbol{\Psi}_1\boldsymbol{\tau}_\mathrm{h}\\ \mathbf{0}_{(\bar{m}-m_1)\times 1}\end{bmatrix},$$

both of which are analyzed next.

10.3 HUMAN INPUT MATCHING CONDITION

The first part of the matching condition (244) is equivalent to the distributed IDA-PBC matching problem of Chapter 6, and can hence be satisfied using the solutions presented in Chapter 8. The combined matching condition is then satisfied if we additionally require that

$$\bar{\mathbf{F}}^\perp\left(-\bar{\mathbf{F}}_\mathrm{d}\bar{\mathbf{K}}_\mathrm{d}\bar{\mathbf{F}}_\mathrm{d}^\top\bar{\mathbf{M}}_\mathrm{d}^{-1}\bar{\boldsymbol{p}} + \bar{\mathbf{F}}_\mathrm{d}\bar{\mathbf{D}}\boldsymbol{\tau}_\mathrm{h}\right) = \boldsymbol{0}, \tag{246}$$

which imposes restrictions on the allowed task-space damping and the allowed human input $\boldsymbol{\tau}_\mathrm{h}$. If we choose block diagonal matrices $\bar{\mathbf{F}}_\mathrm{d}$ and $\bar{\mathbf{K}}_\mathrm{d}$ of the form

$$\bar{\mathbf{F}}_\mathrm{d} = \begin{bmatrix}\mathbf{F}_{\mathrm{d},1} & & \\ & \ddots & \\ & & \mathbf{F}_{\mathrm{d},N}\end{bmatrix}, \quad \bar{\mathbf{K}}_\mathrm{d} = \begin{bmatrix}\mathbf{K}_{\mathrm{d},1} & & \\ & \ddots & \\ & & \mathbf{K}_{\mathrm{d},N}\end{bmatrix}, \tag{247}$$

and if we note that the first block column of $\bar{\mathbf{F}}^\perp$ (243) are zeros, this reduces to $N-1$ matching conditions of the form

$$\mathbf{F}_i^\perp\left(-\mathbf{F}_{\mathrm{d},i}\mathbf{K}_{\mathrm{d},i}\mathbf{F}_{\mathrm{d},i}^\top\mathbf{M}_{\mathrm{d},i}^{-1}\boldsymbol{p}_i + \mathbf{F}_{\mathrm{d},i}\mathbf{D}_i\boldsymbol{\tau}_\mathrm{h}\right) = \boldsymbol{0} \quad \forall \quad i = 2,\dots,N. \tag{248}$$

As anticipated, no conditions are imposed on system 1 because it is fully actuated. For $\mathbf{D}_i = \mathbf{I}_\ell$ the conditions (248) are equal to the single-agent matching condition for input matrix shaping without human input (206). This is also expected, because no physical input force acts on these systems. The condition was previously shown to be satisfied by (208), which gives for each agent, including agent 1,

$$\mathbf{F}_{\mathrm{d},i} = \mathbf{M}_{\mathrm{d},i}\mathbf{M}_i^{-1}\boldsymbol{\Psi}_i \quad \forall \quad i = 1,\dots,N. \tag{249}$$

This choice also satisfies the matching condition if $\mathbf{D}_i = \mathbf{0}_\ell$.

The result is that the direct response of each system ($i = 1,\dots,N$) to the force $\boldsymbol{\tau}_\mathrm{h}$ sensed at system 1 can be adjusted through an appropriate choice of $\mathbf{M}_{\mathrm{d},i}$, or disabled entirely by choosing $\mathbf{D}_i = \mathbf{0}_\ell$.

10.4 DISTRIBUTED CONTROL LAW

The distributed control law (245) consists of two parts. The first line is equivalent to the standard distributed IDA-PBC control law (147), which can be implemented in a distributed fashion as discussed in Chapter 8. This section discusses the implementation aspects of the second line, which concerns the additional control terms for input shaping and canceling the physical human force input.

10.4.1 *Implementation*

The second line of (245) expands to the distributed implementation

$$- \left(\mathbf{F}_1^\top\mathbf{F}_1\right)^{-1}\mathbf{F}_1^\top\mathbf{F}_{\mathrm{d},1}\mathbf{K}_{\mathrm{d},1}\mathbf{F}_{\mathrm{d},1}^\top\mathbf{M}_{\mathrm{d},1}^{-1}\boldsymbol{p}_1 + \left(\mathbf{F}_1^\top\mathbf{F}_1\right)^{-1}\mathbf{F}_1^\top\mathbf{F}_{\mathrm{d},1}\mathbf{D}_1\boldsymbol{\tau}_\mathrm{h} - \boldsymbol{\Psi}_1\boldsymbol{\tau}_\mathrm{h}. \tag{250}$$

for agent 1 and,

$$-\left(\mathbf{F}_i^\top \mathbf{F}_i\right)^{-1} \mathbf{F}_i^\top \mathbf{F}_{\mathrm{d},i} \mathbf{K}_{\mathrm{d},i} \mathbf{F}_{\mathrm{d},i}^\top \mathbf{M}_{\mathrm{d},i}^{-1} \boldsymbol{p}_i + \left(\mathbf{F}_i^\top \mathbf{F}_i\right)^{-1} \mathbf{F}_i^\top \mathbf{F}_{\mathrm{d},i} \mathbf{D}_i \boldsymbol{\tau}_\mathrm{h}. \tag{251}$$

for agents $i = 2, \ldots, N$. In both cases, the first term provides damping of the velocities $\frac{\mathrm{d}}{\mathrm{d}t}\boldsymbol{z}_i$ and the second term provides a virtual input force due to the human input $\boldsymbol{\tau}_\mathrm{h}$ measured at agent 1, which is active if $\mathbf{D}_i = \mathbf{I}_\ell$ and inactive when $\mathbf{D}_i = \mathbf{0}_\ell$. The third term $(-\boldsymbol{\Psi}_1 \boldsymbol{\tau}_\mathrm{h})$ is unique to agent 1, and is used to cancel the physical input force acting on it.

10.4.2 *Remote force transmission*

When choosing to apply $\boldsymbol{\tau}_\mathrm{h}$ to one of the subsystems $i = 2, \ldots, N$, the effect of the measured force $\boldsymbol{\tau}_\mathrm{h}$ at system 1 is transfered to this system, generating an immediate feedforward signal. This allows a group of robots to move at once while maintaining their formation. Coupling forces between the agents serve as feedback to offset errors in the feedforward control signal. Without this feedforward term, the agents $i = 2, \ldots, N$ only follow due to coupling feedback forces that arise from the deformation of the group when agent 1 is set in motion by the human operator.

Communicating this force information to the remote systems can be highly advantageous for haptic control of underactuated agents, as shown in Figure 10. In a direct control approach, there is no easy way for an operator to directly apply a force precisely at $\boldsymbol{z}(\boldsymbol{q})$. Doing so is unintuitive, and any error immediately produces an unwanted torque about this point, possibly destabilizing the UAV. On the other hand, actuation through the haptic manipulator allows arbitrary input motions while the measured force immediately yields a desired feedforward effect on the UAV, providing a transparent control mechanism.

A downside of using the measured force $\boldsymbol{\tau}_\mathrm{h}$ as an input to other agents is that these agents require knowledge of the input force for the actuation signal (251), implying that it must be transfered over the network, which is susceptible to delays.

10.5 INTERACTION AT MICRO AND MACRO SCALE

In some teleoperation tasks, it is practical for the human to operate the input device at a different spatial scale than the remote system. For example, a UAV might operate in a laboratory workspace of tens of meters along all dimensions while the human operator interacts with a haptic device with a workspace of several decimeters. Conversely, a surgeon may wish to perform precision surgery while using a haptic control device at a larger scale. This section shows how scaling of the task-space variables can be incorporated in the proposed control scheme.

10.5.1 *Scaling of the communicated variable*

The distributed IDA-PBC scheme cooperatively controls the quantities $\boldsymbol{z}_i(\boldsymbol{q}_i)$ of each system in the network, but the numeric values need not have the same units of measurement. For example, if $\boldsymbol{z}_1(\boldsymbol{q}_1)$ is an end-effector location measured in centimeters while $\boldsymbol{z}_2(\boldsymbol{q}_2)$ is an end-effector location expressed in meters, synchronization of $\boldsymbol{z}_1(\boldsymbol{q}_1)$ and $\boldsymbol{z}_2(\boldsymbol{q}_2)$ implies that they reach the same numeric value (say, 2.5), but the systems end up at 0.025 m and 2.5 m respectively (see Figure 11).

In general, we may express the communicated numeric value $\boldsymbol{z}_i(q_i)$ in terms of the physical end-effector location $\hat{\boldsymbol{z}}_i(\boldsymbol{q}_i)$, measured in SI units, scaled by a matrix $\boldsymbol{\mathcal{C}}_i = \boldsymbol{\mathcal{C}}_i^\top > \mathbf{0}_\ell$, which gives

$$\boldsymbol{z}_i(\boldsymbol{q}_i) = \boldsymbol{\mathcal{C}}_i \hat{\boldsymbol{z}}_i(\boldsymbol{q}_i), \tag{252}$$

$$\boldsymbol{\Psi}_i(\boldsymbol{q}_i) = \frac{\partial^\top \boldsymbol{z}_i}{\partial \boldsymbol{q}_i} = \frac{\partial^\top \hat{\boldsymbol{z}}_i}{\partial \boldsymbol{q}_i} \boldsymbol{\mathcal{C}}_i = \hat{\boldsymbol{\Psi}}_i \boldsymbol{\mathcal{C}}_i. \tag{253}$$

While most of the control laws remain unchanged due to this scaling, an important modification is that the effect of the physical human input force on the uncontrolled dynamics (234) is not affected by this scaling. Its effect remains the physical generalized force $\hat{\boldsymbol{\Psi}}_1 \boldsymbol{\tau}_\mathrm{h}$. By re-deriving the control law, this can be accounted for by likewise replacing the cancellation force $\boldsymbol{\Psi}_1 \boldsymbol{\tau}_\mathrm{h}$ in (245), (250) by $\hat{\boldsymbol{\Psi}}_1 \boldsymbol{\tau}_\mathrm{h}$.

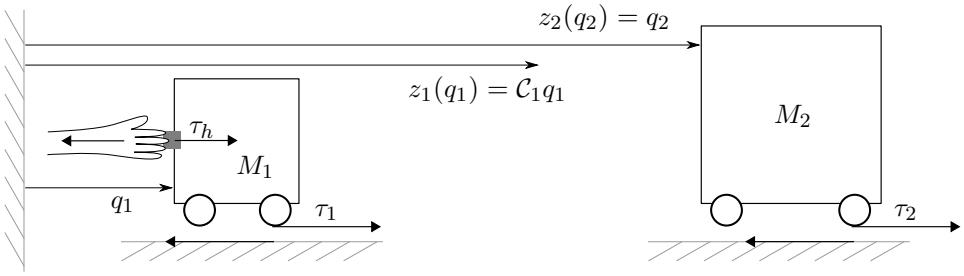

Figure 11: Controlling a remote system at a different spatial scale.

10.5.2 *Scaling the transient response*

Although the scaling procedure does not alter the asymptotic stability result of the distributed IDA-PBC scheme, scaling one system variable affects the transient response of that system as well as those of other systems in the network, which can addressed by a suitable choice of coupling potentials and desired mass matrices.

We illustrate several of these aspects using a simple example, where a point mass input device operating at a centimeter scale ($\mathcal{C}_1 = 100$) is used to telemanipulate a larger point mass at a meter scale ($\mathcal{C}_2 = 1$), when both masses translate horizontally ($\ell = 1$, $V_1 = V_1 = 0$), as shown in Figure 11. This gives $z_2 = q_2$, $z_1 = \mathcal{C}_1 q_1$, $\Psi_1 = \mathcal{C}_1$, $\hat{\Psi}_1 = 1$, and $\Psi_2 = 1$.

The network consists of two agents with one undirected edge that connects them. There are no leaders. With both systems being fully-actuated ($F_1 = F_2 = 1$), there are no matching conditions to be satisfied, and we can choose the coupling potential

$$\bar{V}_\mathrm{c} = \frac{1}{2} k (z_1 - z_2)^2, \quad V_{s,1} = V_{s,2} = 0. \tag{254}$$

Because the end-effectors are merely a scaled version of the actual coordinates, we consider only $\mathbf{K}_v = \mathrm{diag}(K_{v,1}, K_{v,2})$ while setting $\mathbf{K}_\mathrm{d} = \mathbf{0}_2$. We use $\bar{\mathbf{J}} = \mathbf{0}_2$ for simplicity. The previously derived control laws (245), (192), and (250), (251) give

$$\tau_1 = M_{d,1} M_1^{-1} \Psi_1 k (z_2 - z_1) - K_{v,1} M_{d,1}^{-1} p_1 + M_{d,1} M_1^{-1} \Psi_1 D_1 \tau_h - \hat{\Psi}_1 \tau_h, \tag{255}$$

$$\tau_2 = M_{d,2} M_2^{-1} \Psi_2 k (z_1 - z_2) - K_{v,2} M_{d,2}^{-1} p_2 + M_{d,2} M_2^{-2} \Psi_2 D_2 \tau_h. \tag{256}$$

Expressed in physical distances by substituting z_i and Ψ_i, and with $D_1 = D_2 = 1$ to let the force τ_h act on both systems in the desired dynamics, this becomes

$$\tau_1 = M_{d,1} M_1^{-1} \mathcal{C}_1 k (q_2 - \mathcal{C}_1 q_1) - K_{v,1} M_{d,1}^{-1} p_1 + M_{d,1} M_1^{-1} \mathcal{C}_1 \tau_h - \tau_h, \tag{257}$$

$$\tau_2 = M_{d,2} M_2^{-1} k (\mathcal{C}_1 q_1 - q_2) - K_{v,2} M_{d,2}^{-1} p_2 + M_{d,2} M_2^{-1} \tau_h. \tag{258}$$

The first term in both control laws represents the coupling force that steers the systems toward each other until $q_2 = \mathcal{C}_1 q_1$, demonstrating the distance amplification by a factor $\mathcal{C}_1$. The desired spring force for a given extension can be adjusted using the parameter k. The mass $M_{d,2}$ can be selected to adjust the response of the remote system to the measured force τ_h, while $M_{d,1}$ can be used to reduce the forces enacted on the human operator, to account for the amplification factor $\mathcal{C}_1$.

10.6 EXTENSION TO REMOTE FORCE SENSATION

To further enhance the transparency in teleoperation tasks, it can be helpful to explicitly sense external forces acting on the remote systems. In the previously discussed control strategy, the human operator only senses spring-like force feedback when the remote system and input device are not fully synchronized or fully in formation. Enabling such additional force feedback can be accomplished in a similar way as the human input force is transmitted to the other agents.

10.6.1 *Measured force distribution*

This can be accomplished by augmenting the desired dynamics (237) with additional inputs based on the measured force at one or more of the remote system end-effectors. For example, when one a force $\boldsymbol{\tau}_r$ is sensed at one of the remote systems, it can be incorporated by changing the term $\bar{\mathbf{F}}_{\mathrm{d}}\bar{\mathbf{D}}\boldsymbol{\tau}_{\mathrm{h}}$ in (237) to

$$\bar{\mathbf{F}}_{\mathrm{d}} \begin{bmatrix} \mathbf{D}_{1,h} & \mathbf{D}_{1,h} \\ \vdots & \vdots \\ \mathbf{D}_{N,h} & \mathbf{D}_{N,h} \end{bmatrix} \begin{bmatrix} \boldsymbol{\tau}_{\mathrm{h}} \\ \boldsymbol{\tau}_r \end{bmatrix}, \tag{259}$$

where the matrix $\mathbf{D}_{1,h}$ can be assigned to enable ($\mathbf{I}_\ell$) or disable ($\mathbf{0}_\ell$) the force $\boldsymbol{\tau}_{\mathrm{h}}$ acting on system i, and the matrix $\mathbf{D}_{1,r}$ can be assigned likewise to control the desired effect of the force $\boldsymbol{\tau}_r$. For teleoperation tasks with one input device and one remote agent with a force sensor, a transparent force feedback scheme would imply using $\mathbf{D}_{1,h} = \mathbf{D}_{2,h} = \mathbf{D}_{1,r} = \mathbf{D}_{2,r} = \mathbf{I}_\ell$.

The procedure of this chapter can be used to derive the corresponding control law and matching conditions, where the main additional constraint imposes that the remote system has sufficient actuation degrees to cancel the physical and measured force $\boldsymbol{\tau}_r$ if it is desired to shape its mass matrix. Extending this result to groups of robots, this technique can be used to slow down all agents in a group when one or more agents experience an input force due to an obstacle that is encountered.

10.6.2 *A note on generality and notational complexity*

While the presented approach is fairly generic, its notation can be somewhat cumbersome, despite not even covering the most general distributed IDA-PBC case. For example, the solutions given in this chapter do not exploit relative damping between systems (Section 7.2.2) or energy-transfer control using the matrix $\bar{\mathbf{J}}$ to avoid unnecessary complexity.

It is emphasized that the generic procedure of using the uncontrolled dynamics and the desired stable closed-loop dynamics to derive the control law and matching conditions can always be followed directly instead, directly incorporating scaling and force measurements. This leads to control laws and matching conditions expressed in terms of explicit model descriptions, parameters, and scaled variables, while omitting irrelevant terms, which may considerably simplify the resulting solution.

Part V

CASE STUDIES

This part combines and illustrates several results that can be obtained using the methods introduced in Parts III and IV, by providing simulation results for groups of underactuated and heterogeneous systems.

Chapter 11 begins with a simulation of identical but underactuated unmanned aerial vehicles that cooperatively assume a formation at a desired altitude. Another simulation demonstrates how these vehicles can synchronize with a fully-actuated landing platform in order to achieve a soft landing. Chapter 12 highlights the aspect of cooperation between heterogeneous agents, in which an unmanned aerial vehicle autonomously docks with two flexible-joint robotic arms. A second simulation demonstrates how a human operator can interact with the group of systems in order to adjust the final formation location.

11 COOPERATION BETWEEN UNDERACTUATED SYSTEMS

This chapter describes a simulation study that captures the main result of the proposed distributed IDA-PBC method. We demonstrate the asymptotic convergence of a group of underactuated unmanned aerial vehicles to a prescribed formation in the cooperative coordinates, while each agent stabilizes its internal coordinates.

Formations of unmanned aerial vehicles (UAVs) have applications in cooperative transportation and surveillance tasks. UAV formation and synchronization tasks have previously been considered using techniques such as backstepping or second-order consensus [66–68]. This chapter does not necessarily aim to improve these methods or provide a detailed comparison, but rather to demonstrate the implementation and transient behavior of our method for a practical application.

This chapter is built on a single-agent solution for planar UAV models, where each agent can translate vertically and horizontally and rotate about an axis perpendicular to the translation plane. This simpler model allows us to focus on the main contributions of our method, and makes the simulation results easier to interpret. However, single-agent IDA-PBC solutions also exist for the full 3D dynamics [23], and there are solutions for UAVs with robotic manipulators attached to them [69].

Section 11.1 provides the dynamics of two UAV models which can be shown to be equivalent for a suitable coordinate and input transformation. Section 11.2 summarizes a single-agent IDA-PBC solution from literature. Section 11.3 gives two simulations where six UAVs assume a desired formation at a reference altitude. In addition to a standard formation result, Section 11.4 provides a simulation where several UAVs synchronize with a landing platform in order to make a soft landing.

11.1 TWO EQUIVALENT PLANAR UAV MODELS

The results provided in this chapter apply to two classes of unmanned aerial vehicles, which have the same uncontrolled dynamics after a suitable change of inputs. This section gives the equations of motion and an input transformation for each model, as well as the resulting equivalent model used in the subsequent analysis. The model description corresponds to a generic class of thrust propelled vehicles, and may hence be applicable to other systems as well.

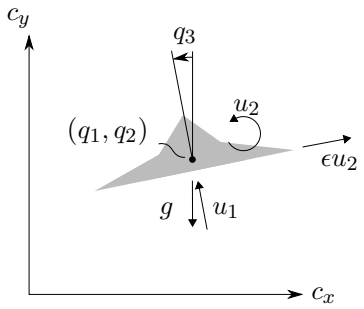

Figure 12: Lateral view of the vertical take-off and landing vehicle discussed in [28], with a center of mass at (q_1, q_2), and a tilt angle q_3. It is actuated with a thrust force u_1 and a tilt torque u_2, which also yields a lateral force ϵu_2.

11.1.1 *Strongly laterally coupled aircraft*

The basis for the developments in this chapter is the vertical take-off and landing vehicle discussed in [28], as shown in Figure 12. It consists of a single body actuated with a vertical thrust force u_1 and a thrust torque u_2. The wing shape results in a coupling between the thrust torque and the lateral motion with a force ϵu_2 for some positive constant ϵ.

For a gravity acceleration g, and normalized body mass and inertia, its dynamics are described by [28]

$$\begin{bmatrix} \ddot{q}_1 \\ \ddot{q}_2 \\ \ddot{q}_3 \end{bmatrix} = \begin{bmatrix} 0 \\ -g \\ 0 \end{bmatrix} + \begin{bmatrix} -\sin q_3 & \epsilon \cos q_3 \\ \cos q_3 & \epsilon \sin q_3 \\ 0 & 1 \end{bmatrix} \begin{bmatrix} u_1 \\ u_2 \end{bmatrix}. \tag{260}$$

Using new inputs $\boldsymbol{\tau} = [\tau_1 \ \ \tau_2]^\top$, and an input transformation corrected from [28] given by

$$\begin{bmatrix} u_1 \\ u_2 \end{bmatrix} = \frac{g}{\epsilon} \begin{bmatrix} \epsilon \cos q_3 \\ \sin q_3 \end{bmatrix} + \frac{1}{\epsilon} \begin{bmatrix} -\epsilon \sin q_3 & \epsilon \cos q_3 \\ \cos q_3 & \sin q_3 \end{bmatrix} \begin{bmatrix} \tau_1 \\ \tau_2 \end{bmatrix}, \tag{261}$$

we obtain the uncontrolled dynamics used throughout this chapter, given by

$$\begin{bmatrix} \ddot{q}_1 \\ \ddot{q}_2 \\ \ddot{q}_3 \end{bmatrix} = \frac{g}{\epsilon} \begin{bmatrix} 0 \\ 0 \\ \sin q_3 \end{bmatrix} + \begin{bmatrix} 1 & 0 \\ 0 & 1 \\ \epsilon^{-1} \cos q_3 & \epsilon^{-1} \sin q_3 \end{bmatrix} \begin{bmatrix} \tau_1 \\ \tau_2 \end{bmatrix}. \tag{262}$$

11.1.2 *Quadrotor model*

We also consider the presently more common quadrotor vehicle, as shown in Figure 13, which does not have an intrinsic lateral coupling force. For a vehicle with a mass M, inertia I, vertical thrust u_1 and torque u_2, a center of mass (c_x, c_y), and a tilt angle q_3, its dynamics are given by

$$\begin{bmatrix} \ddot{c}_x \\ \ddot{c}_y \\ \ddot{q}_3 \end{bmatrix} = \begin{bmatrix} 0 \\ -g \\ 0 \end{bmatrix} + \begin{bmatrix} -\frac{1}{M} \sin q_3 & 0 \\ \frac{1}{M} \cos q_3 & 0 \\ 0 & \frac{1}{I} \end{bmatrix} \begin{bmatrix} u_1 \\ u_2 \end{bmatrix}, \tag{263}$$

where friction and aerodynamic effects are assumed to be negligible.

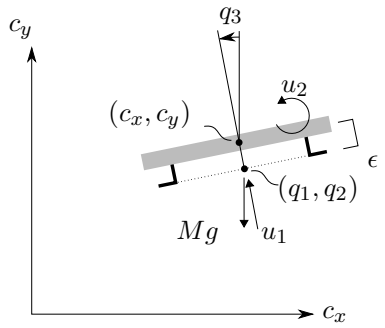

Figure 13: Lateral view of a conventional quadrotor with a center of mass (c_x, c_y), and a tilt angle q_3. It is actuated with a thrust force u_1 and a tilt torque u_2. Its landing gear is placed at a distance ϵ below its center of mass.

For the purpose of landing the vehicle, we are more interested in the dynamics of the landing gear, located at a distance ϵ below its center of mass, at (q_1, q_2), of which the kinematics are related to (c_x, c_y) as

$$\begin{bmatrix} q_1 \\ q_2 \\ q_3 \end{bmatrix} = \begin{bmatrix} c_x + \epsilon \sin q_3 \\ c_y - \epsilon \cos q_3 \\ q_3 \end{bmatrix}, \quad \begin{bmatrix} \ddot{q}_1 \\ \ddot{q}_2 \\ \ddot{q}_3 \end{bmatrix} = \begin{bmatrix} \ddot{c}_x \\ \ddot{c}_y \\ \ddot{q}_3 \end{bmatrix} + \begin{bmatrix} -\epsilon \dot{q}_3^2 \sin q_3 \\ \epsilon \dot{q}_3^2 \cos q_3 \\ 0 \end{bmatrix} + \begin{bmatrix} \cos q_3 \\ \sin q_3 \\ 0 \end{bmatrix} \epsilon \ddot{q}_3. \tag{264}$$

Inserting (263), the equations of motion in the coordinates $\boldsymbol{q} = [q_1 \;\; q_2 \;\; q_3]^\top$ become

$$\begin{bmatrix} \ddot{q}_1 \\ \ddot{q}_2 \\ \ddot{q}_3 \end{bmatrix} = \begin{bmatrix} 0 \\ -g \\ 0 \end{bmatrix} + \begin{bmatrix} -\frac{1}{M} \sin q_3 & \frac{\epsilon}{I} \cos q_3 \\ \frac{1}{M} \cos q_3 & \frac{\epsilon}{I} \sin q_3 \\ 0 & \frac{1}{I} \end{bmatrix} \begin{bmatrix} u_1 \\ u_2 \end{bmatrix} + \begin{bmatrix} -\epsilon \dot{q}_3^2 \sin q_3 \\ \epsilon \dot{q}_3^2 \cos q_3 \\ 0 \end{bmatrix}. \tag{265}$$

These dynamics are similar to the coupled aircraft model (260) except for a quadratic velocity term. Inspired by [28], we propose to use new inputs $\boldsymbol{\tau} = [\tau_1 \;\; \tau_2]^\top$ and the transformation

$$\begin{bmatrix} u_1 \\ u_2 \end{bmatrix} = -\begin{bmatrix} \epsilon M \dot{q}_3^2 \\ 0 \end{bmatrix} + \frac{g}{\epsilon} \begin{bmatrix} \epsilon M \cos q_3 \\ I \sin q_3 \end{bmatrix} + \frac{1}{\epsilon} \begin{bmatrix} -\epsilon M \sin q_3 & \epsilon M \cos q_3 \\ I \cos q_3 & I \sin q_3 \end{bmatrix} \begin{bmatrix} \tau_1 \\ \tau_2 \end{bmatrix}, \tag{266}$$

which yields, after some algebraic manipulation, the model

$$\begin{bmatrix} \ddot{q}_1 \\ \ddot{q}_2 \\ \ddot{q}_3 \end{bmatrix} = \frac{g}{\epsilon} \begin{bmatrix} 0 \\ 0 \\ \sin q_3 \end{bmatrix} + \begin{bmatrix} 1 & 0 \\ 0 & 1 \\ \epsilon^{-1} \cos q_3 & \epsilon^{-1} \sin q_3 \end{bmatrix} \begin{bmatrix} \tau_1 \\ \tau_2 \end{bmatrix}, \tag{267}$$

which is indeed the same model as (262).

11.1.3 *Simple mechanical system model*

The previously obtained equivalent quadrotor model and the strongly coupled aircraft model can be written as a simple mechanical system using the terminology of Chapter 2. For agent i, this gives $n_i = 3$, $m_i = 2$, $\mathbf{M}_i = \mathbf{I}_3$, $\boldsymbol{p}_i = \mathbf{M}_i \dot{\boldsymbol{q}}_i = \dot{\boldsymbol{q}}_i$, and

$$\boldsymbol{q}_i = \begin{bmatrix} q_{1,i} \\ q_{2,i} \\ q_{3,i} \end{bmatrix}, \quad V_i(\boldsymbol{q}_i) = \frac{g}{\epsilon_i} \cos q_{3,i}, \quad \mathbf{F}(\boldsymbol{q}_i) = \begin{bmatrix} 1 & 0 \\ 0 & 1 \\ \epsilon_i^{-1} \cos q_{3,i} & \epsilon_i^{-1} \sin q_{3,i} \end{bmatrix}. \tag{268}$$

Both the quadrotor and the strongly coupled aircraft will henceforth be referred to as an unmanned aerial vehicle, or UAV.

11.2 SINGLE-AGENT UAV IDA-PBC SOLUTION

The UAV model belongs to the class of systems discussed in Chapter 3, for which [28] provides an explicit solution to the single-agent tracking problem. The original goal is to stabilize a desired equilibrium $\boldsymbol{q}^* = [q_1^* \;\; q_2^* \;\; 0]^\top$, corresponding to asymptotic tracking of a desired vertical and horizontal location, with a fixed horizontal attitude angle.

In the distributed control case, the agents control $q_{1,i}$ and $q_{2,i}$ collaboratively while stabilizing the angle $q_{3,i}$ to zero ($\ell = 2$). This section repeats the main result of the example in [28], adopted to the notation of this thesis.

11.2.1 *Kinetic energy matching equation*

The input matrix annihilator is given by

$$\mathbf{F}_i^{\perp} = \begin{bmatrix} \cos q_{3,i} & \sin q_{3,i} & -\epsilon_i \end{bmatrix}. \tag{269}$$

Combined with the simple form of $\mathbf{M}_i$, and because $\mathbf{M}_{\mathrm{d},i}$ will be chosen as a function of $q_{3,i}$, this reduces the kinetic energy matching equation (171) of agent i to

$$\begin{bmatrix} \cos q_{3,i} & \sin q_{3,i} & -\epsilon_i \end{bmatrix} \left(-\mathbf{M}_{\mathrm{d},i} \frac{\partial}{\partial q_{3,i}} \left(\boldsymbol{p}_i^{\top} \mathbf{M}_{\mathrm{d},i}^{-1} \boldsymbol{p}_i \right) + 2\mathbf{J}_i \mathbf{M}_{\mathrm{d},i}^{-1} \boldsymbol{p}_i \right) = 0, \tag{270}$$

where the desired mass matrix $\mathbf{M}_{\mathrm{d},i} > \mathbf{0}_3$ and gyroscopic force interconnection matrix $\mathbf{J}_i = -\mathbf{J}_i^{\top}$ are to be designed to satisfy this equality. A solution is [28]

$$\mathbf{M}_{\mathrm{d},i} = \begin{bmatrix} k_{1,i}\epsilon_i \cos^2 q_{3,i} + k_{3,i} & k_{1,i}\epsilon_i \cos q_{3,i} \sin q_{3,i} & k_{1,i} \cos q_{3,i} \\ k_{1,i}\epsilon_i \cos q_{3,i} \sin q_{3,i} & -k_{1,i}\epsilon_i \cos^2 q_{3,i} + k_{3,i} & k_{1,i} \sin q_{3,i} \\ k_{1,i} \cos q_{3,i} & k_{1,i} \sin q_{3,i} & k_{2,i} \end{bmatrix}, \tag{271}$$

with the constants $k_{1,i} > 0$ and $k_{2,i}, k_{3,i}$ satisfying

$$k_{3,i} > 5k_{1,i}\epsilon_i, \quad \frac{k_{1,i}}{\epsilon_i} > k_{2,i} > \frac{k_{1,i}}{2\epsilon}, \tag{272}$$

in order to ensure that $\mathbf{M}_{\mathrm{d},i}$ is globally positive definite and bounded. The matrix $\mathbf{J}_i$ can be solved from (270) algebraically, which gives [28]

$$\mathbf{J}_i = -\frac{k_{1,i}\gamma_3^0}{2} \begin{bmatrix} 0 & J_{1,i} & J_{2,i} \\ -J_{1,i} & 0 & J_{3,i} \\ -J_{2,i} & -J_{3,i} & 0 \end{bmatrix}, \tag{273}$$

with the scalars

$$J_{1,i} = \boldsymbol{p}^{\top} \mathbf{M}_{\mathrm{d},i}^{-1} \begin{bmatrix} -2\epsilon_i \cos q_{3,i} \\ 2\epsilon_i \sin q_{3,i} \\ 1 \end{bmatrix}, \quad J_{2,i} = \boldsymbol{p}^{\top} \mathbf{M}_{\mathrm{d},i}^{-1} \begin{bmatrix} 0 \\ 1 \\ 0 \end{bmatrix}, \quad J_{3,i} = \boldsymbol{p}^{\top} \mathbf{M}_{\mathrm{d},i}^{-1} \begin{bmatrix} -1 \\ 0 \\ 0 \end{bmatrix},$$

and the constant $\gamma_{3,i}^0 = k_{1,i} - \epsilon_i k_{2,i}$. The constant $\gamma_{3,i}^0$ equals $\gamma_{3,i}$ in the definition of $\boldsymbol{\gamma}_i$ (72):

$$\boldsymbol{\gamma}_i(q_{3,i}) = \begin{bmatrix} \gamma_{1,i} \\ \gamma_{2,i} \\ \gamma_{3,i} \end{bmatrix} = \mathbf{M}_{\mathrm{d},i} \left(\mathbf{F}_i^{\perp} \right)^{\top}, \tag{274}$$

while the remaining terms $\gamma_{1,i}$ and $\gamma_{2,i}$ become

$$\begin{aligned} \gamma_{1,i} &= k_{1,i}\epsilon_i \cos^3 q_{3,i} + k_{3,i} \cos q_{3,i} + k_{1,i}\epsilon_i \cos q_{3,i} \sin^2 q_{3,i} - k_{1,i}\epsilon_i \cos q_{3,i} \\ &= k_{3,i} \cos q_{3,i}, \end{aligned} \tag{275}$$

$$\begin{aligned} \gamma_{2,i} &= k_{1,i}\epsilon_i \cos^2 q_{3,i} \sin q_{3,i} - k_{1,i}\epsilon_i \cos^2 q_{3,i} \sin q_{3,i} + k_{3,i} \sin q_{3,i} - k_{1,i}\epsilon_i \sin q_{3,i} \\ &= (k_{3,i} - k_{1,i}\epsilon_i) \sin q_{3,i}. \end{aligned} \tag{276}$$

11.2.2 *Desired stabilization potential energy*

The desired stabilization potential energy is obtained using (73) which yields

$$b_i(q_{3,i}) = \begin{bmatrix} \cos q_{3,i} & \sin q_{3,i} & -\epsilon_i \end{bmatrix} \begin{bmatrix} 0 \\ 0 \\ -\dfrac{g}{\epsilon_i} \sin q_{3,i} \end{bmatrix} = g \sin q_{3,i}, \tag{277}$$

$$V_{\mathrm{s},i}(\boldsymbol{q}_i) = \frac{1}{\gamma^0_{3,i}} \int_0^{q_{3,i}} b(\mu)\mathrm{d}\mu = \frac{g}{\gamma^0_{3,i}} \int_0^{q_{3,i}} \sin\mu\,\mathrm{d}\mu = \frac{g}{\gamma^0_{3,i}}(1-\cos q_{3,i}). \tag{278}$$

11.2.3 *Communicated variable*

From (71) and the preceding definitions we obtain

$$a_{j,i} = q_{j,i} - \frac{1}{\gamma^0_{3,i}} \int_0^{q_{3,i}} \gamma_{j,i}(\mu)\mathrm{d}\mu, \tag{279}$$

which yields for $j = 1, 2$ and agent i,

$$\begin{aligned} a_{1,i} &= q_{1,i} - \frac{k_{3,i}}{\gamma^0_{3,i}} \int_0^{q_{3,i}} \cos\mu\,\mathrm{d}\mu \\ &= q_{1,i} - \frac{k_{3,i}}{\gamma^0_{3,i}} \sin q_{3,i}, \end{aligned} \tag{280}$$

$$\begin{aligned} a_{2,i} &= q_{2,i} - \frac{k_{3,i} - k_{1,i}\epsilon_i}{\gamma^0_{3,i}} \int_0^{q_{3,i}} \sin\mu\,\mathrm{d}\mu \\ &= q_{2,i} - \frac{k_{3,i} - k_{1,i}\epsilon_i}{\gamma^0_{3,i}}(1-\cos q_{3,i}). \end{aligned} \tag{281}$$

Since $\ell = m_i$, we obtain from (70) that the communicated variable $\boldsymbol{z}_i$ is

$$\boldsymbol{z}_i(\boldsymbol{q}_i) = \begin{bmatrix} a_{1,i} \\ a_{2,i} \end{bmatrix} = \begin{bmatrix} q_{1,i} \\ q_{2,i} \end{bmatrix} - \frac{1}{\gamma^0_{3,i}} \begin{bmatrix} k_{3,i}\sin q_{3,i} \\ (k_{3,i} - k_{1,i}\epsilon_i)(1-\cos q_{3,i}) \end{bmatrix}. \tag{282}$$

When $q_{3,i}$ stabilizes at zero, this reduces to $\boldsymbol{z}_i(q_{1,i}, q_{2,i}, 0) = [q_{1,i}\ \ q_{2,i}]^\top$, meaning that any target formation in $\boldsymbol{z}_i$ can immediately be expressed in absolute and relative distances expressed in the Euclidean coordinates $(q_{1,i}, q_{2,i})$.

11.3 FORMATION FLYING

This section demonstrates the implementation and simulation of a distributed system of six identical UAV systems with the previously given dynamics and single-agent IDA-PBC solutions.

11.3.1 *Formation objective and graph structure*

The control objective of each UAV i is to stabilize its tilt angle at $q^*_{3,i} = 0$ while communicating the variable $\boldsymbol{z}_i$ with neighboring UAVs to assume a desired formation, as shown in Figure 14. The target formation is a pyramid shape composed of four equilateral triangles with sides of length c, which uniquely specifies the inter-agent distances for each edge. For example, $\boldsymbol{r}^*_{23} = -\frac{1}{2}c[1\ \ \sqrt{3}]^\top$ and $\boldsymbol{r}^*_{32} = -\boldsymbol{r}^*_{23}$.

Each agents has either two or four neighbors that exchange the vector signals $\boldsymbol{z}_i$, as shown in Figure 15. Only the leading agents 1 and 2 know a prescribed reference hovering altitude a^*. No horizontal target is specified, meaning that the group comes to standstill at an arbitrary horizontal position but with a fixed geometry and altitude.

For each of the edges $(1,2)$, $(6,3)$, $(3,5)$, $(3,1)$, $(5,2)$, $(2,4)$, $(2,3)$, $(4,1)$, $(1,6)$ and their opposite counterparts $(2,1), \cdots (6,1)$, the adjacency matrices are chosen as $\boldsymbol{\mathcal{A}}_{ij} = \mathrm{diag}(1,2)$. The leader target altitude is specified using $\boldsymbol{z}^*_1 = \boldsymbol{z}^*_2 = [\star\ \ a^*]^\top$ where the undefined horizontal target $\star$ is ignored by selecting the leader matrix gains as $\boldsymbol{\mathcal{B}}_1 = \boldsymbol{\mathcal{B}}_2 = \mathrm{diag}(0,5)$.

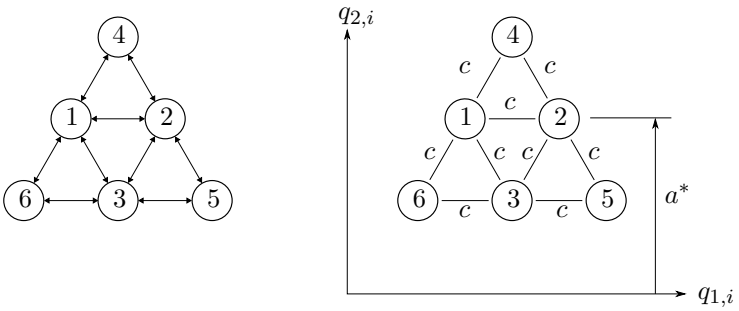

Figure 14: UAV communication graph (left) and target formation (right)

11.3.2 *Single-agent parameters*

The single-agent parameters are selected equal for each agent, as given in Table 2. Note that the open-loop model (268) is already normalized for properties such as mass and inertia through the input transformations (261), (266), meaning that they do not alter the simulation result.

Any parameters satisfying the previously given constraints (such as positive definiteness of $\mathbf{M}_{\mathrm{d},i}$) yield an asymptotically stable result, but the parameters effect the transient response considerably. For this simulation, the parameters have been selected based on trial and error as in [28], to obtain a quickly damped response.

Par.	c	a^*	g	ϵ_i	$k_{1,i}$	$k_{2,i}$	$k_{3,i}$	$\mathbf{K}_{v,i}$	$\mathbf{K}_{\mathrm{d},i}$
Value	1 m	2 m	9.81 m/s^2	0.1	2	6.67	1.02	$\mathrm{diag}(0,0)$	$\mathrm{diag}(2,2)$

Table 2: UAV system and control parameters for all agents i.

11.3.3 *Damping method*

Two damping insertion techniques were discussed in this thesis. The standard IDA-PBC technique is to insert it through the actuated coordinates and the output $\boldsymbol{y}_{\mathrm{d},i}$, by choosing nonzero $\mathbf{K}_{v,i} > \mathbf{0}_{m_i}$, as discussed in Chapter 3 for the single-agent case and in Part III for distributed systems. The other technique is to damp the velocities $\boldsymbol{y}_{e,i} = \frac{\mathrm{d}}{\mathrm{d}t}\boldsymbol{z}_i$ by shaping the input matrix and choosing nonzero $\mathbf{K}_{\mathrm{d},i} > \mathbf{0}_\ell$, as discussed in Part IV. Both techniques can be used simultaneously, either to damp the individual agent outputs or their relative outputs, or both.

For the UAV models used in this chapter, better-damped transient responses were obtained by damping only the velocities $\frac{\mathrm{d}}{\mathrm{d}t}\boldsymbol{z}_i$ using $\mathbf{K}_{\mathrm{d},i} > \mathbf{0}_\ell$ and $\mathbf{K}_{v,i} = \mathbf{0}_{m_i}$.

11.3.4 *Control law*

The solution of the decoupled matching problem and the resulting control law is a direct implementation of the methods discussed in Chapter 8, augmented with the damping technique introduced in Chapter 9. From (192) and (251) we obtain

$$\boldsymbol{\tau}_i = \boldsymbol{\sigma}_i + \boldsymbol{\Phi}_i \left(\boldsymbol{\mathcal{B}}_i(\boldsymbol{z}_i^* - \boldsymbol{z}_i) + \sum_{j=1}^{N} \boldsymbol{\mathcal{A}}_{ij}(\boldsymbol{z}_j - \boldsymbol{z}_i - \boldsymbol{r}_{ij}^*) - \mathbf{K}_{\mathrm{d},i}\boldsymbol{\Psi}_i^\top \mathbf{M}_i^{-1}\boldsymbol{p}_i \right). \quad (283)$$

where the internal stabilization term $\boldsymbol{\sigma}_i$ (194) stabilizes the angle $q_{i,3}$ and the shaped input matrix $\boldsymbol{\Phi}_i$ (194) ensures that the coupling and damping forces on $\boldsymbol{z}_i$ do not violate the matching conditions. Recall that $\boldsymbol{\Psi}_i^\top \mathbf{M}_i^{-1}\boldsymbol{p}_i = \frac{\mathrm{d}}{\mathrm{d}t}\boldsymbol{z}_i$, which reveals the analog with fully-actuated distributed PD controllers.

11.3.5 *Implementation*

The simulations throughout this thesis are a direct implementation of the previously given open-loop dynamics and control laws, with the same idealizations like the absence of time delays. At each time instant, this yields the vectors $\dot{\bar{\boldsymbol{p}}}$ and $\dot{\bar{\boldsymbol{q}}}$ of the whole system (138), which can be represented as a single ordinary differential equation. Given the initial conditions $\bar{\boldsymbol{q}}(0)$ and $\bar{\boldsymbol{p}}(0)$, this equation is integrated to find the trajectories $\bar{\boldsymbol{p}}(t)$ and $\bar{\boldsymbol{q}}(t)$ for a given time range.

The centralized ordinary differential equation is automatically generated from the open-loop dynamics of the agents i, their internal control laws, and their distributed interactions along the network edges (i, j). This generic procedure is implemented in a newly developed Python package called `systemsim`. Further details are given in Appendix b. An animation of each simulation can be viewed at `https://github.com/laurensvalk/underactuated-systems`.

11.3.6 *Formation forming*

The UAVs are initialized with different uniformly distributed pseudo-random initial configurations $\boldsymbol{q}_i$ in the range $-1 \leq q_{1,i} \leq 1$, $1 \leq q_{2,i} \leq 3$, and $-1 \leq q_{3,i} \leq 1$. The momenta $\boldsymbol{p}_i = \mathbf{I}_3 \dot{\boldsymbol{q}}_i = \dot{\boldsymbol{q}}_i$, are all pseudo-randomly initialized in the range $[-0.5, 0.5]$, as shown in Table 3. Figure 15 shows the trajectories of each UAV as they move from their initial configuration towards the desired formation.

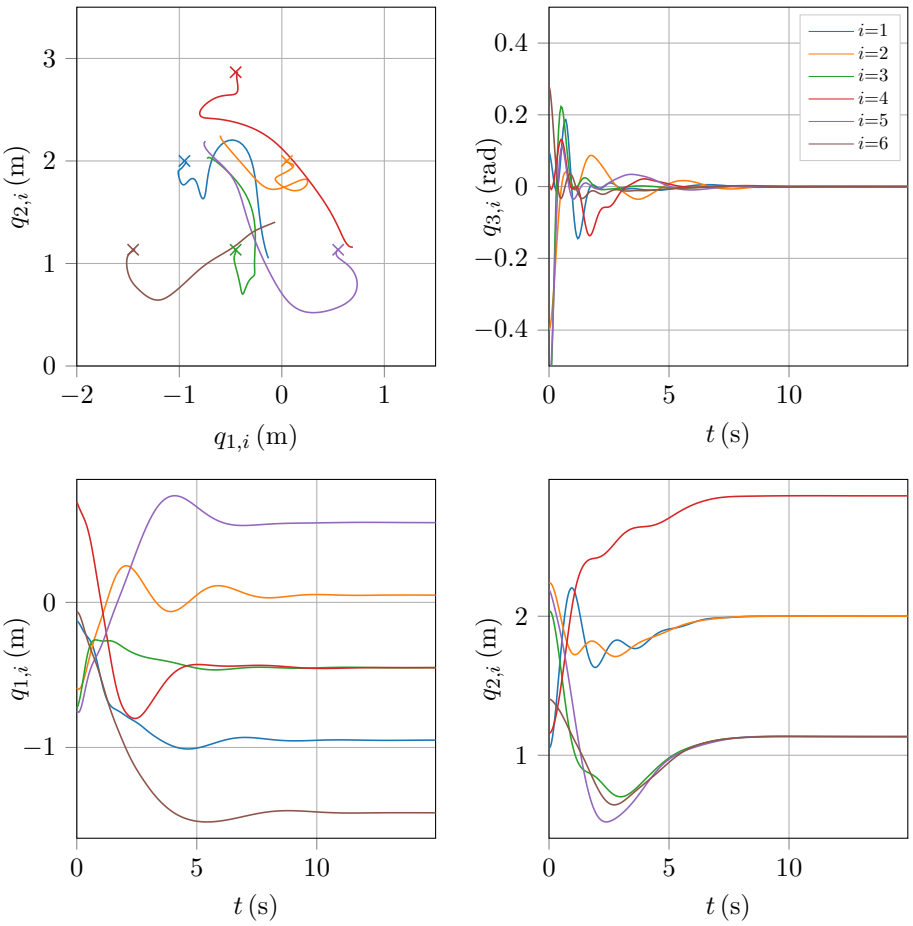

Figure 15: Formation of the pyramid configuration of Figure 14 with six identical UAVs.

The coordinates $(q_{1,i}, q_{2,i})$ reached at the end of the simulation are marked with an $\times$ symbol, which indeed coincide with the required shape pictured in Figure 14. Furthermore, the leading agents 1 and 2 reach the prescribed altitude $a^* = 2\,\mathrm{m}$, whereas agents 3, 5, and 6 synchronize their altitudes at a fixed distance from the leaders. After the horizontal and vertical motion has subsided, all tilt angles also converge to zero. It is also visible that the vertical formation shape converges before the group altitude target converges.

Collisions are not explicitly avoided in this simulation. A possible extension to address this practical problem is discussed in Chapter 13.

Table 3: Initial conditions for all agents i corresponding to Figure 15.

	$q_{1,i}$ (m)	$q_{2,i}$ (m)	$q_{3,i}$ (rad)	$p_{1,i}$ (m/s)	$p_{2,i}$ (m/s)	$p_{3,i}$ (rad/s)
1	-0.1280	1.0519	0.0993	-0.0647	-0.0796	-0.1697
2	-0.5907	2.2385	-0.4007	-0.2332	0.1211	0.0291
3	-0.7308	2.0272	-0.6311	0.2853	0.3540	-0.0058
4	0.6931	1.1593	0.0105	-0.4347	-0.0719	-0.4035
5	-0.7457	2.1935	-0.5480	-0.3931	-0.2797	-0.1502
6	-0.0644	1.4035	0.2808	-0.0169	0.0052	-0.1131

11.3.7 *Inverted initial conditions*

In the next simulation, the UAVs are initialized with pseudo-random initial configurations $\boldsymbol{q}_i$ in the range $-1 \leq q_{1,i} \leq 1$, $2 \leq q_{2,i} \leq 4$, and $\pi - 1 \leq q_{3,i} \leq \pi + 1$, as shown in Table 4. This implies that the UAVs are initialized upside down, to demonstrate the transient response of a more aggressive maneuver. Figure 16 shows the trajectories of each UAV as they move from their initial configuration towards the desired formation.

The result is similar as before, and convergence to the final formation takes little extra time. It is worth noting that some UAVs converge to the tilt angle 2π, which is equivalent to the orientation 0 after making one full rotation. This can happen because the stabilization potential (278) has minimum at every 2π, each of which corresponds to the desired objective.

Table 4: Initial conditions for all agents i corresponding to Figure 16.

	$q_{1,i}$ (m)	$q_{2,i}$ (m)	$q_{3,i}$ (rad)	$p_{1,i}$ (m/s)	$p_{2,i}$ (m/s)	$p_{3,i}$ (rad/s)
1	-0.1660	3.4406	2.1418	-0.1977	-0.3532	-0.4077
2	-0.6275	2.6911	2.9351	0.0388	-0.0808	0.1852
3	-0.5911	3.7562	2.1964	0.1705	-0.0827	0.0587
4	-0.7192	2.3962	3.7431	0.4683	-0.1866	0.1923
5	0.7528	3.7892	2.3117	-0.4609	-0.3302	0.3781
6	-0.8033	2.8422	4.0574	0.0332	0.1919	-0.1845

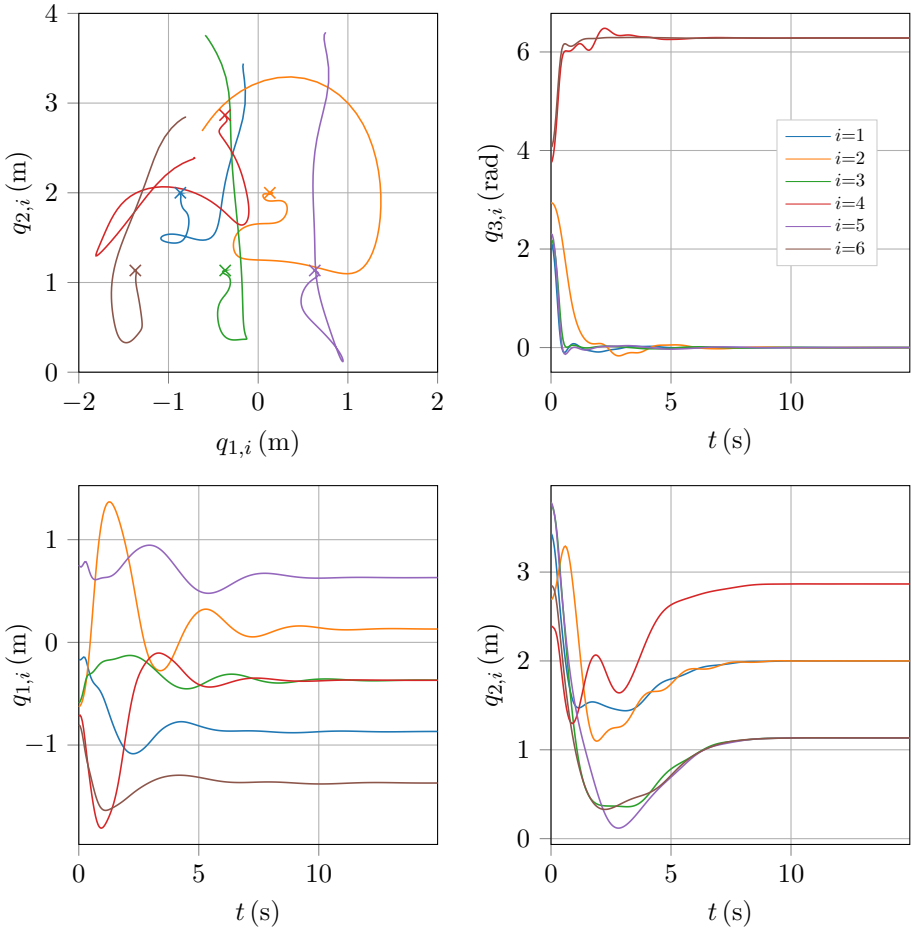

Figure 16: Creation of the formation when all agents are initially upside down.

11.3.8 *Almost global asymptotic stability*

The single-agent solution in [28] is almost globally asymptotically stable, in the sense that if it is initialized stationary, precisely upside down ($q_{3,i} = \pi$), and at its target location, it remains upside down at that location. For all other initial conditions, it recovers to the desired orientation ($q_{3,i} = 0$). The upside down orientation is an (unstable) equilibrium because the gradient of the stabilization potential energy (278) is zero at ($q_{3,i} = 0$). This behavior is similar to a pendulum initialized in its upright orientation.

For the group of UAVs, this occurs only if the group is already in its target configuration, and at the target location if there are leaders. For any deviation from the target formation, the potential forces between the agents would perturb the unstable equilibria, such that the group eventually converges to the desired formation with each UAV in the regular orientation.

11.4 CONTROLLED LANDING ON COOPERATING VEHICLE

This section discusses the distributed control problem of landing a group of three UAVs on an autonomously controlled platform that can translate horizontally, as shown in Figure 17. It is assumed that only one UAV can communicate with the autonomous cart. UAV 3 synchronizes its horizontal translation with the cart while UAVs 2 and 4 synchronize their altitude with UAV 3 while maintaining a fixed relative horizontal distance from UAV 3.

The horizontally translating landing platform is modeled as a fully-actuated frictionless point mass $M_1 > 0$, with $F_1 = 1$ and $V = 0$, whose single-agent control parameters are $M_{\mathrm{d},1} > 0$, $J_1 = 0$, $V_{s,1} = 0$, $K_{v,1} > 0$ and $K_{\mathrm{d},1} = 0$.

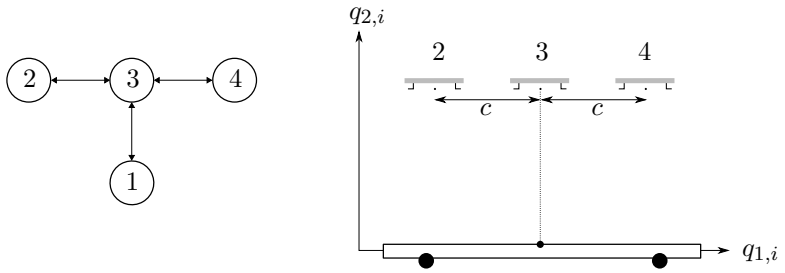

Figure 17: UAV and lander communication graph (left) and intermediate target formation before starting the descent (right).

11.4.1 *Graph structure and the communicated variable*

The previously described communication graph is summarized in Figure 17. The communicated variables $\boldsymbol{z}_i \in \mathbb{R}^2$ of the UAVs are as before (282). Although the autonomous cart does not have a vertical coordinate, we can define its communicated variable as

$$\boldsymbol{z}_1(q_{1,1}) = \begin{bmatrix} q_{1,1} \\ 0 \end{bmatrix}, \quad \boldsymbol{\Psi}_1 = \begin{bmatrix} 1 & 0 \\ 0 & 0 \end{bmatrix}. \tag{284}$$

This definition violates the condition $\ell \leq n_i$ since $\ell = 2 > n_1 = 1$. Hence, this simulation is an example of an extension that not only allows heterogeneous systems but also certain constraints. In this view, the cart may be considered to have a vertical coordinate, but a constraint force keeps it at zero. The desired formations can still be achieved if the targets $\boldsymbol{r}_{ij}^*$ and $\boldsymbol{z}_i^*$ do not violate these constraints.

11.4.2 *Vehicle mass shaping*

Because the autonomous cart is fully-actuated, it is possible to assign an arbitrary desired mass matrix $M_{\mathrm{d},1} > 0$. While doing so is not necessary to achieve the group objective asymptotically, the mass matrix can be shaped to change its relative magnitude with respect to the UAV vehicles.

The horizontal synchronization objective of the landing vehicle with UAV 3 yields a virtual coupling force between these two agents. When we consider a more massive landing vehicle of 50 kg compared to a UAV of 1 kg, this force makes the landing vehicle move much less than the UAV, to an extent that the landing vehicle remains almost stationary.

By choosing a higher $M_{\mathrm{d},1} > M_1$, this relative mass effect can be adjusted to make the landing vehicle contribute more to the group objective. This speeds up the transient response, which may conserve battery power of the UAVs, at the

expensive of higher energy consumption of the landing platform. Recall that the apparent inverse effect of increasing the desired mass matrix $M_{\mathrm{d},1}$ to speed up a system was addressed in Section 9.4.6.

To illustrate this effect in the simulations, we select $M_1 = 50\,\mathrm{kg}$ and choose $M_{\mathrm{d},1} = 2500\,\mathrm{kg}$ to amplify the effect of the coupling forces on the vehicle by a factor 50. This results in perceived mass of 1 kg, which is the same order of magnitude as the UAV models with normalized mass. Because the damping force scaled inversely proportionally with $M_{\mathrm{d},1}$, $K_{v,1} = 2500$ is selected to obtain a well-damped response.

11.4.3 *Formation forming and controlled descent*

The simulation takes place in two separate phases. First, the UAVs attain a desired relative horizontal formation while synchronizing their altitudes. Meanwhile, UAV 3 synchronizes its horizontal translation with the autonomous cart (system 1). After six seconds all three UAVs also steer towards a target altitude of zero, for a controlled descent. The separation of the two phases ensures that the desired formation is attained before the landing is attempted.

To attain the leaderless formation in the initial phase, the adjacency matrices and relative targets are $\boldsymbol{\mathcal{A}}_{23} = \boldsymbol{\mathcal{A}}_{34} = \mathrm{diag}(1, 2)$, $\boldsymbol{r}^*_{23} = \boldsymbol{r}^*_{34} = [c\ 0]^\top$, $c = 1$ while having no leaders implies ($\boldsymbol{\mathcal{B}}_1 = \boldsymbol{\mathcal{B}}_2 = \boldsymbol{\mathcal{B}}_3 = \boldsymbol{\mathcal{B}}_4 = \mathbf{0}_2$). In the second phase ($t > 6$), the UAVs have a target of $\boldsymbol{z}^*_2 = \boldsymbol{z}^*_3 = \boldsymbol{z}^*_4 = [\star\ 0]^\top$ and a corresponding leader matrix of $\boldsymbol{\mathcal{B}}_2 = \boldsymbol{\mathcal{B}}_3 = \boldsymbol{\mathcal{B}}_4 = \mathrm{diag}(0, 1)$, corresponding to a vertical target of 0 while imposing no additional constraints on the horizontal motion.

The UAV parameters are the same as in Table 2. The initial conditions are given in Table 5 and the simulation results are shown in Figure 18.

Table 5: Initial conditions for all agents i corresponding to Figure 18.

	$q_{1,i}$ (m)	$q_{2,i}$ (m)	$q_{3,i}$ (rad)	$p_{1,i}$ (m/s)	$p_{2,i}$ (m/s)	$p_{3,i}$ (rad/s)
1	-1	-	-	0	-	-
1	-0.5560	2.7415	-0.5866	0.4186	-0.0116	0.1117
2	0.5318	2.0368	-0.4064	-0.3123	-0.4193	0.2384
3	-0.1174	1.3166	0.7599	-0.2259	-0.0858	-0.2039

During the first phase ($0 \leq t \leq 6$) the desired formation of the UAVs is achieved in a similar fashion as in the previous simulations. In this case, however, the landing vehicle also synchronizes with the horizontal location of UAV 3. Because of the shaped mass of the landing vehicle, potential forces between the systems yield motion on the same order of magnitude among all vehicles. This means that the landing vehicle actively participates creating the formation, rather than waiting for the UAVs to fly towards it.

During the second phase ($t > 6$), the vehicles slowly descend while maintaining their horizontal formation, resulting in a simulated soft landing.

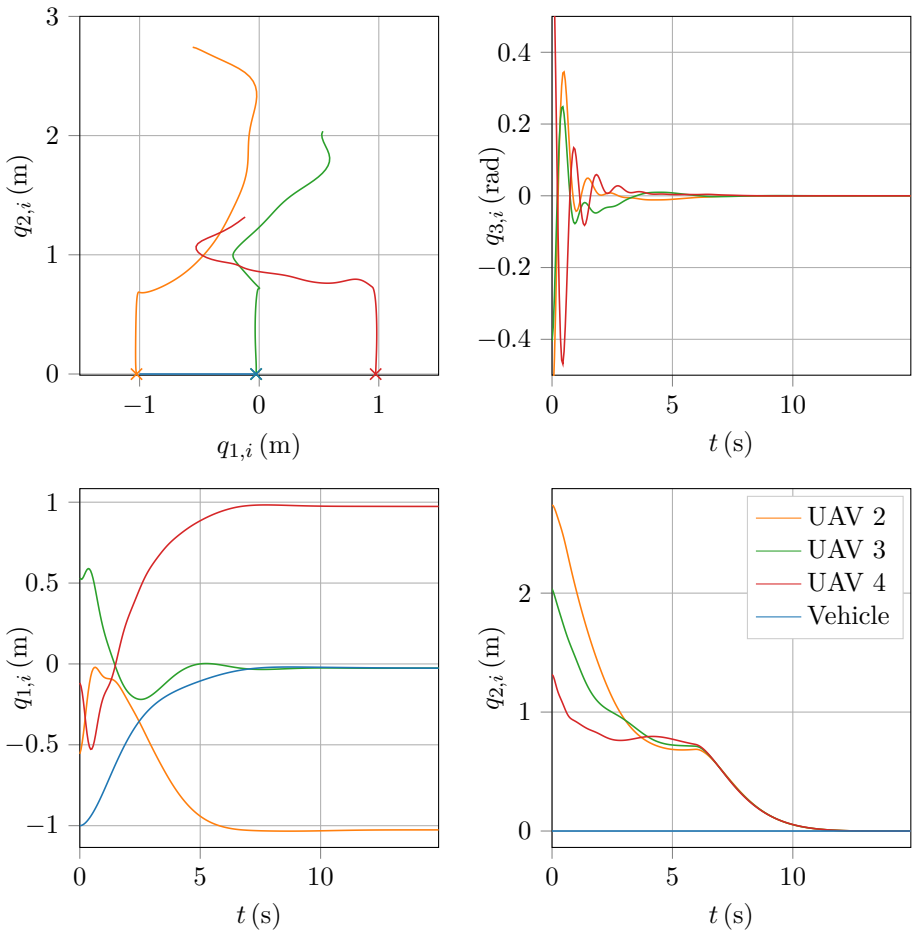

Figure 18: Synchronization of a group of UAVs with an autonomous lander ($0 \leq t \leq 6$) and a subsequent soft landing ($t > 6$).

12

TASK-SPACE COORDINATION AND HUMAN SUPERVISORY CONTROL OF HETEROGENEOUS MECHANICAL SYSTEMS

This chapter combines most of the modeling and control techniques introduced throughout this thesis in two simulations. The first simulation highlights the aspect of creating task-space formations between heterogeneous underactuated systems, where a UAV and two different flexible-joint robotic manipulators agree on a docking location (Section 12.2). The second simulation extends this result with a haptic manipulator, through which a human operator can alter the final docking location while the docking procedure itself remains autonomous (Section 12.3). Before presenting the simulations, a derivation of the single-agent control solution of a flexible-joint manipulator is given in Section 12.1.

12.1 FLEXIBLE-JOINT MANIPULATOR DYNAMICS AND CONTROL

This section derives the equations of motion of a planar m-link flexible-joint manipulator using the modeling techniques discussed in Chapter 2. The manipulator consists of m links with length L_k, and mass M_k. The center of mass of link k is located at the position (x_k, y_k), assumed to be in the middle of the link. The inertia around its center of mass is I_k. The links are connected through frictionless hinges, with α_k defined as the counterclockwise rotation of link k with respect to link $k-1$, as shown in Figure 19. The absolute angle γ_k of link k is the sum of the relative angles, given by

$$\gamma_k = \alpha_1 + \cdots + \alpha_k. \tag{285}$$

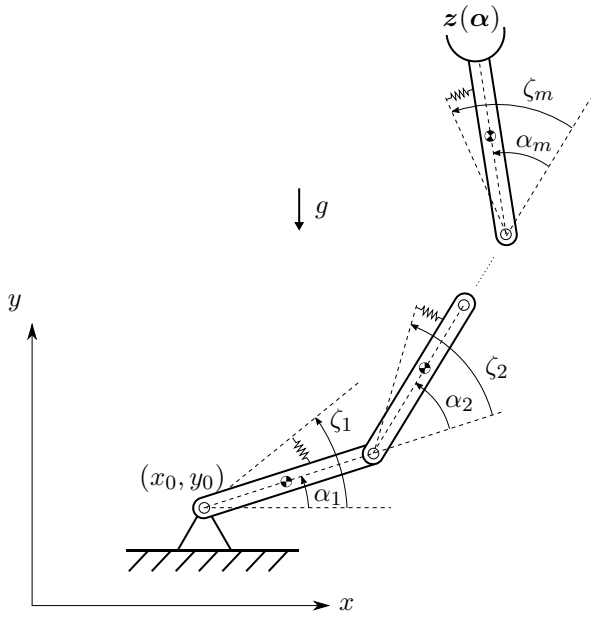

Figure 19: A flexible-joint manipulator with m links and an end-effector location $\boldsymbol{z}(\boldsymbol{\alpha})$. Each link is driven through a linear torsional spring between the link and a motor, with a spring extension angle $\zeta_k - \alpha_k$.

Each link k is driven by a torsional spring with stiffness c_k. The spring connects a motor shaft to the joint segment (at angle ζ_k), such that the spring extension angle is $\zeta_k - \alpha_k$. The motor that drives spring k is mounted at segment $k-1$, embedded in the total mass and inertia of that link. It can be controlled using a torque signal u_k. Finally, gravity acts at each center of mass in the downward direction.

The angles α_k and ζ_k uniquely describe the configuration $\boldsymbol{q} \in \mathbb{R}^{2m}$ of the system:

$$\boldsymbol{\alpha} = \begin{bmatrix} \alpha_1 \\ \vdots \\ \alpha_m \end{bmatrix}, \quad \boldsymbol{\zeta} = \begin{bmatrix} \zeta_1 \\ \vdots \\ \zeta_m \end{bmatrix}, \quad \boldsymbol{q} = \begin{bmatrix} \boldsymbol{\alpha} \\ \boldsymbol{\zeta} \end{bmatrix}. \tag{286}$$

12.1.1 *Kinematics*

If the manipulator base is located at (x_0, y_0), the positions of the center of mass locations (x_k, y_k) of each link $k = 1, \ldots, m$ are given recursively as

$$\begin{aligned} x_1 &= x_0 + \frac{1}{2} L_1 \cos(\gamma_1), \\ y_1 &= y_0 + \frac{1}{2} L_1 \sin(\gamma_1), \\ x_2 &= x_1 + \frac{1}{2} L_1 \cos(\gamma_1) + \frac{1}{2} L_2 \cos(\gamma_2), \\ y_2 &= y_1 + \frac{1}{2} L_1 \sin(\gamma_1) + \frac{1}{2} L_2 \sin(\gamma_2), \\ &\vdots \\ x_m &= x_{m-1} + \frac{1}{2} L_{m-1} \cos(\gamma_{m-1}) + \frac{1}{2} L_m \cos(\gamma_m), \\ y_m &= y_{m-1} + \frac{1}{2} L_{m-1} \sin(\gamma_{m-1}) + \frac{1}{2} L_m \sin(\gamma_m). \end{aligned} \tag{287}$$

The end-effector, presumed to be a gripper, is located at the end-point of the final link, denoted as $\boldsymbol{z}(\boldsymbol{\alpha})$, given by

$$\boldsymbol{z}(\boldsymbol{\alpha}) = \begin{bmatrix} x_m + \frac{1}{2} L_m \cos(\gamma_m) \\ y_m + \frac{1}{2} L_m \cos(\gamma_m) \end{bmatrix}. \tag{288}$$

12.1.2 *Mass matrix*

The mass matrix $\mathbf{M}(\boldsymbol{q})$ can be inferred from the kinetic energy in the system. First, define the joint positions and velocities as

$$\boldsymbol{w} = \begin{bmatrix} \gamma_1 & x_1 & y_1 & \cdots & \gamma_m & x_m & y_m \end{bmatrix}^\top, \quad \dot{\boldsymbol{w}} = \frac{\partial \boldsymbol{w}}{\partial \boldsymbol{\alpha}} \dot{\boldsymbol{\alpha}}. \tag{289}$$

The kinetic energy of the system is the sum of the kinetic translational energy and rotational energy of each link. This sum can be expressed as a quadratic function of the velocities $\boldsymbol{w}$, which gives

$$T_\alpha = \frac{1}{2} \dot{\boldsymbol{w}}^\top \mathrm{diag}(I_1, M_1, M_1, \ldots, I_m, M_m, M_m) \dot{\boldsymbol{w}} \tag{290}$$

$$= \frac{1}{2} \dot{\boldsymbol{\alpha}}^\top \mathbf{M}_\alpha \dot{\boldsymbol{\alpha}}, \tag{291}$$

where

$$\mathbf{M}_\alpha = \frac{\partial^\top \boldsymbol{w}}{\partial \boldsymbol{\alpha}} \mathrm{diag}(I_1, M_1, M_1, \ldots, I_m, M_m, M_m) \frac{\partial \boldsymbol{w}}{\partial \boldsymbol{\alpha}}. \tag{292}$$

The motor shafts and drive train of each link have an inertia I_ζ, which gives a mass matrix of

$$\mathbf{M}_\zeta = I_\zeta \mathbf{I}_m. \tag{293}$$

The total mass matrix $\mathbf{M}(\boldsymbol{q}) > \mathbf{0}_n$ of the system with coordinates $\boldsymbol{q}$ is

$$\mathbf{M}(\boldsymbol{q}) = \begin{bmatrix} \mathbf{M}_\alpha(\boldsymbol{\alpha}) & \mathbf{0}_m \\ \mathbf{0}_m & \mathbf{M}_\zeta \end{bmatrix}. \tag{294}$$

12.1.3 *Potential energy*

The potential energy in the system consists of the gravitational energy and the energy due to the spring extensions, which gives

$$V = V_\alpha + \frac{1}{2}(\boldsymbol{\zeta} - \boldsymbol{\alpha})^\top \boldsymbol{\Upsilon}(\boldsymbol{\zeta} - \boldsymbol{\alpha}), \tag{295}$$

where $\boldsymbol{\Upsilon} = \operatorname{diag}(c_1, \ldots, c_m) > \mathbf{0}_m$ is the spring stifness matrix. The gravitational potential energy is

$$V_\alpha = g \sum_{k=1}^{m} M_k y_k(\boldsymbol{\alpha}). \tag{296}$$

12.1.4 *Gravity compensation*

The equations of motion are the standard Hamiltonian equations (15). Relying on the partitioning (286) and introducing $\boldsymbol{p}_\alpha = \mathbf{M}_\alpha \dot{\boldsymbol{\alpha}}$ and $\boldsymbol{p}_\zeta = \mathbf{M}_\zeta \dot{\boldsymbol{\zeta}}$, the total energy and equations of motion can be written as

$$\begin{bmatrix} \dot{\boldsymbol{q}} \\ \dot{\boldsymbol{p}} \end{bmatrix} = \begin{bmatrix} \mathbf{0}_m & \mathbf{0}_m & \mathbf{I}_m & \mathbf{0}_m \\ \mathbf{0}_m & \mathbf{0}_m & \mathbf{0}_m & \mathbf{I}_m \\ -\mathbf{I}_m & \mathbf{0}_m & \mathbf{0}_m & \mathbf{0}_m \\ \mathbf{0}_m & -\mathbf{I}_m & \mathbf{0}_m & \mathbf{0}_m \end{bmatrix} \begin{bmatrix} \dfrac{\partial \hat{H}}{\partial \boldsymbol{\alpha}} \\ \dfrac{\partial \hat{H}}{\partial \boldsymbol{\zeta}} \\ \dfrac{\partial \hat{H}}{\partial \boldsymbol{p}_\alpha} \\ \dfrac{\partial \hat{H}}{\partial \boldsymbol{p}_\zeta} \end{bmatrix} + \begin{bmatrix} \mathbf{0}_m \\ \mathbf{0}_m \\ \mathbf{0}_m \\ \mathbf{I}_m \end{bmatrix} u \tag{297}$$

$$\hat{H} = \frac{1}{2}\boldsymbol{p}_\alpha^\top \mathbf{M}_\alpha^{-1} \boldsymbol{p}_\alpha + \frac{1}{2}\boldsymbol{p}_\zeta^\top \mathbf{M}_\zeta^{-1} \boldsymbol{p}_\zeta + V_\alpha + \frac{1}{2}(\boldsymbol{\zeta} - \boldsymbol{\alpha})^\top \boldsymbol{\Upsilon}(\boldsymbol{\zeta} - \boldsymbol{\alpha}) \tag{298}$$

The system is underactuated because only the coordinates $\boldsymbol{\zeta}$ are actuated, hampering the ability to directly compensate for gravity. We now define a control law that compensates for the effects of gravity, adapting the Lagrangian formulation from [37] to the Hamiltonian framework. To do so, we introduce a new coordinate $\boldsymbol{\delta} \in \mathbb{R}^m$, with a momentum $\boldsymbol{p}_\delta = \mathbf{M}_\delta \dot{\boldsymbol{\beta}}$, $\mathbf{M}_\delta = \mathbf{M}_\zeta$, and a control law $\boldsymbol{u}$, as

$$\boldsymbol{\delta} = \boldsymbol{\zeta} - \boldsymbol{\Upsilon}^{-1} \frac{\partial V_\alpha}{\partial \boldsymbol{\alpha}}, \tag{299}$$

$$\boldsymbol{u} = \boldsymbol{\tau} + \frac{\partial V_\alpha}{\partial \boldsymbol{\alpha}} + \mathbf{M}_\zeta \boldsymbol{\Upsilon}^{-1} \frac{\mathrm{d}^2}{\mathrm{d}t^2} \frac{\partial V_\alpha}{\partial \boldsymbol{\alpha}}, \tag{300}$$

where $\boldsymbol{\tau} \in \mathbb{R}^m$ is a new input.

This transformation and control law can be implemented without acceleration measurements because the second time derivative of the gravity torque can be expressed as a function of the state variables $\boldsymbol{\alpha}, \boldsymbol{\zeta}, \boldsymbol{p}_\alpha, \boldsymbol{p}_\zeta$ [37].

Substituting the transformations and the control law into the dynamics (297) gives the new dynamics

$$\dot{\boldsymbol{\alpha}} = \mathbf{M}_\alpha^{-1}\boldsymbol{p}_\alpha, \tag{301}$$

$$\dot{\boldsymbol{\beta}} = \mathbf{M}_\delta^{-1}\boldsymbol{p}_\delta, \tag{302}$$

$$\begin{aligned}\dot{\boldsymbol{p}}_\alpha &= -\frac{\partial}{\partial \boldsymbol{\alpha}}\left(\frac{1}{2}\boldsymbol{p}_\alpha^\top \mathbf{M}_\alpha^{-1}\boldsymbol{p}_\alpha + V_\alpha\right) + \boldsymbol{\Upsilon}\left(\boldsymbol{\delta} + \boldsymbol{\Upsilon}^{-1}\frac{\partial V_\alpha}{\partial \boldsymbol{\alpha}} - \boldsymbol{\alpha}\right) \\ &= -\frac{\partial}{\partial \boldsymbol{\alpha}}\left(\frac{1}{2}\boldsymbol{p}_\alpha^\top \mathbf{M}_\alpha^{-1}\boldsymbol{p}_\alpha\right) + \boldsymbol{\Upsilon}\left(\boldsymbol{\delta} - \boldsymbol{\alpha}\right), \end{aligned} \tag{303}$$

$$\begin{aligned}\dot{\boldsymbol{p}}_\delta &= \mathbf{M}_\delta \ddot{\boldsymbol{\zeta}} - \mathbf{M}_\delta \boldsymbol{\Upsilon}^{-1}\frac{\mathrm{d}^2}{\mathrm{d}t^2}\frac{\partial V_\alpha}{\partial \boldsymbol{\alpha}} \\ &= \dot{\boldsymbol{p}}_\zeta - \mathbf{M}_\delta \boldsymbol{\Upsilon}^{-1}\frac{\mathrm{d}^2}{\mathrm{d}t^2}\frac{\partial V_\alpha}{\partial \boldsymbol{\alpha}} \\ &= -\boldsymbol{\Upsilon}(\boldsymbol{\zeta} - \boldsymbol{\alpha}) + u - \mathbf{M}_\delta \boldsymbol{\Upsilon}^{-1}\frac{\mathrm{d}^2}{\mathrm{d}t^2}\frac{\partial V_\alpha}{\partial \boldsymbol{\alpha}} \\ &= -\boldsymbol{\Upsilon}(\boldsymbol{\delta} - \boldsymbol{\alpha}) + \boldsymbol{\tau}. \end{aligned} \tag{304}$$

These dynamics can in turn be written as Hamiltonian equations similar to (297), but now in the coordinates $\boldsymbol{\alpha}$ and $\boldsymbol{\delta}$, and without the gravity term. This gives the flexible-joint model used throughout this chapter, which for agent i is given in the standard notation of (135), with

$$\begin{aligned}\boldsymbol{q}_i &= \begin{bmatrix}\boldsymbol{\alpha}_i \\ \boldsymbol{\delta}_i\end{bmatrix}, \quad \boldsymbol{p}_i = \begin{bmatrix}\boldsymbol{p}_{\alpha,i} \\ \boldsymbol{p}_{\delta,i}\end{bmatrix}, \quad V_i = \frac{1}{2}(\boldsymbol{\delta} - \boldsymbol{\alpha})^\top \boldsymbol{\Upsilon}(\boldsymbol{\delta} - \boldsymbol{\alpha}) \\ \mathbf{M}_i &= \begin{bmatrix}\mathbf{M}_{\alpha,i} & \mathbf{0}_m \\ \mathbf{0}_m & \mathbf{M}_{\delta,i}\end{bmatrix}, \quad \mathbf{F}_i = \begin{bmatrix}\mathbf{0}_m \\ \mathbf{I}_m\end{bmatrix}. \end{aligned} \tag{305}$$

In order to give a physical interpretation of the new angles $\boldsymbol{\delta}$ (299), it is useful to note that the relative angles $\boldsymbol{\delta} - \boldsymbol{\alpha}$ are the torsional spring extensions compensated for the (static) extension due to gravity, given the current arm pose $\boldsymbol{\alpha}$. Alternatively, the angles $\boldsymbol{\delta}$ can be thought of as the motor angles of a corresponding flexible-joint robot operating in a gravity-free environment, as shown in Figure 20.

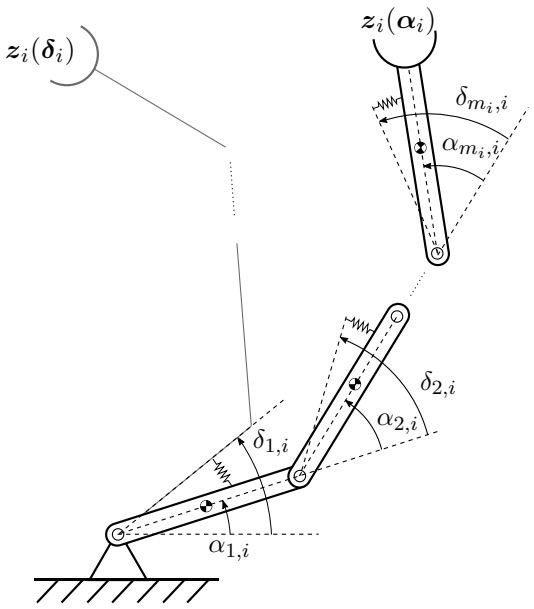

Figure 20: Flexible-joint manipulator i. The physical end-effector is $\boldsymbol{z}_i(\boldsymbol{\alpha}_i)$, but the communicated variable $\boldsymbol{z}_i(\boldsymbol{\delta}_i)$ is evaluated using the angles $\boldsymbol{\delta}_i$.

12.1.5 *Single-agent IDA-PBC solution for task-space coordination*

The system dynamics (305) belong to the class of systems for which an IDA-PBC solution was derived in Section 3.6.3, where it was shown that the communicated variable $\boldsymbol{z}_i$ can be selected as a function of $\boldsymbol{\delta}_i$, while specifying targets $\boldsymbol{z}_i^*$ directly in terms of the link coordinates $\boldsymbol{\alpha}$. An interpretation of this concept is shown in Figure 20, where $\boldsymbol{z}_i(\boldsymbol{\alpha}_i)$ represents the physical end-effector of robot i while $\boldsymbol{z}_i(\boldsymbol{\delta}_i)$ represents the same $\boldsymbol{z}_i(\cdot)$ evaluated using the coordinates $\boldsymbol{\delta}_i$. As $\boldsymbol{\delta}_i$ and $\boldsymbol{\alpha}_i$ converge to each other, the same happens for the physical and virtual end-effector positions.

By coordinating the variable $\boldsymbol{z}_i(\boldsymbol{\delta}_i)$ with other agents in the network, the IDA-PBC conditions for stability and cooperation are satisfied, while still being able to cooperatively control the physical end-effector position with other agents. Although Section 3.6.3 also provides several degrees of freedom to shape the kinetic energy of the robotic manipulator, this chapter uses $\mathbf{M}_{\mathrm{d},i} = \mathbf{M}_i$ and $V_{\mathrm{s},i} = V_i$ for simplicity.

Whereas solutions to the single-agent tracking problem of flexible-joint robots are well known [24, 25], fewer results are available for networks of such robots. Although the work [17] provides a distributed control law for multiple flexible-joint robots, it is restricted to coordinate synchronization of homogeneous systems. Combined with the distributed IDA-PBC control scheme, our proposed solution extends this application to heterogeneous formations in the end-effector space of the robots. This also facilitates formations with very different agents, as discussed next.

12.2 TASK-SPACE COORDINATION OF HETEROGENEOUS SYSTEMS

In this simulation, we consider an autonomous docking task of a UAV with two flexible-joint robotic arms, which are mounted and initialized as shown in Figure 21. We re-use the terrestrial UAV model and control solution from Chapter 11 for brevity, but similar techniques could be used for autonomous docking of spacecraft with a larger space station.

As before, it is assumed that the systems are not in physical contact. We only consider docking process up to the point where the desired formation is achieved and the manipulators are ready to physically couple with the UAV. After grasping the UAV, the three systems become one system with kinematic constraints, which is beyond the scope of this thesis. Some extensions are discussed in Chapter 13.

12.2.1 *Objective, communication graph, and implementation*

The control objective is to obtain a stationary configuration where the UAV is horizontal, while the two manipulator end-effectors coincide with mounting locations on the UAV, presumed to be at 0.2 m to the left and right of its center. A non-unique example of such a leaderless formation is shown in Figure 21. The final docking location and arm poses vary depending on the initial conditions. If desired, the final location can be imposed by designating one or more agents as a leader of the group, with a fixed target.

The formation objective is to be achieved using bidirectional information exchange of the variables $\boldsymbol{z}_i(\boldsymbol{q}_i)$ between the UAV and each robotic arm. This can be accomplished using a network with the undirected edges $(2,1)$, $(1,3)$, the leader matrices $\boldsymbol{\mathcal{B}}_1 = \boldsymbol{\mathcal{B}}_2 = \boldsymbol{\mathcal{B}}_3 = \mathbf{0}_2$, the adjacency matrices $\boldsymbol{\mathcal{A}}_{12} = \boldsymbol{\mathcal{A}}_{23} = \mathbf{I}_2$, and the relative targets $\boldsymbol{r}_{21}^* = \boldsymbol{r}_{13}^* = [0.2 \;\; 0]^\top$.

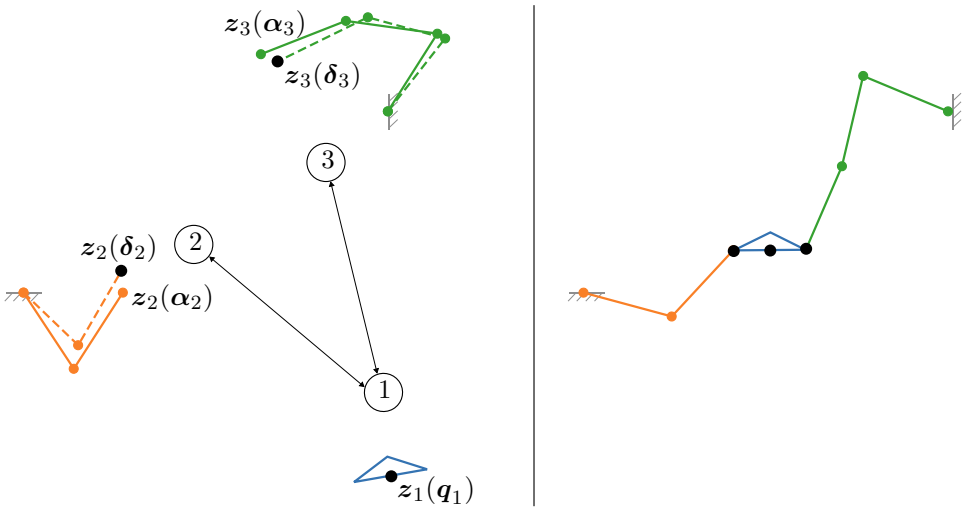

Figure 21: Initial configuration of two flexible-joint manipulators and a UAV (left), and the final docked configuration at the end of the simulation (right). Although the flexible-links are slightly displaced here to highlight the difference between $\boldsymbol{z}_i(\boldsymbol{\alpha}_i)$ and $\boldsymbol{z}_i(\boldsymbol{\delta}_i)$, the initial conditions are chosen as $\boldsymbol{\delta}_i = \boldsymbol{\alpha}_i$.

Although the agents are highly nonlinear, underactuated, and heterogeneous, the control law of each agent is a direct implementation of the method discussed in this thesis. The control law is equal to (283), using the preceding modeling and control definitions for the UAV and the flexible-joint robot. The arm parameters are summarized in Table 6 and the UAV parameters are given in Table 2.

Parameter	2-link arm	3-link arm	haptic manipulator
x_0 (m)	-1	1	-
y_0 (m)	0	1	-
L_k (m)	0.5	0.5	0.1
M_k (kg)	2	2	0.2
c_k (Nm/rad)	10	10	-
I_k (kgm^2)	0.05	0.05	0.005
I_ζ (kgm^2)	0.05	0.05	-
$\mathbf{K}_{v,i}$	$0.5\mathbf{I}_2$	$0.5\mathbf{I}_3$	$0.1\mathbf{I}_2$
$\mathbf{K}_{\mathrm{d},i}$	$0.5\mathbf{I}_2$	$0.5\mathbf{I}_2$	$0.1\mathbf{I}_2$

Table 6: UAV system and control parameters for all agents i. The haptic manipulator is used only in the second simulation.

12.2.2 *Simulation results*

The initial conditions of each system are shown in Table 7. The time traces of the UAV and the end-effectors of the flexible-joint manipulators are shown in Figure 22, where the final end-effector positions are designated with a $\times$ symbol.

First, we observe that the desired formation is achieved, with the end-effectors ultimately at a prescribed horizontal distance of 0.2 m from the center of the UAV. While the true endpoints $\boldsymbol{z}_i(\boldsymbol{\alpha}_i)$ (solid lines) briefly diverge from the communicated variables $\boldsymbol{z}_i(\boldsymbol{\delta}_i)$ (dashed lines) during the maneuver due to the flexibility between

the motors and the physical links, they eventually converge to the same point as the arms come to rest.

The rather nonlinear trajectories of the end-effectors can be explained as follows. Initially, when the UAV is at the lower right, the end-effectors start to move towards it at a comparatively high pace. This initially causes both arms to move towards the lower right. As the UAV approaches more closely, overshooting past the robotic arms, the arms being to reverse. This process repeats once more, leading to a smaller oscillation in all systems, before converging to the final formation. As the UAV approaches its final position, its tilt angle stabilizes at zero.

Table 7: Initial conditions corresponding to Figure 21.

Manipulators	2-link	3-link	UAV	
α_1, δ_1 (rad)	-1	1	$q_{1,i}$ (m)	1
α_2, δ_2 (rad)	2	2	$q_{2,i}$ (m)	-1
α_3, δ_3 (rad)	-	0.5	$q_{3,i}$ (rad)	0.174
$p_{\alpha_1}, p_{\delta_1}$ (Nm s)	0	0	$p_{1,i}$ (m/s)	0
$p_{\alpha_2}, p_{\delta_2}$ (Nm s)	0	0	$p_{2,i}$ (m/s)	0
$p_{\alpha_3}, p_{\delta_3}$ (Nm s)	-	0	$p_{3,i}$ (rad/s)	0

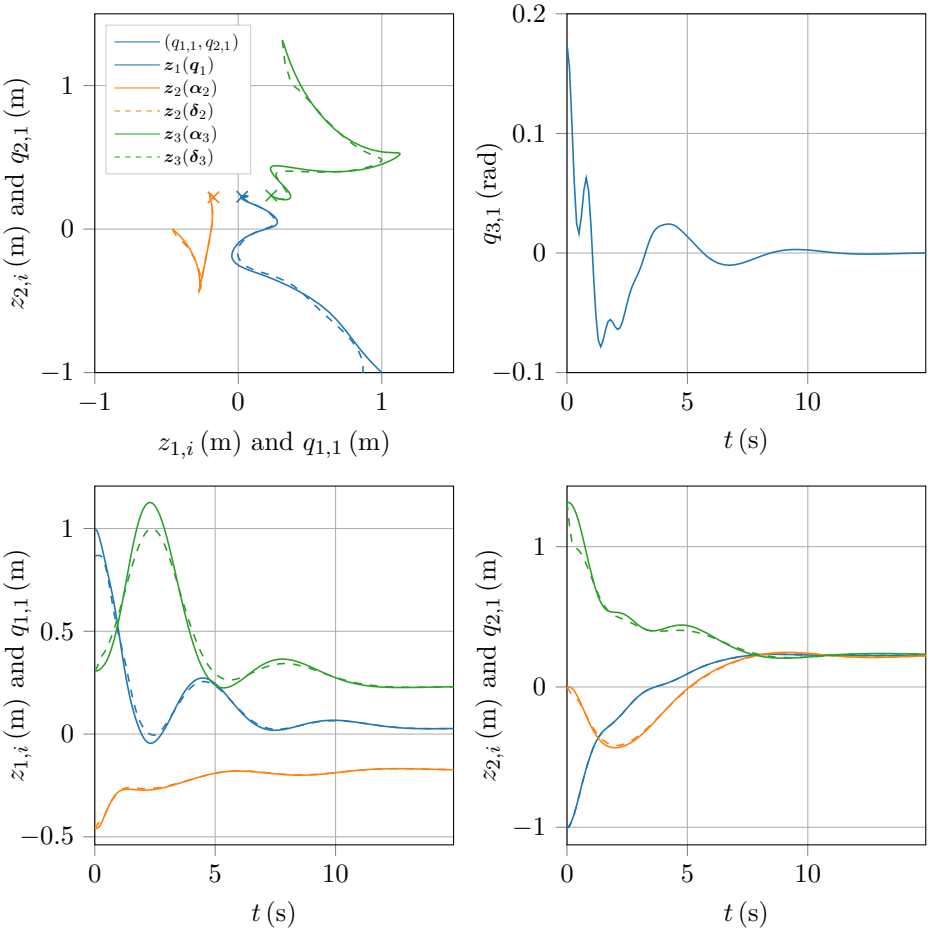

Figure 22: Autonomous docking result with the initial and final configuration corresponding to Figure 21. The dashed lines indicate the communicated variables while the solid lines indicate the physical trajectories.

12.2.3 *Singular configurations*

In robotic manipulator control problems, including in some task-space cooperation tasks [38, 61], the assumption is commonly made that the end-point Jacobian $\boldsymbol{\Psi}_i^\top$ remains full rank during the task, implying that the end-effector can move in any direction at all times. A low-rank configuration occurs when a robotic arm is partially folded (called an "internal singularity") and when it is fully stretched ("external singularity"). Singularities instantaneously prevent the end-effector from moving in one or more directions.

A full-rank assumption prevents the need to address excessive angular rates that can arise with methods that rely on the pseudo-inverse of the Jacobian. This full-rank assumption can be restrictive because it limits the usable workspace, particularly when all robots must maintain the full-rank condition simultaneously.

It is worth noting that the full-rank condition is not strictly necessary in our approach, which is more similar to Jacobian-transpose control [56]. In this case, a low-rank configuration leads to zero angular-rates at worst, implying a local minimum or saddle point of the potential energy in the system. Due to interaction with other agents in the network, however, a robot can recover from a low-rank configuration and continue nominal operation.

In our approach, when a robotic arm is fully stretched, it cannot move further toward a cooperative target, but it rather remains stationary until other agents move towards it instead. For example, consider the task depicted in Figure 21, but assume that the UAV is initially very far away. The arms stretch in the direction of the UAV and effectively pause the docking formation task until the UAV is sufficiently close.

12.3 HUMAN SUPERVISORY CONTROL

This section reconsiders the previous leaderless formation example, and adds a haptic input device that allows a human operator to alter the otherwise arbitrary final docking location. The haptic input device is a small scale, fully-actuated non-flexible two-link manipulator. It coordinates its scaled end-effector position and measured force with the UAV, allowing the human operator to remotely adjust the UAV location.

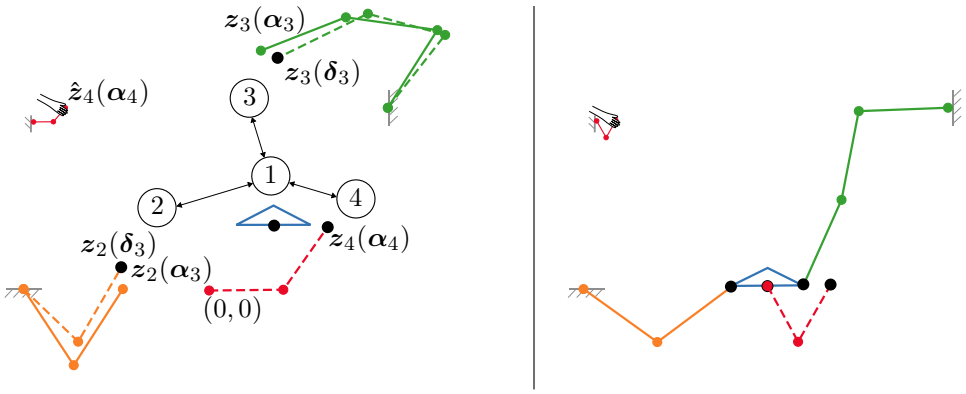

Figure 23: Initial configuration of two flexible-joint manipulators, a UAV, and a haptic input device (left), and the final docked configuration after the simulation (right). The red dashed manipulator represents the virtual, scaled version of the physical haptic input device. Its end-effector (right-most black dot) maintains a relative distance $\boldsymbol{r}_{14}^* = [0.5\ \ 0]^\top$m with respect to the UAV.

12.3.1 *Haptic manipulator*

The haptic input device is a two-link manipulator to which a human operator can apply a force $\boldsymbol{\tau}_\mathrm{h} \in \mathbb{R}^2$, which is also measured. The manipulator dynamics are as in Section 12.1, but without the joint flexibility or dynamic gravity compensation. After canceling gravity with a static feedback law $\boldsymbol{u} = \boldsymbol{\tau} + \frac{\partial V_\alpha}{\partial \boldsymbol{\alpha}}$, the system dynamics are given by (195)

$$\begin{bmatrix} \dot{\boldsymbol{q}}_4 \\ \dot{\boldsymbol{p}}_4 \end{bmatrix} = \begin{bmatrix} \mathbf{0}_2 & \mathbf{I}_2 \\ -\mathbf{I}_2 & \mathbf{0}_2 \end{bmatrix} \begin{bmatrix} \dfrac{\partial H_4}{\partial \boldsymbol{q}_4} \\ \dfrac{\partial H_4}{\partial \boldsymbol{p}_4} \end{bmatrix} + \begin{bmatrix} \mathbf{0}_2 \\ \mathbf{I}_2 \end{bmatrix} \boldsymbol{\tau}_i + \begin{bmatrix} \mathbf{0}_2 \\ \hat{\boldsymbol{\Psi}}_4 \end{bmatrix} \boldsymbol{\tau}_\mathrm{h}, \tag{306}$$

where $\boldsymbol{q}_4 = \boldsymbol{\alpha}_4$, $\mathbf{M}_4 = \mathbf{M}_\alpha$ (292), $V = 0$, and $\hat{\boldsymbol{\Psi}}_4 = \frac{\partial \hat{\boldsymbol{z}}_4}{\partial \boldsymbol{q}_4}$, as defined next.

The physical end-effector location $\hat{\boldsymbol{z}}_4$ is defined with respect to its own origin (x_0, y_0) to allow an arbitrary placement of the haptic device. From (288), this gives

$$\hat{\boldsymbol{z}}_4(\boldsymbol{q}_4) = \begin{bmatrix} L_{1,4}\cos(\alpha_{1,4}) + L_{2,4}\cos(\alpha_{1,4} + \alpha_{2,4}) \\ L_{1,4}\sin(\alpha_{1,4}) + L_{2,4}\sin(\alpha_{1,4} + \alpha_{2,4}) \end{bmatrix}. \tag{307}$$

From (252), the scaled end-effector position is

$$\boldsymbol{z}_4(\boldsymbol{q}_4) = \boldsymbol{\mathcal{C}}_4 \hat{\boldsymbol{z}}_4(\boldsymbol{q}_4), \tag{308}$$

where we choose $\boldsymbol{\mathcal{C}}_4 = 5\mathbf{I}_2$ in this example, amplifying human displacements by a factor 5. This scaling corresponds to a virtual robotic manipulator whose base is at the origin $(0, 0)$ and whose end-effector is at $\boldsymbol{z}_4(\boldsymbol{q}_4)$, as shown by the red dashed manipulator in Figure 23.

12.3.2 *Objective, communication graph, and implementation*

The formation objective and communication graph is the same as discussed in Section 12.2.1, with one additional undirected edge between the haptic manipulator and the UAV, as shown in Figure 23. This edge has $\boldsymbol{\mathcal{A}}_{14} = \mathbf{I}_2$ and $\boldsymbol{r}^*_{14} = [0.5\ \ 0]^\top$m.

The implementation of the distributed control laws follows the strategy of Chapter 10, in which techniques were introduced to optionally apply the measured force $\boldsymbol{\tau}_\mathrm{h}$ directly to other systems. In this simulation, the effect of the human input is applied to the haptic manipulator and the UAV: $\mathbf{D}_1 = \mathbf{D}_4 = \mathbf{I}_2$, $\mathbf{D}_2 = \mathbf{D}_3 = \mathbf{0}_2$, to speed up the response of the UAV to the human input that would result from the formation objective only.

12.3.3 *The human controller*

While the human operator is able to adjust the position of the UAV, the docking task remains autonomous. As the operator moves the haptic device to move the UAV, the manipulator end-effectors automatically follow. This facilitates high-level remote control, without requiring highly skilled operators.

For this simulation, the human operator is modeled as a PD controller that steers the position $\boldsymbol{z}_1$ to zero by moving the haptic manipulator: $\boldsymbol{\tau}_\mathrm{h} = -2\boldsymbol{z}_1 - \boldsymbol{y}_{\mathrm{e},1}$. This rather simplified behavioral model is inspired by the crossover model of [70], which states that an operator tends to control second order systems by acting as a differentiator.

12.3.4 *Simulation results*

The initial conditions for this simulation are given in Table 8, while the position traces of the end-effectors are shown in Figure 24.

Table 8: Initial conditions corresponding to Figure 24.

Manipulators	2-link	3-link	Haptic	UAV	
α_1, δ_1 (rad)	-1	1	0	$q_{1,i}$ (m)	0.3535
α_2, δ_2 (rad)	2	2	$\pi/4$	$q_{2,i}$ (m)	0.3535
α_3, δ_3 (rad)	-	0.5	-	$q_{3,i}$ (rad)	0
$p_{\alpha_1}, p_{\delta_1}$ (Nm s)	0	0	0	$p_{1,i}$ (m/s)	0
$p_{\alpha_2}, p_{\delta_2}$ (Nm s)	0	0	0	$p_{2,i}$ (m/s)	0
$p_{\alpha_3}, p_{\delta_3}$ (Nm s)	-	0	-	$p_{3,i}$ (rad/s)	0

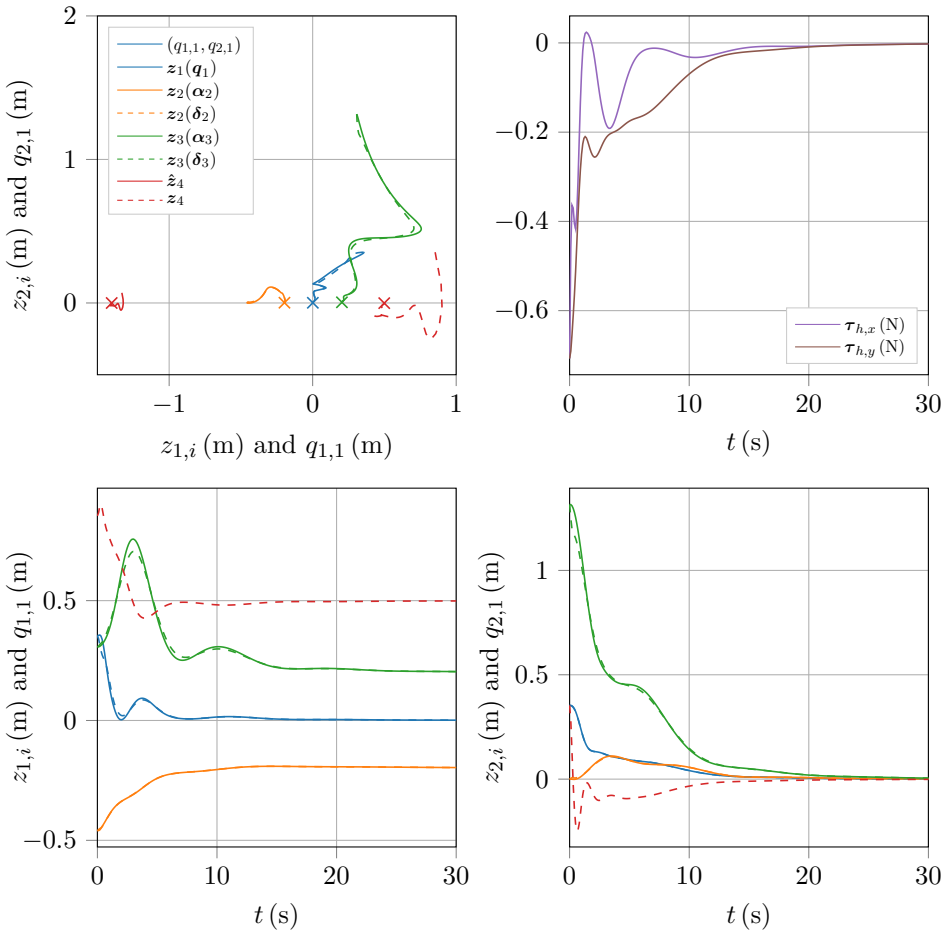

Figure 24: Semi-autonomous docking result with the initial and final configuration corresponding to Figure 23. The haptic manipulator trajectory (solid red) is shown in the top left graph for comparison with its virtual counterpart (red dashed), but its base location is arbitrary.

In this simulation, all systems are initially stationary. Furthermore, the UAV tilt angle is zero and it is already synchronized with the scaled haptic manipulator, at an initial horizontal distance of 0.5 m. This allows us to focus on the subsequent result of both formation forming and the human supervisory control input.

While the formation is being formed, the human operator is already actively controlling the position of the UAV. Since the UAV is initially to the top right of the origin, the operator applies a force in the negative horizontal and vertical direction, as shown in Figure 24 (top right), causing the virtual manipulator to move downward and to the left (red dashed line in bottom figures). This causes the UAV to follow, though at a lower pace as it is held back by virtual coupling forces of the robotic manipulators.

As the human operator continues to apply a force towards the origin, the UAV and ultimately the robotic manipulators follow. Regardless of whether the origin is reached exactly, the robotic manipulators attain the desired formation with respect to the grasping points at the UAV, as shown in Figures 23 and 24.

Although modeled as a PD controller here, the human operator does not necessarily have to insert damping into the system, which is already accomplished by the controlled systems and the haptic manipulator itself. Hence, holding the haptic actuator still at any position will cause the formation to stably converge to the corresponding (scaled) location. In this way, the human operator acts primarily as a supervisory controller, making it possible to adjust the final location of the docked systems without having to control the precise autonomous docking process.

Part VI

CONCLUSIONS

This part provides several extensions of the proposed distributed IDA-PBC method for further research in Chapter 13. Chapter 14 gives a summary and conclusion of the results obtained in this thesis.

13 EXTENSIONS OF DISTRIBUTED IDA-PBC

This final chapter gives several starting points for future research that could extend the proposed methods in this thesis and further establish its relation with currently existing methods. Section 13.1 gives two practical extensions regarding physical contact between systems, which was not considered in this thesis. Section 13.2 exploits the previously derived control by interconnection interpretation to extend the formation control result with applications such as dealing with time delays. Section 13.3 considers applications where some of the agents in the network do not represent physical systems but virtual systems to enhance performance of the physical systems in the network. Section 13.4 extends this idea by discussing energy exchange mechanisms beyond potential energy coupling.

13.1 ENERGY SHAPING FOR COLLISION AVOIDANCE AND CONSTRAINTS

Throughout this thesis, it has been assumed that there is no physical interaction between the agents, thereby ignoring the effects of possible collisions between agents or physical constraints that can arise when agents cooperate. While this is a common assumption in most synchronization literature, it is not very practical in reality. This section gives classes of possible solutions in which the proposed scheme can be adapted or extended to account for these effects.

13.1.1 *Potential energy shaping for collision avoidance*

Although the network coupling energy $\bar{V}_c$ was chosen as a quadratic function (183) of the $\boldsymbol{z}_i$ variables to ensure certain convexity properties and to maintain a generic treatment of rather different applications, other nonnegative functions $\bar{V}_c(\cdot)$ can be chosen to achieve objectives in addition to assuming and maintaining formations.

For collision avoidance, one can use additional potential functions that increase rapidly as any two agents become prohibitively close. This leads to repulsive forces that push them apart as they approach, while decaying to zero when the agents are sufficiently far apart. Such techniques are known to be effective in robotics and cooperative control of fully-actuated point masses, despite not providing hard constraints for collision avoidance [71]. By expressing these potentials in terms of the variables $\boldsymbol{z}_i$, the repulsive forces can be achieved without violating the matching conditions.

13.1.2 *Physical interaction and constraints*

Physical interaction can also arise when one or more agents are kinematically coupled. This is a natural consequence of some cooperative tasks, such as cooperative manipulation of an object.

Although the special case of decoupled matching conditions and control laws (Chapters 7 and 8) may no longer apply, the generic top down procedure of Chapter 6 still holds. In this case, the uncontrolled dynamics (138) and desired network dynamics (144) must be modified to include the physical constraint. Setting the desired dynamics equal to the uncontrolled dynamics then yields the corresponding control law and matching conditions.

Energy shaping of kinematically coupled fully-actuated systems is considered in the Hamiltonian framework in [64]. If the constraints reduce the number of degrees of freedom more than they reduce the number of independent actuators, constraints can even serve to simplify or remove the need to solve matching conditions [72].

13.2 CONTROL BY INTERCONNECTION

In light of the interpretation of the single-agent IDA-PBC solutions as a control by interconnection method in Section 9.3, the resulting internally controlled underactuated systems can possibly be used in some of the existing control schemes [13–17], opening up several useful extensions that relax several conditions imposed in this thesis, such as bidirectional communication without delays.

13.2.1 *Unidirectional communication and directed graphs*

Throughout this thesis, agents were coupled using quadratic potential energies of the form $||\boldsymbol{z}_i - \boldsymbol{z}_j||^2$. Taking gradients of these potentials led to coupling control forces on both agents i and j, driving them toward one another. Both agents required knowledge of the difference $\boldsymbol{z}_i - \boldsymbol{z}_j$ to implement the resulting control laws, which led to the requirement of bidirectional communication and undirected graphs.

When considering the fully-actuated schemes of Chapter 5, the use of undirected graphs is common in some passivity-based distributed control approaches [14, 17]. Other methods provide conditions for this to work on directed graphs as well [13, 15], if the interconnections are linear and certain graph theoretic conditions hold.

With the control by interconnection interpretation, it is anticipated that the proposed single-agent solutions can also be used with certain directed communication graphs, possibly with the control scheme of [13]. The interactions are linear in $\boldsymbol{z}_i(\boldsymbol{q}_i) - \boldsymbol{z}_j(\boldsymbol{q}_j)$, with the nonlinearities and underactuation captured in $\boldsymbol{z}_i(\boldsymbol{q}_i)$.

To support this expectation, Figures 25 and Figure 26 show a directed graph and simulation result corresponding to an adapted version of the simulation of Section 11.3. An important property is that this directed graph is balanced and connected [13]. All parameters and initial conditions remain the same, but only the edges $(1,2)$, $(6,3)$, $(3,5)$, $(3,1)$, $(5,2)$, $(2,4)$, $(2,3)$, $(4,1)$, $(1,6)$ have an adjacency matrix of $\boldsymbol{\mathcal{A}}_{ij} = \text{diag}(1,2)$. The matrices of their counterparts $(2,1), \cdots (6,1)$, are set to zero. Although the transient response is somewhat slower, the agents eventually converge to the desired formation and altitude, despite using only unidirectional communication.

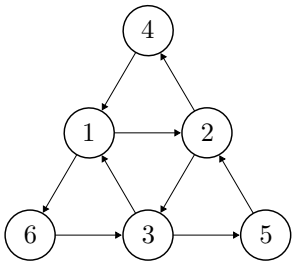

Figure 25: Directed UAV communication graph.

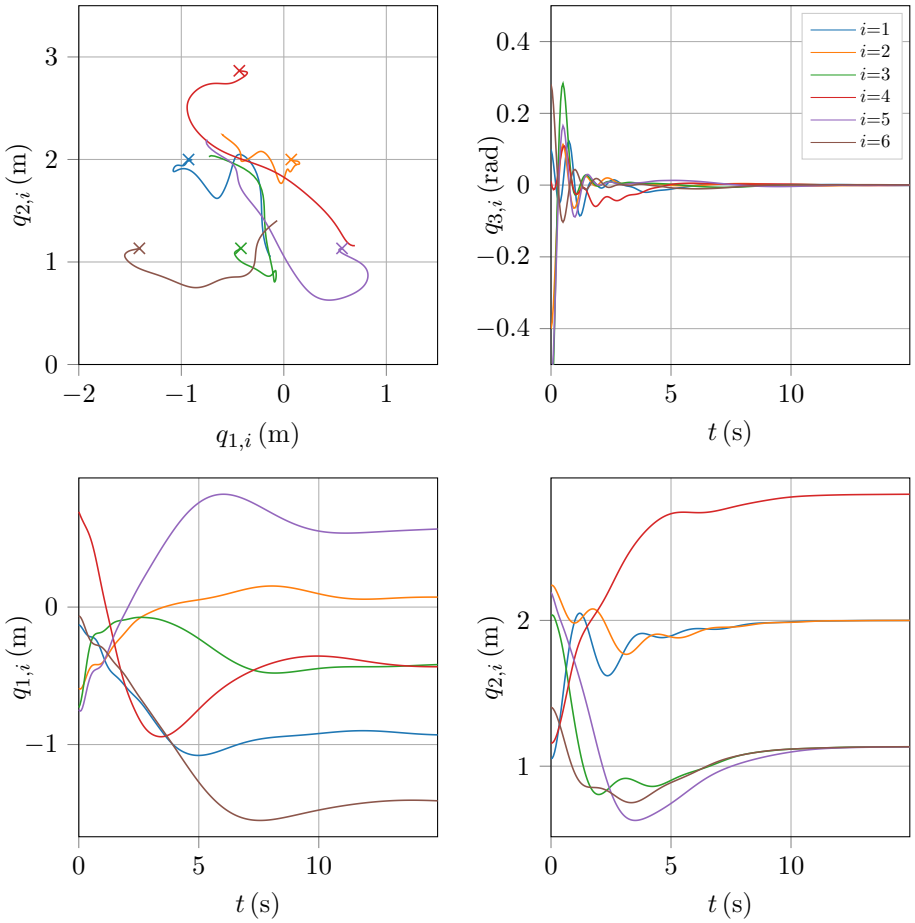

Figure 26: UAV formation using a balanced and connected directed communication graph.

13.2.2 *Time delays and switching graph topologies*

If it is found that the proposed single-agent solutions of the underactuated and heterogeneous agents satisfy the necessary conditions to work with the schemes [13, 14], then existing results regarding delayed inter-agent communication carry over immediately, for the previously given linear couplings.

In addition to being a very practically useful result for networks of underactuated systems, such a solution could be used to investigate how time delays can be captured within the top-down distributed control approach used throughout this thesis. Doing so may allow the presence of time delays even when using more general, nonlinear inter-agent couplings such as nonzero $\mathbf{J}_{ij}$ in (154).

The previously mentioned abstraction to existing passivity-based control methods may also lead to practical extensions such as switching graph topologies, possibly allowing agents to achieve their goals while only communicating with a changing number of neighbors in their vicinity.

13.2.3 *Contraction and passivity for reference tracking and integral control*

It may be possible to adapt or enhance the single-agent solutions to satisfy certain contraction properties, which is investigated for single underactuated systems in [73, 74]. Doing so may allow the systems to work in the contraction-based distributed control scheme [15], providing exponential rather than asymptotic convergence to the desired formation.

Similarly, it may be possible to extend the stationary formation control scheme of this thesis to reference tracking in terms of a suitable (group) reference for the signals $\boldsymbol{z}_i$ or $\frac{\mathrm{d}}{\mathrm{d}t}\boldsymbol{z}_i = \boldsymbol{y}_{e,i}$. A possible intermediate step would be to prove passivity or contraction with respect to a velocity error signal $\boldsymbol{y}_{e,i} - \boldsymbol{y}_{\mathrm{ref}}$, as done in [13–15] for fully-actuated systems and in [58] for generic Hamiltonian systems.

If additionally it is possible to demonstrate passivity or contraction of each system with respect to a signal $\boldsymbol{z}_i + \boldsymbol{\Lambda}\boldsymbol{y}_{e,i}$, then distributed PID control schemes may be feasible, as briefly addressed in Chapter 5. This may lead to improved robustness against disturbances and reduce steady state errors in the presence of unmodeled friction.

13.3 DISTRIBUTED IDA-PBC AND OBSERVER SYSTEMS

In the distributed system analysis throughout this thesis, each system corresponded to a model of a physical system. However, there is no restriction that prevents virtual systems with equivalent models to be included in the network. Doing so can be useful in several applications, two of which are discussed next.

13.3.1 *Absence of velocity measurements*

In some applications, it is not possible to measure the generalized velocity information $\dot{\boldsymbol{q}}_i$ that is needed to obtain $\boldsymbol{p}_i = \mathbf{M}_i^{-1}\dot{\boldsymbol{q}}_i$. Knowledge of $\boldsymbol{p}_i$ is required for agent i to insert damping though a positive dissipation matrix $\mathbf{K}_{v,i} > \mathbf{0}_{m_i}$ or $\mathbf{K}_{\mathrm{d},i} > \mathbf{0}_{\ell}$.

By adding simulated virtual systems with similar models as the physical systems, it is possible to insert damping through the virtual systems instead, by coupling them using potential forces, as shown in Figure 27. This can be achieved by connecting virtual systems to each physical system while keeping the network connection between the physical systems (top figure), or by interconnecting the virtual systems (bottom figure). The main requirement is that the zero state is detectable from the virtual velocity output, implying that sustained zero virtual velocity must also mean that the physical velocities are zero.

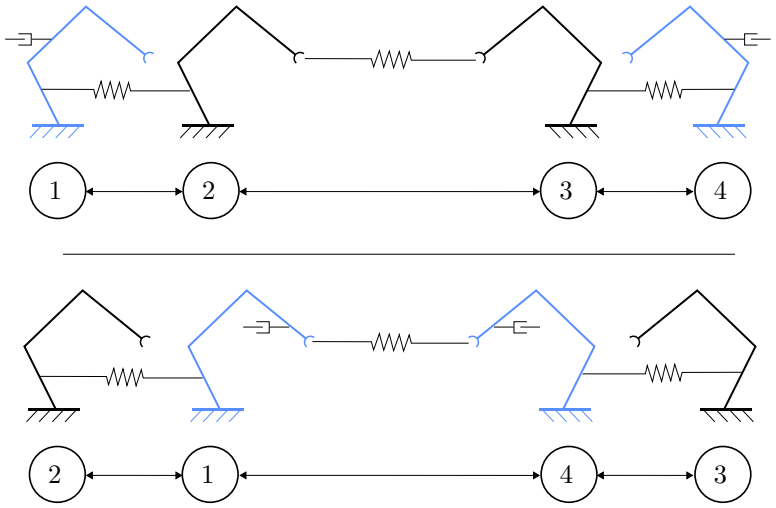

Figure 27: Two possible graph structures for physical robotic manipulators (black) without velocity measurement capability, and virtual systems (blue) that insert damping that propagates to the real systems.

Because it was previously shown that the distributed control method also works for heterogeneous systems, this approach with virtual systems could still work even if the physical model parameters are not known precisely.

The bottom scheme in Figure 27 closely resembles the recently published method for fully-actuated Lagrangian systems without velocity measurements [75]. Further research may allow the method proposed in this thesis to be extended to the absence of velocity measurements in underactuated systems.

13.3.2 *Virtual systems for robustness to parameter uncertainty*

In [76] it was shown that networking can improve robustness of tracking tasks compared to single systems or multiple decentralized systems in the presence of parameter uncertainty. This idea can be used with the proposed distributed IDA-PBC approach as well. Combined with the previously introduced notion of simulated virtual systems, a desired number of virtual systems can be initialized with a desired random distribution of the uncertain parameters. Interconnecting these virtual systems with the physical systems may lead to improved robustness to parameter uncertainty.

13.4 ENERGY-TRANSFER CONTROL

The distributed control solutions given in Chapters 7 and 8 were a special case of the more generic solution of Chapter 6. Although it was found that this special case of agent coupling was sufficient for achieving the formation objective, the more generic solution can possibly be used to achieve other objectives as well as to improve the transient response. In this section we consider the effect of choosing nonzero $\mathbf{J}_{ij}$ in the matrix (154), which leads to interactions between systems called energy-transfer control [77]. A recent publication [64] used a similar technique for teleoperation of a group of fully-actuated robots with physical coupling constraints.

13.4.1 *Force and power balances*

To illustrate several aspects of energy-transfer control in the distributed IDA-PBC method, we consider a network of two agents that are not coupled using potential energy, and focus on the additional control signals $\Delta\boldsymbol{\tau}_1$ and $\Delta\boldsymbol{\tau}_2$ due to selecting a nonzero $\mathbf{J}_{12} = -\mathbf{J}_{21}^\top \in \mathbb{R}^{n_1 \times n_2}$:

$$\Delta\boldsymbol{\tau}_1 = (\mathbf{F}_1^\top \mathbf{F}_1)^{-1}\mathbf{F}_1^\top \mathbf{J}_{12}\mathbf{M}_{\mathrm{d},2}^{-1}\boldsymbol{p}_2, \tag{309}$$

$$\Delta\boldsymbol{\tau}_2 = -(\mathbf{F}_2^\top \mathbf{F}_2)^{-1}\mathbf{F}_2^\top \mathbf{J}_{12}^\top \mathbf{M}_{\mathrm{d},1}^{-1}\boldsymbol{p}_1. \tag{310}$$

Each agent requires both position and velocity information of the other agent to implement the additional control signal. Each system has the desired closed-loop energy $H_{\mathrm{d},i} = \boldsymbol{p}_i^\top \mathbf{M}_{\mathrm{d},i}^{-1}\boldsymbol{p}_i + V_{\mathrm{d},i}$ and the total energy is $H_\mathrm{d} = H_{\mathrm{d},2} + H_{\mathrm{d},2}$. When $\mathbf{K}_{v,i} = \mathbf{0}_{m_i}$ and $\boldsymbol{\tau}_\mathrm{d} = \boldsymbol{0}$, the closed-loop dynamics (144) can be used to obtain

$$\dot{H}_{\mathrm{d},1} = \quad \boldsymbol{p}_1\mathbf{M}_{\mathrm{d},1}^{-1}\mathbf{J}_{12}\mathbf{M}_{\mathrm{d},2}^{-1}\boldsymbol{p}_2, \tag{311}$$

$$\begin{aligned}\dot{H}_{\mathrm{d},2} &= -\boldsymbol{p}_2\mathbf{M}_{\mathrm{d},2}^{-1}\mathbf{J}_{12}^\top\mathbf{M}_{\mathrm{d},1}^{-1}\boldsymbol{p}_1 \\ &= -\dot{H}_{\mathrm{d},1}.\end{aligned} \tag{312}$$

Consistent with the previous observation that the matrix $\bar{\mathbf{J}}$ does not instantaneously effect the rate of decrease of the energy function, we obtain that indeed

$$\dot{H}_{\mathrm{d},1} + \dot{H}_{\mathrm{d},2} = 0. \tag{313}$$

This implies that the systems can exchange energy without a net change in the total energy.

A similar procedure can be carried out for energy-transfer control in terms of the input-output variables $\boldsymbol{\tau}_{e,i}$ and $\boldsymbol{y}_{e,i} = \frac{\mathrm{d}}{\mathrm{d}t}\boldsymbol{z}_i$ with a compatible new definition of $\bar{\mathbf{J}}$, comparable to the definition of $\bar{\mathbf{K}}_{\mathrm{d}}$ as a counterpart to $\bar{\mathbf{K}}_v$. Doing so may provide more physical insight, as $\boldsymbol{y}_{e,i}$ represents physical task-space velocities, with compatible dimensions between the systems.

13.4.2 *Energy routing and energy balancing control*

While the overall power balance balance is zero, the matrix $\mathbf{J}_{12}$ can be used to assign the direction of energy flow between two systems. For example, if we choose

$$\mathbf{J}_{12} = d\,\mathbf{M}_{\mathrm{d},1}^{-1}\boldsymbol{p}_1\boldsymbol{p}_2^{\top}\mathbf{M}_{\mathrm{d},2}^{-1}, \tag{314}$$

where d is a scalar, the energy balances (311), (312) become

$$\begin{aligned}\dot{H}_{\mathrm{d},1} = -\dot{H}_{\mathrm{d},2} &= d\,\boldsymbol{p}_1\mathbf{M}_{\mathrm{d},1}^{-1}\mathbf{M}_{\mathrm{d},1}^{-1}\boldsymbol{p}_1\boldsymbol{p}_2^{\top}\mathbf{M}_{\mathrm{d},2}^{-1}\mathbf{M}_{\mathrm{d},2}^{-1}\boldsymbol{p}_2 \\ &= d\,||\mathbf{M}_{\mathrm{d},1}^{-1}\boldsymbol{p}_1||^2||\mathbf{M}_{\mathrm{d},2}^{-1}\boldsymbol{p}_2||^2.\end{aligned} \tag{315}$$

Because the quadratic terms are nonnegative, a positive d directs energy from system 2 toward system 1, while a negative d directs energy from system 2 to 1. There is only an change of energy when both systems are non-stationary.

A practical application could involve energy distribution between two systems, where the sign of d is chosen based on the difference in energy of two systems using

$$d = (H_{\mathrm{d},2} - H_{\mathrm{d},1} - d_0), \tag{316}$$

where the scalar d_0 is the desired difference in energy. When $d_0 = 0$, this leads to energy balancing, where energy is transfered from one system to the other until the energy of both systems is equal.

13.4.3 *Virtual systems and energy-transfer control*

In addition to routing energy between physical systems, systems can be virtual, analogous to Section 13.3, leading to possible applications for control design.

Because a virtual system can be arbitrarily initialized, it is possible to assign a desired total energy contained initially in the network of systems. By subsequently distributing this energy as described above, the physical system can be made to obtain a desired energy level, provided the systems are sufficiently non-stationary. While this requirement implies that using nonzero $\mathbf{J}_{ij}$ may be of little value for the stationary formation objective of this thesis, it may have applications in controlling single oscillators and oscillator networks.

For example, a physical linear mass spring system with a control force acting on the mass may be oscillating at an initial amplitude corresponding to a constant energy level E_0. By initializing a virtual mass spring system with an energy E_Δ and routing all its energy towards the physical system using a fixed d, the physical system eventually attains the energy $E_0 + E_\Delta$ with a corresponding amplitude. Moreover, the energy required for this amplitude transition is minimal by definition.

14 SUMMARY AND CONCLUSIONS

This chapter summarizes and concludes the report in Section 14.1. Section 14.2 discusses the contributions and limitations of the proposed methods, and gives suggestions for improvement and further research.

14.1 CONCLUSIONS

We have proposed a new, practical distributed control method that enables heterogeneous groups of underactuated and fully-actuated mechanical systems to cooperatively assume desired stationary task-space formations, with or without leaders with absolute targets. This section summarizes the approach and relates it to the previously stated research questions.

14.1.1 *Summary*

This thesis began with a recapitulation of relevant passivity-based modeling and control methodologies from literature, and summarized the single-agent control problem of passivity-based control by interconnection and damping assignment (IDA-PBC). A unified control scheme was presented to compare existing control methods for groups of fully-actuated systems.

Using a top-down distributed control design approach, we have considered the distributed coordination problem of multiple underactuated and fully-actuated systems as the problem of controlling a single, large underactuated mechanical system. By applying the IDA-PBC control technique to assign a desired class of stable dynamics to this large system, we have obtained control laws and matching conditions that allow the group of systems to accomplish a cooperative formation task, while each agent locally stabilizes its own coordinates.

The control objectives are achieved by shaping the total kinetic and potential energy of the systems and the connections between them, such that the energy minimum corresponds to meeting the local and cooperative objectives. The control laws ensure that the systems asymptotically converge to the desired configuration by dissipating the shaped energy until the minimum is reached.

By expressing the potential energy between systems as a positive function of certain task coordinates shared between heterogeneous systems in the network, it was shown that the resulting coupling control forces can achieve the group objectives without violating the total matching conditions. In turn, it was shown that with this choice of potential energy between the systems, the large matching conditions for the group of systems could be decomposed into a set of distributed matching conditions that could be satisfied by each individual agent independent of the network topology. Likewise, the control laws could be implemented in a distributed fashion using bidirectional information exchange over an undirected, connected network.

The per-agent matching conditions were found to be satisfied for a range of single-agent IDA-PBC solutions. By allowing these existing solutions to be reused in a constructive manner, this enables distributed control for a wide range of new applications, while encompassing several existing applications in a generalized control scheme. In addition to providing stable interaction between systems using potential energy gradient forces, several other techniques were identified to adjust the transient response of the systems. These techniques include conservative energy

exchange methods and the ability to shape the relative mass of each system to equalize participation in a group objective when using very different systems.

By extending the energy shaping method to shaping of the input and output behavior of a system, a connection was made between IDA-PBC and the method of control by interconnection. In addition to providing a relation to other passivity-based distributed control methods, this allowed us to study how a human operator can interact with a single system or a distributed system in a stable way. The latter has applications in teleoperation of machines that can operate in environments where humans cannot. For this purpose, techniques were introduced to scale the human input motion and input forces compared to the controlled systems, while preserving passivity with respect to the human power supply.

The practical applicability of the proposed distributed control method was demonstrated using two simulation case studies. These studies highlighted the ability to make underactuated and heterogeneous systems cooperatively achieve task-space formations, with or without leaders in the group. The second case study, concerning formations of flexible-joint robots with an underactuated unmanned aerial vehicle, is novel result that extends existing work on coordinate synchronization of flexible-joint robots.

14.1.2 *Research questions revisited*

We now revisit the research questions of Section 1.2, that have led to the proposed results. It was found that IDA-PBC was valuable to the distributed control problem at two different levels. First, it was used as a tool to study the achievable stabilization and formation objectives of the group of systems as a whole. Subsequently, it was found that the necessary conditions and control laws could be decomposed into local conditions and control laws that are equal to the conditions of certain classes of IDA-PBC solutions. This makes the IDA-PBC method also applicable at this single-agent level, while making it possible to reuse known solutions and couple them in a network.

This result implicitly also encompasses the answers to the subquestions 1.2.1 and 1.2.2, because the choice of coordinates, equilibria and the local conditions for cooperation can be satisfied using existing single-agent IDA-PBC solutions. Additionally, it was shown that the task coordinate $\boldsymbol{z}_i(\boldsymbol{q}_i)$ obtained from existing single-agent solutions is the variable that must be communicated over the network to achieve stable cooperation between systems. The allowable coupling potentials must be a function of these variables, although the function is free. This answers the subquestions 1.2.3 and 1.2.4 regarding the communicated variable and its constraints on the allowed control laws. By reshaping the input-output behavior in addition to shaping the total energy of a system, it became possible to adjust the effects of interaction of systems and groups of systems with their environment, including human operators, which has been used to address question 1.2.5.

14.2 DISCUSSION

Having summarized the working principles of existing and new methods presented in this thesis, we now reflect on the obtained results in relation to existing work and in light of current limitations and recommendations for further research.

14.2.1 *Simplicity and terminology*

The results presented in this thesis have been developed in several stages, a process chronologically similar to the order of the chapters in this thesis. Initially, due to the apparent incompatibility of underactuated systems with existing bottom-up approaches for fully-actuated systems (Chapter 5), we pursued a top-down approach that led to new results for underactuated systems in Chapters 6–8.

Only later while investigating the input-output properties of the shaped mechanical systems for interaction with other systems and human operators (Chapter 9), we found that a control by interconnection approach could also be used for our proposed class of underactuated systems. Hence, by dissecting the obtained top-down result into separate components, we have obtained a system form that can be used in bottom-up approaches similar to those presented in Chapter 5.

Taking this new form as a starting point instead, our method can be presented much more concisely with fewer intermediate steps, reducing the apparent complexity of the method. Similarly, it then naturally embeds the ability to study human interaction and input-output behavior (Chapter 10) from the start, rather than as a seemingly separate addition.

We have deliberately chosen to document the results almost chronologically, both to highlight the development process, but also because the steps to derive the end result are useful on their own, as they reveal control solutions (such as exploiting $\bar{\mathbf{J}}$) not trivially obtained by bottom-up methods. A concise result of the distributed control law with a brief stability proof (without the lengthy derivation thought process) is better served for presentation in a separate paper. An initial attempt at such a presentation, still without the input shaping method, is given in [78].

14.2.2 *Practical value and additions to existing work*

Distributed control methods for fully-actuated systems [13–17] have well-established and constructive solutions for groups of heterogeneous systems, task-space coordination, formation tasks, and leaderless or leader-following tasks. Although some results have been obtained for underactuated systems, these are limited to (coordinate) synchronization [32, 36, 37], to specific applications [37], or they are not constructive or implemented in a distributed sense [36].

The proposed approach of distributed IDA-PBC generalizes these results to heterogeneous groups of underactuated and fully-actuated systems that pursue task-space formations with or without leaders. The method is constructive because suitable single-agent control solutions can be reused to obtain the distributed control laws. These features extend the potential of distributed control applications. For example, we showed how underactuated aerial vehicles can cooperate with robotic manipulators.

The generality and practicality of the proposed method also arises by noting that existing control schemes for fully-actuated systems can be obtained as special cases of the proposed method. This leads to simple distributed control laws for simple systems, while providing sufficient conditions for cooperation with more complex systems. This is promising both for deriving extensions that are already known to hold for fully-actuated systems, and for practical implementation on real systems.

14.2.3 *Practical limitations and recommendations for further research*

As addressed separately in Chapter 13, the presented method can be enhanced by exploiting several features of the distributed control method not yet addressed in this thesis. This includes accounting for time-delays or the absence of velocity measurements, as well as extensions such as conservative energy transfer, communication across directed graphs, reference tracking, and collision avoidance. In this section we consider some more fundamental limitations that may hamper practical implementation depending on the type of application.

Although the proposed method has the potential to be used for various practical applications, this thesis has not addressed many practical and physical challenges of nonlinear control methods for underactuated systems, such as actuator limitations, sensor inaccuracy, measurement and control signal discretization, modeling errors, disturbances, friction, or robustness to parameter uncertainty. Similar concerns could be raised regarding accuracy of force measurements for the application of human interaction with underactuated and distributed systems. All of these aspects are known to adversely affect single underactuated systems, and hence also networks composed of such systems. However, due to the decoupled nature of the conditions for collaboration, it is expected that some solutions to overcome these problems for single agents may also be applicable for distributed systems. The true practical value can only be demonstrated experimentally.

Following Sections 8.6 and 3.1.4, it is also essential to establish a complete, formal proof of the stability result for task-space formations without leaders, and for the case where some coordinates do not have fixed targets other than becoming stationary.

Additionally, some properties intrinsic to this type of control method may give rise to difficulties with avoiding local minima, reaching targets in finite time, imposing hard constraints, or achieving a desired form of optimality. This is in contrast to optimization-based methods, which can embed constraints and optimize for desired metrics, at the expense of higher computational complexity and potentially less certainty about convergence of a solution. In this view, our method is perhaps most relevant for larger networks where optimization-based approaches are not feasible. However, network optimization techniques can be related to passivity-based control approaches [79], meaning that further research could also combine these fields, and exploit the passivity properties of the presented class of single-agent solutions for optimal distributed control techniques.

APPENDIX

A SELECTED DERIVATIONS

This appendix provides a few short derivations for selected equations in this thesis.

A.1 QUADRATIC POTENTIAL FUNCTIONS

This section provides a derivation of (99) by expanding the term $\bar{\boldsymbol{z}}^\top \boldsymbol{\mathcal{L}} \bar{\boldsymbol{z}}$ into a sum of squares. The first step is to use the definition (96) to expand the vector $\boldsymbol{\mathcal{L}}\bar{\boldsymbol{z}}$ as

$$\begin{aligned}
\bar{\boldsymbol{z}}^\top \boldsymbol{\mathcal{L}} \bar{\boldsymbol{z}} &= \bar{\boldsymbol{z}}^\top \begin{bmatrix} (\sum_{j=1}^N \boldsymbol{\mathcal{A}}_{1j}) \boldsymbol{z}_1 - \boldsymbol{\mathcal{A}}_{12} \boldsymbol{z}_2 \ \cdots \ - \boldsymbol{\mathcal{A}}_{1N} \boldsymbol{z}_N \\ \vdots \\ -\boldsymbol{\mathcal{A}}_{1N} \boldsymbol{z}_1 - \boldsymbol{\mathcal{A}}_{2N} \boldsymbol{z}_2 - \cdots + (\sum_{j=1}^N \boldsymbol{\mathcal{A}}_{Nj}) \boldsymbol{z}_N \end{bmatrix} \\
&= \bar{\boldsymbol{z}}^\top \begin{bmatrix} \sum_{j=1}^N \boldsymbol{\mathcal{A}}_{1j} (\boldsymbol{z}_1 - \boldsymbol{z}_j) \\ \vdots \\ \sum_{j=1}^N \boldsymbol{\mathcal{A}}_{Nj} (\boldsymbol{z}_N - \boldsymbol{z}_j) \end{bmatrix} \\
&= \boldsymbol{z}_1^\top \sum_{j=1}^N \boldsymbol{\mathcal{A}}_{1j} (\boldsymbol{z}_1 - \boldsymbol{z}_j) + \cdots + \boldsymbol{z}_N^\top \sum_{j=1}^N \boldsymbol{\mathcal{A}}_{Nj} (\boldsymbol{z}_N - \boldsymbol{z}_j) \\
&= \sum_{i=1}^N \sum_{j=1}^N \boldsymbol{z}_i^\top \boldsymbol{\mathcal{A}}_{ij} (\boldsymbol{z}_i - \boldsymbol{z}_j). \qquad (317)
\end{aligned}$$

Preparing for the next step, we split the previous result into two equal parts:

$$\bar{\boldsymbol{z}}^\top \boldsymbol{\mathcal{L}} \bar{\boldsymbol{z}} = \frac{1}{2} \sum_{i=1}^N \sum_{j=1}^N \boldsymbol{z}_i^\top \boldsymbol{\mathcal{A}}_{ij} (\boldsymbol{z}_i - \boldsymbol{z}_j) + \frac{1}{2} \sum_{i=1}^N \sum_{j=1}^N \boldsymbol{z}_i^\top \boldsymbol{\mathcal{A}}_{ij} (\boldsymbol{z}_i - \boldsymbol{z}_j). \qquad (318)$$

The second sum may be rewritten by reversing the indexes i and j, bringing the minus sign to the front, reversing the indexes of $\boldsymbol{\mathcal{A}}_{ji}$ (allowed because $\boldsymbol{\mathcal{A}}_{ji} = \boldsymbol{\mathcal{A}}_{ij}$), and reversing the order of summation, giving, respectively

$$\begin{aligned}
\frac{1}{2} \sum_{i=1}^N \sum_{j=1}^N \boldsymbol{z}_i^\top \boldsymbol{\mathcal{A}}_{ij} (\boldsymbol{z}_i - \boldsymbol{z}_j) &= \frac{1}{2} \sum_{j=1}^N \sum_{i=1}^N \boldsymbol{z}_j^\top \boldsymbol{\mathcal{A}}_{ji} (\boldsymbol{z}_j - \boldsymbol{z}_i) \\
&= -\frac{1}{2} \sum_{j=1}^N \sum_{i=1}^N \boldsymbol{z}_j^\top \boldsymbol{\mathcal{A}}_{ij} (\boldsymbol{z}_i - \boldsymbol{z}_j) \\
&= -\frac{1}{2} \sum_{i=1}^N \sum_{j=1}^N \boldsymbol{z}_j^\top \boldsymbol{\mathcal{A}}_{ij} (\boldsymbol{z}_i - \boldsymbol{z}_j). \qquad (319)
\end{aligned}$$

Inserting the rewritten summation into (318) gives the end result (99) as

$$\begin{aligned}
\bar{\boldsymbol{z}}^\top \boldsymbol{\mathcal{L}} \bar{\boldsymbol{z}} &= \frac{1}{2} \sum_{i=1}^N \sum_{j=1}^N \boldsymbol{z}_i^\top \boldsymbol{\mathcal{A}}_{ij} (\boldsymbol{z}_i - \boldsymbol{z}_j) - \frac{1}{2} \sum_{i=1}^N \sum_{j=1}^N \boldsymbol{z}_j^\top \boldsymbol{\mathcal{A}}_{ij} (\boldsymbol{z}_i - \boldsymbol{z}_j) \qquad (320) \\
&= \frac{1}{2} \sum_{i=1}^N \sum_{j=1}^N (\boldsymbol{z}_i - \boldsymbol{z}_j)^\top \boldsymbol{\mathcal{A}}_{ij} (\boldsymbol{z}_i - \boldsymbol{z}_j) \geq 0. \qquad (321)
\end{aligned}$$

We now show how (102) is rewritten to derive (103)–(105). We begin by expanding the weighted sums in (102), while leaving the summations unchanged:

$$\begin{aligned}\phi &= \frac{1}{4}\sum_{i=1}^{N}\sum_{j=1}^{N}\left(\boldsymbol{z}_i-\boldsymbol{z}_j+\boldsymbol{r}^*_{ij}\right)^\top\boldsymbol{\mathcal{A}}_{ij}\left(\boldsymbol{z}_i-\boldsymbol{z}_j+\boldsymbol{r}^*_{ij}\right)\\ &\qquad+\frac{1}{2}\sum_{i=1}^{N}\left(\boldsymbol{z}_i-\boldsymbol{z}^*_i\right)^\top\boldsymbol{\mathcal{B}}_i(\boldsymbol{z}_i-\boldsymbol{z}^*_i)\\ &= \frac{1}{4}\sum_{i=1}^{N}\sum_{j=1}^{N}(\boldsymbol{z}_i-\boldsymbol{z}_j)^\top\boldsymbol{\mathcal{A}}_{ij}(\boldsymbol{z}_i-\boldsymbol{z}_j)+\frac{1}{2}\sum_{i=1}^{N}\boldsymbol{z}_i^\top\boldsymbol{\mathcal{B}}_i\boldsymbol{z}_i\\ &\quad+\frac{1}{2}\sum_{i=1}^{N}\sum_{j=1}^{N}(\boldsymbol{r}^*_{ij})^\top\boldsymbol{\mathcal{A}}_{ij}(\boldsymbol{z}_i-\boldsymbol{z}_j)-\sum_{i=1}^{N}(\boldsymbol{z}^*_i)^\top\boldsymbol{\mathcal{B}}_i\boldsymbol{z}_i\\ &\quad+\frac{1}{4}\sum_{i=1}^{N}\sum_{j=1}^{N}(\boldsymbol{r}^*_{ij})^\top\boldsymbol{\mathcal{A}}_{ij}\boldsymbol{r}^*_{ij}+\frac{1}{2}\sum_{i=1}^{N}(\boldsymbol{z}^*_i)^\top\boldsymbol{\mathcal{B}}_i\boldsymbol{z}^*_i.\end{aligned}$$

These three lines are quadratic in $\boldsymbol{z}_i$, linear in $\boldsymbol{z}_i$ and constant, respectively. The quadratic terms on the first line can be written in matrix form using (99). The last line yields the constant c_0. The linear terms are left unchanged for now. We get:

$$\begin{aligned}\phi &= \frac{1}{2}\bar{\boldsymbol{z}}(\boldsymbol{\mathcal{L}}+\boldsymbol{\mathcal{B}})\bar{\boldsymbol{z}}\\ &\quad+\frac{1}{2}\sum_{i=1}^{N}\sum_{j=1}^{N}(\boldsymbol{r}^*_{ij})^\top\boldsymbol{\mathcal{A}}_{ij}(\boldsymbol{z}_i-\boldsymbol{z}_j)-\sum_{i=1}^{N}(\boldsymbol{z}^*_i)^\top\boldsymbol{\mathcal{B}}_i\boldsymbol{z}_i\\ &\quad+c_0,\end{aligned}\tag{322}$$

with

$$c_0 = \frac{1}{4}\sum_{i=1}^{N}\sum_{j=1}^{N}(\boldsymbol{r}^*_{ij})^\top\boldsymbol{\mathcal{A}}_{ij}\boldsymbol{r}^*_{ij}+\frac{1}{2}\sum_{i=1}^{N}(\boldsymbol{z}^*_i)^\top\boldsymbol{\mathcal{B}}_i\boldsymbol{z}^*_i.\tag{323}$$

Now we turn our attention to the linear terms on the second line, which we wish to write in the form $\boldsymbol{c}_1{}^\top\bar{\boldsymbol{z}}$. Noting that $\boldsymbol{\mathcal{A}}_{ij}=\boldsymbol{\mathcal{A}}_{ji}$ and $\boldsymbol{r}^*_{ij}=-\boldsymbol{r}^*_{ji}$ we can write

$$\begin{aligned}\boldsymbol{c}_1{}^\top\bar{\boldsymbol{z}} &= -\sum_{i=1}^{N}(\boldsymbol{z}^*_i)^\top\boldsymbol{\mathcal{B}}_i\boldsymbol{z}_i+\frac{1}{2}\sum_{i=1}^{N}\sum_{j=1}^{N}(\boldsymbol{r}^*_{ij})^\top\boldsymbol{\mathcal{A}}_{ij}\boldsymbol{z}_i-\frac{1}{2}\sum_{i=1}^{N}\sum_{j=1}^{N}(\boldsymbol{r}^*_{ij})^\top\boldsymbol{\mathcal{A}}_{ij}\boldsymbol{z}_j\\ &= -\sum_{i=1}^{N}(\boldsymbol{z}^*_i)^\top\boldsymbol{\mathcal{B}}_i\boldsymbol{z}_i+\frac{1}{2}\sum_{i=1}^{N}\sum_{j=1}^{N}(\boldsymbol{r}^*_{ij})^\top\boldsymbol{\mathcal{A}}_{ij}\boldsymbol{z}_i+\frac{1}{2}\sum_{i=1}^{N}\sum_{j=1}^{N}(\boldsymbol{r}^*_{ij})^\top\boldsymbol{\mathcal{A}}_{ij}\boldsymbol{z}_i\\ &= -\sum_{i=1}^{N}(\boldsymbol{z}^*_i)^\top\boldsymbol{\mathcal{B}}_i\boldsymbol{z}_i+\sum_{i=1}^{N}\sum_{j=1}^{N}(\boldsymbol{r}^*_{ij})^\top\boldsymbol{\mathcal{A}}_{ij}\boldsymbol{z}_i\\ &= \begin{bmatrix}-(\boldsymbol{z}^*_1)^\top\boldsymbol{\mathcal{B}}_1+\sum_{j=1}^{N}(\boldsymbol{r}^*_{1j})^\top\boldsymbol{\mathcal{A}}_{1j} & \cdots & -(\boldsymbol{z}^*_N)^\top\boldsymbol{\mathcal{B}}_N+\sum_{j=1}^{N}(\boldsymbol{r}^*_{Nj})^\top\boldsymbol{\mathcal{A}}_{Nj}\end{bmatrix}\bar{\boldsymbol{z}}\\ &= \begin{bmatrix}-\boldsymbol{\mathcal{B}}_1\boldsymbol{z}^*_1+\sum_{j=1}^{N}\boldsymbol{\mathcal{A}}_{1j}\boldsymbol{r}^*_{1j}\\ \vdots\\ -\boldsymbol{\mathcal{B}}_N\boldsymbol{z}^*_N+\sum_{j=1}^{N}\boldsymbol{\mathcal{A}}_{Nj}\boldsymbol{r}^*_{Nj}\end{bmatrix}^\top\bar{\boldsymbol{z}},\end{aligned}\tag{324}$$

which gives the vector $\boldsymbol{c}_1$.

A.2 UNCONTROLLED NETWORK DYNAMICS

To see that the uncontrolled network dynamics can be written as (138)–(140), take each of the original dynamics (135)–(137), and stack the equations $\dot{\boldsymbol{q}}_i$ and $\boldsymbol{p}_i$ into the vectors $\dot{\tilde{\boldsymbol{q}}}$ and $\dot{\tilde{\boldsymbol{p}}}$ to write

$$\begin{bmatrix} \begin{bmatrix} \dot{\boldsymbol{q}}_1 \\ \vdots \\ \dot{\boldsymbol{q}}_N \end{bmatrix} \\ \begin{bmatrix} \dot{\boldsymbol{p}}_1 \\ \vdots \\ \dot{\boldsymbol{p}}_N \end{bmatrix} \end{bmatrix} = \begin{bmatrix} \mathbf{0}_{\bar{n}} & \mathbf{I}_{\bar{n}} \\ -\mathbf{I}_{\bar{n}} & \mathbf{0}_{\bar{n}} \end{bmatrix} \begin{bmatrix} \begin{bmatrix} \dfrac{\partial H_1}{\partial \boldsymbol{q}_1} \\ \vdots \\ \dfrac{\partial H_N}{\partial \boldsymbol{q}_N} \end{bmatrix} \\ \begin{bmatrix} \dfrac{\partial H_1}{\partial \boldsymbol{p}_1} \\ \vdots \\ \dfrac{\partial H_N}{\partial \boldsymbol{p}_N} \end{bmatrix} \end{bmatrix} + \begin{bmatrix} \mathbf{0}_{\bar{n}\times\bar{m}} \\ \begin{bmatrix} \mathbf{F}_1 & & \\ & \ddots & \\ & & \mathbf{F}_N \end{bmatrix} \end{bmatrix} \begin{bmatrix} \boldsymbol{\tau}_1 \\ \vdots \\ \boldsymbol{\tau}_N \end{bmatrix}, \tag{325}$$

$$\begin{bmatrix} \boldsymbol{y}_1 \\ \vdots \\ \boldsymbol{y}_N \end{bmatrix} = \begin{bmatrix} \mathbf{F}_1 & & \\ & \ddots & \\ & & \mathbf{F}_N \end{bmatrix}^{\top} \begin{bmatrix} \mathbf{M}_1 & & \\ & \ddots & \\ & & \mathbf{M}_N \end{bmatrix}^{-1} \begin{bmatrix} \boldsymbol{p}_1 \\ \vdots \\ \boldsymbol{p}_N \end{bmatrix}, \tag{326}$$

$$\bar{H} = \sum_{i=1}^{N} H_i = \frac{1}{2} \begin{bmatrix} \boldsymbol{p}_1 \\ \vdots \\ \boldsymbol{p}_N \end{bmatrix}^{\top} \begin{bmatrix} \mathbf{M}_1 & & \\ & \ddots & \\ & & \mathbf{M}_N \end{bmatrix}^{-1} \begin{bmatrix} \boldsymbol{p}_1 \\ \vdots \\ \boldsymbol{p}_N \end{bmatrix} + \sum_{i=1}^{N} V_i. \tag{327}$$

This equals (138)–(140) after substituting (142), (143).

A.3 DERIVATIONS FOR THE MATCHED INPUT MATRIX

This section gives a generic expression for the partial derivative of a scalar that is a function of $\boldsymbol{z}(\boldsymbol{q}) \in \mathbb{R}^{\ell}$, both for the single-agent and multi-agent case.

A.3.1 *Single-agent Case*

We wish to know the partial derivative of the scalar

$$c(\boldsymbol{z}(\boldsymbol{q})) = c(z_1(q_1, \ldots, q_n), \ldots, z_\ell(q_1, \ldots, q_n)) \in \mathbb{R}, \tag{328}$$

to the coordinate vector $\boldsymbol{q}$. We first take the derivative of c to each coordinate q_j:

$$\begin{aligned} \frac{\partial c}{\partial q_j} &= \frac{\partial c(z_1(q_1, \ldots, q_n), \ldots, z_\ell(q_1, \ldots, q_n))}{\partial q_j} \\ &= \frac{\partial c}{\partial z_1}\frac{\partial z_1}{\partial q_j} + \cdots + \frac{\partial c}{\partial z_\ell}\frac{\partial z_\ell}{\partial q_j} = \begin{bmatrix} \dfrac{\partial z_1}{\partial q_j} & \cdots & \dfrac{\partial z_\ell}{\partial q_j} \end{bmatrix} \frac{\partial c}{\partial \boldsymbol{z}}. \end{aligned}$$

The complete result is obtained by repeating this derivation for each coordinate and stacking the result:

$$\frac{\partial c}{\partial \boldsymbol{q}} = \begin{bmatrix} \dfrac{\partial c}{\partial q_1} \\ \vdots \\ \dfrac{\partial c}{\partial q_n} \end{bmatrix} = \begin{bmatrix} \dfrac{\partial z_1}{\partial q_1} & \cdots & \dfrac{\partial z_\ell}{\partial q_1} \\ \vdots & & \vdots \\ \dfrac{\partial z_1}{\partial q_n} & \cdots & \dfrac{\partial z_\ell}{\partial q_n} \end{bmatrix} \frac{\partial c}{\partial \boldsymbol{z}} = \boldsymbol{\Psi} \frac{\partial c}{\partial \boldsymbol{z}},$$

where we have defined the matrix $\boldsymbol{\Psi}$ as

$$\boldsymbol{\Psi}(\boldsymbol{q}) = \frac{\partial^\top \boldsymbol{z}}{\partial \boldsymbol{q}} = \begin{bmatrix} \frac{\partial z_1}{\partial q_1} & \cdots & \frac{\partial z_\ell}{\partial q_1} \\ \vdots & & \vdots \\ \frac{\partial z_1}{\partial q_n} & \cdots & \frac{\partial z_\ell}{\partial q_n} \end{bmatrix} \in \mathbb{R}^{n \times \ell}. \tag{329}$$

A.3.2 *Multi-agent Case*

Suppose now that $b \in \mathbb{R}$ is a function of the coordinates of multiple agents:

$$\begin{aligned} b &= b(\boldsymbol{z}_1(\boldsymbol{q}_1), \ldots, \boldsymbol{z}_N(\boldsymbol{q}_N)) \\ &= b \Bigg(z_{1,1}(q_{1,1}, \ldots, q_{n_1,1}), \ldots, z_{\ell,1}(q_{1,1}, \ldots, q_{n_1,1}), \\ &\qquad \ldots, \\ &\qquad z_{1,i}(q_{1,i}, \ldots, q_{n_i,i}), \ldots, z_{\ell,i}(q_{1,i}, \ldots, q_{n_i,i}) \\ &\qquad \ldots, \\ &\qquad z_{1,N}(q_{1,N}, \ldots, q_{n_N,N}), \ldots, z_{\ell,N}(q_{1,N}, \ldots, q_{n_N,N}) \Bigg), \end{aligned} \tag{330}$$

where a subscript α, β pertains to the α-th vector entry of the β-th agent. The constants n_i and ℓ are the number of states and dimension of the communicated variable of each agent.

Each coordinate $\boldsymbol{z}_i$ depends only on $\boldsymbol{q}_i$, such that

$$\frac{\partial z_{j,i}}{\partial q_{k,\ell}} = 0 \quad \forall \quad i \neq \ell. \tag{331}$$

Then we may write

$$\begin{aligned} \frac{\partial b}{\partial q_{j,i}} &= 0 + \cdots + 0 + \frac{\partial b}{\partial z_{1,i}} \frac{\partial z_{1,i}}{\partial q_{j,i}} + \cdots + \frac{\partial b}{\partial z_{\ell,i}} \frac{\partial z_{\ell,i}}{\partial q_{j,i}} + 0 + \cdots + 0 \\ &= \begin{bmatrix} \frac{\partial z_{1,i}}{\partial q_{j,i}} & \cdots & \frac{\partial z_{\ell,i}}{\partial q_{j,i}} \end{bmatrix} \frac{\partial b}{\partial \boldsymbol{z}_i}. \end{aligned} \tag{332}$$

The complete derivative is again obtained by repeating this derivation for each coordinate and stacking the result:

$$\frac{\partial b}{\partial \boldsymbol{q}_i} = \begin{bmatrix} \frac{\partial b}{\partial q_{1,i}} \\ \vdots \\ \frac{\partial b}{\partial q_{n_i,i}} \end{bmatrix} = \begin{bmatrix} \frac{\partial z_{1,i}}{\partial q_{1,i}} & \cdots & \frac{\partial z_{\ell,i}}{\partial q_{1,i}} \\ \vdots & & \vdots \\ \frac{\partial z_{1,i}}{\partial q_{n_i,i}} & \cdots & \frac{\partial z_{\ell,i}}{\partial q_{n_i,i}} \end{bmatrix} \frac{\partial b}{\partial \boldsymbol{z}_i} = \boldsymbol{\Psi}_i \frac{\partial b}{\partial \boldsymbol{z}_i},$$

where it should be noted that matrix $\boldsymbol{\Psi}_i$ depends only on $\boldsymbol{q}_i$:

$$\boldsymbol{\Psi}_i(\boldsymbol{q}_i) = \frac{\partial^\top \boldsymbol{z}_i}{\partial \boldsymbol{q}_i} = \begin{bmatrix} \frac{\partial z_{1,i}}{\partial q_{1,i}} & \cdots & \frac{\partial z_{\ell,i}}{\partial q_{1,i}} \\ \vdots & & \vdots \\ \frac{\partial z_{1,i}}{\partial q_{n_i,i}} & \cdots & \frac{\partial z_{\ell,i}}{\partial q_{n_i,i}} \end{bmatrix} \in \mathbb{R}^{n_i \times \ell}. \tag{333}$$

b

SYSTEMSIM: A PYTHON MULTI-AGENT SIMULATOR

The simulation results presented throughout have been generated using a Python package specifically developed for this thesis, called `systemsim`. It is a general purpose simulator for networks of systems with the dynamics $\dot{\boldsymbol{x}}_i = \boldsymbol{f}(\boldsymbol{x}_i, \boldsymbol{u}_i, \boldsymbol{d}_i, t)$ and the output $\boldsymbol{y}_i = \boldsymbol{h}(\boldsymbol{x}_i, t)$.

B.1 OBJECT ORIENTED SYSTEM REPRESENTATIONS

Each system is represented as a `System` object, characterized by an implementation of the equations of motion $\boldsymbol{f}(\cdot)$, the output $\boldsymbol{h}(\cdot)$, an optional state feedback law, and a set of initial conditions. Given an optional exogenous input $\boldsymbol{d}$ as a function of time and a simulation time range, the object can call an ODE integration routine to obtain and store state and output trajectories for the given time range.

Inheritance of the `System` class is used to generate classes for more specific types of systems, such as linear time invariant systems, or Lagrangian and Hamiltonian mechanical systems. The generic `System` attributes and methods remain the same, but the equations of motion are parametrized by constant or state-dependent system matrices to simplify the process of initializing such systems.

B.2 NETWORK INTERACTIONS

Any number of heterogeneous systems with compatible input and output dimensions can be interconnected into a single large system of the class `Interconnection`. Such an object is initialized from a previously initialized set of `System` objects and a set of edges and adjacency matrices that specify how the inputs and outputs of systems are interconnected. Upon initialization, it extracts the equations of motion of each subsystem and their interconnections to construct a single ODE for the networked system.

For example, such a scheme can be used to combine a linear integrator with a nonlinear mechanical system through a negative feedback interconnection. Because the `Interconnection` class is itself inherited from the `System` class, the resulting closed-loop system is treated as a regular system and can again be included in a higher level network of systems.

A further specialization is the `DistributedMechanicalSystem` class used for the simulations in this thesis. Though largely similar to the `Interconnection` class, it implements the interactions between mechanical systems through the variables $\boldsymbol{z}_i$ rather than the velocity outputs $\boldsymbol{y}_i$.

B.3 INSTALLATION AND EXAMPLES

The `systemsim` package is available from the Python Package Index (`pypi.org`) using standard installation tools such as `pip`. It is compatible with Python 3 and requires `numpy` for matrix and vector operations, `sympy` for symbolic derivations, and `scipy` for ODE integration. Installation instructions are provided at `https://github.com/laurensvalk/systemsim`. This page also provides links to several of the example simulations included in this thesis. The `systemsim` package is released under the MIT license.

BIBLIOGRAPHY

[1] R. Ortega, A. van der Schaft, I. Mareels, and B. Maschke, "Putting energy back in control," *IEEE Control Systems Magazine*, vol. 21, no. 2, pp. 18–33, 2001.

[2] Y. Cao, W. Yu, W. Ren, and G. Chen, "An overview of recent progress in the study of distributed multi-agent coordination," *IEEE Transactions on Industrial Informatics*, vol. 9, no. 1, pp. 427–438, 2013.

[3] D. Jia, K. Lu, J. Wang, X. Zhang, and X. Shen, "A survey on platoon-based vehicular cyber-physical systems," *IEEE Communications Surveys and Tutorials*, vol. 18, no. 1, pp. 263–284, 2016.

[4] D. P. Scharf, F. Y. Hadaegh, and S. R. Ploen, "A survey of spacecraft formation flying guidance and control (part I): Guidance," pp. 1733–1739, 2003.

[5] D. P. Scharf, F. Y. Hadaegh, and S. R. Ploen, "A survey of spacecraft formation flying guidance and control (part II): Control," in *Proceedings of the American Control Conference*, IEEE, vol. 4, 2004, pp. 2976–2985.

[6] D. Mellinger, M. Shomin, N. Michael, and V. Kumar, "Cooperative grasping and transport using multiple quadrotors," in *Distributed Autonomous Robotic Systems*, Springer, 2013, pp. 545–558.

[7] T. Huntsberger, P. Pirjanian, A. Trebi-Ollennu, H. D. Nayar, H. Aghazarian, A. J. Ganino, M. Garrett, S. S. Joshi, and P. S. Schenker, "Campout: A control architecture for tightly coupled coordination of multirobot systems for planetary surface exploration," *IEEE Transactions on Systems, Man, and Cybernetics - Part A: Systems and Humans*, vol. 33, no. 5, pp. 550–559, 2003.

[8] B. Sinopoli, C. Sharp, L. Schenato, S. Schaffert, and S. S. Sastry, "Distributed control applications within sensor networks," *Proceedings of the IEEE*, vol. 91, no. 8, pp. 1235–1246, 2003.

[9] J. Cortes, S. Martinez, T. Karatas, and F. Bullo, "Coverage control for mobile sensing networks," *IEEE Transactions on Robotics and Automation*, vol. 20, no. 2, pp. 243–255, 2004.

[10] M. Rubenstein, A. Cornejo, and R. Nagpal, "Programmable self-assembly in a thousand-robot swarm," *Science*, vol. 345, no. 6198, pp. 795–799, 2014.

[11] J. Werfel and R. Nagpal, "Three-dimensional construction with mobile robots and modular blocks," *The International Journal of Robotics Research*, vol. 27, no. 3-4, pp. 463–479, 2008.

[12] W. Ren and Y. Cao, *Distributed Coordination of Multi-agent Networks: Emergent Problems, Models, and Issues*. Springer Science & Business Media, 2011.

[13] N. Chopra and M. W. Spong, "Passivity-based control of multi-agent systems," in *Advances in Robot Control*, Springer, 2006, pp. 107–134.

[14] M. Arcak, "Passivity as a design tool for group coordination," *IEEE Transactions on Automatic Control*, vol. 52, no. 8, pp. 1380–1390, 2007.

[15] S.-J. Chung and J.-J. Slotine, "Cooperative robot control and concurrent synchronization of Lagrangian systems," *IEEE Transactions on Robotics*, vol. 25, no. 3, pp. 686–700, 2009.

[16] W. Ren, "Distributed leaderless consensus algorithms for networked Euler–Lagrange systems," *International Journal of Control*, vol. 82, no. 11, pp. 2137–2149, 2009.

[17] E. Nuno, I. Sarras, and L. Basanez, "Consensus in networks of nonidentical Euler–Lagrange systems using P+D controllers," *IEEE Transactions on Robotics*, vol. 29, no. 6, pp. 1503–1508, 2013.

[18] J. C. Willems, "The generation of Lyapunov functions for input-output stable systems," *SIAM Journal on Control*, vol. 9, no. 1, pp. 105–134, 1971.

[19] S. Arimoto and M Takegaki, "A new feedback method for dynamic control of manipulators," *Journal of Dynamic Systems, Measurement, and Control*, vol. 102, pp. 119–125, 1981.

[20] J.-J. Slotine and W. Li, "On the adaptive control of robot manipulators," *The International Journal of Robotics Research*, vol. 6, no. 3, pp. 49–59, 1987.

[21] R. Ortega and M. W. Spong, "Adaptive motion control of rigid robots: A tutorial," *Automatica*, vol. 25, no. 6, pp. 877–888, 1989.

[22] R. Ortega, A. Loría, P. J. Nicklasson, and H. Sira-Ramirez, *Passivity-based Control of Euler-Lagrange systems: Mechanical, Electrical and Electromechanical Applications*, ser. Communications and Control Engineering. Springer Science & Business Media, 1998.

[23] B. Yüksel, C. Secchi, H. H. Bülthoff, and A. Franchi, "Reshaping the physical properties of a quadrotor through IDA-PBC and its application to aerial physical interaction," in *IEEE International Conference on Robotics and Automation*, IEEE, 2014, pp. 6258–6265.

[24] M. W. Spong, "Modeling and control of elastic joint robots," *Journal of Dynamic Systems, Measurement, and Control*, vol. 109, no. 4, pp. 310–319, 1987.

[25] B. Brogliato, R. Lozano, B. Maschke, and O. Egeland, *Dissipative Systems Analysis and Control: Theory and Applications*, ser. Communications and Control Engineering. Springer Science & Business Media, 2013.

[26] R. Ortega, A. Donaire, and J. G. Romero, "Passivity-based control of mechanical systems," in *Feedback Stabilization of Controlled Dynamical Systems*, Springer, 2017, pp. 167–199.

[27] R. Ortega, M. W. Spong, F. Gómez-Estern, and G. Blankenstein, "Stabilization of a class of underactuated mechanical systems via interconnection and damping assignment," *IEEE Transactions on Automatic Control*, vol. 47, no. 8, pp. 1218–1233, 2002.

[28] J. A. Acosta, R. Ortega, A. Astolfi, and A. D. Mahindrakar, "Interconnection and damping assignment passivity-based control of mechanical systems with underactuation degree one," *IEEE Transactions on Automatic Control*, vol. 50, no. 12, pp. 1936–1955, 2005.

[29] P. Ogren, E. Fiorelli, and N. E. Leonard, "Cooperative control of mobile sensor networks: Adaptive gradient climbing in a distributed environment," *IEEE Transactions on Automatic Control*, vol. 49, no. 8, pp. 1292–1302, 2004.

[30] M. W. Spong and N. Chopra, "Synchronization of networked Lagrangian systems," in *Lagrangian and Hamiltonian Methods for Nonlinear Control*, Springer, 2007, pp. 47–59.

[31] E. Vos, *Formation control in the port-Hamiltonian framework*. PhD Thesis. University of Groningen, 2015.

[32] S. Nair and N. E. Leonard, "Stable synchronization of mechanical system networks," *SIAM Journal on Control and Optimization*, vol. 47, no. 2, pp. 661–683, 2008.

[33] A. M. Bloch, N. E. Leonard, and J. E. Marsden, "Controlled Lagrangians and the stabilization of mechanical systems I: The first matching theorem," *IEEE Transactions on Automatic Control*, vol. 45, no. 12, pp. 2253–2270, 2000.

[34] A. M. Bloch, D. E. Chang, N. E. Leonard, and J. E. Marsden, "Controlled Lagrangians and the stabilization of mechanical systems II: Potential shaping," *IEEE Transactions on Automatic Control*, vol. 46, no. 10, pp. 1556–1571, 2001.

[35] G. Blankenstein, R. Ortega, and A. van der Schaft, "The matching conditions of controlled Lagrangians and IDA-passivity based control," *International Journal of Control*, vol. 75, no. 9, pp. 645–665, 2002.

[36] D. Zhu, D. Zhou, J. Zhou, and K. L. Teo, "Synchronization control for a class of underactuated mechanical systems via energy shaping," *Journal of Dynamic Systems, Measurement, and Control*, vol. 134, no. 4, p. 410 071, 2012.

[37] E. Nuño, D. Valle, I. Sarras, and L. Basañez, "Leader–follower and leaderless consensus in networks of flexible-joint manipulators," *European Journal of Control*, vol. 20, no. 5, pp. 249–258, 2014.

[38] Y.-C. Liu and N. Chopra, "Controlled synchronization of heterogeneous robotic manipulators in the task space," *IEEE Transactions on Robotics*, vol. 28, no. 1, pp. 268–275, 2012.

[39] A. J. van der Schaft, *L2-Gain and Passivity Techniques in Nonlinear Control*, ser. Communications and Control Engineering. Springer Science & Business Media, 2000.

[40] M. Arcak, C. Meissen, and A. Packard, *Networks of Dissipative Systems: Compositional Certification of Stability, Performance, and Safety*. Springer, 2016.

[41] R. Ortega, A. van der Schaft, F. Castanos, and A. Astolfi, "Control by interconnection and standard passivity-based control of port-Hamiltonian systems," *IEEE Transactions on Automatic Control*, vol. 53, no. 11, pp. 2527–2542, 2008.

[42] R. Ortega and E. García-Canseco, "Interconnection and damping assignment passivity-based control: A survey," *European Journal of control*, vol. 10, no. 5, pp. 432–450, 2004.

[43] A. Astolfi and R. Ortega, "Immersion and invariance: A new tool for stabilization and adaptive control of nonlinear systems," *IEEE Transactions on Automatic control*, vol. 48, no. 4, pp. 590–606, 2003.

[44] L. Wang, F. Forni, R. Ortega, Z. Liu, and H. Su, "Immersion and invariance stabilization of nonlinear systems via virtual and horizontal contraction," *IEEE Transactions on Automatic Control*, vol. 62, no. 8, pp. 4017–4022, 2017.

[45] W. Lohmiller and J.-J. Slotine, "On contraction analysis for non-linear systems," *Automatica*, vol. 34, no. 6, pp. 683–696, 1998.

[46] J. Jouffroy and T. I. Fossen, "A tutorial on incremental stability analysis using contraction theory," *Modeling, Identification and Control*, vol. 31, no. 3, p. 93, 2010.

[47] P. Kokotovic, M Krstic, and I. Kanellakopoulos, "Backstepping to passivity: Recursive design of adaptive systems," in *IEEE Conference on Decision and Control*, IEEE, 1992, pp. 3276–3280.

[48] H. K. Khalil, *Nonlinear Systems*. Prentice-Hall, New Jersey, 1996.

[49] W. M. Haddad and V. Chellaboina, *Nonlinear Dynamical Systems and Control: A Lyapunov-Based Approach*. Princeton University Press, 2011.

[50] M. Ryalat and D. S. Laila, "A simplified IDA-PBC design for underactuated mechanical systems with applications," *European Journal of Control*, vol. 27, pp. 1–16, 2016.

[51] G. Viola, R. Ortega, R. Banavar, J. Á. Acosta, and A. Astolfi, "Total energy shaping control of mechanical systems: Simplifying the matching equations via coordinate changes," *IEEE Transactions on Automatic Control*, vol. 52, no. 6, pp. 1093–1099, 2007.

[52] M. Zhang, R. Ortega, Z. Liu, and H. Su, "A new family of interconnection and damping assignment passivity-based controllers," *International Journal of Robust and Nonlinear Control*, vol. 27, no. 1, pp. 50–65, 2017.

[53] A. Donaire, R. Mehra, R. Ortega, S. Satpute, J. G. Romero, F. Kazi, and N. M. Singh, "Shaping the energy of mechanical systems without solving partial differential equations," *IEEE Transactions on Automatic Control*, vol. 61, no. 4, pp. 1051–1056, 2016.

[54] K. Nunna, M. Sassano, and A. Astolfi, "Constructive interconnection and damping assignment for port-controlled Hamiltonian systems," *IEEE Transactions on Automatic Control*, vol. 60, no. 9, pp. 2350–2361, 2015.

[55] A. Donaire, R. Ortega, and J. G. Romero, "Simultaneous interconnection and damping assignment passivity-based control of mechanical systems using dissipative forces," *Systems & Control Letters*, vol. 94, pp. 118–126, 2016.

[56] J. J. Craig, *Introduction to Robotics: Mechanics and Control*. Pearson/Prentice Hall, 2005.

[57] J Van Der Burg, R Ortega, J Scherpen, J Acosta, and H Siguerdidjane, "An experimental application of total energy shaping control: Stabilization of the inverted pendulum on a cart in the presence of friction," in *Proceedings of the European Control Conference*, IEEE, 2007, pp. 1990–1996.

[58] K. Fujimoto, K. Sakurama, and T. Sugie, "Trajectory tracking control of port-controlled hamiltonian systems via generalized canonical transformations," *Automatica*, vol. 39, no. 12, pp. 2059–2069, 2003.

[59] H. Bai, M. Arcak, and J. Wen, *Cooperative Control Design: A Systematic, Passivity-Based Approach*. Springer Science & Business Media, 2011.

[60] L. Valk and T. Keviczky, "Unified passivity-based distributed control of mechanical systems," in *37th Benelux Meeting on Systems and Control*, 2018.

[61] E. Nuño, C. I. Aldana, and L. Basañez, "Task space consensus in networks of heterogeneous and uncertain robotic systems with variable time-delays," *International Journal of Adaptive Control and Signal Processing*, vol. 31, no. 6, pp. 917–937, 2017.

[62] T. Hatanaka, N. Chopra, M. Fujita, and M. W. Spong, *Passivity-based control and estimation in networked robotics*. Springer, 2015.

[63] A. Franchi, C. Secchi, H. I. Son, H. H. Bulthoff, and P. R. Giordano, "Bilateral teleoperation of groups of mobile robots with time-varying topology," *IEEE Transactions on Robotics*, vol. 28, no. 5, pp. 1019–1033, 2012.

[64] M. Angerer, S. Musić, and S. Hirche, "Port-hamiltonian based control for human-robot team interaction," in *IEEE International Conference on Robotics and Automation*, IEEE, 2017, pp. 2292–2299.

[65] G. R. Luecke, "Haptic interactions using virtual manipulator coupling with applications to underactuated systems," *IEEE Transactions on Robotics*, vol. 27, no. 4, pp. 730–740, 2011.

[66] D. Lee, "Distributed backstepping control of multiple thrust-propelled vehicles on a balanced graph," *Automatica*, vol. 48, no. 11, pp. 2971–2977, 2012.

[67] A. Abdessameud, I. G. Polushin, and A. Tayebi, "Motion coordination of thrust-propelled underactuated vehicles with intermittent and delayed communications," *Systems & Control Letters*, vol. 79, pp. 15–22, 2015.

[68] H. Wang, "Second-order consensus of networked thrust-propelled vehicles on directed graphs," *IEEE Transactions on Automatic Control*, vol. 61, no. 1, pp. 222–227, 2016.

[69] J. Acosta, M. Sanchez, and A. Ollero, "Robust control of underactuated aerial manipulators via IDA-PBC," in *IEEE Conference on Decision and Control*, IEEE, 2014, pp. 673–678.

[70] D. T. McRuer and H. R. Jex, "A review of quasi-linear pilot models," *IEEE Transactions on Human Factors in Electronics*, no. 3, pp. 231–249, 1967.

[71] N. E. Leonard and E. Fiorelli, "Virtual leaders, artificial potentials and coordinated control of groups," in *IEEE Conference on Decision and Control*, IEEE, vol. 3, 2001, pp. 2968–2973.

[72] Y.-H. Liu, Y. Xu, and M. Bergerman, "Cooperation control of multiple manipulators with passive joints," *IEEE Transactions on Robotics and Automation*, vol. 15, no. 2, pp. 258–267, 1999.

[73] J. Acosta, R. Ortega, A. Astolfi, and I. Sarras, "A constructive solution for stabilization via immersion and invariance: The cart and pendulum system," *Automatica*, vol. 44, no. 9, pp. 2352–2357, 2008.

[74] L. Wang, F. Forni, R. Ortega, Z. Liu, and H. Su, "Immersion and invariance stabilization of nonlinear systems via virtual and horizontal contraction," *IEEE Transactions on Automatic Control*, vol. 62, no. 8, pp. 4017–4022, 2017.

[75] E. Nuño and R. Ortega, "Achieving consensus of Euler-Lagrange agents with interconnecting delays and without velocity measurements via passivity-based control," *IEEE Transactions on Control Systems Technology*, 2017.

[76] E. Nuño, R. Ortega, B. Jayawardhana, and L. Basañez, "Coordination of multi-agent Euler–Lagrange systems via energy-shaping: Networking improves robustness," *Automatica*, vol. 49, no. 10, pp. 3065–3071, 2013.

[77] A. van der Schaft and D. Jeltsema, "Port-Hamiltonian systems theory: An introductory overview," *Foundations and Trends® in Systems and Control*, vol. 1, no. 2-3, pp. 173–378, 2014.

[78] L. Valk and T. Keviczky, "Distributed control of heterogeneous underactuated mechanical systems," in *Proceedings of the Conference on Distributed Estimation and Control in Networked Systems*, IFAC, 2018 (Submitted).

[79] M. Bürger, D. Zelazo, and F. Allgöwer, "Duality and network theory in passivity-based cooperative control," *Automatica*, vol. 50, no. 8, pp. 2051–2061, 2014.